

CFD Modelling of Fluid Flow and Contaminant Transport in Hydrogeological Systems



Nageena Kiani Frost

Ph.D.

October 2006

CFD Modelling of Fluid Flow and Contaminant Transport in Hydrogeological Systems

Centre for Numerical Modelling and Process Analysis
School of Computing and Mathematical Sciences
the University of Greenwich
London, United Kingdom.

A thesis submitted in partial fulfilment of the requirements of the
University of Greenwich for the degree of Doctor of Philosophy.

Copyright © 2006 University of Greenwich

All Rights Reserved. Except as permitted under current
legislation, no part of this work may be photocopied, stored
in a retrieval system, published, adapted, transmitted,
recorded or reproduced in any form or by any means,
without the prior permission of the copyright owner.
Enquiries should be addressed to the University of
Greenwich.

The right of the University of Greenwich to be identified as
the author of this work has been asserted in accordance
with the Copyright, Designs and Patents Act 1988.

ABSTRACT

This study provides an understanding of various aspects of hydrogeological systems modelling and the use of computational techniques to predict and optimise hydrological parameter assessment, anisotropic scaling, macrodispersion and solute flux measurements under unsteady, uniform/non-uniform flow conditions.

The incorporated models are structured around multi-physics continuum mechanics analysis to investigate fluid flow and solute transport in hydrogeological systems. The control-volume unstructured mesh configuration, based on cell-centred or vertex-based FV algorithms for CFD and CSM problems is employed. The non-linear material behaviour exhibited by porous soils and the fluid flow evaluation under system stresses is described by elasto-visco-plastic constitutive relationships and the coupling between CFD and CSM processes.

The designed simulation models are used to calibrate the flow problems associated with regional groundwater levels estimation, determination of soil hydraulic properties and moisture distribution in dry soils in response to infiltration of compressible or incompressible fluids. For solute transport problems, investigations of spatial distribution of solute species in homogeneous/layered heterogeneous systems are undertaken by accounting for chemical, geochemical and biological reactions caused by particle deposition processes and liquid-solid interactions in natural subsurface systems. The simulated shape and spread of contaminant plume are effectively influenced by the governing transport mechanism for solutes. The attenuation in leachate is predicted to have a significant role in reducing the level of contaminant concentration and its potential impact on the attainable groundwater resources.

ACKNOWLEDGEMENTS

I would like to express my sincere gratitude to Dr. Mayur Patel and Dr. Choi-Hong Lai for their assistance, guidance and supervision throughout the completion of this research project.

I would also like to thank friends and colleagues as well as academic, research and technical staff associated with the School of Computing and Mathematical Sciences at the University of Greenwich for their support and academic contribution towards this work.

Acknowledgements are also due to Dr. Adrian Butler and the Department of Earth Sciences at Imperial College for the research associated with the thesis in conducting the numerical validations for Burnstump (Nottingham) case study.

I would also extend my sincere thanks and deepest gratitude to my family for the motivation, financial support and co-operative behaviour displayed by them over the years.

TABLE OF CONTENTS

ABSTRACT	III
ACKNOWLEDGEMENTS	IV
TABLE OF CONTENTS	V
LIST OF FIGURES	X
LIST OF TABLES	XV
NOMENCLATURE	XVI
INTRODUCTION	1
1.1 WATER: FACTS AND ISSUES	1
1.2 THE HYDROLOGIC CYCLE	4
1.3 LEGISLATIVE FRAMEWORK	6
1.3.1 List I of Families and Groups of Substances	8
1.3.2 List II of Families and Groups of Substances	9
1.3.3 Water Quality Standards	9
1.4 RISK ASSESSMENT	10
1.4.1 The Risk-based Approach in the UK	11
1.4.2 Stages of Risk Assessment Framework	12
1.4.2.1 Identification of Potential Risk	12
1.4.2.2 Assessment of Risk	12
1.4.2.3 Implementation	13
1.4.3 Conceptual Model	13
1.4.4 Source/Pathway/Receptor Assessment	14
1.4.4.1 Source Characterisation	14
1.4.4.2 Pathways	15
1.4.4.3 Receptors	16
1.4.5 Groundwater Tier Analysis	17
1.5 RESEARCH OBJECTIVES	18
1.5.1 Water-Quantity	19
1.5.2 Water-Quality	19
1.6 LITERATURE REVIEW	20
NUMERICAL METHODOLOGIES	24
2.1 INTRODUCTION	24
2.2 HYDROGEOLOGICAL MODELS	24

2.3	ABOUT PHYSICA	26
2.4	COMPUTATIONAL FLUID DYNAMICS	28
2.4.1	Implicit Discretisation of the Governing Equations	29
2.4.1.1	Diffusion Term on an Orthogonal Mesh	29
2.4.1.2	Transient Term.....	30
2.4.1.3	Source Term.....	31
2.4.1.4	Convection Term	31
2.4.1.5	Diffusion Term on a Non-Orthogonal Mesh	32
2.4.2	The Exact Solution.....	33
2.4.3	Difference Schemes	34
2.4.3.1	The Two Point Schemes for Convection Diffusion Problems	35
2.4.3.2	A Generalized Formulation of the Transport Equation	40
2.4.3.3	Higher Order Difference Schemes.....	41
2.4.4	PHYSICA Modules	43
2.4.4.1	Scalar Module.....	43
2.5	COMPUTATIONAL SOLID MECHANICS	45
2.5.1	Tensor Definition.....	45
2.5.2	Engineering Definition	46
2.5.3	General Discretisation.....	48
2.5.3.1	Cell-vertex FV Method.....	51
2.6	ADAPTED APPROACH.....	53
2.7	IMPLEMENTATION	53
FLOW AND TRANSPORT MODELS: HOMOGENEOUS SYSTEMS.....		55
3.1	GROUNDWATER IN STORAGE	55
3.1.1	Porosity	55
3.1.1.1	Porosity of Sedimentary Rocks	57
3.1.1.2	Porosity of Plutonic and Metamorphic Rocks.....	57
3.1.1.3	Porosity of Volcanic Rocks	58
3.1.2	Specific Yield and Specific Retention	58
3.2	GROUNDWATER MOVEMENT	58
3.2.1	Darcy's Law.....	59
3.2.2	Darcy's Velocity and Hydraulic Head.....	59
3.2.3	Hydraulic Conductivity and Permeability	60
3.2.4	Aquifers	62
3.2.4.1	Confined and Unconfined Aquifers.....	62
3.2.4.2	Cones of Depression and Flow Nets.....	63
3.2.5	Properties of Aquifers.....	64
3.2.5.1	Homogeneity/Heterogeneity.....	64
3.2.5.2	Isotropy/Anisotropy.....	64
3.2.5.3	Darcy's Law for Anisotropic Materials.....	65
3.2.5.4	Principal Directions of Hydraulic Conductivity.....	65

3.2.6	General Flow Equations.....	67
3.2.7	Finite Volume Approximation for Anisotropic Hydraulic Conductivity.....	68
3.3	CONTAMINANT TRANSPORT MECHANISMS	70
3.3.1	Advection.....	70
3.3.2	Diffusion	71
3.3.3	Mechanical Dispersion	71
3.3.4	Hydrodynamic Dispersion	72
3.3.5	Transport Equation of Conservative Solutes	72
3.3.6	Reactive Transport.....	73
3.3.6.1	Adsorption	73
3.3.6.2	Degradation.....	77
3.3.6.3	Colloid Transport.....	78
3.4	FLOW AND TRANSPORT MODELS: VALIDATION	80
3.4.1	Constant Withdrawals from Aquifer Systems	81
3.4.1.1	Case 1.....	84
3.4.1.2	Case 2.....	85
3.4.2	Flow Field Evaluation for Anisotropic Geologic Formations	87
3.4.2.1	Mesh Specific Predictions	87
3.4.2.2	Comparison Case.....	93
3.4.3	Conservative Solute Transport in Uniform Flow Fields.....	95
3.4.3.1	Case 1.....	95
3.4.3.2	Case 2.....	96
3.4.4	Reactive Solute Transport under Non-Linear Sorption and Decay	98
3.4.5	Colloid Transport in Geochemically Heterogeneous Porous Media	100
3.5	CONCLUDING REMARKS.....	102
FLOW AND TRANSPORT MODELS: VADOSE ZONE		104
4.1	INTRODUCTION	104
4.2	SOIL WATER STORAGE	105
4.2.1	Physical Properties of Soil Water System	105
4.2.2	Pressure Head and Water Content	106
4.2.3	Soil Water Constants	107
4.3	SOIL WATER MOVEMENT	108
4.3.1	Water Movement during Infiltration.....	109
4.3.2	Governing Flow Equations	110
4.3.3	Constitutive Relationships	112
4.3.3.1	van Genuchten Model.....	112
4.3.3.2	Haverkamp Model	113
4.3.4	Initial and Boundary Conditions for Flow	113
4.3.4.1	Initial Conditions	113
4.3.4.2	Boundary Conditions.....	113
4.3.5	Governing Transport Equations.....	115

4.3.5.1	Volatilization	115
4.4	NUMERICAL SIMULATIONS AND VALIDATIONS	118
4.4.1	Flow Modelling.....	118
4.4.1.1	Flow Field Analysis Subject to Infiltration	118
4.4.1.2	Sensitivity Analysis of Flow Parameters.....	122
4.4.2	Transport Modelling	125
4.4.2.1	Transport of Conservative Contaminants	125
4.4.2.2	Transport of Reactive Contaminants	131
4.5	CONCLUDING REMARKS.....	142
FLOW AND TRANSPORT MODELS: HETEROGENEOUS (LAYERED) SYSTEMS		144
5.1	INTRODUCTION	144
5.2	LAYERED HETEROGENEITY.....	144
5.2.1	Test Cases	145
5.2.1.1	Flow Problems	145
5.2.1.2	Transport Problems.....	147
5.2.2	Case Study: Burnstump	150
5.2.2.1	Site Characterisation and Details.....	150
5.2.2.2	Simulation Results and Discussions	152
5.3	CONCLUDING REMARKS.....	165
STRESS ANALYSIS		166
6.1	INTRODUCTION	166
6.2	ASSESSMENT OF MECHANICAL BEHAVIOUR OF SOILS	167
6.2.1	Stress State Variables for Unsaturated Soils.....	168
6.2.2	Volume Change Analysis	170
6.2.2.1	Constitutive Relationships.....	171
6.2.3	Use of SWCC in Volume Change Prediction.....	176
6.2.4	Stress-Deformation Analysis	177
6.3	IMPLEMENTATION	179
6.3.1	Comparisons and Validation.....	180
6.3.2	Concluding Remarks.....	185
CONCLUSIONS		187
7.1	FINITE VOLUME METHODOLOGY	187
7.2	INTEGRATED MODELLING FRAMEWORK	187
7.3	VALIDATION OF RESULTS	187
7.4	FLUID FLOW ANALYSIS.....	188
7.5	SOLUTE TRANSPORT ANALYSIS	188
7.6	EFFECTIVENESS OF THE MODEL	189

FUTURE WORK 190

 8.1 HEAT TRANSFER190

 8.2 RANDOM HETEROGENEITY190

 8.3 ANALYSIS OF FLOW THROUGH FRACTURES.....191

 8.4 COMPLEX CHEMICAL REACTIONS191

 8.5 SHEAR STRENGTH ANALYSIS191

 8.6 MULTI-PHASE FLOW192

APPENDICES 193

 A BOREHOLE DATA FOR BURNSTUMP CASE STUDY194

 A1 Borehole survey for chloride concentration.....194

 A2 Borehole survey for ammonocal-nitrogen196

 B PRINCIPAL DIRECTIONS AND ANISOTROPY198

 C CALCULATION OF COEFFICIENT OF WATER STORAGE199

REFERENCES 200

LIST OF FIGURES

Figure 1-1. Distribution of water on earth	2
Figure 1-2. Groundwater use as a percentage of public supply	2
Figure 1-3. UK water resource use by industry and public, 1997/98	2
Figure 1-4. Common sources of groundwater contamination	3
Figure 1-5. Hazardous waste produced by type in UK, 2002	4
Figure 1-6. Diagrammatic representation of hydrologic cycle	5
Figure 1-7. Schematic representation of hydrological cycle. Source: Fetter[2].	7
Figure 1-8. Pollutant linkages	12
Figure 1-9. Assessment framework. Box numbers refer to numbered steps in section 1.4.2. Source: Marsland and Carey [4].	14
Figure 1-10. Tier assessment of groundwater. Source: Marsland and Carey [4].	18
Figure 1-11. Research objectives.	19
Figure 2-1. Example of deterministic models, air pressure contours around a moving car...25	25
Figure 2-2. Example of deterministic models, computed Mach contours in a transonic flow around a generic fighter configuration.	26
Figure 2-3. Example of stochastic models, spectrum of design event lengths against the number of occurrences.	26
Figure 2-4. Physica model architecture.	27
Figure 2-5. Adjacent Control Volumes.	29
Figure 2-6. Non-Orthogonal Control Volumes.	32
Figure 2-7. Normal and shear stresses on a cubical element of infinitesimal dimension.	48
Figure 3-1. Relation between texture and porosity. (a) Well-sorted sedimentary deposit having high porosity; (b) poorly sorted sedimentary deposit having low porosity; (c) well-sorted sedimentary deposit consisting of pebbles that are themselves porous, so that the deposit as a whole has a very high porosity; (d) well-sorted sedimentary deposit whose porosity has been diminished by the deposition of mineral matter in the interstices; (e) rock rendered porous by solution; (f) rock rendered porous by fracturing. Source: Domenico and Schwartz [52].	57
Figure 3-2. Physical representation of confined and unconfined aquifers. Source: http://www.epa.gov/seahome/groundwater/src/geo3.htm	63
Figure 3-3. Definition of principal directions in orthogonal coordinate system.	66
Figure 3-4. Equilibrium and non-equilibrium adsorption.	74
Figure 3-5. Fluid flow profile under transient conditions in an idealized aquifer.	82
Figure 3-6. Fluid flow profile for water withdrawal under transient conditions in an idealized aquifer.	83

Figure 3-7. Comparison of drawdown from a single well after one year.	84
Figure 3-8. Comparison between Physica (coloured contours) and PMWIN (line contours) hydraulic head distribution results. Red squares represent position of abstraction wells.	86
Figure 3-9 Interconnection of nodes through cell faces.	88
Figure 3-10. Geometry of case1 (top) and case2 (bottom) for flow field evaluation.	89
Figure 3-11. Geometry of case 3 (top) and case 4 (bottom) for flow field evaluation.	90
Figure 3-12. Geometry of case 5.	91
Figure 3-13. Hydraulic head contours for (a) isotropic (b) anisotropic conductivity for cases 1 and 2.	91
Figure 3-14. Hydraulic head contours for case 3. (a) isotropic hydraulic conductivity, (b) $K_{yy} = K_{xx}/10$, (c) $K_{yy} = K_{xx}/100$, (d) $K_{yy} = K_{xx}/1000$	92
Figure 3-15. Head distribution for case 4 with (a) isotropic, (b) anisotropic hydraulic conductivity.	92
Figure 3-16. Head distribution for case 5 with (a) isotropic and (b) anisotropic hydraulic conductivity.	93
Figure 3-17. Problem description.	94
Figure 3-18. Comparison of flowlines and simulated hydraulic head contours for isotropic medium in Physica (bottom) and PMWIN (top) results.	94
Figure 3-19. Comparison of flowlines and simulated hydraulic head contours for anisotropic medium in Physica (bottom) and PMWIN (top) results.	94
Figure 3-20. Concentration profiles at 4 different times for the case 1 with constant concentration at the entrance of the column.	96
Figure 3-21 Problem description of case 2.	96
Figure 3-22. Simulated concentration distribution under anisotropic flow conditions at four different times subject to advection and dispersion.	97
Figure 3-23. Comparison of concentration profiles subject to no-decay and linear/non-linear decay with (a) $C_0 > 1$, (b) $C_0 < 1$. Numbers 1, 2 and 3 represent cases with no decay, non-linear decay and linear decay respectively.	99
Figure 3-24. Comparison of concentration profiles subject to no sorption and linear/non-linear adsorption.	99
Figure 3-25. Effect of (a) geochemical heterogeneity, (b) hydraulic conductivity values variation on colloid transport for a period of 0.75 days.	101
Figure 3-26. Effect of longitudinal dispersivity variation on colloid transport at 0.75 days.	101
Figure 4-1. Soil water constants for different soil types. Source: Fetter [2].	108
Figure 4-2. Moisture zones during ponded water infiltration. Source: Ward and Robinson [54].	110
Figure 4-3. Graphical representation of flow processes under infiltration.	119

Figure 4-4. Comparison of results for case 1. Physica 1 ($\Delta t = 1$ sec, $\Delta z \approx 0.0021$ mm), Physica 2 ($\Delta t = 1$ min, $\Delta z \approx 0.0021$ mm), Physica 3 ($\Delta t = 1$ sec, $\Delta z \approx 1.11$ mm).....	120
Figure 4-5. Water content profile for case 2 at times: 0.1, 0.2 and 0.8 hours.....	120
Figure 4-6. Pressure head profile for case 3 for (a) loam, (b) clay loam soil texture.....	122
Figure 4-7. Water content (a) and unsaturated conductivity (b) profiles for loam and clay loam materials.....	122
Figure 4-8. Flow profiles for sensitivity analysis.....	124
Figure 4-9. Concentration Profiles at 0, 0.5, 1, 1.5, 2, 2.5, 3 and 3.5 days. Symbols, solid lines and broken lines represent Physica, McGrail and analytical solutions respectively.....	127
Figure 4-10. Pure advection of solutes at constant and Darcy velocity.....	129
Figure 4-11. Advection and dispersion of solutes at Darcy's velocity.....	130
Figure 4-12. Fate of organic contaminants in subsurface.....	131
Figure 4-13 Concentration profile at 1 day for different K_d values.....	133
Figure 4-14. Concentration profile for case I at $t = 2$ days. (a) without adsorption, (b) with adsorption.....	134
Figure 4-15. (a) Concentration profile for case II, (b) concentration profile for case III at $t = 2$ days.....	134
Figure 4-16. Contaminant distribution for different values of the Langmuir parameter K_1	134
Figure 4-17. Concentration profile for case I at three different times.....	136
Figure 4-18. Comparison results for case I (sensitivity analysis) showing concentration profiles at (a) $t = 50$ d and (b) $t = 100$ d.....	136
Figure 4-19. Concentration profiles comparison at 0.25, 0.5, 1, 2 and 4 days.....	136
Figure 4-20. Comparison of total concentrations: (a)-(d) and aqueous phase concentrations: (e) & (f).....	139
Figure 4-21. Gas concentration profiles (a) without and with (b) modification in gas diffusion coefficient according to equation (4.32).....	141
Figure 4-22. Effect of gas-phase advection for case B: (a) $V_G = 0.333$ cm/d, $C_0 = 100$ $\mu\text{g}/\text{cm}^3$, (b) $V_G = 0.0$ cm/d, $C_0 = 100$ $\mu\text{g}/\text{cm}^3$, (c) $V_G = 3.36$ cm/d, $C_0 = 1000$ $\mu\text{g}/\text{cm}^3$ and (d) $V_G = 0.0$ cm/d, $C_0 = 1000$ $\mu\text{g}/\text{cm}^3$	142
Figure 5-1. Layering configuration of a heterogeneous medium. Soil materials sand, clay, loam and silt possess different hydraulic properties.....	145
Figure 5-2. Water content profile with initial pressure head of -10,000 cm at 48 hours.....	146
Figure 5-3. Water content profile with initial pressure head of -1000 cm at 4 different times.....	146
Figure 5-4. Concentration profile for Freundlich isotherm at three different times.....	148
Figure 5-5. Concentration contours showing the effect of (a) physical layered heterogeneity, (b) geochemical layered heterogeneity, (c) dispersivity ratio $R = 1$ and (d) dispersivity ratio $R = 10$ on colloid transport at an observation time of	

0.75 day. (e) & (f) show combined effect of physical and geochemical heterogeneity. The basic parameters used are given in table (3.5).	149
Figure 5-6. Hydrogeological map of the area.	152
Figure 5-7. Conceptual model of the subsurface underneath Burnstump.	153
Figure 5-8. Calibrated soil water characteristic curve for homogeneous geologic settings.	154
Figure 5-9. Observed (broken lines with symbols) and simulated (solid lines) chloride concentration profiles. The predicted profiles consider the conserved behaviour of chloride.	155
Figure 5-10. Comparison of observed and simulated chloride concentration profiles with an associated half-life of 12 years.	155
Figure 5-11. Comparison of observed and simulated NH ₃ -N concentration profiles under homogeneous geologic setting.	156
Figure 5-12. Simulated water content profile at one year for three soil types case.	156
Figure 5-13. Comparison of observed and simulated chloride concentration profiles for three soil type case.	157
Figure 5-14. Geologic profile setting for four clay lenses case. Turquoise, light turquoise and yellow colours represent materials of type sand1, sand2 and clay respectively.	157
Figure 5-15. Comparison of observed and simulated chloride concentration profiles for four clay lenses case.	157
Figure 5-16. Comparison of observed and simulated NH ₃ -N concentration profiles for four clay lenses case.	158
Figure 5-17. Geologic profile of 2-d model. Left: one clay lens, right: two offset clay lenses cases. Dbgl = depth below ground level.	159
Figure 5-18. Geometry of 3-d case.	159
Figure 5-19. Contours of chloride concentration for two-d simulation (one clay lens case). Plots a-j show transport at Julian date 2001-20001 with a time interval of two years.	160
Figure 5-20. Contours of chloride concentration for two-d simulation (two offset clay lenses case). Plots a-j show transport at Julian date 2001-20001 with a time interval of two years.	161
Figure 5-21. 3D results of simulated chloride concentration at different time intervals.	164
Figure 6-1. Idealized elastic-plastic behaviour giving rise to two categories of deformation analysis. Source: Fredlund and Rahardjo [51].	167
Figure 6-2. Semi-logarithmic plot of void ratio versus net normal stress and matric suction. Source: Fredlund and Rahardjo [51].	179
Figure 6-3. Geometry of the example problem with flow conditions.	181
Figure 6-4. Geometry of the problem with flow conditions and applied load.	181
Figure 6-5. Matric suction distribution at day 100. (a) Hung and Fredlund [89]. (b) Physica results.	182
Figure 6-6. Matric suction distribution at day 200.	182

Figure 6-7. Comparison of matric suction development below the cover versus depth with time. Solid lines = Physica results, symbols = Hung and Fredlund.183

Figure 6-8. Contours of SWCC (a) and permeability function (b) at 100 day.183

Figure 6-9. Contours of vertical displacement (m) due to loading at 100 days.....184

Figure 6-10. Contours of total displacement due to wetting and loading at 100 days.....184

Figure 6-11. Distribution of deformation vectors due to loading and wetting after 100 days.185

Figure 6-12. Cumulative total displacements at the surface at five different times.185

Figure 8-1. Route map for future work. Blue boxes = modelling environment, Turquoise boxes = tasks accomplished, pink boxes = future work.192

LIST OF TABLES

Table 2-1. An example of some available commercial software to model fluid flow and contaminant transport problems.	25
Table 2-2. Definition of Differencing Schemes.....	39
Table 2-3. Work plan – Tasks accomplished and implemented in PHYSICA’s simulation environment.	54
Table 3-1. Soil classification, total porosity and effective porosity of geologic formations. Source: Roscoe Moss Company [53].	56
Table 3-2. Representative values of hydraulic conductivity for various rock types. Source: Domenico and Schwartz [52].	61
Table 3-3. Parameter values used to calculate drawdown in two idealized aquifers. Source: Alley et al [58].	84
Table 3-4. Mesh orientation and element types for 5 cases.....	88
Table 3-5. Parameters and the basic values for colloid transport model. Source: Sun et al [55].	102
Table 4-1 Hydrologic Soil Groups.....	106
Table 4-2. Case 3 parameters.....	121
Table 4-3. Material properties for Langmuir isotherm.	133
Table 4-4. Basic parameters used for concentration calculations. * properties of TCE	140
Table 4-5. Parametric values for TCE.	142
Table 5-1. Soil parameters.	147
Table 5-2. Parametric values for simulated cases for colloid transport.....	149
Table 5-3. Soil parameters values for the calibrated simulations.	152
Table 5-4. Contaminant parameters and associated values.	153
Table 6-1. Assumed soil properties for flow analysis.....	181
Table 6-2. Assumed soil properties for stress-deformation analysis.	181

NOMENCLATURE

Roman Letters

A.....	Area.....	m^2
Nodal point of a CV	
C.....	Constant	
Concentration	$mg.l^{-1}$
CV.....	Control Volume	
FV.....	Finite Volume	
C.....	Concentration.....	$kg.m^{-3}$
D.....	Diffusion Coefficient	
E.....	Energy.....	J
F.....	Vector	
K.....	Hydraulic conductivity	ms^{-1}
K	Global stiffness matrix	
P.....	Pressure.....	Pa
Central point of a CV	
R.....	Retardation factor	
S.....	Source	
Surface	m^2
Storativity.....	m
V.....	Volume.....	m^3
J	Total flux.....	$m^3 s^{-1}$
D	Dispersion coefficient.....	$m^2 s^{-1}$
E.....	Youngs modulus	
R.....	Outward normal operator	
W.....	Weighting function	
N.....	Shape function	
H.....	Modulus of elasticity	
I	Identity matrix	
f	Global nodal force vector	
b	Source Vector	
b.....	Body force	
d.....	Distance	m
e.....	Natural Logarithm.....	2.718281
<i>f</i>	Face	
k.....	Permeability	m^2
l.....	Length	m
h.....	Hydraulic head.....	m
n.....	Normal	
Pore size distribution	
n	Unit Outward Normal	

q	Flow Rate	$m^3 s^{-1}$
r	Radius	m
t	Time	s
u	Velocity	$m.s^{-1}$
u	Velocity Vector	$m.s^{-1}$
x	Distance, direction x-axis	m
y	Distance, direction y-axis	m
z	Distance, direction z-axis	m

Greek Letters

Γ	Diffusion Coefficient	
θ	Water content	$m^3 m^{-3}$
Angle between two faces	
Fractional surface coverage of deposited colloids	
μ	Poisson's ratio	
ν	Kinematic Viscosity	$m^2 s^{-1}$
Average linear velocity	ms^{-1}
Lame's constant	
λ	Lame's constant	
Decay constant	s^{-1}
α	Dispersivity	m
Width of capillary fringe	m^{-1}
ρ	Density	$kg.m^{-3}$
τ	Shear Stress	$N.m^{-2}$
η	Porosity	
ϕ	Solved Variable/Quantity	

Letters with Sub-scripts

C_t	Coefficient of Convection Term	
C_c	Constant Part of Source Term	
d_{AP}	Distance between point A and P	
S_c	Constant part of source term	
S_p	Value of source term at central Element	
η_e	Effective porosity	
S_y	Specific yield	
S_r	Specific retention	
S_s	Specific storage	m
D_m	Diffusion coefficient	$m^2 s^{-1}$
D_d	Mechanical dispersion	$m^2 s^{-1}$
S_a	Adsorbed concentration	$mg.kg^{-1}$
K_d	Distribution coefficient	$m^2 s^{-1}$

K_1	Langmuir constant of absorbed bond strength	$m^3 g^{-1}$
K_2	Maximum adsorption capacity	
K_f	Coefficient of Freundlich isotherm	
k_1	Sorption finite rate constant	$m.h^{-1}$
k_2	Desorption finite rate constant	h^{-1}
a_p	Colloid particle radius	
S_e	Effective saturation	
θ_s	Saturated water content	
θ_r	Residual water content	
K_s	Saturated hydraulic conductivity	$m.s^{-1}$
ρ_b	Bulk density	
K_{oc}	Partitioning coefficient	
f_{oc}	Fraction of organic carbon	
u_w	Pore water pressure	
u_a	Pore air pressure	

Super-scripts

O	Old/Previous Value
T	Total
Th	Thermal
vp	Visco-Plastic

Mathematical Operators

%	Modulus
∂	Partial Differential
Δ	Gradient, rate of change
∇	Divergence
\sum	Summation
$\sqrt{\quad}$	Square Root
erfc	Error function

Dimensionless Groups

Pe	Peclet Number
Re	Reynolds Number
K_H	Henry's Constant

CHAPTER 1

INTRODUCTION

The work discussed in this thesis is aimed at examining the processes responsible for movement, distribution and quality of water below the surface of earth through the use of computational modelling techniques. The aspects for the need of conventional model and sustainable technologies that will allow preserving an intact environment are discussed in this chapter. The water quality issues are looked into a brief detail to be acquainted with the legal framework.

1.1 Water: Facts and Issues

Water, a natural resource, is vital to the existence of life on earth. Though almost present everywhere on, over and under the surface of earth, its uneven distribution, occurrence and movement are central reasons and subject matter of hydrological system studies. Only three percent of all water that occurs on earth contributes towards the fresh water (Figure 1-1). Subsurface or groundwater that appears as about a quarter of this percentage represents the largest accessible store of fresh water as the best and in some cases the only solution to the problem of providing water for drinking and irrigation in the developing countries.

The demand for groundwater for public and industrial supplies is higher due to the fact that it requires less extensive and expensive treatment than those of equivalent surface-water resources. Figure 1-2 is an example of groundwater usage for public supplies in some of the European countries in 1986. A research carried out by the Environment Agency provides an estimated consumption of over 16.8 billion cubic meters of water (Figure 1-3) in England and Wales in 1997/98. The non-domestic usage accounted for 13.5 billion cubic meters while 3.3 billion cubic meters were used by households through the public supply network. Direct abstraction from groundwater amounted to nearly 9.6 billion cubic meters of the total consumption.

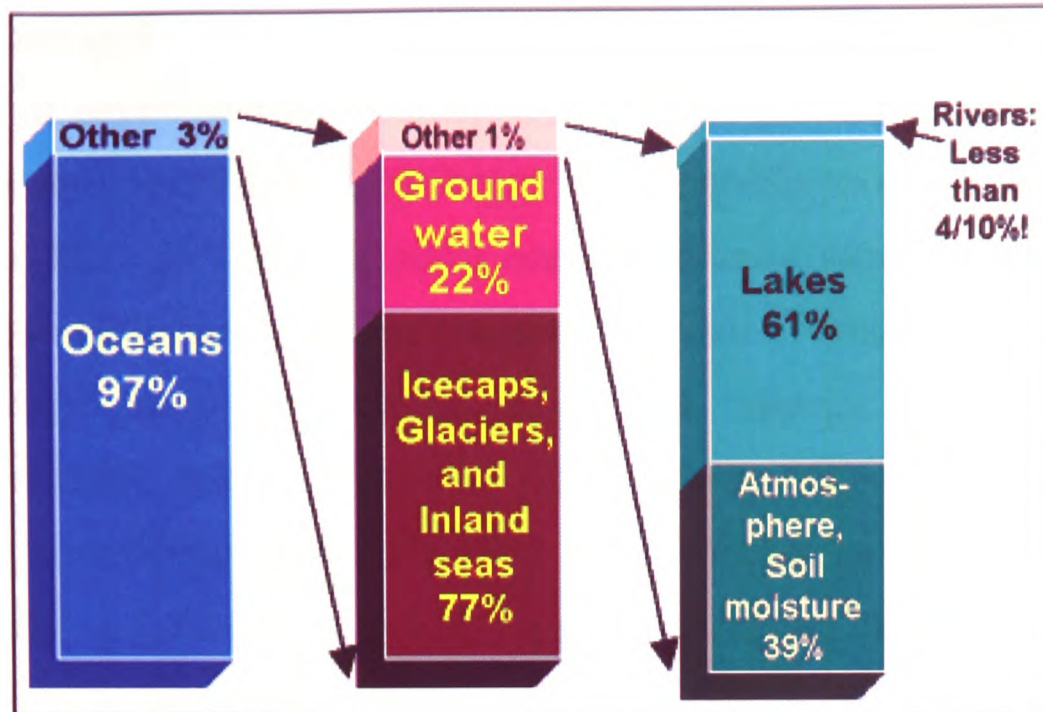


Figure 1-1. Distribution of water on earth

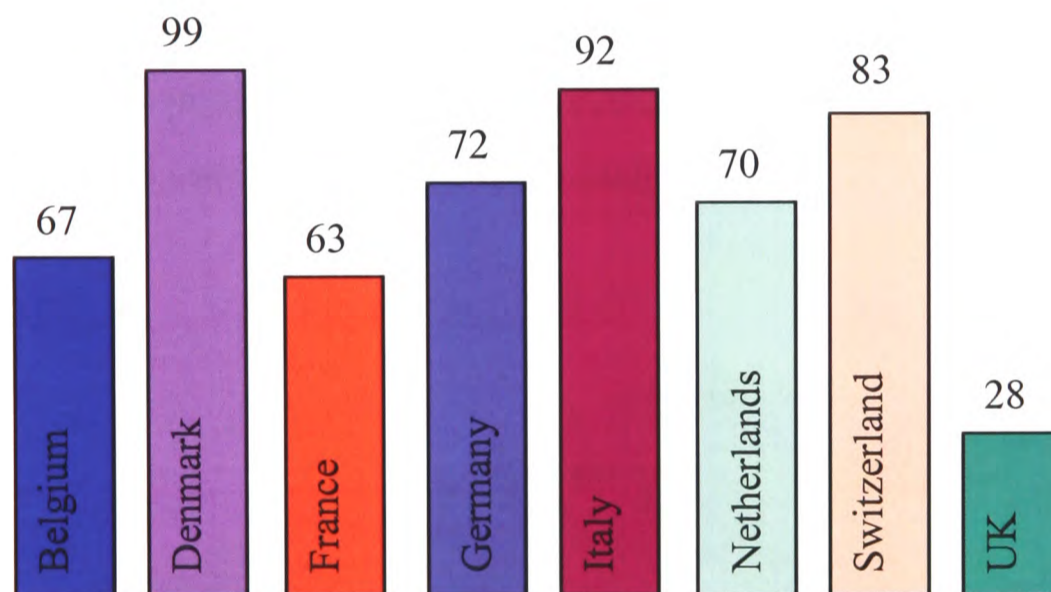


Figure 1-2. Groundwater use as a percentage of public supply

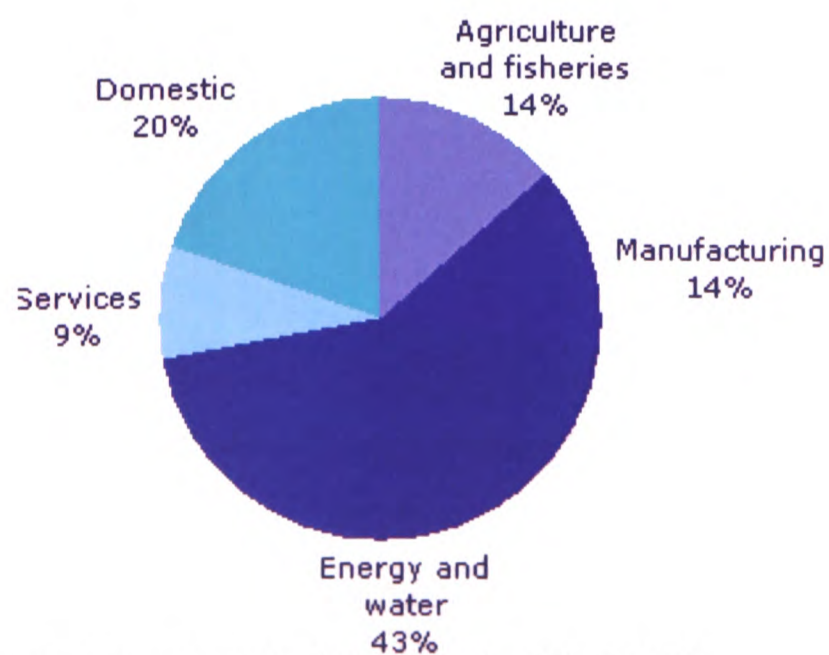


Figure 1-3. UK water resource use by industry and public, 1997/98

Measure of water quality is another critical issue and an aspect of increasing concern for a wide range of environmental problems and geologic processes. Although safer and reliable under most conditions groundwater is vulnerable to contamination in many different ways. Most problems regarding contamination of subsurface water resources are result of human impact on water chemistry in form of waste-disposal practices or other uncontrolled activities such as septic tank seepage, fertilizers infiltration, agricultural pesticides, mining, highway de-icing salts etc (Figure 1-4). For example a chemical spill at industrial plant miles away could infiltrate the ground and eventually enter the aquifer system that an entire community uses for their private wells. This situation could have devastating effects.

The UK produces around 400 million tonnes of waste each year. The vast majority of this is aggregates, sewage and sludge, construction and demolition waste. The remaining 170 million tonnes is produced by industry, commerce and households (Figure 1-5). About 100 million tonnes of waste is landfilled each year.

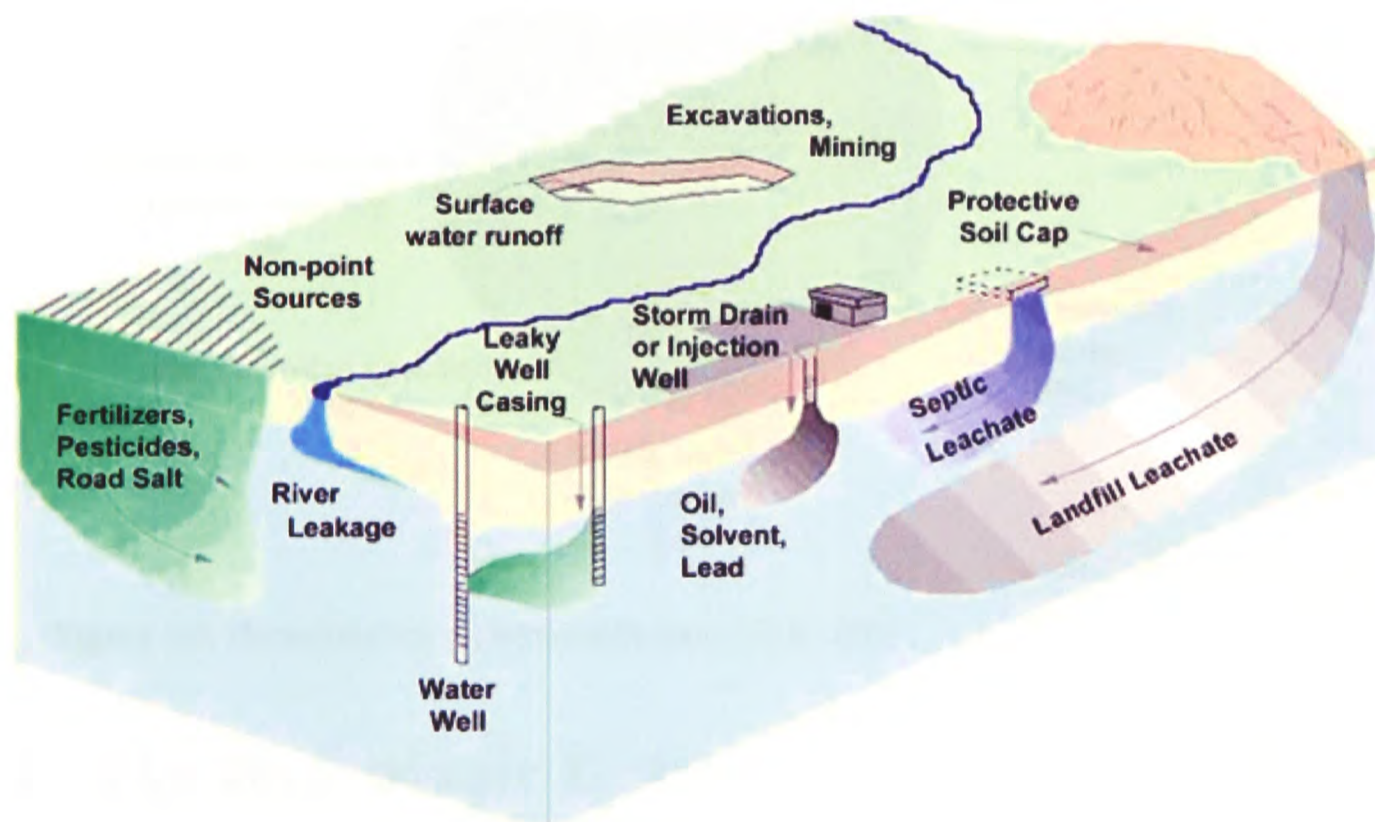
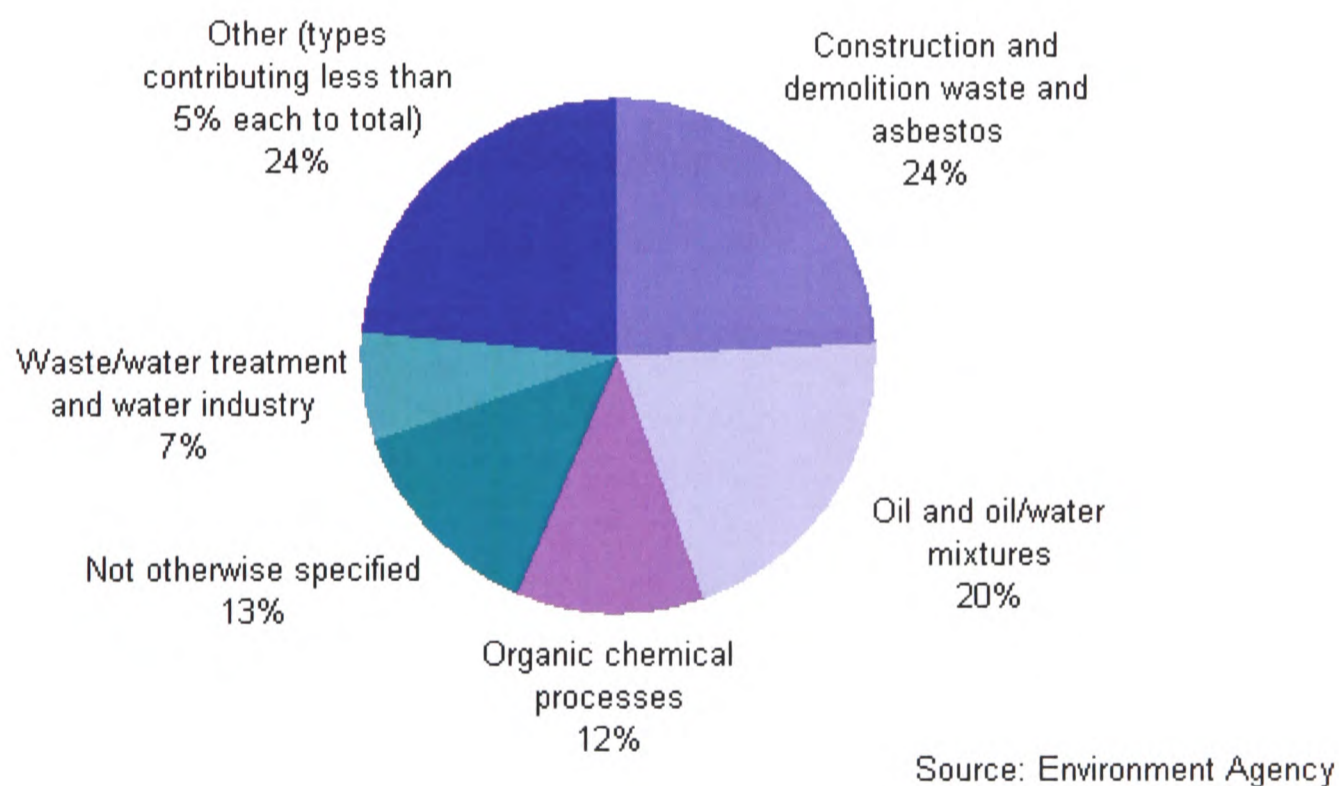


Figure 1-4. Common sources of groundwater contamination

The Environment Agency (1999) estimates that some 300 000 ha of land across Britain may be affected either by industrial, non-industrial or natural contamination. Although not all these sites will pose immediate concern, the Agency estimates that there may be 5000 to 20000 problem sites. A contaminated land can pose toxicological affect on human health, animals, plants, air, soil, groundwater and surface water.

As water becomes scarcer and as competition for its use expands, the issues of quality and quantity reinforce the need to understand, preserve and protect existing resources. The knowledge of basic physical processes is thus important to identify relationship of groundwater with hydrologic cycle as the first step and other phenomena related to its occurrence, replenishment and direction of motion in subsurface systems. Subsequent sections will also provide a guide to the major aspects of legislative control and assessment methodologies for the remedial targets and protection of natural resources.



1.2 The Hydrologic Cycle

The hydrologic cycle is a continuous process by which water is transported from the oceans to the atmosphere to the land and back to the sea, Viessman [1].

Figure 1-6 illustrates the various ways that water is distributed over the earth and various pathways that it takes to move through the cycle. An essential requirement of Figure 1-6

is that of water balance- that the rate of flow into any of stores; ocean, ice-cap or groundwater, is equal to rate of flow out of it.

Water circulation in hydrologic cycle is solar driven. Annually, over 3 feet of water is evaporated off the ocean surface as pure water under the effect of solar radiation. The condensed water returns as precipitation with over 90 percent falling on the oceans. Water that precipitates on land may take several routes through the remainder of the cycle. Some water may temporarily store on the land surface as ice and snow or water in puddles known as depression storage. This water will evaporate or runoff these surfaces into natural or artificial channels. If the surface soil is porous, some rain or melting snow will seep into the ground as infiltration, which is the process whereby water enters the ground at the surface. An exceptionally heavy rainfall can exceed the infiltration capacity, the maximum rate at which water can enter the soil, hence leading to flow over the surface as overland flow as soon as any depression is filled.

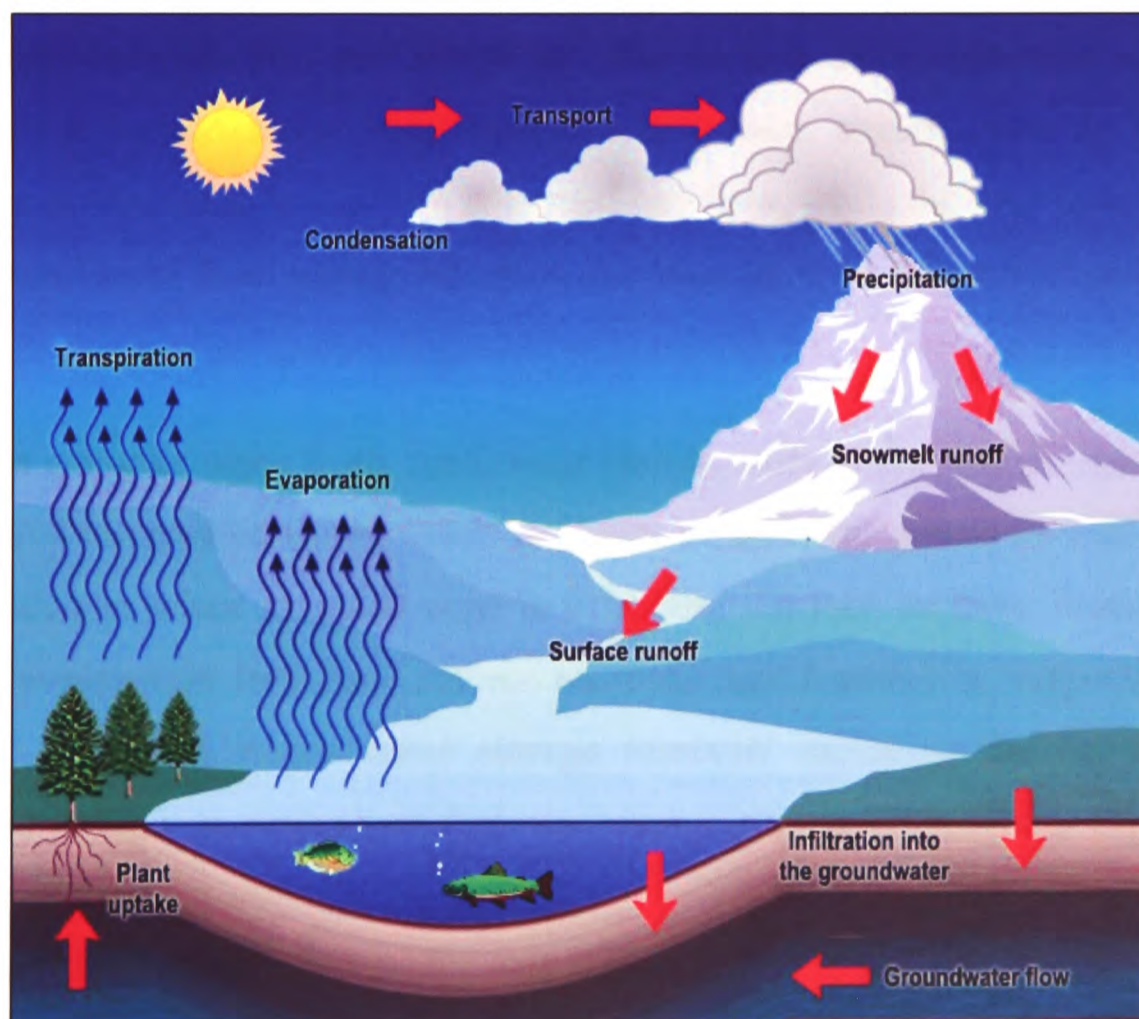


Figure 1-6. Diagrammatic representation of hydrologic cycle

Below the land surface the soil pores contain both air and water. This region is known as the unsaturated or vadose zone. At the top of the vadose zone is the belt of soil water up to where the roots of plants can reach. As the plant uses the water, it is transpired as vapour to the atmosphere. If the rocks beneath the soil are impermeable, or if there are layers of contrasting permeability, there will be a tendency for water to move laterally through the unsaturated zone, a process known as interflow. Water vapour in the vadose zone can also migrate back to land surface to evaporate. The excessive water in vadose zone is pulled downward by gravity, a process known as gravity drainage. It passes through the intermediate belt to the capillary fringe. In the capillary fringe, the pores are filled with capillary water so that the saturation reaches 100 percent; however, the water is held in place by capillary forces.

Below the capillary fringe the pores of the soil or rock are saturated with water completely. Water stored in this saturated zone is known as groundwater. The top of the saturated zone is often referred to as the water table. The storage of water is replenished through the recharge which is the precipitation reaching water table. Water in this zone flows through the rock and soil layers of earth until it discharges as a spring or as seepage into a surface water body such as pond, lake, stream, river or ocean. The groundwater contribution to a stream is termed baseflow, while the total flow in a stream is runoff, contributed from surface runoff as overland flow, interflow and baseflow.

Evaporation can take place from open water bodies, such as the oceans, lakes, streams, reservoirs and intercepted storage such as leaves of trees and plants as well as directly from groundwater when saturated zone is at or near the land surface. Transpiration by plants and evaporation from land surface are combined together as evapotranspiration. Figure 1-7 shows the major water storage reservoir excluding the oceans and the pathways by which water can move from one reservoir to the other (Fetter [2]).

1.3 Legislative Framework

The increased awareness of groundwater vulnerability and the effects of anthropogenic activities on natural systems have increased the concern of human health and environmental protection by giving added impetus to legal control with time.

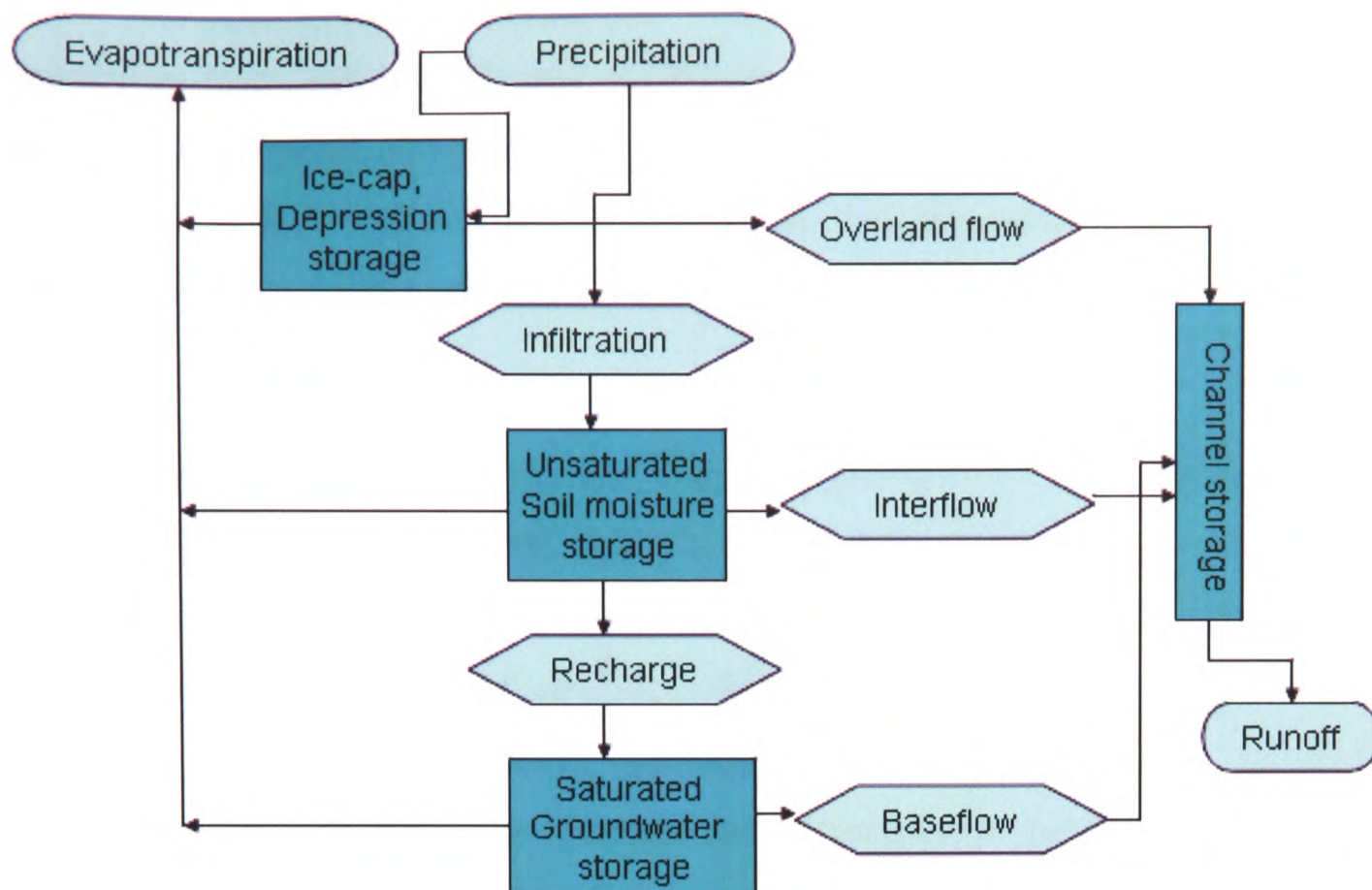


Figure 1-7. Schematic representation of hydrological cycle. Source: Fetter[2].

Since 1972, the protection of the environment has been a stated objective of the European Union and a large amount of legislation has been developed dealing with the issues surrounding air quality, waste and water. The protection of groundwater against pollution caused by certain dangerous substances and guidelines on its suitable practices are specified by European Communities Directives. The principal legislation relevant to groundwater may be identified as follows

- Groundwater Directive (80/68/EEC)
- Drinking Water Directive (80/778/EEC)
- Freshwater Fish Directive (78/659/EEC)
- Surface Waters Directive (75/440/EEC)
- Dangerous Substances Directive (76/464/EEC)
- Bathing Waters Directive (76/160/EEC)

In the United Kingdom, the legislative control to groundwater resources complies with Groundwater Protection Policy, first issued in 1992. The main sections of the policy are

divided into (1) conceptual basis for risk-based decision making supported by vulnerability maps and groundwater protection zones (2) policy statements in activity areas such as physical disturbance of aquifers and groundwater flow, waste disposal, control of groundwater abstraction, contaminated land, disposal of liquid effluents and slurries, underground discharges and diffuse pollution of groundwater.

Transposition of the EC Groundwater Directive (80/68/EEC) was completed by the Groundwater Regulations 1998 (SI 1998 No. 2746) in England, Wales and Scotland and Groundwater Regulations 1998 in Northern Ireland (SR 1998 No. 401). The Directive classifies groups and families of substances that are undesirable in groundwater into two lists on the basis of their toxicity, persistence and bioaccumulation. The directive prevents the entry of List I substances into groundwater directly or indirectly. A discharge of a List I substance is only permitted if the quantities and concentrations of discharge are small enough to cause any subsequent deterioration of groundwater quality. List II substances, according to the Directive must be controlled to prevent pollution of groundwater then or in the future. Regulation 15 of the Waste Management Licensing Regulations 1994 also has some of the provisions of the EC Groundwater Directive (80/68/EEC) relating to the protection of groundwater in relation to the authorised disposal of waste.

1.3.1 List I of Families and Groups of Substances

List I contains the individual substances which belong to the families and groups of substances enumerated below, in exception of those which are considered inappropriate to List I on the basis of a low risk of toxicity, persistence and bioaccumulation.

1. Organohalogen compounds and substances which may form such compounds in the aquatic environment
2. Organophosphorus compounds
3. Organotin compounds
4. Substances which possess carcinogenic mutagenic properties in or via the aquatic environment
5. Mercury and its compounds
6. Cadmium and its compounds

7. Mineral oils and hydrocarbons
8. Cyanides

1.3.2 List II of Families and Groups of Substances

List II contains the individual substances and the categories of substances belonging to the families and groups of substances listed below which could have a harmful effect on groundwater.

1. The following metalloids and metals and their compounds:

Zinc	Selenium	Barium	Cobalt
Copper	Arsenic	Beryllium	Thallium
Nickel	Antimony	Boron	Silver
Chrome	Titanium	Uranium	Tellurium
Lead	Tin	Vanadium	Molybdenum

2. Biocides and their derivatives not appearing in List I.
3. Substances which have a deleterious effect on the taste and/or odour of groundwater, and compounds liable to cause the formation of such substances in water to render it unfit for human consumption.
4. Toxic or persistent organic compounds of silicon and substances which may cause the formation of such compounds in water excluding those which are biologically harmless or are rapidly converted in water into harmless substances.
5. Inorganic compounds of phosphorus and elemental phosphorus.
6. Fluorides
7. Ammonia and nitrites

1.3.3 Water Quality Standards

In particular, the purpose of guidelines is to protect natural groundwater quality and meet the requirements of all relevant legislation. Where groundwater contamination has been identified, the approach is to use a water quality standard relevant to the current or

intended use of the aquifer. The water quality standards that are likely to be applicable (Rudland et al [3]) are given below:

- UK Water Supply (Water Quality) Regulations 1989
- UK Private Water Supplies Regulations 1991
- UK quality standards for water to be used for direct abstraction to potable supply, e.g. Surface Water (Abstraction for Drinking Water) Regulation 1996
- UK Environmental Quality Standards for the protection of Aquatic Life
- UK quality standards for fresh and saline waters used for bathing and contact water sports, e.g. Bathing Waters Regulations 1991
- UK quality standards for freshwaters required to support fish
- River Water Quality Objectives
- EC Drinking Water Standards
- EC Water quality Standards
- ADAS water quality standards for water used for irrigation and livestock watering
- World Health Organisation (WHO) Guidelines for Drinking Water Quality
- Environmental Health Regulations

1.4 Risk Assessment

Contamination of water resources and land potentially poses risks to human health and the environment. The severity of harm is usually determined on the basis of risk assessment methodologies to establish whether action is needed to reduce or control these risks. A properly conducted risk assessment can reduce potential risks as well as leads to positive benefits in form of cost savings or the avoidance of regulatory action.

The industrialisation of Britain over last couple of centuries has often caused the ground to become contaminated with substances once handled at these sites. A land may be classified as contaminated land by virtue of actual or likely pollution of controlled waters caused by materials on or in the land (Rudland et al [3]). In UK, the contaminated land is controlled by various legislative regulations related to planning, waste

management and water resources. More specifically, the remediation of contaminated land and provisions for the regulation of historical groundwater pollution is evolved under Part IIA of the Environmental Protection Act 1990.

When pollution of controlled waters is an issue and consideration of “Specific Sites”, where contamination is caused by List I substances of EC Groundwater Directive, is taken into account a need exists for the identification of associated risks with such sites in order to reduce or control detrimental effects.

1.4.1 The Risk-based Approach in the UK

The risk assessment approach in the UK is based on a “source-pathway-receptor” relationship also known as pollutant linkage that leads to the derivation of on-site remediation criteria based on an assessment of the potential impact at the identified receptor. The contents of the pollutant linkage are defined as follows

Source: The hazardous substance or agent present at concentrations that are deemed potentially hazardous.

Receptor: The entity (e.g. human, animal, water, vegetation, building services etc.) that is vulnerable to the adverse effects of the hazardous substance.

Pathway: The means by which a hazardous substance comes into contact or otherwise affects a receptor.

In order to illustrate the pollutant linkage an example from CIRIA Publication C553 has been included with the background information on the site as follow

Site details: A former natural valley with a small stream flowing along the valley floor has been infilled over a period of 30 years with scrap car tyres. A fire has developed within the car tyres and the valley was covered with soil in an attempt to smother the fire. The fire has since continued to burn underground, generating noxious gases and tarry residues. A small farmhouse is situated on the edge of the tip. The stream feeds into a major river from which water is extracted for drinking water purposes.

The risk assessment of this site identifies the possible contaminants, receptors and linkage between them via the flow chart (Figure 1-8). It also suggests that the affect of contaminated surface water in the river from which water is extracted for drinking

purposes is being neglected. That is, the humans living beyond the site boundary are at risk.

1.4.2 Stages of Risk Assessment Framework

The key stages in determining remedial targets (Marsland and Carey [4]) to protect surface water or groundwater receptors are summarised as below (Figure 1-9).

1.4.2.1 Identification of Potential Risk

1. Identification and characterisation of the source, including preliminary assessment of the contaminant spatial distributions and concentrations, together with their physical and chemical properties.
2. Identification and characterisation of potential environmental receptor(s).
3. Identification of the transport and exposure pathways of contaminants to a potential environmental (water-based) receptor.

This stage largely involves desk-based study supplemented by the results of an initial site investigation. If no receptor or pathway is identified then no further action is taken.

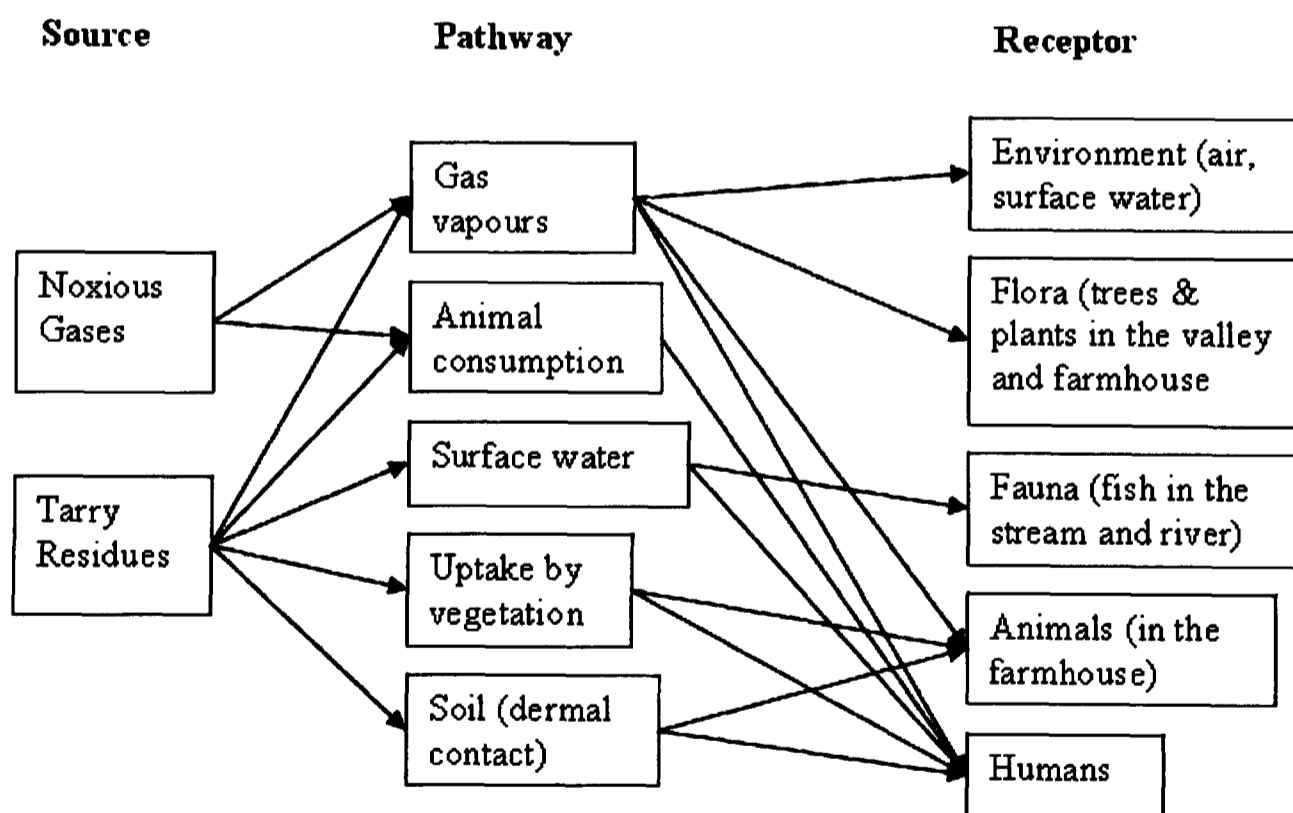


Figure 1-8. Pollutant linkages

1.4.2.2 Assessment of Risk

4. Preliminary assessment (described below in section 1.4.3) which involves estimation of timescale for undertaking a more detailed risk assessment and the

need for interim corrective action where the source has already affected water quality or where the source is in close proximity to the receptor.

5. Determination of remedial targets for soil and groundwater to protect identified receptor (s) based on a tiered approach.
6. Comparison of soil or groundwater contaminant concentrations with the remedial targets to determine which of the following actions are appropriate:
 - a. No action is required, as the observed concentration do not represent a risk to water quality at the receptor
 - b. Update tier assessment including further data collection and analysis
 - c. Undertake remedial action to protect the receptor

1.4.2.3 Implementation

In the event that remedial action is required, the following will be needed:

7. Design remedial actions to prevent or minimise the impact on the identified receptor taking account of environmental benefit and cost.
8. Construction and operation of the remedial scheme
9. Environmental monitoring to verify the effectiveness of remediation
10. Decommissioning of the scheme once remediation is effectively completed.

1.4.3 Conceptual Model

At an early stage of the risk assessment, the formation of a conceptual model of the soil and groundwater is essential based on all the physical and chemical data available and local knowledge of historic and current use of the site and surrounding area. The physical and chemical components of the model will form the framework within which conclusions regarding the chemical data can be drawn. The conceptual model plays a key role to the risk assessment. If the basic physical and hydraulic data are substantially inadequate, conclusions drawn from the chemical data may be seriously in error. The conceptual model should also take account of any assumptions or simplifications made in the tier assessment process. The ensuing decisions on the need for and extent of remedial measures should have regard to the uncertainties in the conceptual model.

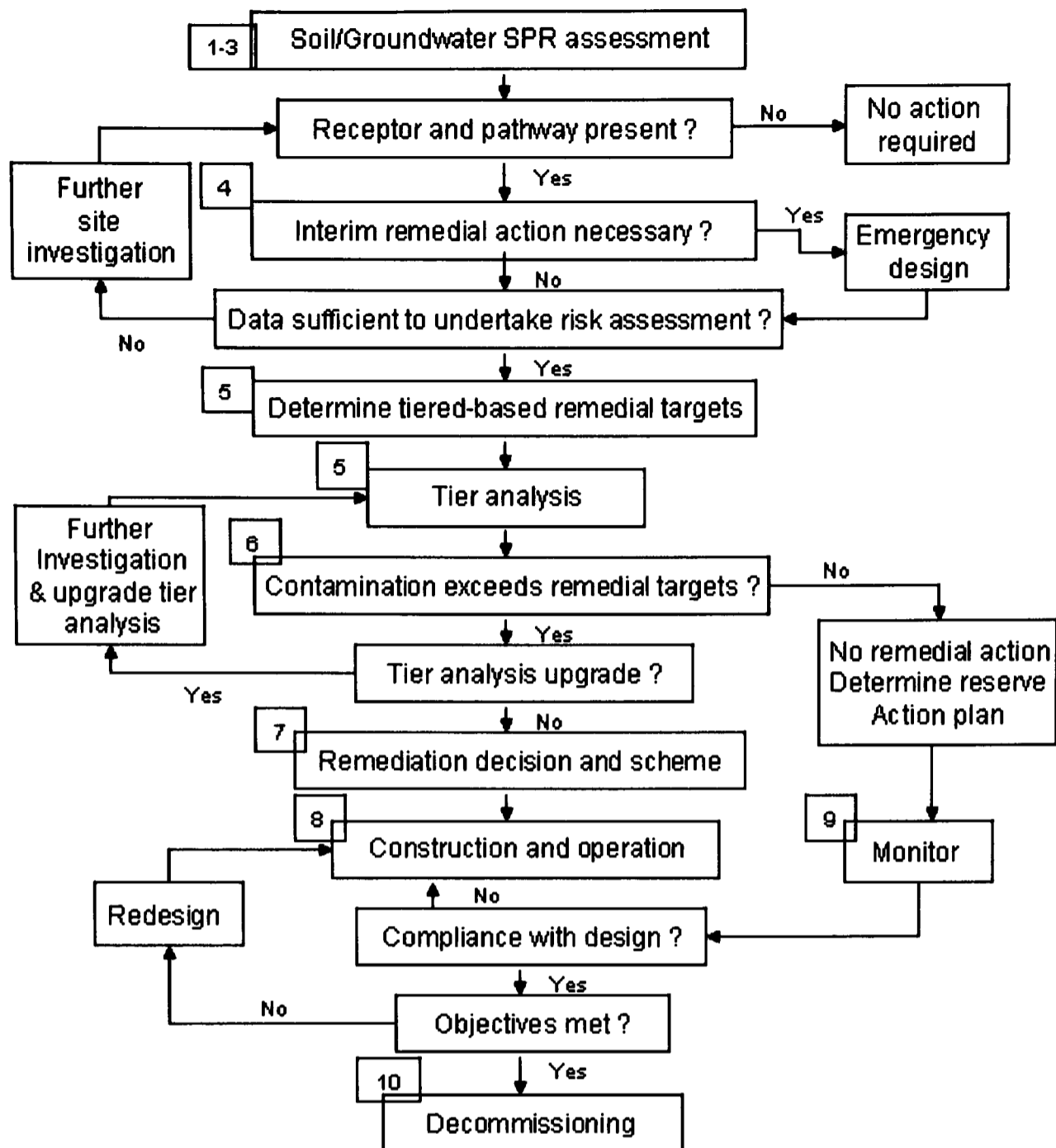


Figure 1-9. Assessment framework. Box numbers refer to numbered steps in section 1.4.2. Source: Marsland and Carey [4].

1.4.4 Source/Pathway/Receptor Assessment

1.4.4.1 Source Characterisation

The source of contamination can be defined in terms of following

Origin and extent

- Primary
 - liquid spillage/leak from containment or distributed system
 - deposit of solid/sludge waste that contains leachable constituents
- Secondary
 - historically contaminated soil
 - vapour in unsaturated soil or aquifer pore space

- dissolved in groundwater (pore water or fissure water)
- dissolved in surface water (effluent to groundwater)

Depth/location

- Soil zone
- Unsaturated zone
- Saturated zone
- Perched horizons
- Free/dissolved/vapour phase
- Into natural ground or artificial structures
- Vertical and lateral extent

Physical and chemical properties

- Density
- Mobility
- Solubility
- Volatility
- Toxicity
- Type of contaminant, inorganic, organic
- Degradability
- Soil/water partitioning
- Persistence
- Present as free product or dissolved phase (single- or multi-phase flow)
- Viscosity
- Leachability
- Material (contaminant)/water partitioning (for primary sources)

1.4.4.2 Pathways

The potential contaminant pathways can be identified in terms of the following

- Pathway length (distance to the receptor)
- Rate of contaminant movement and time to reach the receptor
- Character of hydrogeological pathway
- Processes that will affect contaminant concentrations along the pathway such as:
 - diffusion/dispersion
 - dilution
 - attenuation including volatilisation, sorption and degradation (chemical/biological)
- Influence of artificial pathways and barriers such as culverts, foundations, pipelines etc
- Chemical environment (oxidising, reducing)
- Groundwater/surface water interaction
- Microbiological environment
- Potential of transfer between environmental components, e.g. aqueous to sediment phases
- Background water quality
- Physical and chemical properties (particle size, organic carbon content, intergranular and/or fissure porosity)
- Possible changes to pathways through time (seasonal abstractions, rate of infiltration, flow conditions in culverts etc)

This information is determined in detail with each tier based assessment.

1.4.4.3 Receptors

The possible receptors include the following

- Groundwater abstraction
- Springs
- Groundwater within aquifer
- Estuaries and near-shore environments

- Wetlands

1.4.5 Groundwater Tier Analysis

The assessment of risks to groundwater and surface water receptors is based on the tiered approach involving structured decision-making, cost-effective considerations and progressive data collection and analysis (Marsland and Carey [4]). The approach undertakes the comparison of contaminant concentration in groundwater with the remedial targets to set the need for remediation strategy. The four assessment tiers proposed (Figure 1-10) are described as below:

Tier 1 compares the pore water quality in contaminated soil to relevant criteria such as environmental quality standards, drinking water standards, background water quality etc. ignoring the effects of dilution, dispersion and attenuation along the pathway.

Tier 2 compares the observed contaminant concentrations in groundwater, C_O [mg/l] with target concentration, C_T [mg/l] by taking the effects of dilution into account. The comparison leads to the following

1. $C_O > C_T$ implies a remedial action or an upgrade in tier assessment such as further site-investigation is required.
2. $C_O < C_T$ implies further monitoring for the future prediction is required.

In case of stream or groundwater abstraction receptors, the dilution factor is determined by taking the ratio of the groundwater abstraction or stream flow to the contaminated groundwater flow at plume centre.

Tiers 3 & 4 consider natural attenuation as contaminated groundwater moves to the receptor. C_T for Tiers 3 and 4 is derived by multiplying concentration at receptor by the dimensionless attenuation factor AF , defined as

$$AF = C_O/C_R$$

Where C_R = simulated concentration at receptor [mg/l].

Tier 3 assessment considers the use of analytical contaminant transport models to predict the concentrations as a result of dispersion, retardation and degradation. Tier 4

assessment emphasises on the level of contaminant that would result in an unacceptable impact at the receptor. More sophisticated numerical modelling approach is considered to be undertaken at this stage.

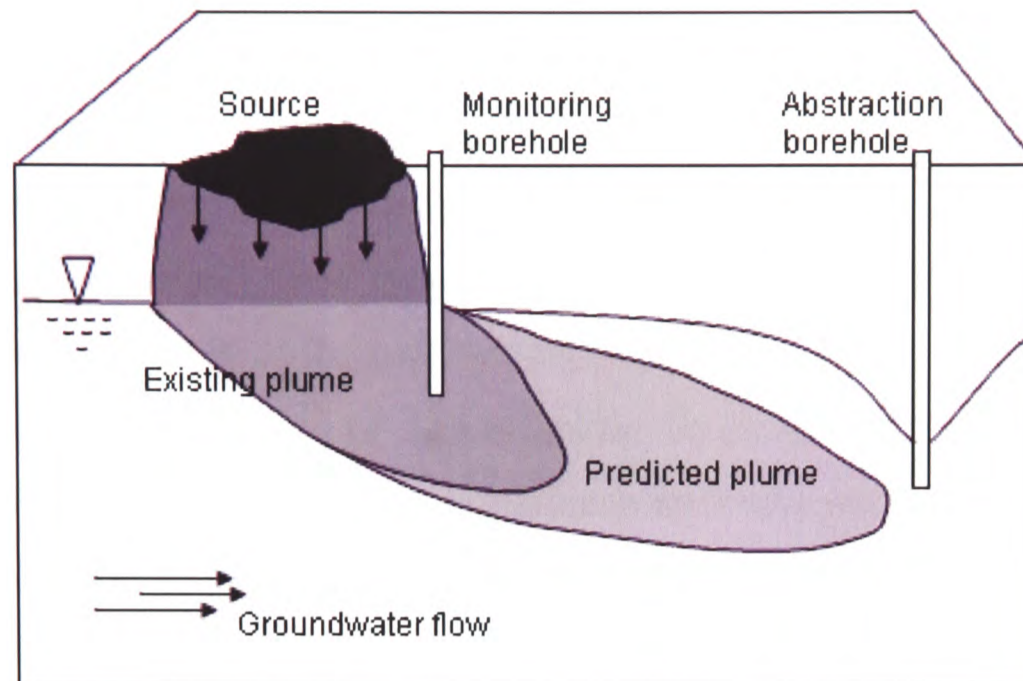


Figure 1-10. Tier assessment of groundwater. Source: Marsland and Carey [4].

1.5 Research Objectives

Assessment of the water-supply potential of aquifers is one of the main driving forces for hydrogeologic studies. The development of the appropriate management systems requires the detailed evaluation, characterisation and analysis of the existing groundwater resources.

Flow of water plays a central role in the transport of chemicals in the subsurface environment. Water quality research is becoming one of the most rapidly expanding aspects of hydrologic studies. To gain a qualitative understanding of fate and transport of conventional pollutants there is a need to investigate geochemical and physical processes involved as well as the rate and pathways of water movement in subsurface systems.

The aim of research is to develop the understanding of various aspects of concern in an integrated framework through the use of computational techniques (Figure 1-11). The research objectives are structured around subsurface water quantity and quality problems as follows

1.5.1 Water-Quantity

- Analysis of long-term approach to sustainability in terms of groundwater withdrawals by pumping and replenishment by recharge from time to time with homogeneous physical properties of transmissivity/hydraulic conductivity and storage.
- Prediction of groundwater movement in geologic formations where physical properties of material are anisotropic in nature.
- Investigation of soil water movement under infiltration in vadose zone which controls the recharge to the underlying groundwater.
- Quantitative description of heterogeneity (layering soils type) of geologic formations by taking large scale variation in hydraulic properties into account.
- Determination of elasticity and compressibility of aquifer materials in response in to addition or removal of imposed system stresses.

1.5.2 Water-Quality

- Prediction of the fate of contaminants subject to advection and dispersion processes in homogeneous and isotropic/anisotropic media to evaluate risk of subsurface pollutions.
- Investigation of spatial distribution of solute species in heterogeneous soils.
- Analysis of chemical, geochemical and biological reactions caused by liquid-solid interactions in natural subsurface systems to describe the transport of radiogenic and toxic waste products.

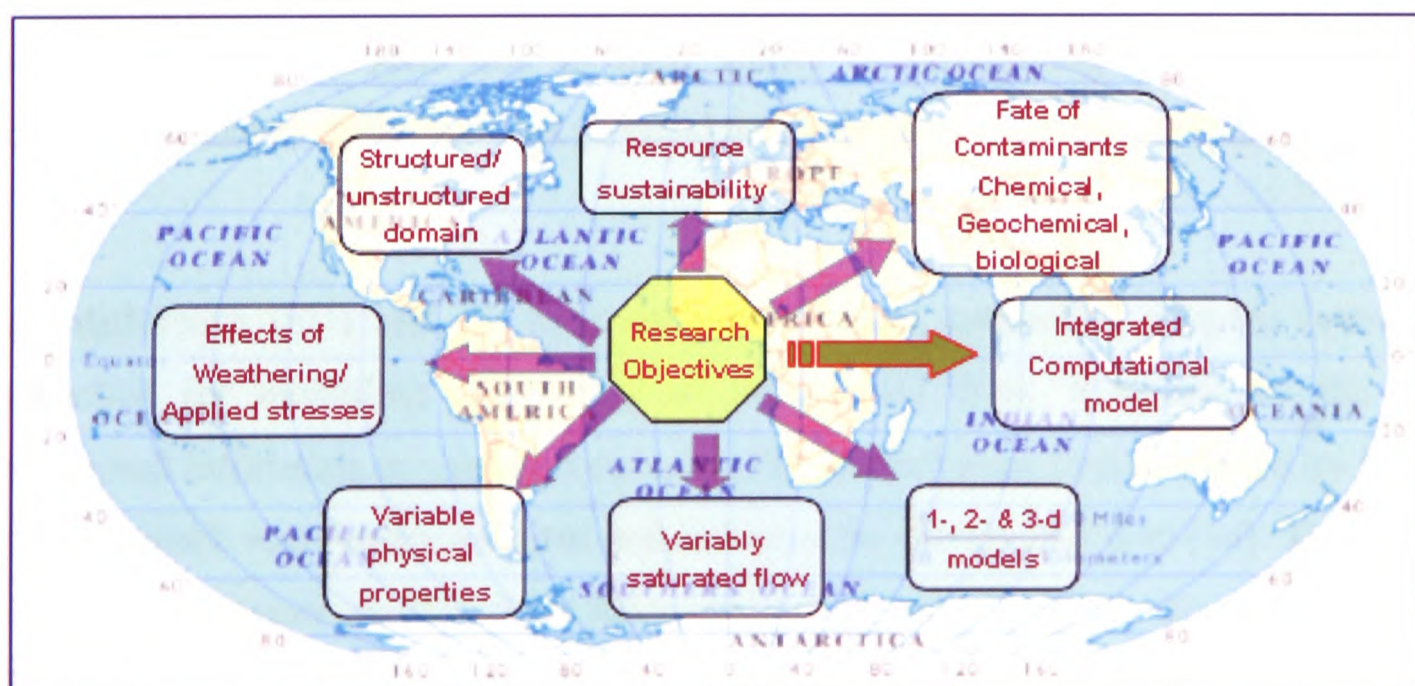


Figure 1-11. Research objectives.

1.6 Literature Review

The study of water movement and fate of contaminants in hydrological systems is important in many aspects and has become a part of scientific research over last few decades. Field applications involve the issues regarding groundwater quality, recharge, evapotranspiration, infiltration, soil consolidation, vegetation and subsurface transport of pollutants; key phenomena dealt in many branches of hydrology, soil mechanics, fluid dynamics and agriculture and environmental engineering.

The use of mathematical models for the eloquent analysis of hydrological systems is quite common and has been studied theoretically in the literature together with the development of computer technology enabling to present sophisticated solutions to complex problems. Analytical methods of flow field simulation for groundwater problems involve use of Fourier or Laplace transforms performed on a series of piecewise linear elements (Manglik and Rai [5], Zhan et al [6]). These methods are useful to obtain the approximations of water table fluctuation and drawdowns of multiple basins and wells in real time domain. Analysis of regional groundwater systems, however, can be established in an efficient way by making use of numerical methods and design techniques (Moore [7], Prickett [8], Freeze and Cherry [9], van Dam and Feddes [10], Ataie-Ashtiani et al [11], Bakker [12]).

Numerical methods appear as key tool and are vastly employed to study the water movement in vadose zone due to their ability of interpreting model architecture, geometry, boundary conditions and physical properties in a discriminate manner.

Finite-difference (FD) and FE methods are the most commonly adopted numerical approaches for modelling the theory of unsaturated flow. Solutions to the one-dimensional infiltration in vadose zone using FD method were first presented by Freeze [13]. This work was further revisited and reviewed by Haverkamp et al [14]. Their work involves the comparison of various discretisation schemes to obtain the solution to the infiltration problems in terms of execution time, accuracy and programming considerations. A comparison between FD and FE methods based on numerous approximations in time is demonstrated by Celia et al [15]. They employed a fully

implicit time approximation to alleviate the mass-balance problems while preserving spatial symmetry. More recently Parsad et al [16] performed a sensitivity analysis of gravity drainage and infiltration processes in unsaturated soils by making use of Galerkin FE discretisation in space and FD discretisation in time.

FD and FE methods can also be employed to examine the effect of water partitioning at the soil-bedrock interface and the seepage faces. In recent years many theories based on the two approaches have been proposed to predict the water movement under variably saturated flow conditions (Cooley [17], van Genuchten [18], Paniconi et al [19], Simpson and Clement [20]). These theories give an insight into the determination of position of seepage surfaces.

Robust solution for flow in non-uniform porous media largely depends on the approximation methods of governing equation, evaluation of constitutive relationships and methods for approximating relative conductivity (Miller et al [21]). The non-homogeneous material properties are observed to have a great impact on both magnitude and direction of flow/transport of fluids/pollutants in geologic systems. A great deal of work has been carried out to investigate the effects of spatial variability in layered soil profiles (Kim and Parizek [22], Pruess [23], Ng [24], Butts and Jensen [25], Mattson et al [26], Prechtel et al [27]). One-dimensional water flow in relatively dry layered soils is modelled by Hills et al [28] using water content formulation of Richards equation based on FD approximations. Their work illustrates the advantages and disadvantages of water content formulation over the pressure based formulation. Gottardi and Venutelli [29] documented infiltration simulations in homogeneous layered soils utilising five schemes derived from FD and FE methods for integrating the three forms (moisture content based, pressure head based, mixed) of Richards equation.

Prediction of solute transport in natural media is a critical requirement in controlling the quality of groundwater and surface water bodies on field scale. Studies show that long-term evolution of chemical and biological effluent in the unsaturated zone generally tends to extend to large depths as a result of dewatering (Gerke et al [30], Wu et al [31]). Contaminant transport in hydrological systems is usually described by the well-

established advective-diffusive transport processes. Diffusion is an important mechanism and controls the mass transport at low Peclet numbers. At high Peclet numbers advection generally serves as the dominant process of contaminant transport in real problems. Searching for a suitable method for solving advection-diffusion problems has been one of the main interests of numerical studies in the last decades. The principal difficulty in the solution comes from the numerical instability caused by artificial dispersion in approximating the advective term. The scientific approach commonly used to remedy the problem of numerical diffusion is the adoption of discretisation schemes with the order of accuracy higher than classical first order upwind differencing scheme (Zalesak [32], Gupta et al [33], Rubin [34], Morton [35]).

A wide variety of geochemical processes such as toxic metals, organics and radionuclides are the result of reactive transport in the subsurface (Schnoor [36], Lichtner et al [37]). Several studies have evaluated various aspects of reactive transport processes (Indelman et al [38], Thomasson and Wierenga [39], Morshed and Kaluarachchi [40], Piggott and Cawfield [41]). The approaches used in these studies to simulate the transport of reactive contaminants assume that it is governed by sorption and decay subject to linear or non-linear isotherm. The sensitivity of migrating plume is described in response to linearity or non-linearity of contaminant parameters. The mathematical methods adopted for the solution of these problems are based on probabilistic, stochastic or artificial neural network analysis.

Fluid flow in deformable porous media is also an aspect of great interest and concern due to a variety of relevant geoenvironmental applications. Several studies have indicated that volume change behaviour of soils can impact the vegetation, infrastructures and species mass transport (Kim et al [42], Mazzieri et al [43]). The purpose of the current study is to construct an integrated modelling environment to investigate the processes of fluid flow and contaminant transport in complex 3-dimensional hydrogeological systems. The structure of thesis and the contents of subsequent chapters are organised as follows

A theoretical background on the mathematical formulation in terms of governing partial differential equation, their discretisation, adopted differencing schemes and implementation strategies are defined in second chapter.

Chapter 3, 4 and 5 are dedicated to the numerical prediction of fluid flow and solute transport in porous soils. Several one-, two- and three-dimensional simulations are performed to investigate the changes in hydraulic head as a result of varying geologic conditions, effects of reactive and conservative solutes and medium heterogeneity in the hydrology on plume migration for transient flow and transport mechanisms. For each chapter, the theoretical basis, formulation, and the Finite Volume solution for the related set of partial differential equations as well as the evaluation of the parameters that control the predicted behaviour and their effects on flow and transport are presented. A good match in the comparison of numerical results and analytical solution or selected results from literature is achieved for most test cases.

The sixth chapter presents the results of model function and properties for consolidating soils. The problems related to the volume change behaviour of expansive soils such as clays are studied and the system deformations under applied loads are computed. Chapters 7 and 8 present the research conclusions and further work followed by appendices and references.

NUMERICAL METHODOLOGIES

This chapter deals with the numerical methods for the presented flow and transport analysis in hydrological systems. The CFD modelling approach is presented in a comprehensive detail to formulate flow and transport problems whereas vertex-based Finite Volume approximation is discussed for modelling of CSM problems.

2.1 Introduction

The use of numerical techniques in deriving and simplifying the dynamics of realistic and non-realistic systems and processes are highly in demand and cover a variety of disciplines including industrial, environmental, biological and computational sciences. Numerical methods are regarded as primary tool for analyzing the configuration of deterministic systems, function approximation, operation research and many stochastic processes. Their scope and importance has improved to a great extent with the rapidly-increasing advances in computer technology. Nowadays they serve as an important ingredient for the commercial codes used by researchers and engineers for modelling many aspects of the real world.

2.2 Hydrogeological Models

The models representing systems can be either deterministic or stochastic or a combination of both deterministic and stochastic. Deterministic models are one of the major classes of mathematical models widely used today for simulating the subsurface hydrology. They are based on conservation of mass, energy and momentum and describe the cause-effect relations of the physical system under study from its known characteristics. Consequently, any operation to be performed contains all the information necessary to predict its future behaviour. A large variety of commercial codes (Table 2-1) uses deterministic, distributed-parameters, computer simulation models for analysing water movement, dispersion, dissolution and retardation of chemical contaminants and the ability of low-conductivity materials to contain contaminated ground water.

In Stochastic models in contrast to the deterministic models there are a range of possible outcomes for any one input reflecting randomness, or uncertainty, in the system (Hardisty [44]). These models are based on empirical evidence of human designing activity and utilize experimental hypothesis (Figure 2-3). Many hydrologic processes are so complicated that they can be interpreted and explained only in a probabilistic sense (Viessman [1]). Precipitation, evaporation, runoff and random heterogeneity of aquifer materials are a few examples of natural phenomena whose outcomes are governed by laws of chance and the sequence of various variables that describe randomness.

The numerical methods covered in this chapter are those commonly used for the analysis of deterministic processes (Figure 2-1 and Figure 2-2) and are based around PHYSICA's multi-physics simulation environment.

3DFEMFAT	WinTran	SEVIEW
AQUA3D	Aquifer Win32	SoilVision
BIOPLUME III	AQTESOLV	SOLUTRANS
HST3D	GMS	SVFlux3D
MIGRATEv9	FEFLOW	WinFlow
MT3D99	ModelCAD	HST3D
POLLUTE	RMP View	MODFE
ChemPoint	Modflow-Surfact 2.2	SEAWAT
3DFEMFAT		

Table 2-1. An example of some available commercial software to model fluid flow and contaminant transport problems.

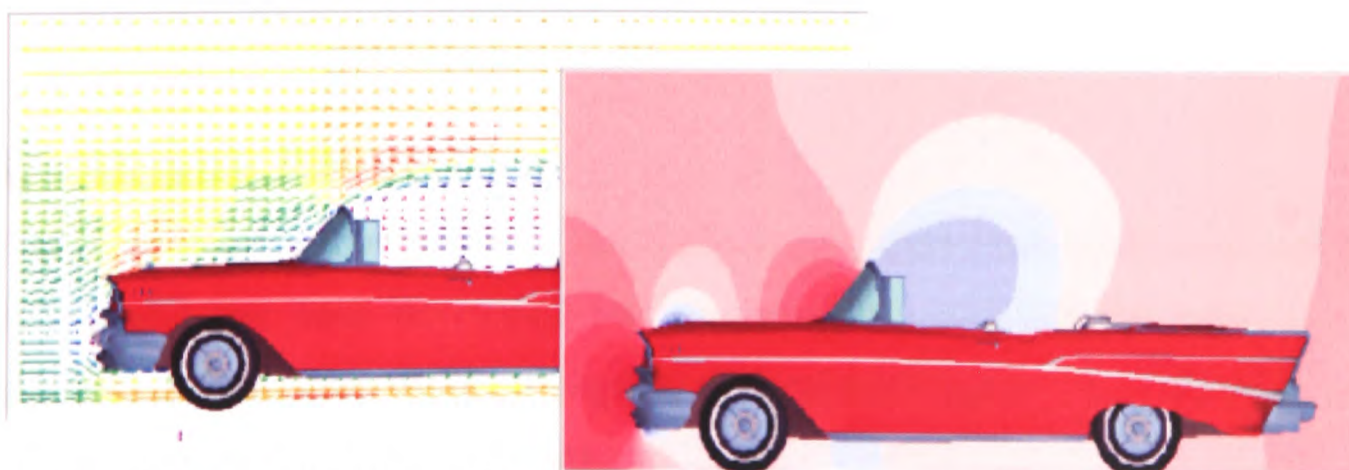


Figure 2-1. Example of deterministic models, air pressure contours around a moving car.

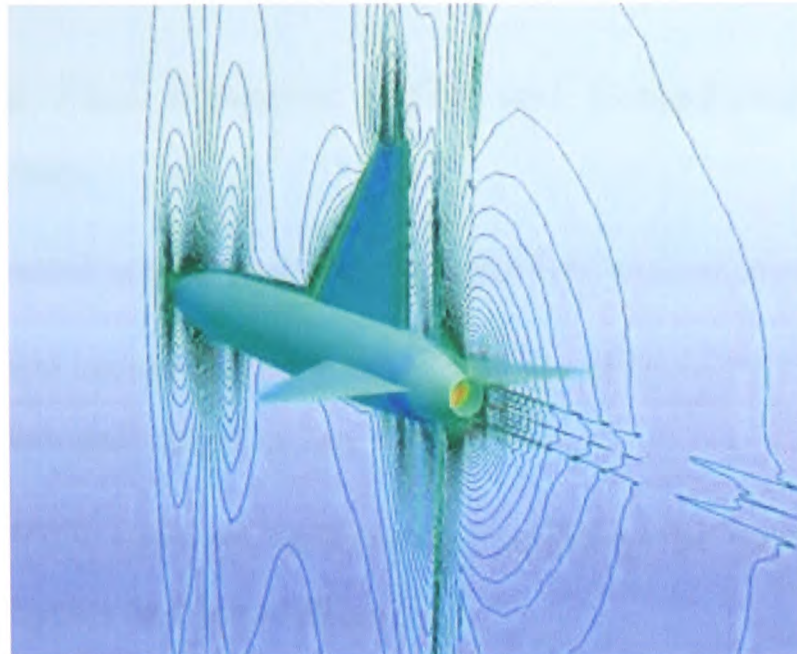


Figure 2-2. Example of deterministic models, computed Mach contours in a transonic flow around a generic fighter configuration.

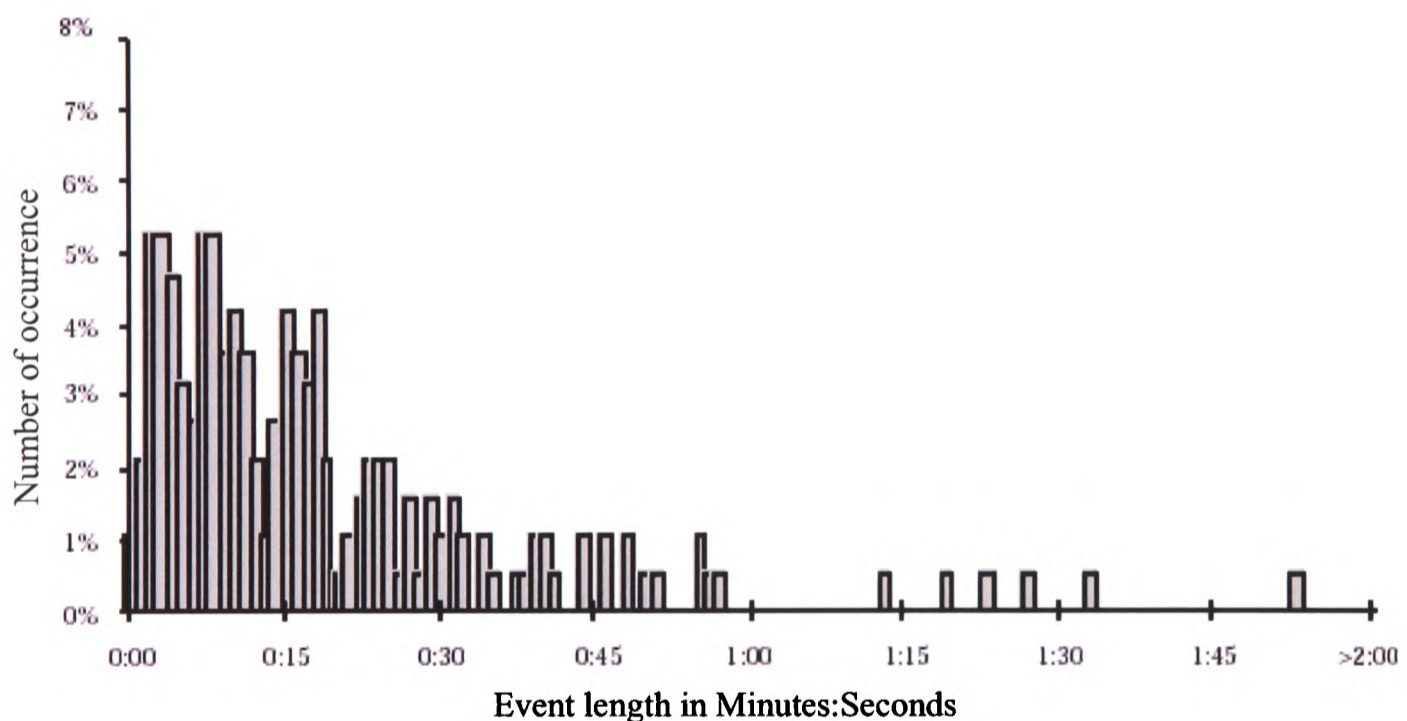


Figure 2-3. Example of stochastic models, spectrum of design event lengths against the number of occurrences.

2.3 About PHYSICA

PHYSICA is an open framework for multi-physics computational continuum mechanics modelling and has been developed for simulating the complex processes that may involve coupling between different physical phenomena (Figure 2-4). Following are the key features of program's functionality:

- Multi-physics simulation environment which provides interaction amongst continuum phenomena, e.g. fluid-structure interaction, magneto-hydrodynamics

with heat transfer and solidification/melting, heat transfer-material defects, aero-acoustics etc.

- Computational Fluid Dynamics (CFD) and Computational Solid Mechanics (CSM) techniques.
- Three dimensional unstructured mesh capability with multi-material domains.
- Well established comprehensive user interface (FEMGV) for geometry creation, mesh generation and visualization.
- Essentially OPEN software architecture, enabling the users to insert their own constitutive physics and interactions.
- Parallel implementation.
- Finite volume discretisation method that is well suited to solve highly non-linear problems.
- Iterative solution procedures, e.g. Jacobi, Conjugate Gradient (CG), BiCG.

The equations and algorithm used in the Physica code have been divided into CFD and CSM sections and are scrutinized separately in this chapter.

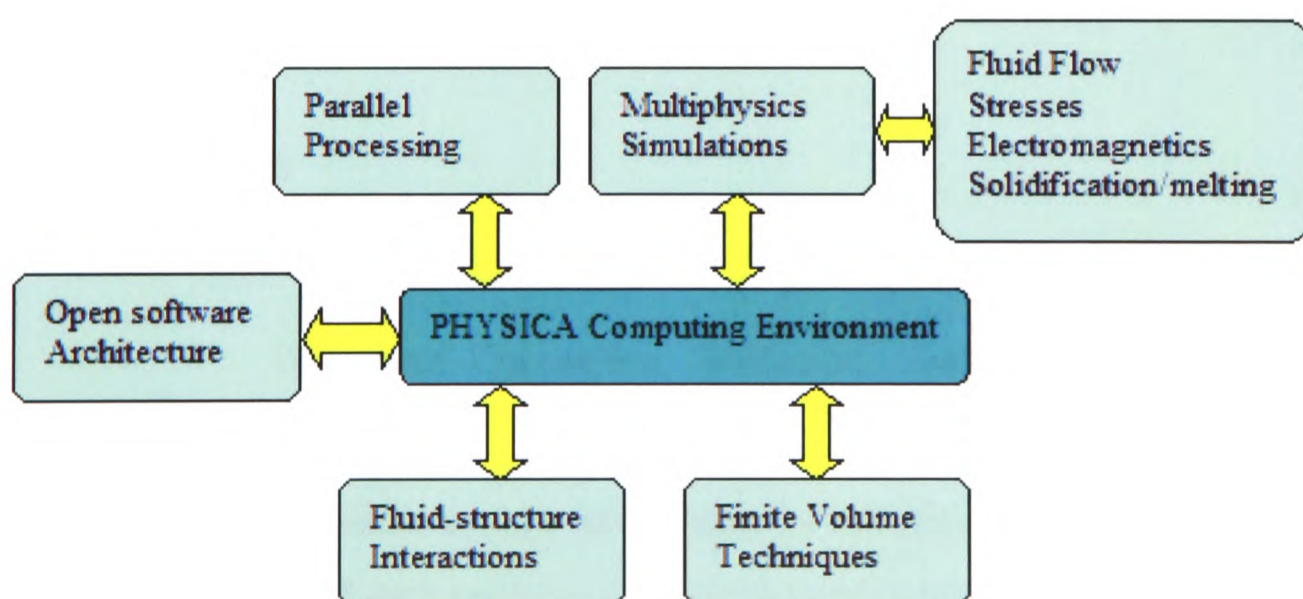


Figure 2-4. Physica model architecture.

2.4 Computational Fluid Dynamics

CFD is the analysis of systems involving fluid flow, heat transport and the associated phenomena by means of computer-based simulation (Versteeg and Malalasekera [45]). The technique is very powerful and spans a variety of industrial and non-industrial applications. In a CFD code the numerical algorithms that serve as the basis of the solver consists of the following steps:

- Formal integration of the governing equations of fluid flow over all the control volumes of the solution domain.
- Discretisation of the terms of integrated equation by means of finite-volume method. This converts the integral equation into a system of algebraic equations.
- Solution of algebraic equations by an iterative method.

The transport phenomena which describe the conservation of a general flow variable ϕ within a finite control volume can be expressed as a balance between the various processes tending to increase or decrease it (Versteeg and Malalasekera [45]).

Representing in words

$$\left[\begin{array}{l} \text{Rate of increase} \\ \text{of } \phi \text{ of fluid} \\ \text{element} \end{array} \right] + \left[\begin{array}{l} \text{Net rate of flow} \\ \text{of } \phi \text{ out of fluid} \\ \text{element} \end{array} \right] = \left[\begin{array}{l} \text{Rate of increase} \\ \text{of } \phi \text{ due to} \\ \text{diffusion} \end{array} \right] + \left[\begin{array}{l} \text{Rate of increase} \\ \text{of } \phi \text{ due to} \\ \text{sources} \end{array} \right]$$

In mathematical form

$$\frac{\partial(C_t)\phi}{\partial t} + \text{div}(C_c \mathbf{u}\phi) = \text{div}(\Gamma_\phi \text{grad}\phi) + S_\phi \quad (3.1)$$

Transient Convection Diffusion Source

The solution of a deterministic system represented by equation (2.1) can be achieved by suitable approximations of each term in (2.1) which transform it in a linearized form

$$\mathbf{A}\phi = \mathbf{b} \quad (3.2)$$

where ϕ is a vector of values of ϕ at a finite number of selected points.

The key step of FV method is the integration of the transport equation over a control volume CV yielding

$$\int_{CV} \frac{\partial(C_c \phi)}{\partial t} dV + \int_{CV} \text{div}(C_c \mathbf{u} \phi) dV = \int_{CV} \text{div}(\Gamma_\phi \text{grad}(\phi)) dV + \int_{CV} S_\phi \quad (3.3)$$

The discretisation of transient, diffusion, convection and source terms based on cell-centred FV formulation is described as follows:

2.4.1 Implicit Discretisation of the Governing Equations

2.4.1.1 Diffusion Term on an Orthogonal Mesh

The discretisation of diffusion term requires the conversion of volume integral into surface integral by making use of Gauss Divergence Theorem which, for a vector \mathbf{F} states as

$$\int_V \text{div} \mathbf{F} dV = \int_S \mathbf{F} \cdot \mathbf{n} dS \quad (3.4)$$

Hence

$$\int_V \text{div}(\Gamma_\phi \text{grad}(\phi)) dV = \int_S \Gamma_\phi \text{grad}(\phi) \cdot \mathbf{n} dS \quad (3.5)$$

or

$$\int_V \text{div}(\Gamma_\phi \text{grad}(\phi)) dV = \sum_f \int_f \Gamma \frac{\partial \phi}{\partial n} dS \quad (3.6)$$

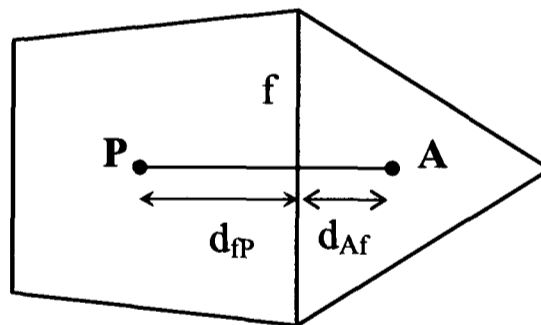


Figure 2-5. Adjacent Control Volumes.

Transformation of (2.5) to (2.6) is based on the fact that the surface of a control volume can be expressed as the sum of surface integrals over each face bounding it.

The normal gradient for a fully orthogonal mesh can be approximated as

$$\frac{\partial \phi}{\partial n} \approx \frac{\phi_A - \phi_P}{d_{AP}} \quad (3.7)$$

If f is the face shared by two elements (Figure 2-5) then the discretised form of equation (2.6) is

$$\sum_f (\Gamma_\phi)_f A_f \frac{(\phi_A - \phi_P)}{d_{AP}} \quad (3.8)$$

2.4.1.1.1 Approximation of Diffusion Coefficient

To calculate fluxes at the control volume faces an approximate distribution of diffusion coefficient between nodal points P and A is made. Hence Γ_ϕ on a face f can be represented as the arithmetic mean

$$(\Gamma_\phi)_f = \alpha_f (\Gamma_\phi)_P + (1 - \alpha_f) (\Gamma_\phi)_A \quad (3.9)$$

where

$$\alpha_f = \frac{d_{Af}}{d_{Af} - d_{fP}} \quad (3.10)$$

or the harmonic mean

$$(\Gamma_\phi)_f = \frac{(\Gamma_\phi)_A (\Gamma_\phi)_P}{\alpha_f (\Gamma_\phi)_P + (1 - \alpha_f) (\Gamma_\phi)_A} \quad (3.11)$$

for each variable. If face f is the part of boundary, arithmetic mean is used otherwise physical properties across each face are averaged through harmonic mean.

2.4.1.2 Transient Term

The approximation of transient term over a control volume over time leads to

$$T_Term = \int_{t-\Delta t}^t \int_V C_t \frac{\partial \phi}{\partial t} dV dt \quad (3.12)$$

For a stationary mesh where V is constant over time the equation (2.12) implies

$$\begin{aligned} T_Term &= \int_V (C_t \phi - C_t^0 \phi^0) dV \\ &= V_P ((C_t)_P \phi_P - C_t^0 \phi^0) \end{aligned} \quad (3.13)$$

where the superscript 0 and subscript P indicate the values at previous time step and average value at the centre of control volume respectively. For every other term in the conservation equation (2.1) fully implicit assumptions are used. Thus the final form of the discretised transient term is

$$T_Term = V_p \left((C_t)_p \phi_p - C_t^0 \phi^0 \right) / \Delta t \quad (3.14)$$

where Δt is the multiplying factor.

2.4.1.3 Source Term

In practical situation the source term in equation (2.1) may be a function of dependent variable. In such a case the FV method approximates the average value of source by means of a linear form

$$S_\phi = S_C - S_P \phi \quad (3.15)$$

The choice of value of S_C and S_P can significantly affect both the rate of convergence and stability of the solution procedure. FV discretisation of source term over a control volume yields

$$\int (S_c - S_p \phi) dV = V_p (S_C - S_P \phi_p) \quad (3.16)$$

2.4.1.4 Convection Term

The volume integral in convection term as appeared in equation (2.3) is transformed to surface integral using the divergence theorem

$$\int_V \text{div}(C_c \mathbf{u} \phi) dV = \int_S C_c (\mathbf{u} \cdot \mathbf{n}) \phi dS \quad (3.17)$$

$$\sum_f C_c (\mathbf{u} \cdot \mathbf{n})_f A_f \phi_f \quad (3.18)$$

here (2.18) is formulated from (2.17) by splitting surface integral into a set of integrals over each of faces bounding the control volume and estimating the integrand on the faces. The value of C_c is the given value in the upwind element. Thus

$$\begin{aligned} C_c &= (C_c)_p \quad \text{if } (\mathbf{u} \cdot \mathbf{n})_f > 0.0 \\ \text{and} & \\ C_c &= (C_c)_A \quad \text{if } (\mathbf{u} \cdot \mathbf{n})_f < 0.0 \end{aligned} \quad (3.19)$$

In order to calculate the face value of ϕ arithmetic averaging is used. Hence ϕ_f can be approximated as

$$\phi_f = \alpha_f \phi_p + (1 - \alpha_f) \phi_A \quad (3.20)$$

where α_f is given by equation (2.10). The discretised form of convection term while taking the arithmetic averaging into account becomes

$$\sum_f C_c(\mathbf{u}\cdot\mathbf{n})_f A_f [\alpha_f \phi_p + (1-\alpha_f)\phi_A] \quad (3.21)$$

2.4.1.5 Diffusion Term on a Non-Orthogonal Mesh

In case of unstructured mesh generating the mesh that accurately fit the solution region with complex boundaries or around the regions where specific mesh characteristics have been positioned leads to mesh skewness which in most cases affects the diffusion term. The accurate modelling of transport phenomena through the regions of mesh skewness requires a correction to be made to the usual discretisation of the diffusion term. Integration of the diffusion term over a control volume leads to the necessity to estimate the derivative of ϕ with respect to face normal. For the fully orthogonal mesh, as discussed earlier, the line connecting the nodes on either side of a face lies along the face normal. Hence the derivative can be estimated by using equation (2.7). In the non-orthogonal case the line connecting the two adjacent nodes is no longer parallel to the face normal vector, i.e. the angle θ in Figure 2-6 is no longer 90 degrees. Hence (2.5) requires an adjustment accordingly. If \mathbf{v} represents the vector along the line connecting the adjacent nodes then

$$\frac{\partial\phi}{\partial\mathbf{v}} = \frac{\phi_A - \phi_P}{d_{AP}} \quad (3.22)$$

The normal vector can be written as a component in the \mathbf{v} direction and a tangential component of the form

$$\mathbf{n} = (\mathbf{v}\cdot\mathbf{n})\mathbf{v} + \beta \quad (3.23)$$

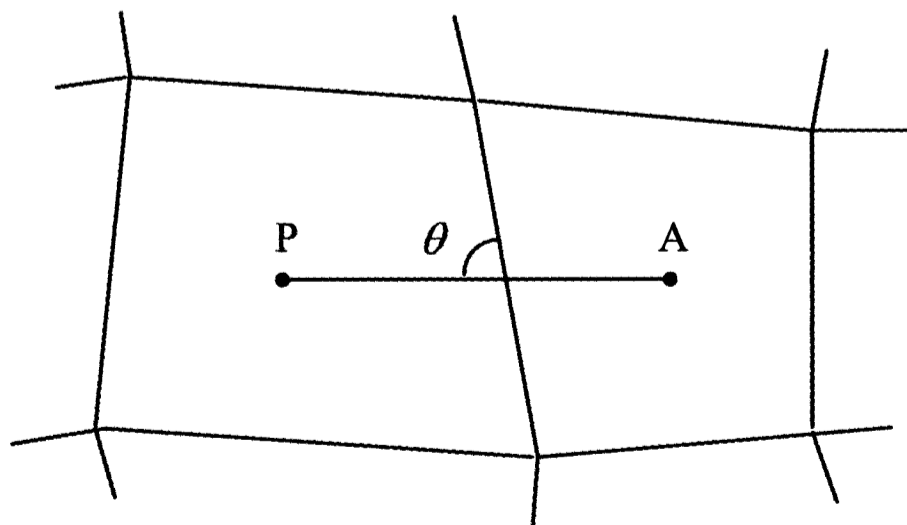


Figure 2-6. Non-Orthogonal Control Volumes

This formulation of normal vector makes it possible to represent the derivative of ϕ with respect to normal in terms of the derivative of ϕ with respect to the vector connecting the nodes

$$\frac{\partial \phi}{\partial n} = (\mathbf{v} \cdot \mathbf{n}) \frac{\partial \phi}{\partial \mathbf{v}} + \beta \frac{\partial \phi}{\partial t} \quad (3.24)$$

where t is the unit vector in the direction β . Writing β as sum of its Cartesian components equation (2.24) can be expressed in the form

$$\frac{\partial \phi}{\partial n} = (\mathbf{v} \cdot \mathbf{n}) \frac{\partial \phi}{\partial \mathbf{v}} + \beta_x \frac{\partial \phi}{\partial x} + \beta_y \frac{\partial \phi}{\partial y} + \beta_z \frac{\partial \phi}{\partial z} \quad (3.25)$$

In order to calculate the Cartesian derivatives of ϕ at a node the derivative is integrated over the control volume about the node in the following ways

$$\int_V \frac{\partial \phi}{\partial x} dV = V \left\{ \frac{\partial \phi}{\partial x} \right\}_p \quad (3.26)$$

Applying divergence theorem (2.26) leads to

$$\begin{aligned} \int_V \frac{\partial \phi}{\partial x} dV &= \int_S \phi n_x dS \\ &= \sum_f A_f \phi_f n_x \end{aligned} \quad (3.27)$$

Together these give an equation for the nodal value of the derivative in terms of a sum of the face values of ϕ . Linear interpolation between nodal values of the derivatives allows the face values to be calculated. Thus the strength of diffusion term is changed under the affect of non-orthogonality as follows

$$D_f = A_f \frac{(\Gamma_\phi)_f}{d_{AP}} (\mathbf{v} \cdot \mathbf{n})_f \quad (3.28)$$

and there is an extra source term equal to

$$A_f (\Gamma_\phi)_f \left(\beta_x \frac{\partial \phi}{\partial x} + \beta_y \frac{\partial \phi}{\partial y} + \beta_z \frac{\partial \phi}{\partial z} \right) \quad (3.29)$$

2.4.2 The Exact Solution

The governing equation (2.1) can be solved exactly if Γ is taken to be constant. The exact solution of one dimensional convection-diffusion problem

$$\frac{d}{dx}(\rho u \phi) = \frac{d}{dx} \left(\Gamma_\phi \frac{d\phi}{dx} \right) \quad (3.30)$$

in a domain $0 \leq x \leq L$ with the boundary conditions

$$\begin{aligned} \text{At } x = 0 \quad \phi &= \phi_0 \\ \text{At } x = L \quad \phi &= \phi_L \end{aligned} \tag{3.31}$$

the solution is

$$\frac{\phi - \phi_0}{\phi_L - \phi_0} = \frac{\exp(Px/L) - 1}{\exp(P) - 1} \tag{3.32}$$

where P is the Peclet number

$$P = \frac{\rho u L}{\Gamma_\phi} \tag{3.33}$$

which is the ratio of the strength of the convection to the strength of the diffusion. It can be seen that for approximately zero values of the Peclet number the problem reduces to the pure diffusion which reveals that the variation of ϕ between the elements centroids is nearly linear. When the flow is in the positive direction, u and hence P being positive, the values of ϕ in the domain are influenced more by ϕ_0 , which is the upstream value of ϕ . For a large positive value of P the value of ϕ remains very close to the upstream value ϕ_0 over much of domain. Similarly for negative flow the value of ϕ is dependent on ϕ_L which again is the upstream value. Hence for a large negative P the value of ϕ over most of the region is very nearly equal to ϕ_L . Thus it is concluded that ϕ is linear only for small values of $|P|$. If $|P|$ increases then $\frac{d\phi}{dx}$ tends to zero at the centre of region indicating that diffusion is nearly absent.

2.4.3 Difference Schemes

The final discretised form of the transport equation (2.1) can be obtained by simply adding the expressions for the discretised form of each of the term described in section (2.3.1). However, this approach faces two problems in order to gain physically realistic numerical results. Firstly, the resulting linear system is not guaranteed to be diagonally dominant. This leads to problems when solution is being sought by using most iterative linear solvers. Secondly, simply adding the discretised terms can lead to an over prediction of the influence of the diffusion term.

The problem of diagonal dominance can be overcome by subtracting ϕ_p multiplied by the continuity equation from the conservation equation for ϕ . To address the problems caused by diffusion term difference schemes are used (Table 2-2). The two point and the higher order difference schemes are described below in details.

2.4.3.1 The Two Point Schemes for Convection Diffusion Problems

2.4.3.1.1 The Central Differencing Scheme

The use of arithmetic averaging in the evaluation of the face value of ϕ in the convection term leads to the following form of discretised equation for convection and diffusion terms

$$\sum_f A_f \left[(C_c)_f (\mathbf{u} \cdot \mathbf{n})_f \left\{ \alpha_f \phi_P + (1 - \alpha_f) \phi_A \right\} + (\Gamma_\phi)_f \left(\frac{\phi_P - \phi_A}{d_{AP}} \right) \right] = 0 \quad (3.34)$$

The strength of convection of ϕ , F_f and diffusion conductance, D_f can be introduced as follows

$$F_f = A_f (C_c)_f (\mathbf{u} \cdot \mathbf{n})_f, \quad D_f = \frac{A_f (\Gamma_\phi)_f}{d_{AP}} \quad (3.35)$$

Utilizing the convention of (2.35), equation (2.34) now can be written as

$$a_P \phi_P = \sum_{nb} a_{nb} \phi_{nb} \quad (3.36)$$

where the summation is all over neighbouring elements. The equations for the coefficients in equation (2.36) are

$$\begin{aligned} a_{nb} &= D_f - (1 - \alpha_f) F_f \\ a_P &= \sum_f (D_f + \alpha_f F_f) \\ &= \sum_{nb} a_{nb} + \sum_f F_f \end{aligned} \quad (3.37)$$

The discretisation techniques can be applied to the steady state continuity equation

$$\text{div}(\rho \mathbf{u}) = 0 \quad (3.38)$$

which is a special case of general conservation equation (2.1), with ϕ equal to 1.0 and Γ_ϕ equal to 0.0. Substituting these values of ϕ and Γ_ϕ in equation (2.34), the discretised form of continuity equation becomes

$$\sum_f F_f = 0 \quad (3.39)$$

Substitution of (2.39) into equation (2.37) gives

$$a_P = \sum_{nb} a_{nb} \quad (3.40)$$

The assessment of central differencing scheme can be made under the following implications. (1) As there is no guarantee for coefficients to remain positive, the solution of discretised equation can become unbounded, $\phi_P > \phi_{nb}$ for all neighbours, which is physically unrealistic in the absence of a source. (2) The central differencing scheme introduces influence at node P from the directions of all its neighbours to calculate the convective and diffusive flux irrespective of the direction of flow or the strength of convection relative to diffusion. (3) The scheme is stable and accurate only if $P < 2$ which is the case of diffusion-dominant low Reynolds number flows or small grid spacing. Owing to this limitation central differencing is not suitable discretisation practice for general purpose flow calculations.

2.4.3.1.2 The Upwind Scheme

In order to avoid the problems observed in the central differencing scheme a well-known remedy is the use of upwind scheme, first suggested by Courant et al [46]. Upwind scheme adopts no alteration to the handling of diffusion term but the convection term uses the upstream nodal value of ϕ for the estimated interface value. Thus

$$\begin{aligned} \phi_f &= \phi_P \quad \text{if } F_f > 0.0 \\ \text{and} & \\ \phi_f &= \phi_A \quad \text{if } F_f < 0.0 \end{aligned} \quad (3.41)$$

In view of (2.41) the coefficients in equation (2.37) take the form

$$\begin{aligned} a_{nb} &= D_f + \max(-F_f, 0.0) \\ a_P &= \sum_f [D_f + \max(F_f, 0.0)] \\ &= \sum_{nb} a_{nb} + \sum_f F_f \end{aligned} \quad (3.42)$$

The upwind approach guarantees that all the coefficients remain positive and consequently leads to a bounded solution. However, it produces erroneous results if flow is not aligned with the grid lines. In such cases the distributions of the transported properties become smeared. The upwind scheme always uses a linear relationship between ϕ and the coordinate axes and hence at large $|P|$ values it overestimates the influence of the diffusion term.

2.4.3.1.3 The Exponential Scheme

If \mathbf{J} represents the total flux as the sum of the diffusion flux and convective flux then it can be presented as

$$\mathbf{J} = C_c \mathbf{u} \phi - \Gamma_\phi \text{grad}(\phi) \quad (3.43)$$

The convection-diffusion equation then can be written as

$$\text{div}(\mathbf{J}) = 0 \quad (3.44)$$

Integration of equation (2.44) over a control volume transform into the discretised equation

$$\sum_f A_f (\mathbf{J} \cdot \mathbf{n})_f = 0 \quad (3.45)$$

In the exponential scheme the exact solution of the equation (2.32) is used as a profile between points P and A . The suffices 0 and L are replaced by P and A and d_{AP} replaces L . Under this assumption the expression for $(\mathbf{J} \cdot \mathbf{n})_f$ is

$$(\mathbf{J} \cdot \mathbf{n})_f = F_f \left(\phi_P + \frac{\phi_P - \phi_A}{\exp(P_f) - 1} \right) \quad (3.46)$$

where

$$P_f = \frac{F_f}{D_f} = \frac{(C_c)_f (\mathbf{u} \cdot \mathbf{n})_f}{(\Gamma_\phi)_f} \quad (3.47)$$

In view of equation (2.46) the coefficients in the discretised equation become

$$\begin{aligned} a_{nb} &= \frac{F_f}{\exp(P_f) - 1} \\ a_p &= \sum_{nb} a_{nb} + \sum_f F_f \end{aligned} \quad (3.48)$$

Exponential scheme provides the exact solution for the steady state one dimensional problem given any value of the Peclet number and for any number of grid points. However, exponentials are expensive in terms of computation time and for dimensions greater than one the scheme is not exact and hence the computation time can not be justified.

2.4.3.1.4 The Hybrid Scheme

By considering the equation (2.48) the variation of a_{nb} / D_f with the Peclet number can be observed through the following certain properties

$$\text{For } P_f \rightarrow \infty \quad \frac{a_{nb}}{D_f} \rightarrow 0.0$$

$$\text{For } P_f \rightarrow -\infty \quad \frac{a_{nb}}{D_f} \rightarrow -P_f$$

$$\text{At } P_f = 0 \quad \frac{a_{nb}}{D_f} = 1 - \frac{P_f}{2}$$

The Hybrid scheme, developed by Spalding [47], uses three straight line sections to approximate these properties, such that

$$\text{For } P_f < -2 \quad \frac{a_{nb}}{D_f} = -P_f$$

$$\text{For } |P_f| < 2 \quad \frac{a_{nb}}{D_f} = 1 - \frac{P_f}{2}$$

$$\text{For } P_f > 2 \quad \frac{a_{nb}}{D_f} = 0$$

Combining these expressions into a compact form

$$a_{nb} = \max\left(-F_f, D_f - \frac{F_f}{2}, 0\right) \tag{3.49}$$

$$a_p = \sum_{nb} a_{nb} + \sum_f F_f$$

It can be noted that the hybrid scheme is identical with the central difference scheme when the Peclet number is in the range -2 to 2 and outside this range it uses a

modification of the upwind scheme where the diffusion has been set to zero. In this way the shortcomings of the upwind scheme are not shared by the hybrid scheme.

2.4.3.1.5 The Power Law Scheme

The power law scheme, described by Patankar [48], is a more accurate approximation to the one dimensional exact solution and produces better results than hybrid scheme. The difficulties arising in the hybrid scheme around $|P_f| = 2$ due to the fact that the diffusion is set to zero at these values can be overcome by adopting a slightly more complex algorithm which is not that expensive to compute. The power law expressions can be written as

$$\text{For } P_f < -10 \quad \frac{a_{nb}}{D_f} = -P_f$$

$$\text{For } -10 < P_f < 0 \quad \frac{a_{nb}}{D_f} = (1 + 0.1P_f)^5 - P_f$$

$$\text{For } 0 < P_f < 10 \quad \frac{a_{nb}}{D_f} = (1 - 0.1P_f)^5$$

$$\text{For } P_f > 10 \quad \frac{a_{nb}}{D_f} = 0$$

It can be seen that for $|P_f| > 10$ the power law and the hybrid schemes are identical. It also gives an extremely close approximation to the exponential scheme with the advantage of being less computationally expensive for use.

Scheme	Formula for $A(P)$
Central Differencing	$1 - 0.5 P $
Upwind	1
Hybrid	$\max(0, 1 - 0.5 P)$
Power Law	$\max(0, (1 - 0.1 P)^5)$
Exponential	$ P / [\exp(P) - 1]$

Table 2-2. Definition of Differencing Schemes

2.4.3.2 A Generalized Formulation of the Transport Equation

Writing the discretised convection-diffusion equation in a form independent of the differencing scheme being used

$$\sum_f \left[D_f A(|P_f| + \max(-F_f, 0.0)) \right] (\phi_P - \phi_A) + F_f \phi_P = 0 \quad (3.50)$$

where the formulae used for the function $A(|P|)$ for the various first order differencing schemes are given in Table (2.2). Combining the discretised forms of each term in the equation on an orthogonal mesh gives

$$\frac{(C_t)_P \phi_P V_P - (C_t)_P^0 \phi_P^0 V_P^0}{\Delta t} + \sum_f \left[(C_c)_f (\mathbf{u}\cdot\mathbf{n})_f \phi_f A_f - (\Gamma_\phi)_f \left(\frac{\phi_A - \phi_P}{d_{AP}} \right) A_f \right] = (S_C - S_P \phi_P) V_P \quad (3.51)$$

Writing equation (2.51) in a form independent of differencing scheme being used leads to

$$\frac{(C_t)_P \phi_P V_P - (C_t)_P^0 \phi_P^0}{\Delta t} + \sum_f \left[\left\{ D_f A(|P_f|) + \max(-F_f, 0.0) \right\} (\phi_P - \phi_A) + F_f \phi_P \right] = (S_C - S_P \phi_P) V_P \quad (3.52)$$

Similarly the discretisation of continuity equation

$$\frac{\partial \rho}{\partial t} + \text{div}(\rho \mathbf{u}) = 0 \quad (3.53)$$

leads to

$$\frac{\rho_P V_P - \rho_P^0 V_P^0}{\Delta t} + \sum_f F_f = 0 \quad (3.54)$$

Replacing C_t by ρ in equation (2.53), substitution of (2.54) after being multiplied by ϕ_P into (2.53) gives

$$a_P \phi_P = \sum_{nb} a_{nb} \phi_{nb} + b_P \quad (3.55)$$

where the summation is over all elements which share a face with element P . the coefficients in equation (2.55) are calculated element P and are given by the formulae

$$\begin{aligned}
 a_{nb} &= D_f A(|P_f|) + \max(-F_f, 0.0) \\
 b_p &= S_C V_P + \frac{V_P^0 \rho_P^0}{\Delta t} \phi_P^0 \\
 a_p &= \sum_{nb} a_{nb} + \frac{V_P^0 \rho_P^0}{\Delta t} + S_P V_P
 \end{aligned}
 \tag{3.56}$$

Equation (2.56) is the final form of discretised equation which can be solved using linear solvers to give the value of ϕ at all the element centroids.

2.4.3.3 Higher Order Difference Schemes

The accuracy of upwind and hybrid schemes is only first-order in terms of Taylor series truncation error which makes them prone to numerical diffusion errors. Higher order schemes are used to minimize such errors. All higher order schemes are currently implemented by means of source based methods. They treat the upwind scheme as their base method and deviation from the upwind scheme as a source term. The value of the dependent variable ϕ on a face is estimated by using a third element as follows

$$\phi_f = F(\phi_C, \phi_D, \phi_U)
 \tag{3.57}$$

where C , D and U represent the elements on the upwind, downwind and “upwind upwind” side of the face. The upwind scheme is used for a boundary face or a face where the upwind upwind element is external to the solution domain.

2.4.3.3.1 Calculation of Upwind Upwind Element

The calculation of upwind upwind element is performed on the basis of geometry of the mesh rather than on the flow pattern. If the face under consideration is a boundary then the upwind upwind element is set to zero otherwise, the element on the upwind side of the face is determined. A value

$$\frac{(r_C - r_D)(r_U - r_C)}{|r_C - r_D||r_U - r_C|}
 \tag{3.58}$$

for each face of upwind element is calculated where r_C is the centroid of element C and the upwind upwind element, U , is the element of the other side of the face of upwind element. For the boundary face the centroid of the face is used for r_U . The element sharing the face with the upwind element is the upwind upwind element. If the face was a boundary face the upwind upwind element is set to the negative of the upwind element.

2.4.3.3.2 Quick

The quadratic upstream interpolation for convective kinetics (QUICK) scheme, developed by Leonard [49] and generalised by Hayas et al [50], uses above described three point upstream-weighted quadratic interpolation for cell face values. The face value of ϕ is given by the equation

$$\phi_f = \phi_C + 0.125(3\phi_D - 2\phi_C - \phi_U) \quad (3.59)$$

this leads to a source contribution for both elements associated with the face equal to

$$-fa0.125((3\phi_D - 2\phi_C - \phi_U)) \quad (3.60)$$

where fa is the convective flux out of the element. Obviously fa is positive for the upwind element and negative for the downwind.

2.4.3.3.3 SMART

The face value of ϕ using SMART scheme can be expressed as

$$\phi_f = \phi_C + 0.5\psi(r)(\phi_C - \phi_U) \quad (3.61)$$

where r and $\psi(r)$ are given as

$$r = \frac{(\phi_D - \phi_C)}{(\phi_C - \phi_U)} \quad (3.62)$$

$$\psi(r) = \max[0.0, \min(2r, 0.75r + 0.25, 4)] \quad (3.63)$$

The SMART scheme leads to a source contribution for both elements associated with the face equal to

$$-fa0.5\psi(r)(\phi_C - \phi_U) \quad (3.64)$$

2.4.3.3.4 Van Leer (Transient)

The source contribution for the Van Leer Transient scheme is given by

$$-fa \frac{\Delta\phi}{\Delta x} (1.0 - cr) \quad (3.65)$$

where

$$cr = (\mathbf{u} \cdot \mathbf{n})_f \frac{\Delta t}{V_C}$$

where V_C is the upwind element volume. $\Delta\phi/\Delta x$ in equation (2.65) is given by the formula

$$\left| \frac{\Delta\phi}{\Delta x} \right| = \min(|\phi_D - \phi_C|, |\phi_C - \phi_U|) \quad (3.66)$$

where $\Delta\phi/\Delta x$ takes the sign of $\phi_D - \phi_C$. If $\phi_D - \phi_C$ and $\phi_C - \phi_U$ differ in sign then $\Delta\phi/\Delta x$ is set to 0.0.

2.4.4 PHYSICA Modules

PHYSICA toolkit provides a modular suite of software components to solve problems involving steady-state or transient fluid flow, heat transfer, phase-change and thermal stresses on structured or unstructured meshes. A number of Utility, Toolset and Physical modules are provided for this purpose. Utility modules handle the algorithms involving database, input/output, memory management and post-processing etc. Toolset modules handle the algorithms based on general equation, geometry and linear solvers etc. The analysis of physical phenomena such as turbulence, particle tracking, solidification, heat transfer and stresses are dealt by Physical module. The software modules are part of an open software framework that allows modules to be constructed either reusing existing ones or creating the new modules according to the user's requirements.

2.4.4.1 Scalar Module

In the scalar module the basic form of the conservation equation for a scalar variable ϕ is given by equation (2.1). The scalar module allows any number of scalar variables to be solved or stored, within the limitations of memory available to PHYSICA. It is possible to specify the coefficients to be used for transient, convection and diffusion terms in the scalar equation. The default coefficients are

Transient	ρ
Convection	ρ
Diffusion	$\rho(v_L + v_T)$

where v_L is the laminar viscosity and v_T is the turbulent viscosity which is set to zero if the turbulence module is not on. User can select their own equations for each of the

coefficient which are defined as constant values or can be calculated by the addition of their own code.

Following are the INFORM (the script file containing problem information by means of controls, switches and physical configuration of the current simulation) entries for the scalar module in PHYSICA.

SCALAR_MODULE

```

NUMERICAL_ZERO_VALUE<real value>                (System default)
SOLVE_<var_name>
BOUNDARY_CONDITIONS
  PATCH <integer no.> WALL          COEFF <real value> VALUE <real value>
  PATCH <integer no.> COEFF_VALUE COEFF <real value> VALUE <real value>
  PATCH <integer no.> FIXED_VALUE VALUE <real value>
  PATCH <integer no.> FIXED_FLUX  VALUE <real value>
  PATCH <integer no.> USER_ROUTINE <char string> <integer value> <real value(s)>
                                          Eqn. Ident  no. of constants  constnts
END
CONVECTON_COEFFICIENT
  ALL                <eqn_type>        <values>
  MATERIAL <mat_num>  <eqn_type>        <values>
  <valid_eqn_types>   DEFAULT
  CONSTANT          <value>
  USER_ROUTINE     <ident> <num_vals> <values>
END
CONVECTION_TERM    <ON, OFF>      (ON)
DIFFERENCE_SCHEME <GENERAL_EQUATION DIFFERENCE_SCHEME>
DIFFUSION_COEFFICIENT
  ALL                <eqn_type>        <values>
  MATERIAL <mat_num>  <eqn_type>        <values>
  <valid_eqn_types>   DEFAULT
  CONSTANT          <value>
  USER_ROUTINE     <ident> <num_vals> <values>
END
DIFFUSION_TERM    <ON, OFF>      (ON)
EXPLICIT_FACTOR   <real value>    (0.0)
EXPLICIT_SOLUTION_STAGE <START_OF_TIME_STEP, END_OF_TIME_STEP>
                                          (END_OF_TIME_STEP)

```

```

FALSE_TIMESTEP      <real value>      (-1.0, -ve = OFF)
HARMONIC_MEAN      <ON, OFF>      (ON)
INITIAL_VALUES    ALL    <real value>
INITIAL_VALUES    PER_MATERIAL
    MATERIAL <integer no.> <real value>
END
INITIAL_VALUES    USER_ROUTINE <char. string> <integer value> <real values>
LINEAR_SOLVER    <JOR, SOR, JCG, BICG>      (JCG)
END

```

2.5 Computational Solid Mechanics

This section describes the Finite Volume procedure for solving the elastic solid mechanics equations regarding thermal and mechanical loads on unstructured meshes. A general description of elastic and plastic material behaviour due to the application of loading condition is presented in terms of Elasto-Visco-Plastic module. Some basic concepts from the mathematical theory of elasticity are provided first, followed by the discretisation techniques based on the FV formulation.

2.5.1 Tensor Definition

The general three dimensional stress state σ_{ij} at a point in elastic equilibrium in tensor form is represented as

$$\sigma_{ij} = \begin{pmatrix} \sigma_{xx} & \sigma_{xy} & \sigma_{xz} \\ \sigma_{yx} & \sigma_{yy} & \sigma_{yz} \\ \sigma_{zx} & \sigma_{zy} & \sigma_{zz} \end{pmatrix} \quad (3.67)$$

The state of strain at a point in terms of deformation or displacement tensor can be given as

$$e_{ij} = \begin{pmatrix} e_{xx} & e_{xy} & e_{xz} \\ e_{yx} & e_{yy} & e_{yz} \\ e_{zx} & e_{zy} & e_{zz} \end{pmatrix} = \begin{pmatrix} \frac{\partial u}{\partial x} & \frac{\partial u}{\partial y} & \frac{\partial u}{\partial z} \\ \frac{\partial v}{\partial x} & \frac{\partial v}{\partial y} & \frac{\partial v}{\partial z} \\ \frac{\partial w}{\partial x} & \frac{\partial w}{\partial y} & \frac{\partial w}{\partial z} \end{pmatrix} \quad (3.68)$$

Representing the deformation tensor in terms of strain and rotation tensors

$$\begin{aligned}
 e_{ij} &= \varepsilon_{ij} + w_{ij} \\
 &= \frac{1}{2}(e_{ij} + e_{ji}) + \frac{1}{2}(e_{ij} - e_{ji})
 \end{aligned} \tag{3.69}$$

In view of equations (2.68) and (2.69) the symmetric second rank tensor definition of strain is expressed as

$$\varepsilon_{ij} = \begin{pmatrix} \varepsilon_{xx} & \varepsilon_{xy} & \varepsilon_{xz} \\ \varepsilon_{yx} & \varepsilon_{yy} & \varepsilon_{yz} \\ \varepsilon_{zx} & \varepsilon_{zy} & \varepsilon_{zz} \end{pmatrix} = \begin{pmatrix} \frac{\partial u}{\partial x} & \frac{1}{2}\left(\frac{\partial u}{\partial y} + \frac{\partial v}{\partial x}\right) & \frac{1}{2}\left(\frac{\partial u}{\partial z} + \frac{\partial w}{\partial x}\right) \\ \frac{1}{2}\left(\frac{\partial v}{\partial x} + \frac{\partial u}{\partial y}\right) & \frac{\partial v}{\partial y} & \frac{1}{2}\left(\frac{\partial v}{\partial z} + \frac{\partial w}{\partial y}\right) \\ \frac{1}{2}\left(\frac{\partial w}{\partial x} + \frac{\partial u}{\partial z}\right) & \frac{1}{2}\left(\frac{\partial w}{\partial y} + \frac{\partial v}{\partial z}\right) & \frac{\partial w}{\partial z} \end{pmatrix} \tag{3.70}$$

The constitutive relation between strain and stress tensors can be expressed as

$$\sigma_{ij} = C_{ijkl} \varepsilon_{kl} \tag{3.71}$$

Under the assumption of isotropic and homogeneous conditions with symmetrical tensor properties the fourth rank tensor C_{ijkl} can be reduced significantly. This allows equation (2.71) to be simplified to

$$\sigma_{ij} = 2\nu\varepsilon_{ij} + \lambda\varepsilon_{kk}\delta_{ij}$$

where λ and ν are the Lamé' constants, which can be defined in terms of the Young's modulus E and the Poisson's ratio μ as

$$\begin{aligned}
 \nu &= \frac{E}{2(1+\mu)} \\
 \lambda &= \frac{\mu E}{(1+\mu)(1-2\nu)}
 \end{aligned}$$

2.5.2 Engineering Definition

The elastic constitutive relationship between stress and strain for isotropic and homogeneous material undergoing small strains is defined in a matrix form as follows

$$\boldsymbol{\sigma} = \mathbf{D}\boldsymbol{\varepsilon}^{(e)} \tag{3.72}$$

where $\boldsymbol{\sigma} = [\sigma_x, \sigma_y, \sigma_z, \tau_{xy}, \tau_{yz}, \tau_{zx}]^T$ is the stress vector with normal and shear stresses in cartesian coordinate system as shown in Figure 2-7 (Fredlund and Rahardjo [51]) and $\boldsymbol{\varepsilon}^{(e)} = [\varepsilon_x^{(e)}, \varepsilon_y^{(e)}, \varepsilon_z^{(e)}, \gamma_{xy}^{(e)}, \gamma_{yz}^{(e)}, \gamma_{zx}^{(e)}]^T$ are the elastic strains. The matrix \mathbf{D} contains the elastic material terms which in three dimensions are given by

$$\mathbf{D} = \frac{E}{(1+\mu)(1-2\mu)} \begin{bmatrix} 1-\mu & \mu & \mu & 0 & 0 & 0 \\ \mu & 1-\mu & \mu & 0 & 0 & 0 \\ 0 & 0 & 1-\mu & 0 & 0 & 0 \\ 0 & 0 & 0 & \frac{1-2\mu}{2} & 0 & 0 \\ 0 & 0 & 0 & 0 & \frac{1-2\mu}{2} & 0 \\ 0 & 0 & 0 & 0 & 0 & \frac{1-2\mu}{2} \end{bmatrix}$$

The total strains are related to the displacement via the following equation

$$\boldsymbol{\varepsilon}^{(T)} = \mathbf{L}\mathbf{d} \quad (3.73)$$

where $\boldsymbol{\varepsilon}^{(T)}$ = total strain, $\mathbf{d} = (u, v, w)^T$ = displacement vector representing displacements in the x -, y - and z -directions and L = differential operator which is given as

$$\mathbf{L} = \begin{bmatrix} \frac{\partial}{\partial x} & 0 & 0 \\ 0 & \frac{\partial}{\partial x} & 0 \\ 0 & 0 & \frac{\partial}{\partial x} \\ \frac{\partial}{\partial y} & \frac{\partial}{\partial x} & 0 \\ \frac{\partial}{\partial z} & 0 & \frac{\partial}{\partial x} \\ 0 & \frac{\partial}{\partial z} & \frac{\partial}{\partial y} \end{bmatrix}$$

The constitutive equation states that the stresses are dependent on the elastic strains. These strains depend on the total $\boldsymbol{\varepsilon}^{(T)}$, thermal $\boldsymbol{\varepsilon}^{(Th)}$ and the visco-plastic $\boldsymbol{\varepsilon}^{(vp)}$ strains as follows

$$\boldsymbol{\varepsilon}^{(e)} = \boldsymbol{\varepsilon}^{(T)} - \boldsymbol{\varepsilon}^{(Th)} - \boldsymbol{\varepsilon}^{(vp)} \quad (3.74)$$

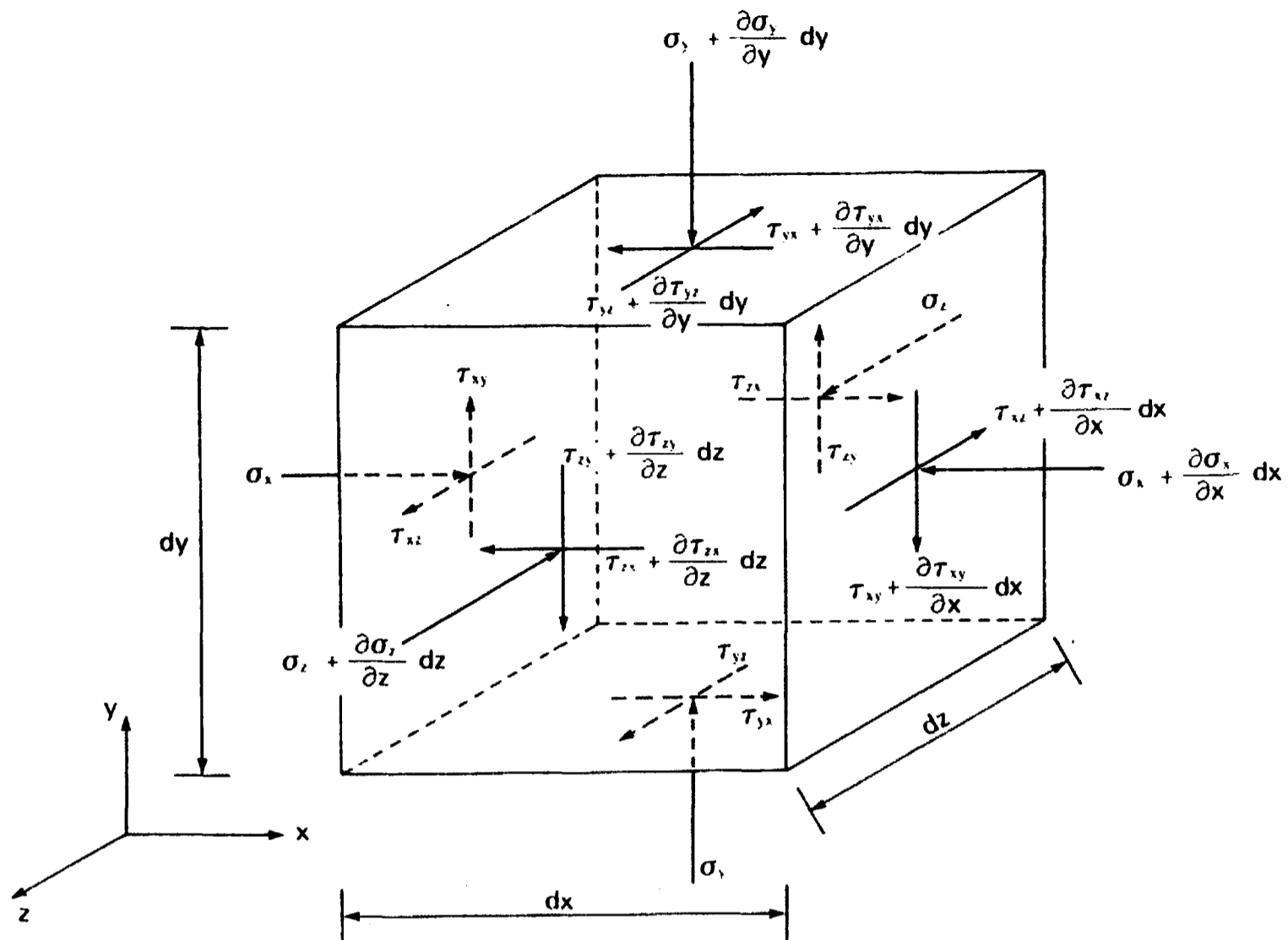


Figure 2-7. Normal and shear stresses on a cubical element of infinitesimal dimension.

2.5.3 General Discretisation

The governing equation concerning the conservation of momentum for a complete analysis within a continuum is given by Cauchy's equation of motion as

$$\nabla \cdot \sigma_{ij} + b_i = \rho a_i \quad (3.75)$$

where b_i = body force per unit volume and a_i = local acceleration. While considering the analysis of quasi-static problems the equation (2.75) can be represented as

$$\nabla \cdot \sigma_{ij} + b_i = 0 \quad (3.76)$$

The discretisation of the governing equations is performed by applying the method of weighted residuals to the displacement formulation. The governing equilibrium equation (2.76) in matrix form is

$$\mathbf{L}^T \boldsymbol{\sigma} + \mathbf{b} = 0 \quad \text{in } \Omega \quad (3.77)$$

The boundary conditions on the surface $\Gamma = \Gamma_t \cup \Gamma_u$ of the domain can be defined as

$$\begin{aligned} \mathbf{R}^T \boldsymbol{\sigma} &= \mathbf{t}_p & \text{on } \Gamma_t \\ \mathbf{u} &= \mathbf{u}_p & \text{on } \Gamma_u \end{aligned}$$

where \mathbf{t}_p are the prescribed tractions on the boundary Γ_t , \mathbf{u}_p are the prescribed displacements on the boundary Γ_u and

$$\mathbf{R} = \begin{bmatrix} n_x & 0 & 0 \\ 0 & n_y & 0 \\ 0 & 0 & n_z \\ n_y & n_x & 0 \\ 0 & n_z & n_y \\ n_z & 0 & n_x \end{bmatrix}$$

is the outward normal operator. Applying the strain-displacement relationship of equation (2.73) to equations (2.72) and (2.74) and substituting the resulting equation in the traction boundary conditions as defined above, one can obtain

$$\mathbf{R}^T (\mathbf{D}\mathbf{L}\mathbf{u} - \mathbf{D}\boldsymbol{\varepsilon}^{th} - \mathbf{D}\boldsymbol{\varepsilon}^{vp}) - \mathbf{t}_p = 0 \quad \text{on } \Gamma_t$$

Also performing the same substitution on the governing equilibrium equation (2.77):

$$\mathbf{L}^T (\mathbf{D}\mathbf{L}\mathbf{u} - \mathbf{D}\boldsymbol{\varepsilon}^{th} - \mathbf{D}\boldsymbol{\varepsilon}^{vp}) + \mathbf{b} = 0 \quad \text{in } \Omega$$

Applying the method of weighted residuals to last two equations and assuming the displacement boundary conditions are satisfied by the displacement vector \mathbf{u} ,

$$\begin{aligned} & \int_{\Omega} \mathbf{W}^T \left[\mathbf{L}^T (\mathbf{D}\mathbf{L}\mathbf{u} - \mathbf{D}\boldsymbol{\varepsilon}^{th} - \mathbf{D}\boldsymbol{\varepsilon}^{vp}) \right] d\Omega + \int_{\Omega} \mathbf{W}^T \mathbf{b} d\Omega \\ & + \int_{\Gamma_t} \bar{\mathbf{W}}^T \left[\mathbf{R}^T (\mathbf{D}\mathbf{L}\mathbf{u} - \mathbf{D}\boldsymbol{\varepsilon}^{th} - \mathbf{D}\boldsymbol{\varepsilon}^{vp}) \right] d\Gamma - \int_{\Gamma_t} \bar{\mathbf{W}}^T \mathbf{t}_p d\Gamma = 0 \end{aligned}$$

where \mathbf{W} and $\bar{\mathbf{W}}$ are arbitrary weighting functions. Assigning $\mathbf{W} = -\bar{\mathbf{W}}$ and applying Green's first theorem to the first volume integral term, the above equation transforms to

$$\begin{aligned} & - \int_{\Omega} [\mathbf{L}\mathbf{W}]^T [\mathbf{D}\mathbf{L}\mathbf{u} - \mathbf{D}\boldsymbol{\varepsilon}^{th} - \mathbf{D}\boldsymbol{\varepsilon}^{vp}] d\Omega + \int_{\Omega} \mathbf{W}^T \mathbf{b} d\Omega \\ & + \int_{\Gamma_u} [\mathbf{R}\mathbf{W}]^T [\mathbf{D}\mathbf{L}\mathbf{u} - \mathbf{D}\boldsymbol{\varepsilon}^{th} - \mathbf{D}\boldsymbol{\varepsilon}^{vp}] d\Gamma + \int_{\Gamma_t} \mathbf{W}^T \mathbf{t}_p d\Gamma = 0 \end{aligned} \tag{3.78}$$

The form of equation (2.78) is the weak form of the equilibrium equation as it permits discontinuous first derivatives of the displacement. The unknown displacement at this point is approximated as

$$\mathbf{u} \approx \hat{\mathbf{u}} = \sum_{j=1}^n \mathbf{N}_j \bar{\mathbf{u}}_j = \sum_{j=1}^n \mathbf{I} \mathbf{N}_j \bar{\mathbf{u}}_j$$

where the unknown variable $\hat{\mathbf{u}}_j$ represents the displacement in this case, $N_j =$ shape function associated with the unknown displacement and $\mathbf{I} =$ third order identity matrix. The displacement approximation can be introduced into equation (2.78) if the arbitrary weighting function \mathbf{W} is replaced by a finite set of prescribed functions defined as

$$\mathbf{W} = \sum_{i=1}^n \mathbf{W}_i$$

where \mathbf{W}_i is the weighting function associated with an unknown displacement. In terms of prescribed functions the equation (2.78) yields a set of algebraic equations of the following form

$$\begin{aligned} & -\int_{\Omega} [\mathbf{L}\mathbf{W}_i]^T [\mathbf{D}\mathbf{L}\hat{\mathbf{u}} - \mathbf{D}\boldsymbol{\varepsilon}^{th} - \mathbf{D}\boldsymbol{\varepsilon}^{vp}] d\Omega + \int_{\Omega} \mathbf{W}_i^T \mathbf{b} d\Omega \\ & + \int_{\Gamma_u} [\mathbf{R}\mathbf{W}_i]^T [\mathbf{D}\mathbf{L}\hat{\mathbf{u}} - \mathbf{D}\boldsymbol{\varepsilon}^{th} - \mathbf{D}\boldsymbol{\varepsilon}^{vp}] d\Gamma + \int_{\Gamma_i} \mathbf{W}_i^T \mathbf{t}_p d\Gamma = 0 \end{aligned}$$

for $i = 1, \dots, n$.

The above equation can be expressed as a linear system of equations of the form

$$\mathbf{K}\bar{\mathbf{u}} - \mathbf{f} = 0$$

where $\mathbf{K} =$ global stiffness matrix, $\bar{\mathbf{u}} =$ global displacement approximation and $\mathbf{f} =$ global equivalent nodal force vector. \mathbf{K} and \mathbf{f} can be formed from the summation of the following contributions

$$\mathbf{K}_{ij} = \int_{\Omega_i} [\mathbf{L}\mathbf{W}_i]^T \mathbf{D}\mathbf{L}N_j d\Omega - \int_{\Gamma_{u_i}} [\mathbf{R}\mathbf{W}_i]^T \mathbf{D}\mathbf{L}N_j d\Gamma \quad (3.79)$$

$$\begin{aligned} \mathbf{f}_i = & \int_{\Omega_i} \mathbf{W}_i^T \mathbf{b} d\Omega - \int_{\Omega_i} [\mathbf{L}\mathbf{W}_i]^T \mathbf{D}\boldsymbol{\varepsilon}^{th} d\Omega - \int_{\Omega_i} [\mathbf{L}\mathbf{W}_i]^T \mathbf{D}\boldsymbol{\varepsilon}^{vp} d\Omega \\ & + \int_{\Gamma_i} \mathbf{W}_i^T \mathbf{t}_p d\Gamma + \int_{\Gamma_{u_i}} [\mathbf{R}\mathbf{W}_i]^T \mathbf{D}\boldsymbol{\varepsilon}^{th} d\Gamma + \int_{\Gamma_{u_i}} [\mathbf{R}\mathbf{W}_i]^T \mathbf{D}\boldsymbol{\varepsilon}^{vp} d\Gamma \end{aligned} \quad (3.80)$$

where Ω_i is the control volume associated with the node i and $\Gamma_i = \Gamma_{u_i} \cup \Gamma_{t_i}$ is the boundary of the control volume.

Up to this stage the discretisation has been performed in a general fashion with no specification of finite weighting functions. The discretisation approach described in the next section uses the vertex based Finite Volume method with regard to the control volume.

2.5.3.1 Cell-vertex FV Method

In the cell-vertex FV method the weighting functions associated with a node are equal to unity within the control volume i.e.

$$\mathbf{W}_i = \mathbf{I}$$

and zero elsewhere. Where \mathbf{I} is the third order identity matrix in three dimensional case. The weighting functions defined in this way allow a variety of possibilities with regard to the control volume definition which is due to non-restricted direct association with the cell as oppose to the standard Bubnov-Galerkin Finite Element method. This makes the cell-vertex FV method a discretisation technique in its own right. Hence the contributions to the overall system of equations for the cell-vertex FV method as described in terms of \mathbf{K} and \mathbf{f} are

$$\mathbf{K}_{ij} = - \int_{\Gamma_{u_i}} \mathbf{R}^T \mathbf{D} \mathbf{L} \mathbf{N}_j d\Gamma \quad (3.81)$$

$$\mathbf{f}_i = \int_{\Omega_i} \mathbf{b} d\Omega + \int_{\Gamma_{u_i}} \mathbf{R}^T \mathbf{D} \boldsymbol{\varepsilon}^{th} d\Gamma + \int_{\Gamma_{u_i}} \mathbf{R}^T \mathbf{D} \boldsymbol{\varepsilon}^{vp} d\Gamma + \int_{\Gamma_i} \mathbf{t}_p d\Gamma \quad (3.82)$$

In FV method the unit virtual displacements are prescribed as opposed to arbitrary virtual displacements in the Bubnov-Galerkin FE method. A collection of discrete control volumes, each independently conservative within the solution domain is thus possible to define. These can be cell-centred or cell-vertex control volumes. As the stress, strain and displacements are all stored at the cell centres, in the cell centred FV method a decoupling phenomenon can occur between stress and displacement. This phenomenon is analogous to that occurs in CFD when the pressure field is decoupled from the velocity field. This similarity allows the solution to this problem in CSM to be compared with those in CFD. On the other hand, the cell-vertex FV method stores the displacements at the vertices and stress and strain at the integration points which can be within the cell or element. The shape function derivatives are used in this case in order to approximate the required derivatives at integration points. As a result this method inherently avoids the problem of decoupling in the same fashion as the standard Bubnov-Galerkin FE method and is referred to as partial staggering.

Following are the INFORM entries for evp module in PHYSICA

```

EVP_MODULE
  FIXED_TIME_STEP
  VARIABLE_TIME_STEP
    INITIAL_TIME_STEP
    TIME_STEP_FACTOR
    TIME_STEP_LIMIT
  END
  SET_LAST_TIME_STEP
  SET_EVP_INTERVAL
  SET_MAX_ITERATION_TO
  SET_TOLERANCE_TO
  SET_EVP_OUTPUT_STEP
  SET_RELOAD
  SET_RATE_DEPENDENT
  LINEAR_SOLVER
    METHOD
    OP_FREQUENCY
    TOLERANCE
  END
  SET_LIQUID_STIFFNESS
  SET_COHERENCE_TEMPERATURE
  SET_UPDATE_GEOMETRY
  BOUNDARY_CONDITIONS
    P_PATCH <integer no.> FORCE          VALUE <non-zero real value>
    P_PATCH <integer no.> DISPLACEMENT VALUE <real value>
    P_PATCH <integer no.> CONSTRAINT    VALUE <non-zero integer value>
  END
  SAVE_DISPLACEMENTS
  SAVE_STRESS
  SAVE_STRAIN
  SAVE_V-P_STRAIN
  SAVE_V-P_STRAIN_RATE
  SAVE_EFFECTIVE_STRESS
  SAVE_EFFECTIVE_STRAIN
  SAVE_EFFECTIV_V-P_STRAIN
  SAVE_EFFECTIV_V-P_STRAIN_RATE
END

```

2.6 Adapted Approach

- Cell-centred finite volume convention implemented over structured/unstructured domain to model large variation in scale efficiently.
- Deterministic modelling approach to describe fluid flow and contaminant transport in homogeneous hydrologic systems by employing CFD techniques for time dependent convection-diffusion problems.
- Deterministic large-scale variability due to stratigraphic layers with contrasting material properties to monitor downward flow and transport under saturated/variably saturated conditions.
- Coupling between fluid flow and contaminant transport equations to quantify the effects of advection and velocity dependent hydrodynamic dispersion on the spread of fresh water plume in two and three-dimensional problems.
- Total variation diminishing (TVD) schemes to accurately track the solute migration with minimized numerical diffusion and spurious oscillations for advection dominated problems.
- Coupling between flow simulations for CFD and structure simulations of CSM to compute fluid-structural interaction.

2.7 Implementation

Tasks accomplished	Setting in Physica's working environment	Addition in Physica's working environment
1. Fluid flow in homogeneous and isotropic porous medium (saturated groundwater flow)	SCALAR MODULE	
2. Groundwater/soil water flow velocities (described by Darcy's flux)		USER, SCALAR MODULE
3. Anisotropic material properties (diffusion coefficient)		GENERAL EQUATION, SCALAR MODULE
4. Non-reactive solute transport	SCALAR MODULE	USER MODULE
5. Reactive solute transport subject to linear adsorption,	SCALAR MODULE	USER MODULE

decay and volatilization		
6. Unsaturated flow, constitutive relationships (described by van Genuchten, Haverkamp and Maulem models)		USER MODULE
7. Differencing schemes for advection-dominated transport problems	SCALAR MODULE	USER MODULE
8. Flow in heterogeneous systems.	SCALAR MODULE	USER MODULE
9. Reactive solute transport (non-linear and kinetic isotherm) in homogeneous systems		USER MODULE
10. System stresses		USER, EVP MODULE
11. Solute transport in geochemically heterogeneous porous media		USER MODULE

Table 2-3. Work plan – Tasks accomplished and implemented in PHYSICA’s simulation environment.

**FLOW AND TRANSPORT MODELS:
HOMOGENEOUS SYSTEMS**

In this chapter the numerical computations of groundwater flow and transport models using CFD techniques as described in the previous chapter are developed. A theoretical analysis of models formation is presented first, followed by the implementation and validation via the examples cases and problems available in the literature. A brief discussion on simulation results is provided for the adopted numerical approach.

3.1 Groundwater in Storage

Being under the influence of constant physical and chemical weathering processes the uppermost portion of earth's crust is subject to continuous decomposition and disintegration. As a result, the sediments and rocks occurring near earth's surface contain pore spaces between the solid grain particles and cracks or fractures. These void spaces and cracks in earth material are of great importance as the occurrence and storage of groundwater and soil moisture depend on their presence and distribution.

3.1.1 Porosity

Total porosity is the percentage of the total volume of the earth material which is represented by its voids. In mathematical form it is stated as

$$\eta = \left(\frac{V_V}{V_T} \right) 100$$

where η = (percentage) porosity, V_V = voids volume ($V_V = V_v^c =$ connected voids volume + $V_v^{nc} =$ non-connected voids volume) and V_T = total volume of the sample. As the flow of water takes place through the portion of total interconnected voids. The porosity available for fluid flow, termed the effective porosity, η_e is expressed as

$$\eta_e = \left(\frac{V_v^c}{V_T} \right) 100$$

Table 3-1 lists the values for total and effective porosity for different materials. Nature of voids is commonly classified on the basis of their mode of origin. Primary porosity is associated with the void spaces that were created at the time formation was deposited. Secondary porosity results from structural deformation and erosion caused by geological of climatic processes on the original rock long after its formation. Faults and fractures in hard and crystalline rocks are common examples (Domenico and Schwartz [52]).

The porosity of a porous medium is controlled by many factors, including the shape, grain packing, degree of sorting and the extent to which changes resulting from compaction, cementation and cracking have occurred. Grain shape is measured in terms of sphericity and roundness. For example, the quartz grains in sand material have high porosity whereas clay particles are plate-like and have low porosity. Sphere-shaped grains pack more tightly and have less porosity than any other shape particles. Grain packing describes the arrangement of individual grains. The most open type of packing of uniform shape will result in a porosity of 48 %, whereas the closest packing exhibits a porosity of 26 % (Company [53]). The uniformity in grain size of a porous medium is described in terms of degree of sorting. A sediment containing mixture of grains sizes where smaller particles fill the voids between the larger ones exhibits poor sorting. Porosity of such a medium is much smaller as compared to a ‘well-sorted’ medium with uniform grain sizes. The combined effect of these factors is illustrated in Figure 3-1.

Material	Diameter (mm)	Total porosity (%)	Effective porosity (%)
Coarse gravel	64.0 – 16.0	28	23
Medium gravel	16.0 – 8.0	32	24
Fine gravel	8.0 – 2.0	34	25
Coarse sand	– 0.5	39	27
Medium sand	0.5 – 0.25	39	28
Fine sand	0.25 – 0.162	43	23
Silt	0.062 – 0.004	46	8
Clay	<0.004	42	3

Table 3-1. Soil classification, total porosity and effective porosity of geologic formations. Source: Roscoe Moss Company [53].

3.1.1.1 Porosity of Sedimentary Rocks

Sedimentary rocks such as sandstone, siltstone, dolomite and shale are formed through diagenesis. This involves compaction, addition or removal of material and transformation of minerals in buried sediment subject to the weight of overlying materials and physical and chemical reactions with the pore fluid. The processes of cementing and compaction reduce the porosity whereas dissolution can cause increase in the porosity in silica, dolomite and limestone materials. In fine grained sediments such as silt, diagenesis results in a primary porosity of sedimentary rock less than that of the original sediment. Reported values for limestone and dolomites range from less than 1% to 30 % (Fetter [2]).

3.1.1.2 Porosity of Plutonic and Metamorphic Rocks

Plutonic and metamorphic rocks such as fractured crystalline rocks, dense crystalline rocks and weathered granite are formed by igneous processes and the impact of temperature and pressure on pre-existing rocks. The processes of erosion and stresses cause the fracture and faulting in these formations yielding an increase in porosity by about 2% to 5%. Weathering caused by chemical decomposition and physical disintegration in plutonic and metamorphic rocks results in porosities ranging from 30% to 60%.

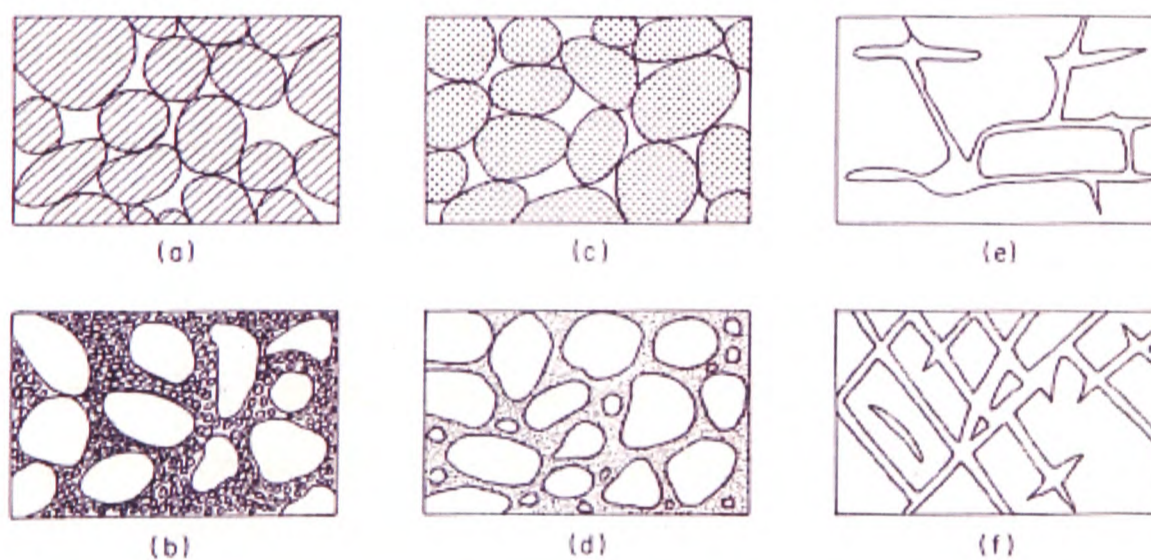


Figure 3-1. Relation between texture and porosity. (a) Well-sorted sedimentary deposit having high porosity; (b) poorly sorted sedimentary deposit having low porosity; (c) well-sorted sedimentary deposit consisting of pebbles that are themselves porous, so that the deposit as a whole has a very high porosity; (d) well-sorted sedimentary deposit whose porosity has been diminished by the deposition of mineral matter in the interstices; (e) rock rendered porous by solution; (f) rock rendered porous by fracturing. Source: Domenico and Schwartz [52].

3.1.1.3 Porosity of Volcanic Rocks

Volcanic rocks, formed by cooling of magma include lava flows, basalt, deposits of ash and cinders and rocks such as welded tuff. Rapidly cooling lava at the surface results in holes due to trapped degassing products and shrinkage cracks in the rock. Porosity of basalt, the crystalline rock formed from magma with low gas content, generally ranges from 1% to 12%. Porosity of pumice, a glass rock formed from magma with very high gas content can be as high as 87%. Similarly porosity of welded tuff ranges from 14% to 40%. Most volcanic ash has a porosity of 50% (Fetter [2]).

3.1.2 Specific Yield and Specific Retention

Specific yield is the volume of water that can drain freely from a saturated soil or rock under the influence of gravity. The remaining volume of water, retained by surface tension forces as thin film around individual grains and in capillary openings is the specific retention. These quantities are expressed as

$$S_Y = \frac{V_{wd}}{V_T} \quad (3.1)$$

$$S_r = \frac{V_{wr}}{V_T} \quad (3.2)$$

where S_Y = specific yield, S_r = specific retention, V_{wd} = volume of water drained and V_{wr} = volume of water retained against gravity force.

The sum of two is equal to porosity i.e.

$$\eta = S_Y + S_r \quad (3.3)$$

Decrease in pore size increases specific retention. Hence a clay material can have a porosity of 50% with a specific yield of 48%. These physical characteristics control the ability of a saturated soil to store and retain water but the flow of water in saturated soils depends on the balance between recharge and discharge as well as the ability of rock to transmit water.

3.2 Groundwater Movement

Water present in interconnected pore spaces of soil and rock is in continuous motion from recharge to discharge areas. The speed and direction of groundwater flow in a porous medium can be calculated from hydraulic gradients and physical properties related to the ease of flow in the medium by the use of Darcy equation.

3.2.1 Darcy's Law

Henry Darcy in 1856 presented the experimental method to describe the laws of water flow through sand. The law, named after Darcy states that the rate of water flow through a porous bed is proportional to the difference in the height of water between the two ends of the bed and inversely proportional to the length of the flow path. In mathematical form

$$\frac{Q}{A} = \mathbf{q} = \frac{\mathbf{K}(h_2 - h_1)}{L} = -\mathbf{K} \frac{dh}{dl} \quad (3.4)$$

where q = volumetric flow rate per unit surface area [L/T], K = constant of proportionality [L/T], h_1, h_2 = water height above a reference level [L], L = length of the flow path [L].

Negative sign in equation (3.4) indicates that the flow is in the direction of decreasing elevation. For fluid flow along x, y and z axes equation (3.4) can be written as

$$\mathbf{q} = -\mathbf{K} \text{grad}(h) = -\mathbf{K} \nabla h \quad (3.5)$$

Darcy's law holds for laminar flow and is valid for most granular materials.

3.2.2 Darcy's Velocity and Hydraulic Head

The average linear velocity or seepage velocity at which water moves through the connected pores comes from equation (3.4) and can be expressed as

$$v = \frac{Q}{An_e} = \frac{-\mathbf{K}dh}{\eta_e dl} \quad (3.6)$$

where v = average linear velocity [L/T], $\eta_e A$ = effective area of flow.

Average linear velocity is always larger than specific discharge q and increases with decreasing effective porosity. The total energy of the fluid flowing through a porous medium is described in terms of conventional Bernoulli equation. This equation states that under conditions of steady flow, the total energy of an incompressible fluid is constant at all positions along a flow path in a closed system (Domenico and Schwartz [52]). This can be written as

$$gz + \frac{P}{\rho_w} + \frac{v^2}{2} = \text{constant} \quad (3.7)$$

where g = acceleration due to gravity [L²/T²], z = elevation above a datum [L], P = pressure exerted by water column and ρ_w = density of fluid (water).

Dividing through by g , equation (3.7) transforms to

$$z + \frac{P}{g\rho_w} + \frac{v^2}{2g} = \text{constant} \quad (3.8)$$

Equation (3.8) describes the total energy contained by the fluid. The first term, the energy of position, is referred to as elevation head. The second term, the energy due to sustained fluid pressure, is pressure head. The third term, the energy due to fluid flow, is the velocity head. Since groundwater velocities are very slow, varying from a few millimetres to a few meters per day on average, velocity head is generally ignored. The total mechanical energy per unit weight of water, termed as hydraulic head is thus given as

$$h = z + \frac{P}{g\rho_w} \quad (3.9)$$

Thus the hydraulic head at a point is found by measuring the elevation of the water level in a piezometer above a datum usually sea level.

3.2.3 Hydraulic Conductivity and Permeability

The factor of proportionality appearing in Darcy's law equation (3.4) is termed hydraulic conductivity and is expressed as

$$\mathbf{K} = \frac{N\rho_w g d^2}{\mu} = \frac{k\rho_w g}{\mu} \quad (3.10)$$

where N = shape factor of the porous medium [dimensionless], d = mean grain diameter [L], μ = kinematic viscosity of the fluid [L^2T] and $k = Nd^2$ = intrinsic permeability [L^2].

As obvious from equation (3.10) hydraulic conductivity contains properties of the medium and the fluid and characterizes the capacity of a medium to transmit water. On the other hand the intrinsic permeability contains properties of the medium only and is independent of the fluid flowing through it. It is commonly used to study three-phase flow in porous media such as oil, gas and water.

The hydraulic conductivity of different geologic materials varies widely being greatest for materials with high effective porosity such as gravels, karstic or reef limestones and

permeable basalts and lowest values for unfractured igneous and metamorphic rocks (Table 3-2).

Material	Hydraulic conductivity (m/s) range
Sedimentary	
1. Gravel	$3 \times 10^{-4} - 3 \times 10^{-2}$
2. Coarse sand	$9 \times 10^{-7} - 6 \times 10^{-3}$
3. Medium sand	$9 \times 10^{-7} - 5 \times 10^{-4}$
4. Fine sand	$2 \times 10^{-7} - 2 \times 10^{-4}$
5. Silt, loess	$1 \times 10^{-9} - 2 \times 10^{-5}$
6. Till	$1 \times 10^{-12} - 2 \times 10^{-6}$
7. Clay	$1 \times 10^{-11} - 4.7 \times 10^{-9}$
8. Unweathered marine clay	$8 \times 10^{-13} - 2 \times 10^{-9}$
Sedimentary Rocks	
1. Karst and reef limestone	$1 \times 10^{-6} - 2 \times 10^{-2}$
2. Limestone, dolomite	$1 \times 10^{-9} - 6 \times 10^{-6}$
3. Sandstone	$3 \times 10^{-10} - 6 \times 10^{-6}$
4. Siltstone	$1 \times 10^{-11} - 1.4 \times 10^{-8}$
5. Salt	$1 \times 10^{-12} - 1 \times 10^{-10}$
6. Anhydrite	$4 \times 10^{-13} - 2 \times 10^{-8}$
7. Shale	$1 \times 10^{-13} - 2 \times 10^{-9}$
Crystalline Rocks	
1. Permeable basalt	$4 \times 10^{-7} - 2 \times 10^{-2}$
2. Fractured igneous and metamorphic rock	$8 \times 10^{-9} - 3 \times 10^{-4}$
3. Weathered granite	$3.3 \times 10^{-6} - 5.2 \times 10^{-5}$
4. weathered gabbro	$5.5 \times 10^{-7} - 3.8 \times 10^{-6}$
5. Basalt	$2 \times 10^{-11} - 4.2 \times 10^{-7}$
6. Unfractured igneous and metamorphic rocks	$3 \times 10^{-14} - 2 \times 10^{-10}$

Table 3-2. Representative values of hydraulic conductivity for various rock types. Source: Domenico and Schwartz [52].

3.2.4 Aquifers

Aquifers are saturated geologic formations capable of storing and yielding significant amount of freshwater for usage. Most of the major aquifers are composed of unconsolidated sand and gravel, limestones, sandstones, dolomite, basalt and fractured plutonic and metamorphic rocks.

Geologic formations some times occur as stratigraphic layers of contrasting hydraulic conductivity values. A geologic unit represents a confining layer if it is impermeable or has little value of hydraulic conductivity. Confining layers are sometimes subdivided into aquitards, aquicludes and aquifuges. Aquicludes are saturated formations that store and yield little groundwater. Aquitard is a geologic unit whose hydraulic conductivity is significantly smaller than adjacent formations and can transmit water at much lower rates, although can hold appreciable amount of water. An aquifuge on the other hand is an absolutely impermeable unit incapable of transmitting any water. Major classification of aquifers (Figure 3-2) as confined or unconfined is made on the basis of presence or absence of an overlying confining layer or aquitard.

3.2.4.1 Confined and Unconfined Aquifers

Unconfined aquifers are generally close to the land surface possessing high hydraulic conductivity but a shallow water table. Such aquifers receive recharge directly from the vadose zone through percolation of infiltration or a surface water body. As the water table is contained within the aquifer, it rises or falls in response to change in recharge and discharge. A confined or artesian aquifer is underlined by a confining unit of relatively small permeability. Under such a confinement water in confined aquifers occurs at a pressure greater than atmospheric. Water level in a well tapping these types of aquifers rises above the upper boundary of the aquifer. In some cases water may rise to the ground surface and flow without pumping thus forming a flowing well. The level to which water rises is represented by potentiometric surface which is the imaginary surface coinciding with the pressure level of water in the aquifer. Recharge to confined aquifer occurs in an area up to which the confining unit does not extend and aquifer receives infiltration through direct percolation or as leakage through confining unit.

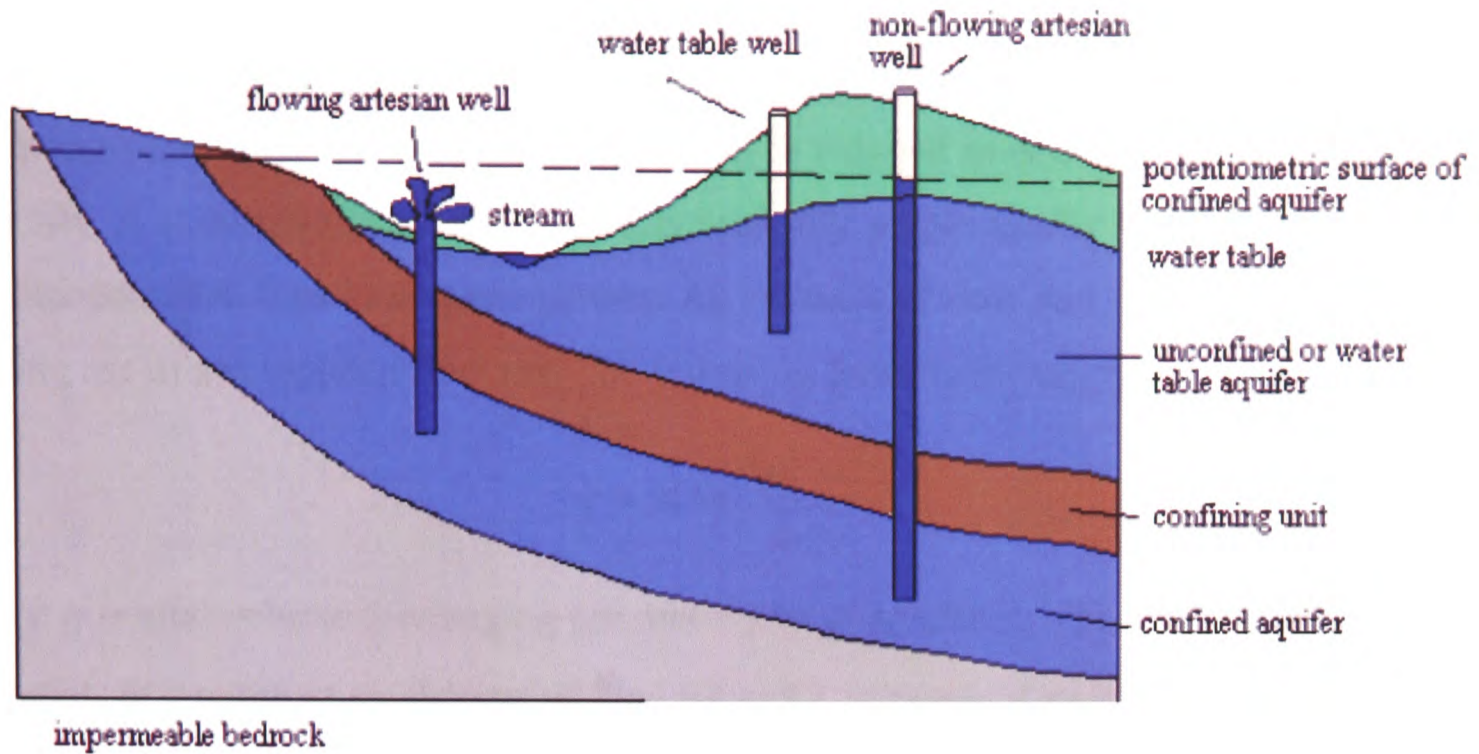


Figure 3-2. Physical representation of confined and unconfined aquifers. Source: <http://www.epa.gov/seahome/groundwater/src/geo3.htm>

Both confined and unconfined aquifers form part of a single unified system. The distinction between the two is made to represent the flow of groundwater under pressure or as free field.

3.2.4.2 Cones of Depression and Flow Nets

Confined and unconfined aquifers response markedly different to pumping. The difference in response is determined in terms of drawdown resulting from pumping the same quantity of water from a single well in each type of aquifers. Drawdown in confined aquifer occurs at much larger area around the pumping well and is always larger as compared to the drawdown in the unconfined aquifers. The cone of depression which describes the amount of drawdown and related volumes is much more areally extensive and deeper in a confined aquifer compared to the cone of depression in the unconfined aquifer. Pumping in unconfined aquifer causes dewatering of saturated space between grains or cracks by releasing significant amount of water from storage within the cone. In confined aquifer, on the other hand pumping causes decrease in head and an accompanying reduction in pressure without changing the saturated thickness. This reduction in water pressure increases the overburden load on the solid skeleton of earth material resulting in compression of the aquifer. Volume of water released from storage within the cone is comparatively small in these aquifer types.

To visualize the storage changes and flow of groundwater, the properties describing the relationship between flow and distribution of groundwater potential are used. A network of equipotential lines and associated flow lines is mapped in two dimensions to form a flow net. A groundwater flow net reflects mutually perpendicular flow or streamlines and equipotential lines in a square pattern. An estimate of flow rate can also be made by making use of a completed flow net. The following formula is employed for this purpose

$$q' = K\Delta\phi\left(\frac{W}{L}\right) \quad (3.11)$$

where q' = total volume discharging per unit width of aquifer [L^3/T], $\Delta\phi$ = increment of potential, W = width of an element of flow net and L = length of an element of flow net.

3.2.5 Properties of Aquifers

3.2.5.1 Homogeneity/Heterogeneity

According to the classical definition, a heterogeneous formation is one that considers position dependency of hydraulic conductivity at all locations. A homogeneous formation, on the other hand, is one in which hydraulic conductivity possesses same value from place to place within a geologic unit.

A simple example of a homogeneous formation is a sandstone aquifer whose porosity, grain-size distribution, thickness and degree of cementation vary only within small limits.

3.2.5.2 Isotropy/Anisotropy

The geometry of pores and voids in a porous medium mostly follows the directional properties of hydraulic conductivity. If the hydraulic conductivity is independent of direction of measurement at a certain point in a geologic deposit, it is said to be isotropic. However, if hydraulic conductivity at a point has a direction dependency, the formation is anisotropic at that point. For example, in undistributed unconsolidated alluvial materials the individual particles are not completely spherical and they tend to rest with their flat sides down when deposited underwater. Thus such a porous medium will have a greater conductivity parallel to the grains than crossing the grain orientation.

3.2.5.3 Darcy's Law for Anisotropic Materials

For an isotropic material Darcy's law was expressed in the form

$$\mathbf{q} = -\mathbf{K} \text{grad}(h)$$

which is correct only if the material is isotropic .ie. $K_x = K_y = K_z$.

For an anisotropic porous medium, Darcy's Law takes the form

$$\begin{aligned} q_x &= -K_{xx} \frac{\partial h}{\partial x} - K_{xy} \frac{\partial h}{\partial y} - K_{xz} \frac{\partial h}{\partial z} \\ q_y &= -K_{yx} \frac{\partial h}{\partial x} - K_{yy} \frac{\partial h}{\partial y} - K_{yz} \frac{\partial h}{\partial z} \\ q_z &= -K_{zx} \frac{\partial h}{\partial x} - K_{zy} \frac{\partial h}{\partial y} - K_{zz} \frac{\partial h}{\partial z} \end{aligned} \quad (3.12)$$

Equation (3.12) expresses a linear relationship between x, y, z components q_x, q_y, q_z of the specific discharge vector \mathbf{q} and x, y, z components of hydraulic gradient. These two sets of components are related to each other by the coefficients of conductivity which is a second order tensor. The components of conductivity tensor in matrix form are represented as

$$\begin{bmatrix} K_{xx} & K_{xy} & K_{xz} \\ K_{yx} & K_{yy} & K_{yz} \\ K_{zx} & K_{zy} & K_{zz} \end{bmatrix}$$

The hydraulic conductivity tensor is symmetric, that is,

$$K_{ij} = K_{ji} \text{ for } i, j = 1, 2, 3$$

which implies

$$K_{xy} = K_{yx}, K_{xz} = K_{zx}, K_{yz} = K_{zy}$$

3.2.5.4 Principal Directions of Hydraulic Conductivity

It is always possible to find three mutually orthogonal coordinate directions which will transform the hydraulic conductivity tensor to a diagonal matrix. That is

$$K_{ij} = 0 \text{ for all } i \neq j \text{ and } K_{ij} \neq 0 \text{ for } i = j$$

In this case, the x-, y-, and the z axes are regarded as the principal directions of anisotropy of a porous medium. The conductivity tensor for the principal directions then becomes

$$\begin{bmatrix} K_{xx} & 0 & 0 \\ 0 & K_{yy} & 0 \\ 0 & 0 & K_{zz} \end{bmatrix}$$

so that eq (3.12) reduces to

$$q_x = K_{xx} \frac{\partial h}{\partial x}, q_y = K_{yy} \frac{\partial h}{\partial y}, q_z = K_{zz} \frac{\partial h}{\partial z}$$

If the coordinates are not aligned with three orthogonal directions, the off-diagonal terms in hydraulic conductivity tensor are non zero. The off-diagonal terms of hydraulic conductivity tensor, in 2-D case (Appendix B), can be obtained from the available principal directions (e.g. $K_{\xi\xi}, K_{\eta\eta}$) using the following relationships

$$\begin{aligned} K_{xx} &= K_{\xi\xi} \cos^2 \theta + K_{\eta\eta} \sin^2 \theta \\ K_{yy} &= K_{\xi\xi} \sin^2 \theta + K_{\eta\eta} \cos^2 \theta \\ K_{xy} &= K_{yx} = (K_{\xi\xi} - K_{\eta\eta}) \sin \theta \cos \theta \end{aligned} \quad (3.13)$$

where θ is the angle between x and ξ or y and η (Figure 3-3). A simple example of orthogonal anisotropic system is marine deposits which usually have the bedding plane parallel to the sand strata. However, cross-bedded deposits have bedding planes that are not parallel to the sand strata and hence non zero off diagonal terms will exist.

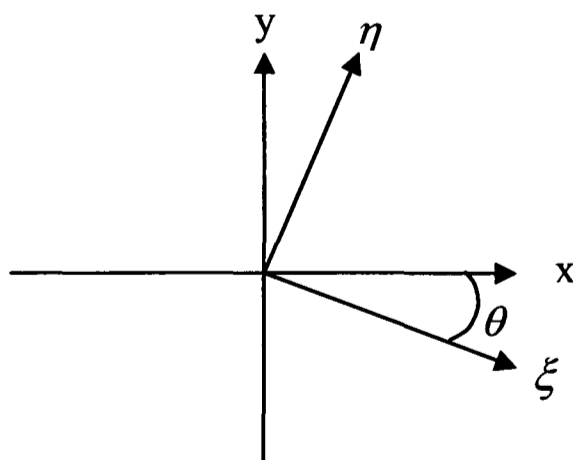


Figure 3-3. Definition of principal directions in orthogonal coordinate system.

3.2.6 General Flow Equations

General form of equation describing unsteady flow of groundwater in a heterogeneous and anisotropic aquifer can be derived by combining water balance equation

$$\text{Inflow} - \text{outflow} = -\text{div}\mathbf{q} - W = S \frac{\partial h}{\partial t} \quad (3.14)$$

with the Darcy's law equation (3.5) and can be written as

$$-\text{div}(-\mathbf{K}\text{grad}(h)) - W = S \frac{\partial h}{\partial t}$$

or

$$\frac{\partial}{\partial x} \left(K_x \frac{\partial h}{\partial x} \right) + \frac{\partial}{\partial y} \left(K_y \frac{\partial h}{\partial y} \right) + \frac{\partial}{\partial z} \left(K_z \frac{\partial h}{\partial z} \right) - W = S \frac{\partial h}{\partial t} \quad (3.15)$$

where W represents the volumetric flux of sources (recharge) and sinks (abstraction wells) per unit volume of the aquifer. S is the storage coefficient or storativity. It is the measure of volume of water withdrawn from or added to the unit volume per unit change in the hydraulic head. In case of a confined aquifer it is represented by specific storage S_s i.e.

$$S = bS_s \quad (3.16)$$

which is the amount of water per unit volume of a saturated formation that is stored or released from storage in response to compression and expansion of aquifer skeleton per unit change in hydraulic head. b represents the aquifer thickness. In case of an unconfined aquifer where saturation varies with the rise and fall of water table it is given by the sum of specific yield and specific storage i.e.

$$S = S_y + hS_s$$

The specific storage values ($<1 \times 10^{-4}$) are generally several orders of magnitude smaller than specific yield. Hence the storativity of an unconfined aquifer approximates its specific yield. For a homogeneous aquifer equation (3.15) transforms to

$$S \frac{\partial h}{\partial t} + W = K_x \frac{\partial^2 h}{\partial x^2} + K_y \frac{\partial^2 h}{\partial y^2} + K_z \frac{\partial^2 h}{\partial z^2} \quad (3.17)$$

Employing the definitions of storage coefficient and transmissivity ($T = K/b$) the flow equation for a confined, homogeneous and isotropic aquifer in absence of source/sink can be written as

$$\frac{S_s}{T} \frac{\partial h}{\partial t} = \frac{\partial^2 h}{\partial x^2} + \frac{\partial^2 h}{\partial y^2} + \frac{\partial^2 h}{\partial z^2} \quad (3.18)$$

which takes the form of Laplace equation if steady-state conditions prevail. As the saturated thickness varies with the variation in hydraulic head in an unconfined aquifer the transmissivity also varies with time. The flow equation in this case is given by

$$S_y \frac{\partial h}{\partial t} = \frac{\partial}{\partial x} \left(K_x h \frac{\partial h}{\partial x} \right) + \frac{\partial}{\partial y} \left(K_y h \frac{\partial h}{\partial y} \right) + \frac{\partial}{\partial z} \left(K_z h \frac{\partial h}{\partial z} \right) \quad (3.19)$$

Under homogeneous and isotropic conditions equation (3.19) transforms into an equation known as Boussinesq equation and is given by

$$\frac{S_y}{K} \frac{\partial h}{\partial t} = \frac{\partial}{\partial x} \left(h \frac{\partial h}{\partial x} \right) + \frac{\partial}{\partial y} \left(h \frac{\partial h}{\partial y} \right) + \frac{\partial}{\partial z} \left(h \frac{\partial h}{\partial z} \right) \quad (3.20)$$

If the variations in saturated thickness h are small it can be replaced with the constant average thickness b . Equation (3.20) then can be linearized to

$$\frac{S_y}{T} \frac{\partial h}{\partial t} = \frac{\partial^2 h}{\partial x^2} + \frac{\partial^2 h}{\partial y^2} + \frac{\partial^2 h}{\partial z^2} \quad (3.21)$$

3.2.7 Finite Volume Approximation for Anisotropic Hydraulic Conductivity

The accurate analysis of fluid flow in complex and intrinsically non-uniform geologic structure demands construction of a computational grid which closely represents their geometrical description. A numerical model to produce correct results and stable solution is thus obtained by employing a discretisation technique on these grids/meshes. Grid should be flexible enough to incorporate certain important features such as wells, tunnels, faults, variably dipping layers and curved boundaries in space in models. Grids are classified into two major types.

Structured grids: Structured grids, logically Cartesian, are usually defined by arrays of ordered cells. Each cell can be assigned an index such as (i, j, k) and shares a regular and well-defined connectivity with its neighbours on left-right, north-south and top-bottom in terms of indices $(i \pm 1, j, k)$, $(i, j \pm 1, k)$ and $(i, j, k \pm 1)$. An irregular structured grid is one which is stretched or deformed in space such that all the intersections of mesh lines are at 90° and none of the connections are broken. Such a mesh will still be a regular orthogonal. On the other hand, a mesh would be thought of as non-orthogonal if there is

no restriction on the angles of intersections of mesh lines. Computing with structured grids is relatively simple as they ensure consistent accuracy and resolution throughout the simulation procedure. These grids are very useful for simple flow problems such as fluid flow and heat transfer analyses.

Unstructured grids: An unstructured grid is comprised of arrays of transmutable cells and is defined in terms of number of nodes or vertices. These grids can be constructed from a variety of elements of triangular, quadrilateral, tetrahedral or hexahedral form. Unstructured grids provide more flexibility in representing complex geometries. However, this flexibility comes at a higher cost due to irregular connectivity of cells to each other. As there is no logical relationship between two connected cells, their special relationship needs to be stated explicitly. The number of connections a particular node has can vary greatly.

Unstructured approach necessitates more computing but are useful for modelling flows, dynamic surfaces and shapes that would need lots of empty spaces if modelled on a structured grid.

Rocks and soils exhibiting favourable orientations for flow in their structures present potential flow pathways indicating the possibility of anisotropic hydraulic conductivity. The steady flow of water in a homogeneous and incompressible porous medium with anisotropic hydraulic conductivity can be represented by Poisson's equation in the following form

$$\frac{\partial}{\partial x} \left(K_{xx} \frac{\partial h}{\partial x} \right) + \frac{\partial}{\partial y} \left(K_{yy} \frac{\partial h}{\partial y} \right) + \frac{\partial}{\partial z} \left(K_{zz} \frac{\partial h}{\partial z} \right) + W = 0 \quad (3.22)$$

The form of equation (3.22) implies that the principal directions of hydraulic conductivity coincide with coordinate axes. Integration of diffusion term in equation (3.22) over a control volume and use of divergence theorem on an unstructured mesh leads to

$$\int_V \left[\frac{\partial}{\partial x} \left(K_{xx} \frac{\partial h}{\partial x} \right) + \frac{\partial}{\partial y} \left(K_{yy} \frac{\partial h}{\partial y} \right) + \frac{\partial}{\partial z} \left(K_{zz} \frac{\partial h}{\partial z} \right) \right] dV = \int_S \left(K_{xx} \frac{\partial h}{\partial x} n_x + K_{yy} \frac{\partial h}{\partial y} n_y + K_{zz} \frac{\partial h}{\partial z} n_z \right) dS \quad (3.23)$$

Approximation of hydraulic gradient on orthogonal/non-orthogonal mesh and discretisation of equation (3.23) along the control volume faces as described in equation (2.6)-(2.8) transforms the right hand side of (3.23) to

$$\sum_f \left[(K_{xx})_f n_x A_f \frac{(h_A - h_P)}{dx} n_x + (K_{yy})_f n_y A_f \frac{(h_A - h_P)}{dy} n_y + (K_{zz})_f n_z A_f \frac{(h_A - h_P)}{dz} n_z \right]$$

which can be simplified to

$$\sum_f \kappa_f \frac{A_f}{d} (h_A - h_P)$$

where

$$\kappa_f = K_{xx} n_x^2 + K_{yy} n_y^2 + K_{zz} n_z^2 \quad (3.24)$$

3.3 Contaminant Transport Mechanisms

There are several processes that control the movement of contaminants dissolved in natural subsurface systems. Transport of solute species may depend on physical processes such as advection, diffusion and mechanical dispersion as well as the chemical, geochemical and biological processes that can cause phase changes or conversion of solutes from one species to another. Inorganic compounds generally go through chemical attenuation by oxidation/reduction, solution, volatilization/precipitation and sorption/desorption processes. However, transport of organic chemical occurs by ion exchange processes of adsorption, degradation and microbiological reactions.

3.3.1 Advection

Advection describes transport of dissolved solute simply due to flow of water. In the absence of other processes, the rate and direction of transport are the same as that of water. The velocity of advective transport can be determined from Darcy's law as

$$v = -\frac{K}{\eta_e} \frac{\partial h}{\partial l} \quad (3.25)$$

where v is the transport velocity (linear groundwater velocity) and dh/dl is the hydraulic gradient. Advection is the simplest and dominant processes of solute transport governed by the mean flow velocity. Mass flux due to advection is given by

$$F_a = v_x C \eta_e \quad (3.26)$$

where C is the concentration of mass per unit volume of solution.

3.3.2 Diffusion

Diffusion or molecular diffusion describes solute movement from areas of higher concentration to those of lower concentration. This phenomena result from the random thermal-kinetic motion of molecular species dissolved in water. It occurs regardless of net water movement. Diffusion can be a dominant transport process in systems with very slow flow rates. Diffusion of solute through water under steady-state condition is described by Fick's law

$$F_d = -D_m \frac{dC}{dx} \quad (3.27)$$

where F_d represents mass flux of solute per unit area per unit time, D_m = diffusion coefficient [L^2/T] and dC/dx = concentration gradient.

Negative sign in (3.27) indicates that the solute movement is from higher to lower concentration. The effective diffusion coefficient which describes the diffusion through connected pore spaces in soils can be determined from the relationship

$$D^* = \tau D_m \quad (3.28)$$

where τ is the tortuosity of the flow path of the diffused species.

3.3.3 Mechanical Dispersion

Mechanical dispersion is the mechanical mixing of molecules caused by velocity variation through different flow paths in the porous medium. Flows in a porous medium vary due to the tortuosity of pore network and are faster through large pores and across the centre of pores than through small pores and near the pore walls (Ward and Robinson [54]). The net effect of dispersion process is the dilution of the contaminant concentration. Mathematically the process of mechanical dispersion is described by

$$D_d = v_x \alpha_L \quad (3.29)$$

where α_L = longitudinal dispersivity [L]. If there is a significant transverse dispersivity, α_T , the medium is anisotropic.

3.3.4 Hydrodynamic Dispersion

The combined effect of diffusion and mechanical dispersion is generally lumped into hydrodynamic dispersion. The coefficient of hydrodynamic dispersion that takes both mechanical mixing and diffusion into account is represented as

$$D_L = D_d + D^* \quad (3.30)$$

where D_L = longitudinal coefficient of hydrodynamic dispersion. The total mass flux due to hydrodynamic dispersion is given by

$$F = \eta_e D_L \frac{dC}{dx} \quad (3.31)$$

3.3.5 Transport Equation of Conservative Solutes

The equation describing the transport of conservative (non-reactive) solutes in porous medium can be derived from the principle of conservation of mass. If F_x represents the total mass of solute per unit cross-sectional area transported per unit time in x-direction, then

$$F_x = v_x \eta_e C - \eta_e D_x \frac{\partial C}{\partial x} \quad (3.32)$$

The net mass of solute entering and leaving a cubic element ($dx dy dz$) is

$$(\nabla \cdot F) dx dy dz = \left(\frac{\partial F_x}{\partial x} + \frac{\partial F_y}{\partial y} + \frac{\partial F_z}{\partial z} \right) dx dy dz$$

this must be equal to accumulation of loss of mass stored in that volume during that interval i.e.

$$-\eta_e \frac{\partial C}{\partial t} dx dy dz$$

Thus the conservation of mass requires

$$\frac{\partial F_x}{\partial x} + \frac{\partial F_y}{\partial y} + \frac{\partial F_z}{\partial z} = -\eta_e \frac{\partial C}{\partial t} \quad (3.33)$$

For a homogeneous medium with uniform velocity it can be written as

$$\left[\frac{\partial}{\partial x} \left(D_x \frac{\partial C}{\partial x} \right) + \frac{\partial}{\partial y} \left(D_y \frac{\partial C}{\partial y} \right) + \frac{\partial}{\partial z} \left(D_z \frac{\partial C}{\partial z} \right) \right] - \left[\frac{\partial}{\partial x} (v_x C) + \frac{\partial}{\partial y} (v_y C) + \frac{\partial}{\partial z} (v_z C) \right] = \frac{\partial C}{\partial t} \quad (3.34)$$

The effect of concentration flux at source or sink can be incorporated by employing the term Src where

$$Src = \frac{q_s}{\eta_e} C_s$$

where q_s is the volumetric flux at source/sink and C_s is the concentration there. Equation (3.33) then takes the form

$$\frac{\partial C}{\partial t} = \nabla \cdot (\mathbf{D} \nabla C) - \nabla \cdot (\mathbf{v} C) + \frac{q_s C_s}{\eta_e} \quad (3.35)$$

The effectiveness of mass transport by advection to the effectiveness of mass transport by hydrodynamic dispersion can be described by the dimensionless Peclet number given by

$$P_e = \frac{v d_m}{D_d} \quad (3.36)$$

where d_m is the mean grain size.

3.3.6 Reactive Transport

3.3.6.1 Adsorption

Adsorption is the one of mass transfer processes that controls the attenuation of organic/inorganic compounds in hydrogeological systems. It involves the partitioning of dissolved contaminants from aqueous phase (groundwater) onto the solid phase (aquifer surfaces) thereby retarding the entire process of contaminant migration.

Adsorption occurs mainly due to van der Waals forces and electrostatic forces between the surface and ions. Natural physical systems such as clays, oxides, protein and organic polysaccharides consist of particles and surfaces of many types. These surfaces and particles possess an electrical charge due to broken bonds and lattice defects caused by physical disintegration and chemical decomposition. The electrical charge allows them to attract and adsorb the dissolved complexing and competing ions.

Many soil factors control adsorption mechanism. A large specific surface area and high amount of organic matter provide large adsorption capacity. The specific surface depends on shape and size of soil particles and it increases as grain size and sphericity decreases. Hence the pore size distribution is another important property for characterizing adsorption property of adsorbing phases. Surface polarity also tends to have effects on adsorptivity of adsorbents. Polar adsorbents termed as hydrophilic have more affinity with water molecules (a polar substance). Their tendency to partition from soil water and adsorb to soil surfaces is smaller. Zeolites, porous alumina, silica gel or silica-alumina are examples of polar adsorbents. Non-polar adsorbents generally termed as hydrophobic on the other hand, have more affinity with solid soils (hydrocarbons) than water thus having greatest effect on adsorptions. Carbonaceous and polymer adsorbents and silicate are typical non-polar adsorbents.

Clay soils are generally considered as strong adsorbers owning large specific surface area per unit volume and significant electrical charges at the surface.

Adsorption processes may be classified either as fast/instantaneous or equilibrium adsorption where the chemical reactions are reversible and locally in thermodynamic equilibrium or slow/kinetic or non-equilibrium adsorption where the reactions are irreversible and require a kinetic rate law to determine the reaction rate (Figure 3-4).

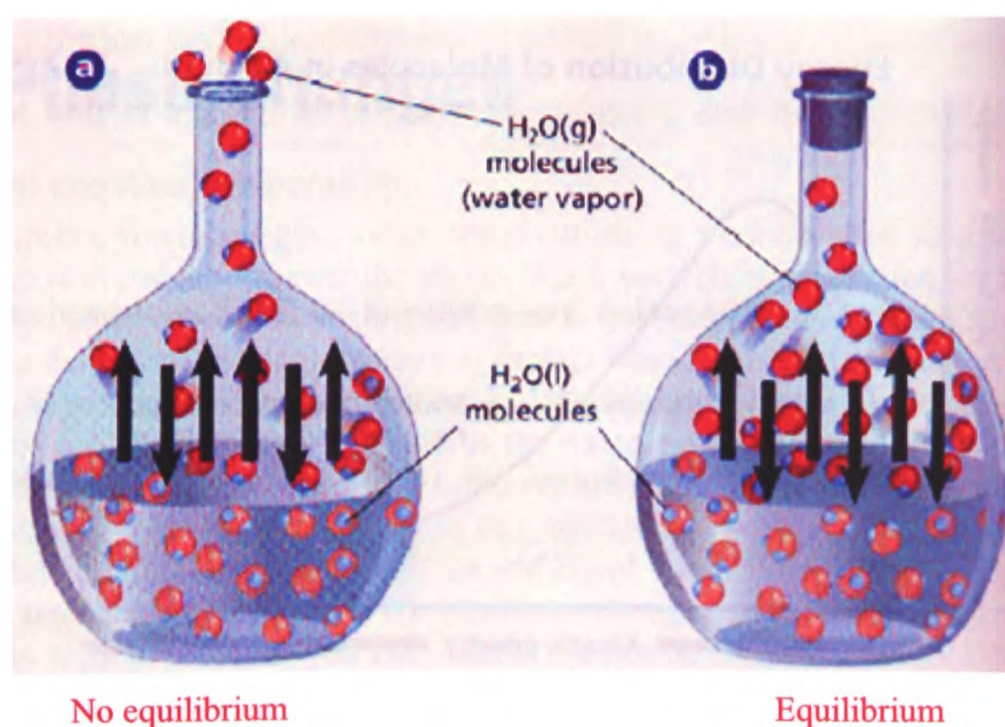


Figure 3-4. Equilibrium and non-equilibrium adsorption.

3.3.6.1.1 Adsorption model

The governing reactive transport equation for a homogeneous saturated medium taking the effects of advection, dispersion and adsorption into account can be represented as

$$\frac{\partial C}{\partial t} = \nabla \cdot (\mathbf{D} \nabla C) - \nabla \cdot (\mathbf{v} C) + \frac{\rho_b}{\eta} \frac{\partial S_a}{\partial t} \quad (3.37)$$

where, C = concentration of solute [mg/l], S_a = adsorbed solute concentration [mg/kg], D = dispersion coefficient [m^2/sec], \mathbf{v} ($= \mathbf{q}/\eta$) = pore water velocity [m/sec], ρ_b = bulk density of the medium [kg/m^3].

The dispersion tensor \mathbf{D} is defined as

$$D_{ij} = \alpha_T |\mathbf{v}| \delta_{ij} + (\alpha_L - \alpha_T) \frac{v_i v_j}{|\mathbf{v}|} + D_m \tau \delta_{ij} \quad (3.38)$$

where δ_{ij} = Kronecker delta.

3.3.6.1.2 Adsorption isotherm

Laboratory study to determine amount of solute partitioning between solid and liquid phases involves mixing of contaminant solutions of different concentrations with specific soils. After equilibrium between the two phases is reached, the adsorbed concentration is determined by calculating the difference between the concentration prior to the experiment and the concentration at equilibrium. The relationship between adsorbed concentration and concentration of solute remaining in solution is expressed as a graphical plot and is termed as adsorption isotherm due the fact that the experiments are performed at constant temperature.

3.3.6.1.3 Instantaneous (Fast) or Equilibrium Adsorption

An equilibrium adsorption reaction is fast in relation to contaminant transport process at groundwater velocity thus resulting in an instantaneous mass transfer in the porous medium. Most transport models use three types of instantaneous adsorption isotherms: linear, Langmuir and Freundlich.

Linear Isotherm

Linear isotherm is the simplest adsorption isotherm. It describes the linear relationship between S_a and C and is valid for dissolved species present at low concentrations. Transport of BTEX through soils is the example of this type of adsorption isotherm. It can be expressed mathematically as

$$S_a = K_d C \quad (3.39)$$

where K_d is the distribution coefficient which describes the partitioning between liquid and solids for the linear isotherm. A dimensionless retardation factor R which takes into account the effect of sorption on contaminants transport by retarding the actual contaminant velocity in groundwater system can be defined by using equation (3.39) in (3.37) as

$$R = 1 + \frac{\rho_b K_d}{\eta} \quad (3.40)$$

Langmuir Isotherm

Langmuir isotherm assumes that there is a finite number of adsorption sites available on the solid surface. At low solute concentration adsorbed concentration increases linearly with increase in solute concentration whereas it becomes constant at higher concentrations. The equation describing single-component Langmuir isotherm is given by

$$S_a = \frac{K_1 K_2 C}{1 + K_1 C} \quad (3.41)$$

where K_1 = Langmuir constant which is the measure of the adsorbate bond strength [m^3/g], K_2 = maximum adsorption capacity.

The retardation factor for Langmuir-type adsorption is given by

$$R = 1 + \frac{\rho_b}{\eta} \left(\frac{K_1 K_2}{(1 + K_1 C)^2} \right) \quad (3.42)$$

Freundlich Isotherm

Freundlich isotherm describes a nonlinear relationship between adsorbed and solute concentrations. It assumes that the number of available adsorption sites is unlimited.

It is expressed as

$$S_a = K_f C^n \quad (3.43)$$

where K_f = coefficient of Freundlich isotherm [m^3/g^n], n = power law coefficient for the adsorption isotherm [dimensionless].

The value of n varies between 0.4 (heavy metals) to near 1.0 (organic solutes). In case $n = 1.0$, Freundlich isotherm reduces to linear isotherm. The retardation factor for Freundlich isotherm is defined as

$$R = 1 + \frac{\rho_b K_f}{\eta} n C^{n-1} \quad (3.44)$$

3.3.6.1.4 Kinetic (Slow) or Non-Equilibrium Adsorption

For cases where the equilibrium condition does not satisfy e.g. the layered heterogeneous medium with contrasting permeability values resulting decelerated solute transport in less permeable layer, kinetic or slow adsorption models are incorporated more commonly.

First-order Kinetically-controlled Adsorption

The rate of adsorption for a first-order kinetically-controlled model can be described as

$$\frac{\partial S_a}{\partial t} = k_1 C - k_2 S_a \quad (3.45)$$

where k_1 = finite rate constant, sorption [m/h], k_2 = finite rate constant, desorption [h^{-1}].

3.3.6.2 Degradation

Many organic contaminants such as petroleum hydrocarbons and chloride compounds undergo biological degradation or break down over time. These degradation reactions can be straight chemical reactions or can occur as a result of energy and carbon

utilization of micro organisms provided by dissolved organic compounds. Chlorinated organic compounds such as methane, ethane, propane, butane, brominated organic compounds, alkylbenzene and halogenated acetates are some of examples that undergo either biotic or abiotic degradation. Experiments show that a slow decay of contaminant results in plume shrinkage over time as concentrations decrease. The first order decay of a constituent due to radioactive decay or biodegradation can be presented as (Domenico and Schwartz [52])

$$r = -\lambda\eta_e C \quad (3.46)$$

where λ is the decay constant for radioactive decay or some reaction rate coefficient for biodegradation processes.

3.3.6.3 Colloid Transport

Micro-organisms such as viruses and bacteria with a range in size from 0.001 to 1 micron are termed colloids. Colloids are ubiquitous in subsurface systems and can play a crucial role in transport of strongly sorbing solute species, heavy metals and pesticides. In some cases, colloids can themselves be contaminant or promote chemical reactions in soils due to high surface area per unit mass and negative charge at the surface of their cell wall. The sources of colloids in groundwater include the following:

- Detached soil, mineral or contaminant particles.
- Changes in redox conditions from mixing with percolated surface water in the solutes undergoing geochemical precipitation.
- Formation of micelles initialized by macromolecules such as humic acids.
- Emulsions of fine droplets from free phase hydrocarbons.
- Colloids introduced directly into the groundwater from landfills, septic tanks or other contaminant sources.

The transport of colloidal particles takes place under some mechanical and adsorptive processes and can be determined from their physical/chemical properties. The removal and accumulation of bacterial cells occur by straining within the aquifer matrix. The pore entrance size which is a function of grain size is important in this aspect. The mechanical removal takes place when the particles enter the soil matrix but are caught by the smaller pore spaces as it traverses the matrix.

Adsorptive interactions of colloids are effected by increasing ionic strength of groundwater which increases the capability of bacteria to adhere to soil surfaces. Increased ionic strength also enhances the ability of colloidal particles to combine, thus forming on the whole a large particle which is more likely to be captured in pore spaces. Increased ionic strength, on the other hand, also decreases the thickness of electric double layer formed due to the collection of positive ions on the negatively charged surfaces and anions in the solution. This results in the attachment of colloids to the matrix surface. The physical and mechanical behaviour of colloids, their migration and colloid-facilitated transport in groundwater systems can be examined through the use of reactive chemical transport models.

3.3.6.3.1 Transport model

The general advection-dispersion equation describing transfer of colloidal particles from liquid suspension onto stationary surfaces through colloid deposition and release (Sun et al [55]) can be described as

$$\frac{\partial N}{\partial t} = \nabla \cdot (D \nabla N) - \nabla \cdot (\mathbf{v} N) - \frac{f}{\pi a_p^2} \frac{\partial \theta}{\partial t} \quad (3.47)$$

where N = colloid number concentration [m^{-3}], θ = fractional surface coverage of deposited colloids [dimensionless], f = specific surface area [m^2/m^3] and a_p = colloid particle radius [μm].

The particle surface coverage rate of the porous medium for patchwise geochemically heterogeneous model is given by (Johnson et al [56])

$$\frac{\partial \theta}{\partial t} = \lambda \frac{\partial \theta_f}{\partial t} + (1 - \lambda) \frac{\partial \theta_u}{\partial t} \quad (3.48)$$

where λ and $(1 - \lambda)$ represent the favourable and unfavourable representative elementary volume surface fractions respectively. The favourable and unfavourable surface coverage rates while taking the dynamic aspects of colloid deposition and first-order kinetic release into account can be represented as

$$\frac{\partial \theta_f}{\partial t} = \pi a_p^2 k_{dep,f} B(\theta_f) N - k_{det,f} \theta_f \quad (3.49)$$

$$\frac{\partial \theta_u}{\partial t} = \pi a_p^2 k_{dep,u} B(\theta_u) N - k_{det,u} \theta_u \quad (3.50)$$

The dynamic blocking function B characterizes the probability of colloid deposition by quantifying the fraction of collector surface still available for deposition of colloids (Sun et al [55]). Two types of dynamic blocking functions are generally recognized. The Langmuirian blocking function derived from the molecular adsorption model of Langmuir is presented as

$$B(\theta_s) = 1 - \frac{\theta_s}{\theta_{\max}} \quad (3.51)$$

where subscript s denotes favorable (f) or unfavorable (u) surface fractions, θ_{\max} is the maximum attainable surface coverage, k_{dep} = colloid deposition rate constant [m/s] and k_{det} = colloid release rate constant [s^{-1}]. According to recent research studies, the dynamics of particle deposition in hydrogeological systems can be better described by random sequential adsorption (RSA) dynamic blocking function expressed as

$$B(\theta_s) = 1 - a_1 \left(\frac{\theta_s}{\theta_{\max}} \right) + a_2 \left(\frac{\theta_s}{\theta_{\max}} \right)^2 + a_3 \left(\frac{\theta_s}{\theta_{\max}} \right)^3 \quad (3.52)$$

where the coefficients a_1 , a_2 and a_3 in the model are chosen as those given by Johnson and Elimelech [57].

3.4 Flow and Transport Models: Validation

Issues of changes in water quantity and quality subject to social, economical and legal constraints are critical for hydrological implications and waste contaminant design and remediation. The development of appropriate management system requires the detailed evaluation, characterisation and analysis of existing groundwater resources. The use of computational models for description of flow and transport phenomena has played an increasing role to provide a quantitative representation of the cause and effect relationships for these systems during past several decades.

Physical model presented for water movement and contaminant transport are required to solve numerically to establish flow and transport processes taking place in complex hydrological environments. The conventions of cell-centred finite volume method described in chapter 2 are implemented over structured/unstructured domain to model large variation in scale efficiently. The accuracy and capability of numerical approach

adopted is accomplished by means of several benchmark problems. In order to validate the model implementation, following test cases have been investigated

- Section (3.4.1)** Constant withdrawals from aquifer systems
- Section (3.4.2)** Flow field evaluation for anisotropic geologic formations
- Section (3.4.3)** Conservative solute transport in uniform flow fields
- Section (3.4.4)** Reactive solute transport under non-linear sorption and decay
- Section (3.4.5)** Colloid transport in geochemically heterogeneous porous media

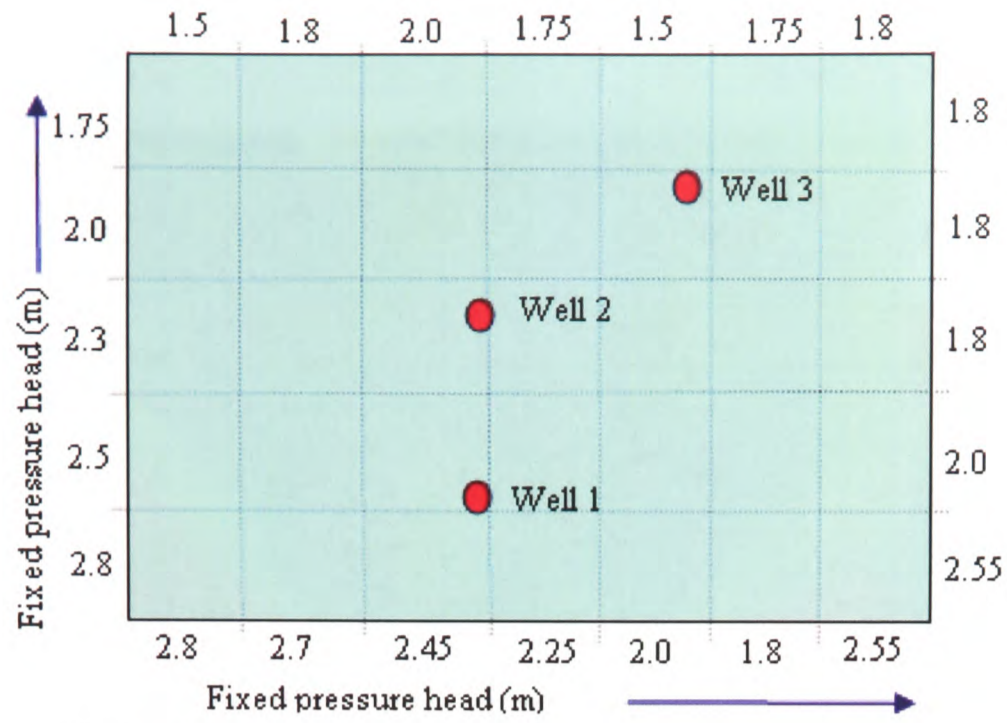
3.4.1 Constant Withdrawals from Aquifer Systems

Evaluation of water-supply potential of aquifers is a crucial issue for many real life problems. A large body of work is focused on methods of evaluating the effects of groundwater pumping on an aquifers long term capacity to yield water to wells.

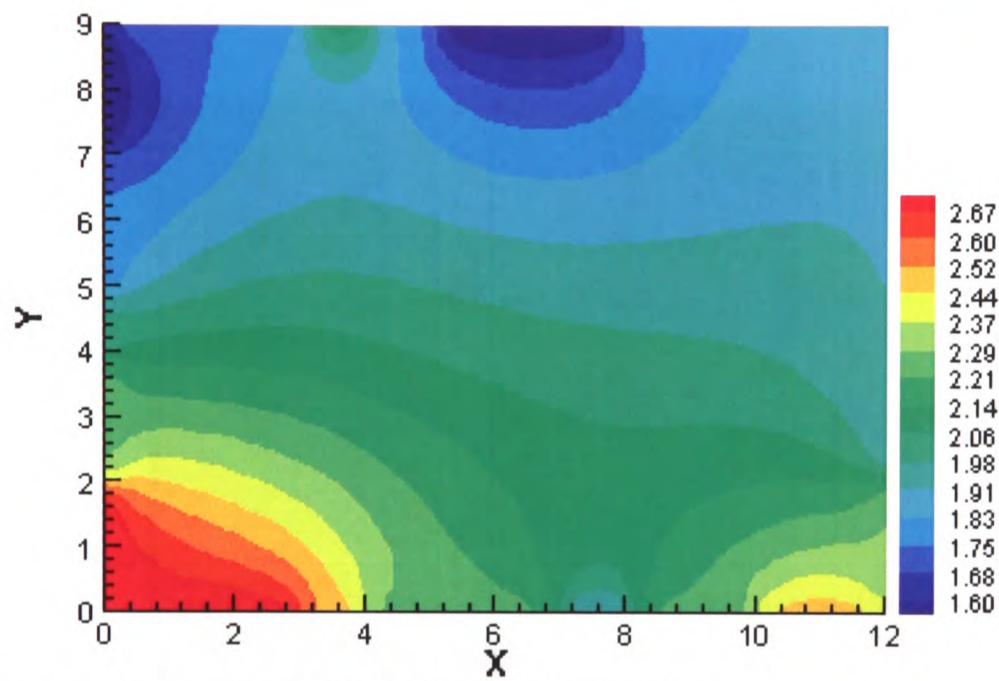
A simple example is presented first in this section to visualize the flow field variation in response to the pumping from an idealized aquifer with the help of hydraulic head contours and flow nets (Figure 3-5 and Figure 3-6).

The developed groundwater model predicts the dynamic behaviour of water table in response to pumpage and net recharge for a shallow water table aquifer with a constant hydraulic head across its boundaries as shown in Figure 3-5a. The flow process is governed by equation (3.20) with the parameteric values of hydraulic conductivity, transmissivity and specific yield range from 1.5 to 3 m per day, 100 to 200 m² per day and 8% respectively. This problem is followed by the two test cases to evaluate the time scale and time varying response of withdrawals.

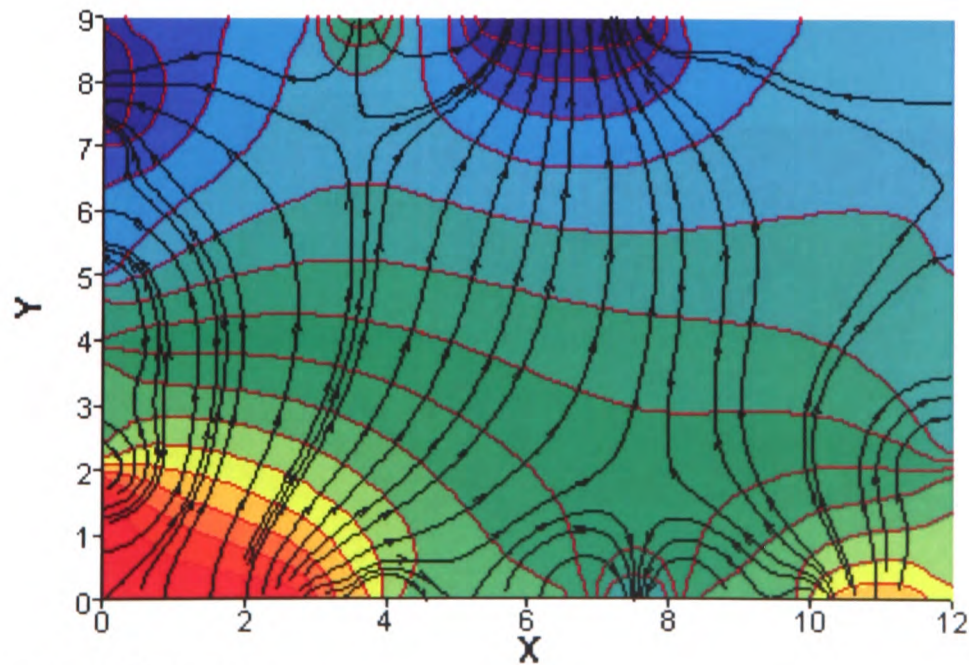
Figure 3-5b and c show the distribution of hydraulic head under a constant recharge rate and the formation of flow nets respectively after a simulation time of 50 days. Once the system reaches the equilibrium a constant withdrawal rate is applied to the aquifer in form of three abstraction wells. Figure 3-6 shows a decrease in the overall hydraulic head of the aquifer after 50 days of pumping. The drawdown at the abstraction points are shown in terms of cones of depression (Figure 3-6c).



(a) Geometry of the problem

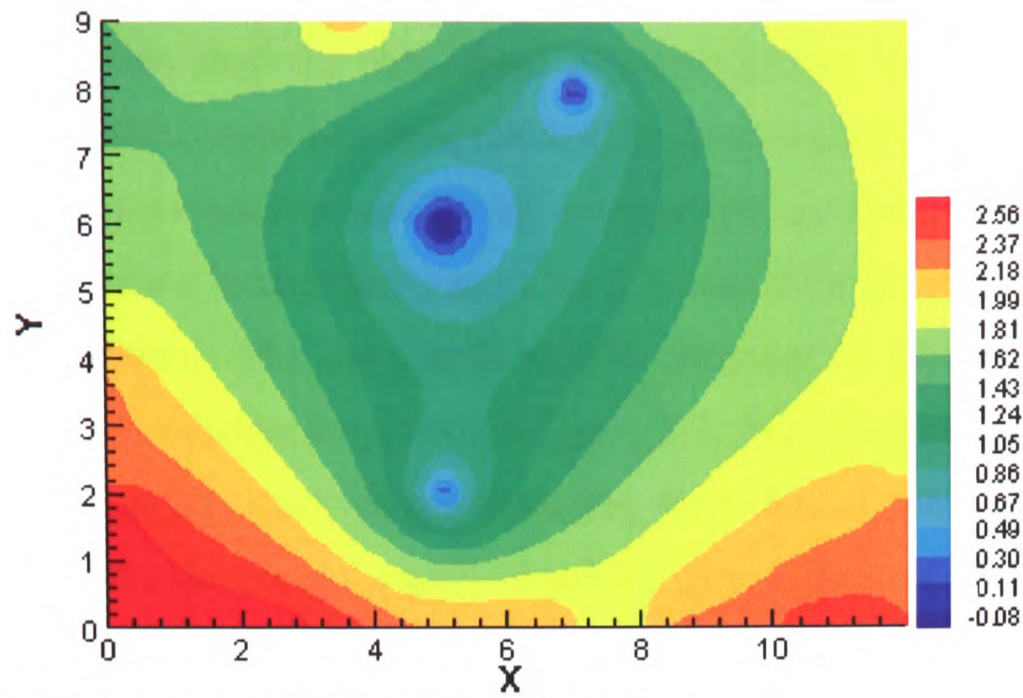


(b) Head distribution (in meters) at 50 days prior to pumping.

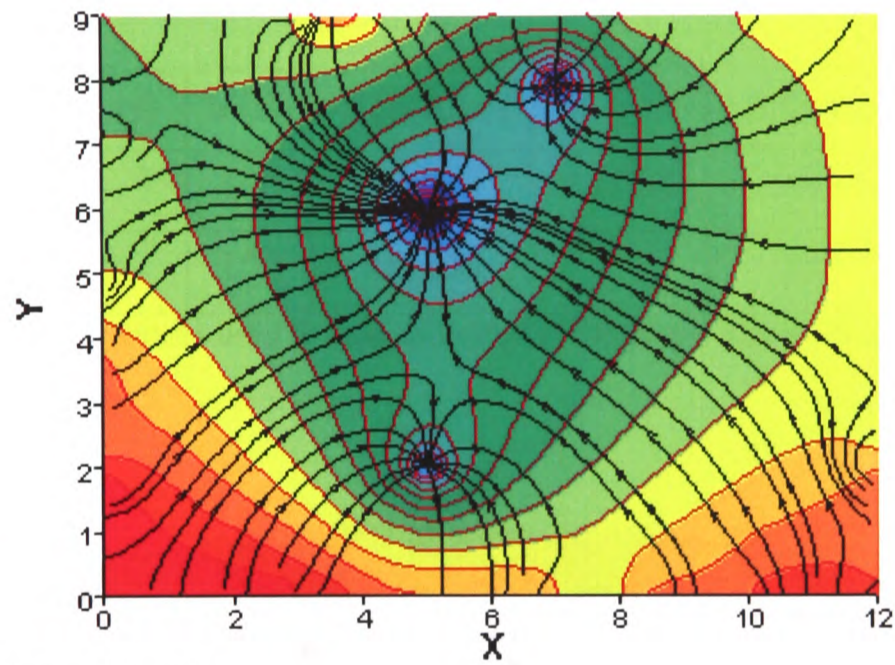


(c) Representation of flownet.

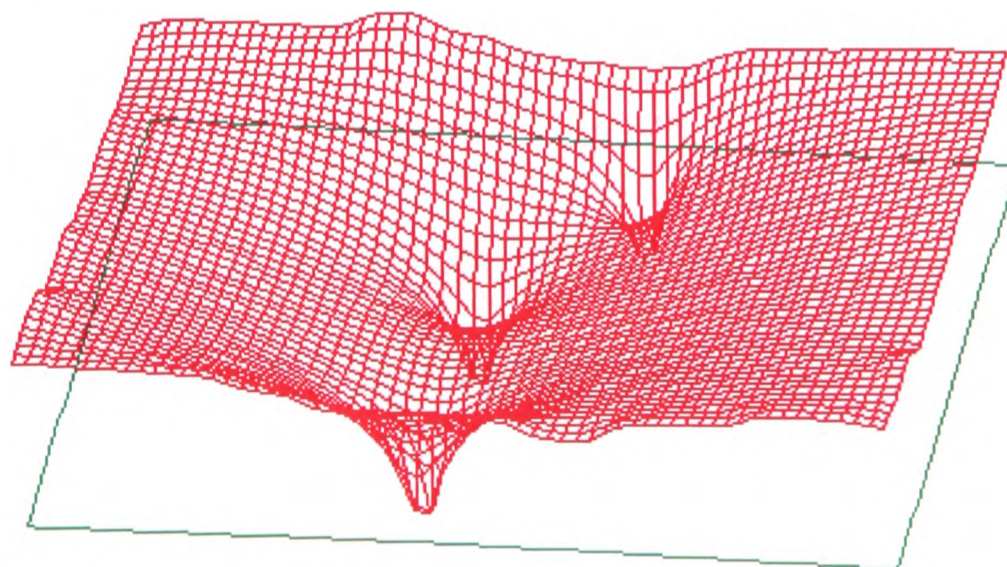
Figure 3-5. Fluid flow profile under transient conditions in an idealized aquifer.



(a) Head distribution (in meters) after 50 days of pumping.



(b) Representation of flownet



(c) Representation of cones of depression after 50 days of pumping.

Figure 3-6. Fluid flow profile for water withdrawal under transient conditions in an idealized aquifer.

3.4.1.1 Case 1

First case describing the constant withdrawals from aquifer systems compares the amount of drawdown in idealized unconfined (equation (3.20)) and confined (equation (3.18)) aquifers subject to same pumping rate applied to a single pumping well (Alley et al [58]). The physical parameters used in the calculations are listed in Table 3-3. The prescribed boundaries are located far enough away so that they do not have an effect on the simulation conditions. The simulation results computed in Physica for one year pumping from the two aquifers are shown in Figure 3-7. Inspection of Figure 3-7 shows that drawdown appear at much larger distances from the abstraction point in the confined aquifer with a deeper and areally extensive cone of depression as compared to the unconfined aquifer. The response to pumping of many real aquifers lies somewhere between the responses in these idealized examples.

Aquifer type	K (ft/day)	b (ft)	T (ft ² /day)	S	t (days)	Q (ft ³ /day)
Confined	100	100	10,000	0.0001	365	192,500
Unconfined	100	100	10,000	0.2	365	192,500

Table 3-3. Parameter values used to calculate drawdown in two idealized aquifers. Source: Alley et al [58].

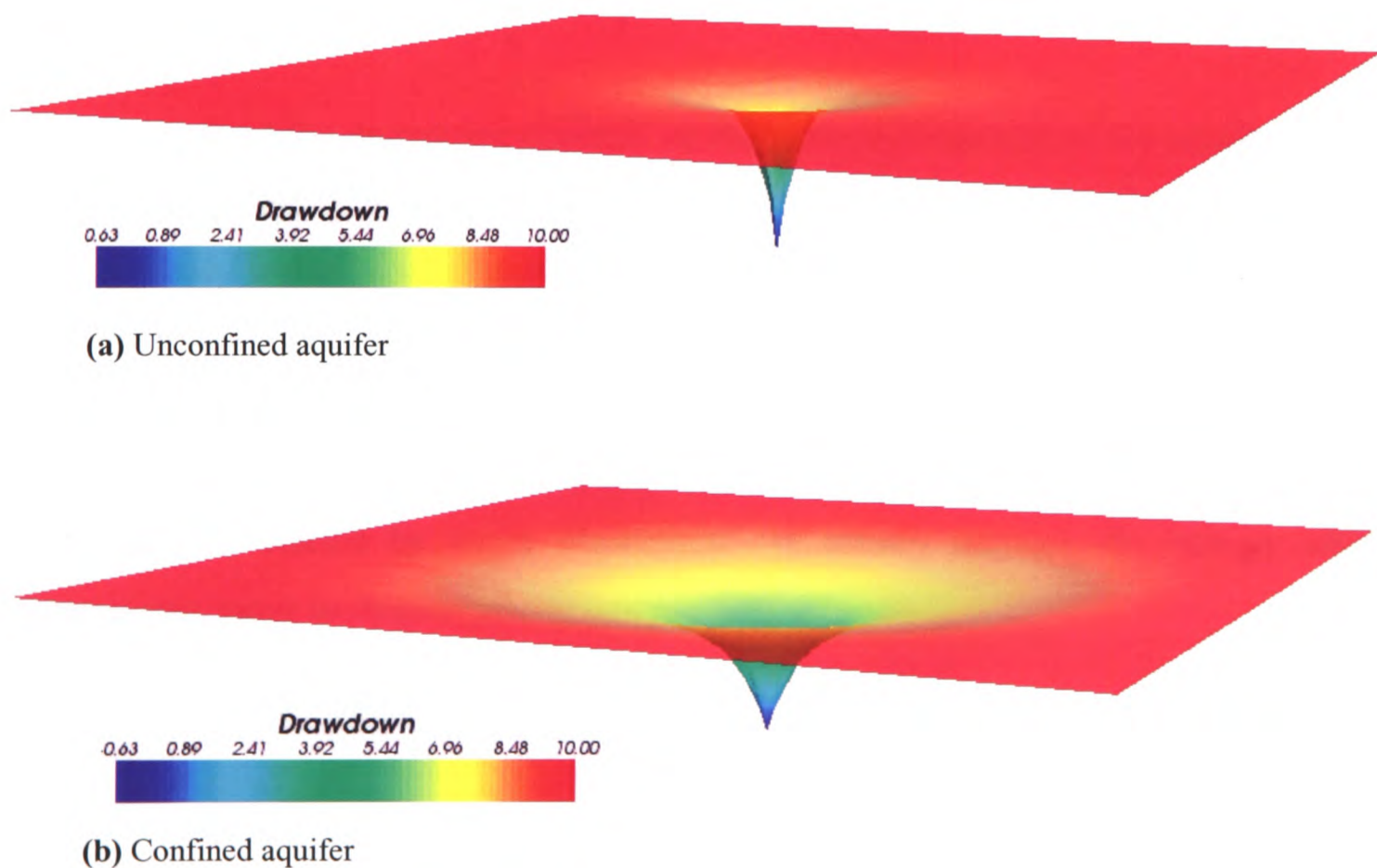


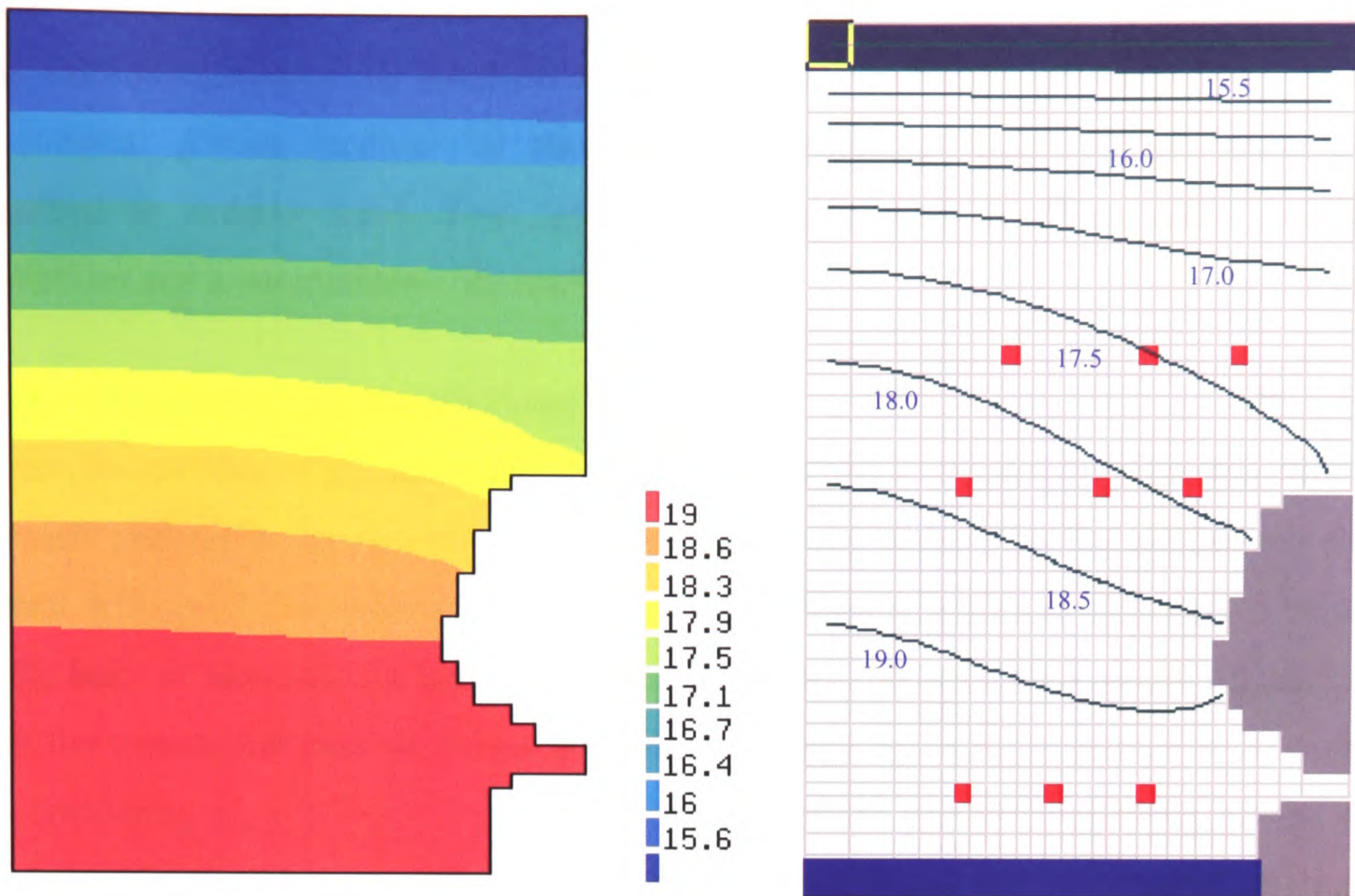
Figure 3-7. Comparison of drawdown from a single well after one year.

3.4.1.2 Case 2

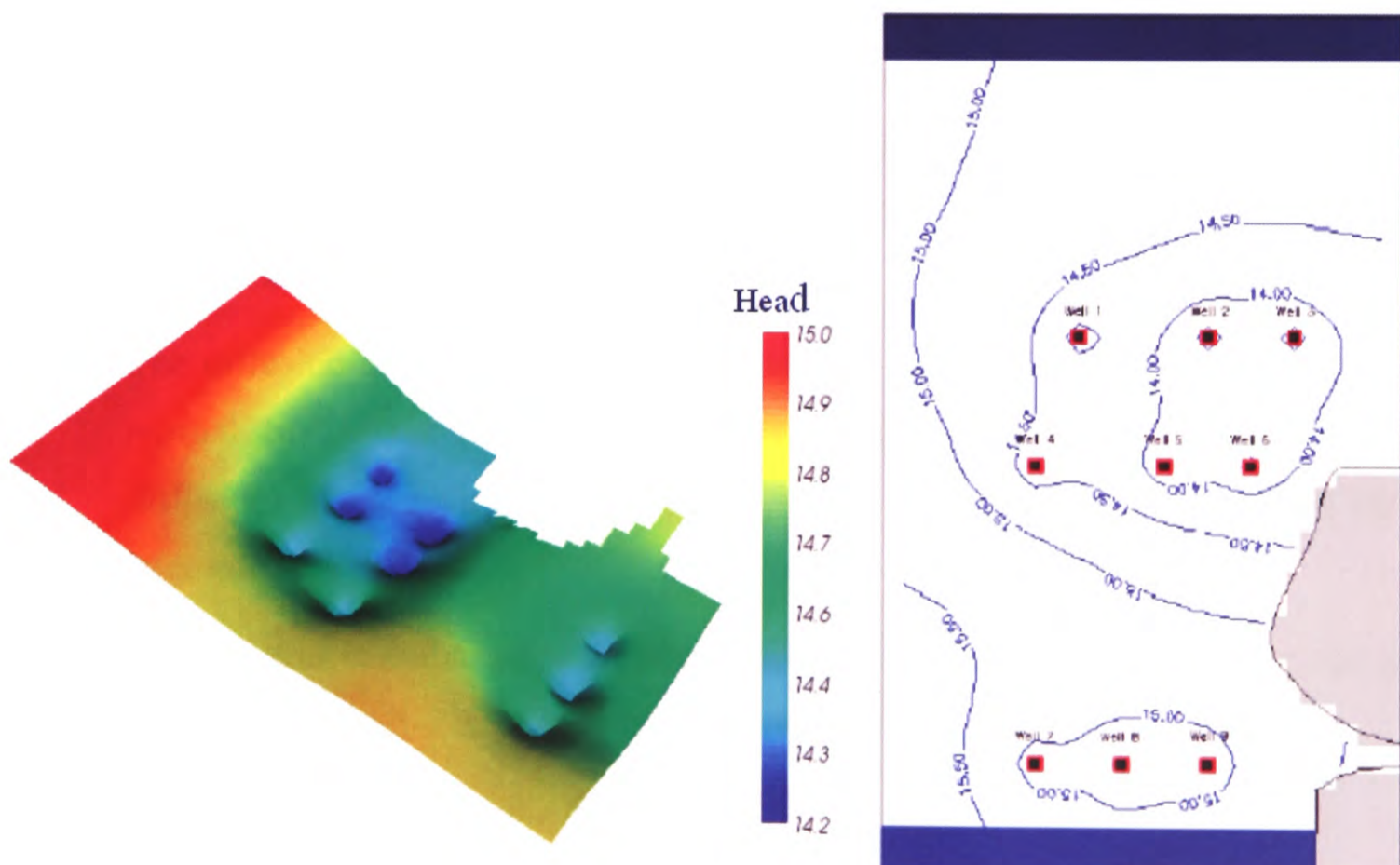
The second case demonstrates the prediction of water levels in an unconfined aquifer system under steady state and transient conditions with the flow field governed by equation (3.20). The aquifer is homogeneous coarse grained sand material with a measured isotropic hydraulic conductivity of 160 m/day; the specific yield has been assessed as 0.06. The elevations of aquifer top and bottom are 25 m and 0 m respectively. The area of interest is 10 km long and 6 km wide and is bounded by no flow zones to the east and west. There is also a volcanic mountain in the south east corner of the model area. To the north an area of constant hydraulic head existed with a value of 15 m. The southern boundary is a specified flux boundary with an inflow rate of $0.0672 \text{ m}^3/\text{day}$ per meter. A total of nine wells in the area are pumped at 45 l/s each during the 8 month of dry season to supply water for irrigation and domestic purposes.

To access the water level in the aquifer, simulations are performed on a grid of 947 elements taking (a): steady-state condition with the mean recharge rate of 0.00025 m/day (Figure 3-8a) and (b): after 8 months pumping during the dry season (Figure 3-8b). Results are compared with PMWIN (Processing MODFLOW for Windows) which is a 3D finite-difference based integrated simulation system for modelling groundwater flow and transport processes.

The time scale of the drawdown depends on the storage properties of the aquifer and its ability to yield water across the capture zone of the well. Groundwater pumping can affect not only water supply consumption but also the maintenance of aquatic life and other environmental needs. Long term reduction in water levels and induced changes in the flow direction can affect vegetation along streams and temperature, oxygen levels and nutrient concentration in the natural hydrologic environments. In some settings, steep gradients caused by water abstraction can greatly increase the rate at which contaminants move to deeper groundwater.



(a) Head distribution for steady state case at 120 days of recharge period.



(b) Head distribution for transient case at 240 days of pumping.

Figure 3-8. Comparison between Physica (coloured contours) and PMWIN (line contours) hydraulic head distribution results. Red squares represent position of abstraction wells.

3.4.2 Flow Field Evaluation for Anisotropic Geologic Formations

This example presents the estimation of anisotropic hydraulic conductivity in a 3-dimensional porous medium by taking into account the discretisation procedure described in section 3.2.7. Two test cases are presented to show mesh specific predictions and a comparison with another code.

3.4.2.1 Mesh Specific Predictions

To test the validity of algorithm and the capability of the model to determine the effects of mesh orientation on the flow field, simulations are carried out by accounting for several different 2-dimensional grid types. The grid discrimination in each case is made on the basis of element type and degree of inclination (orthogonality/non-orthogonality) from the rectangular axes as shown in Table 3-4. Equation (3.22) is solved in all cases by considering $K_{xx} = 1.0 \times 10^{-5}$ m/s, $K_{yy} = 1.0 \times 10^{-6}$ m/s (or 1.0×10^{-7} m/s) and a source of constant flux at grid centre. The geometries of cases 1-5 are shown in Figure 3-10 to Figure 3-12.

The simulation results for 5 cases are shown in Figure 3-13 to Figure 3-16. The grid orientation and element types are observed to have great impact on the distribution of hydraulic head for anisotropic material properties. Comparison of results for cases 2b, 3b and 4b predicts that a grid structure generated according to case 2 is unable to account for anisotropy for the following two reasons

- The diffusion coefficient is defined along x, y and z-axes. The contribution of normals to diffusion term results in having same diffusion term (same amount of diffusion) along each direction which makes anisotropic case to behave like isotropic one.
- When a grid is deformed at an angle of 45° the face diffusion flux for a cell as shown in Figure 3-9 is defined in terms of connectivity of
 - Node1 with node2 through f_1
 - Node1 with node3 through f_2
 - Node1 with node4 through f_3
 - Node1 with node5 through f_4

Node1 has no defined connectivity with a node in x, y or z-direction. For case 2 the normal to the face $n_x = n_y = \pm 1/\sqrt{2}$. Hence

$$\kappa_f = \frac{K_{xx}}{2} + \frac{K_{yy}}{2}$$

If e.g. $K_{xx} = 100$ m/day and $K_{yy} = 50$ m/day then $\kappa_f = 75$ will appear to be the same for all faces f_1 - f_4 which would result in showing isotropic behaviour instead of anisotropic. It is concluded that the grid structure generated according to case 3, 4 or 5 can better describe the flow through anisotropic geologic formations where the flow field is not aligned along the coordinate axes.

Case no.	Element type	Degree of inclination
Case 1	Rectangular	0
Case 2	Rectangular	45
Case 3	Rectangular + trapezoid	45
Case 4	Delaunay	45
Case 5	Rectangular + trapezoid	0

Table 3-4. Mesh orientation and element types for 5 cases.

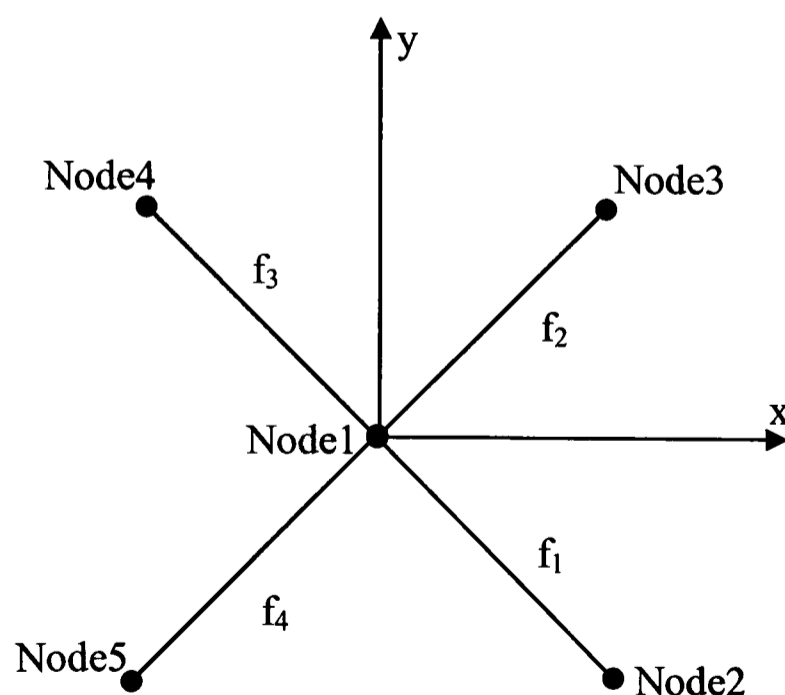


Figure 3-9 Interconnection of nodes through cell faces.

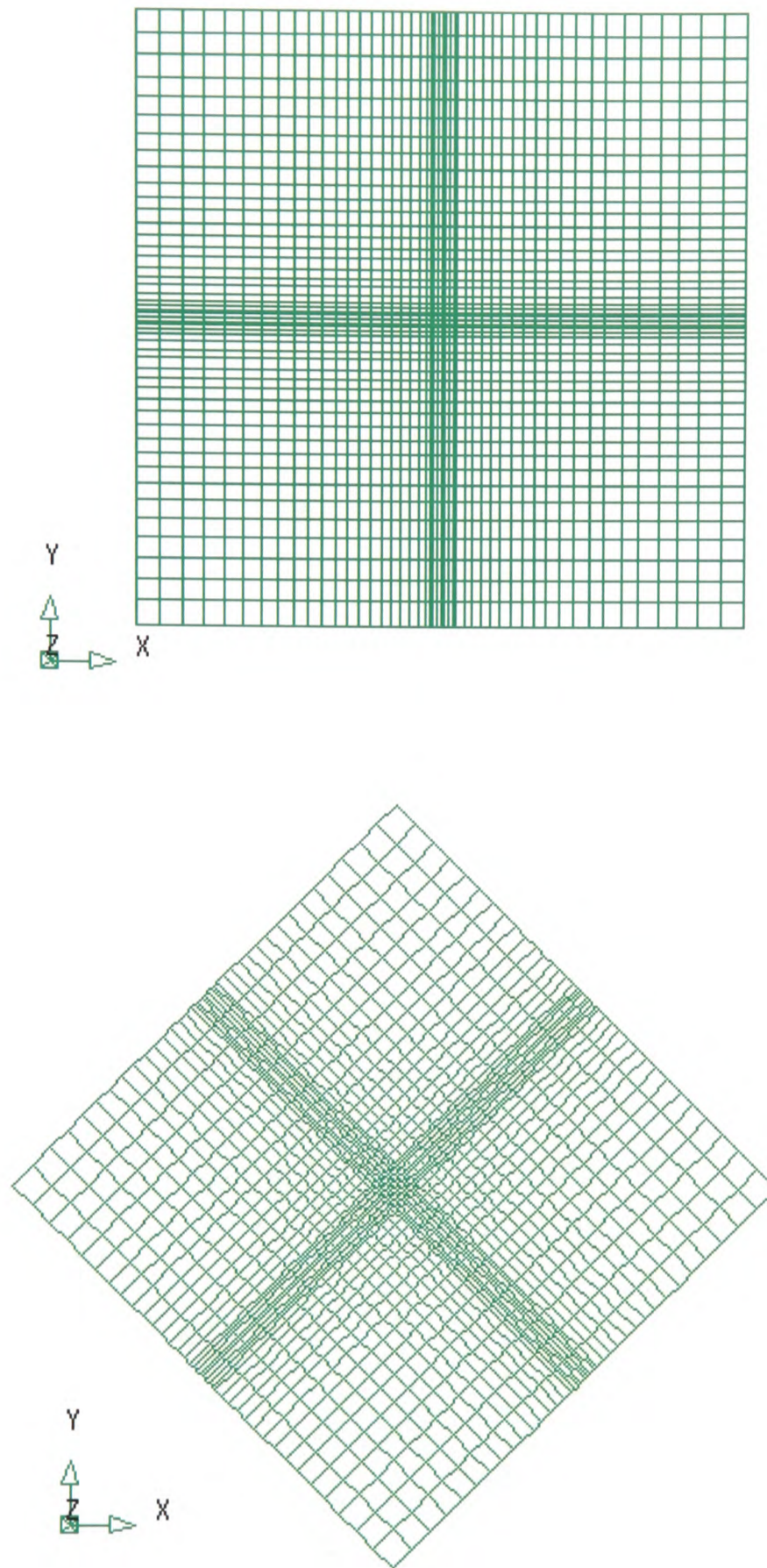


Figure 3-10. Geometry of case1 (top) and case2 (bottom) for flow field evaluation.

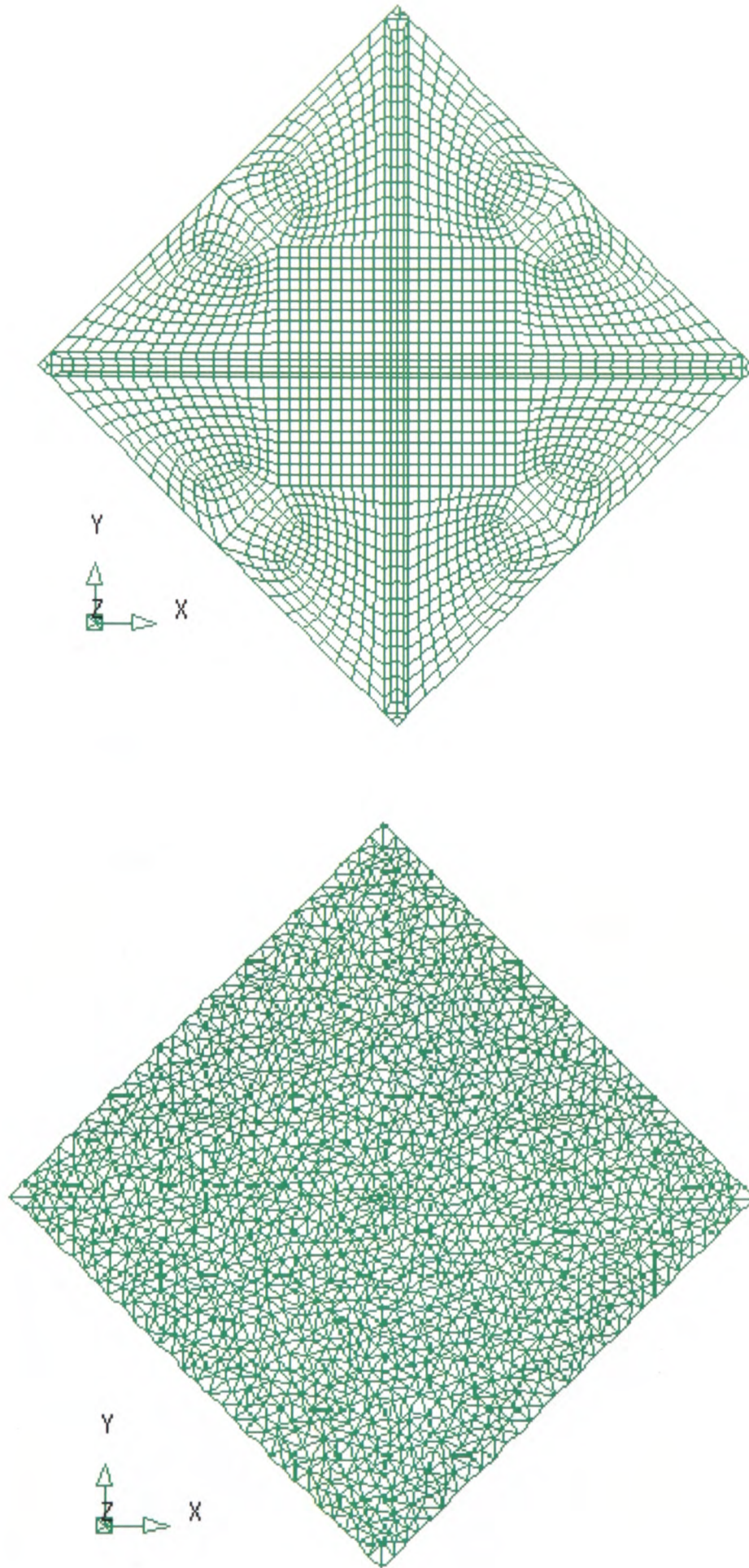


Figure 3-11. Geometry of case 3 (top) and case 4 (bottom) for flow field evaluation.

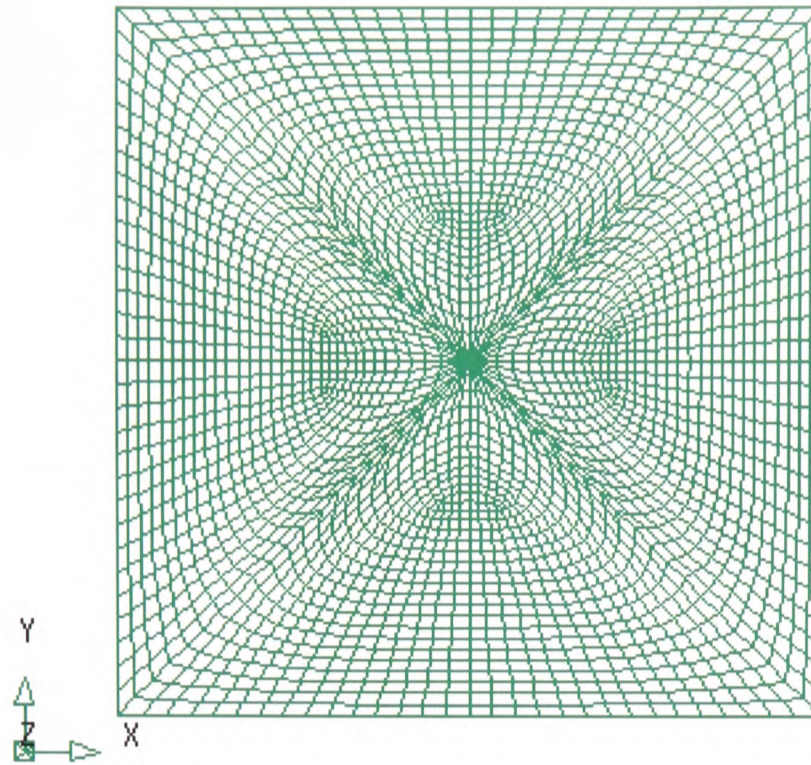


Figure 3-12. Geometry of case 5.

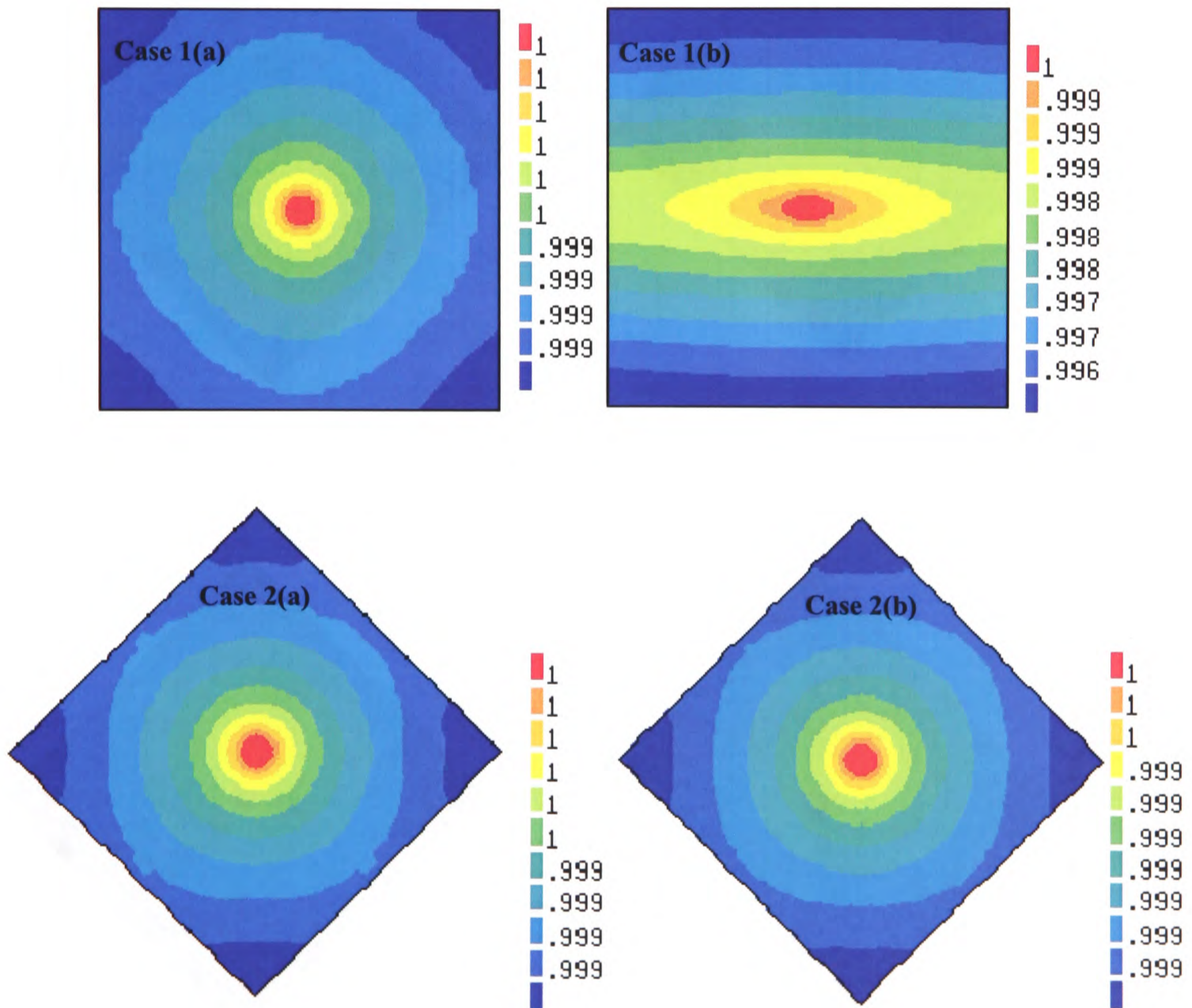


Figure 3-13. Hydraulic head contours for (a) isotropic (b) anisotropic conductivity for cases 1 and 2.

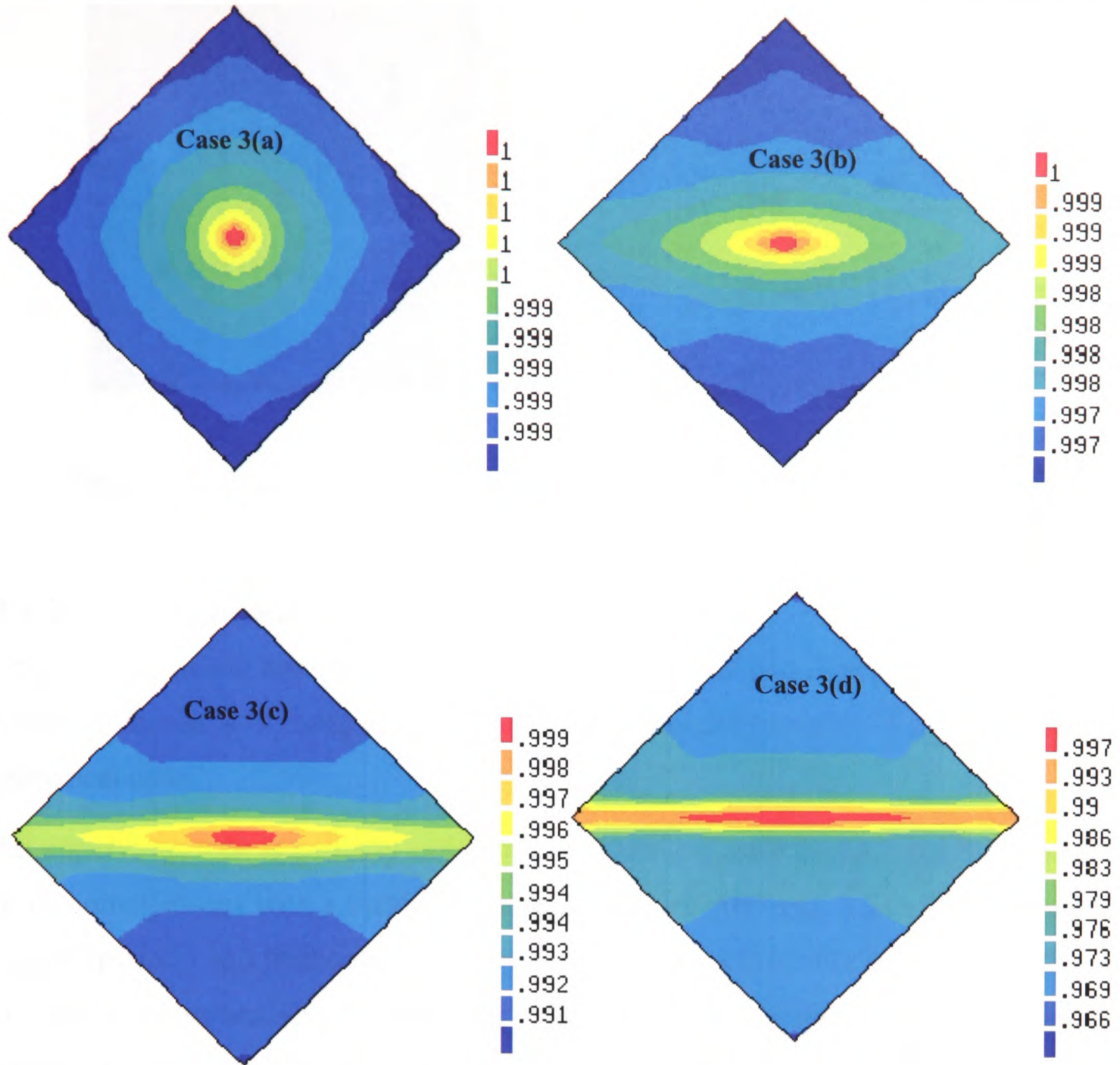


Figure 3-14. Hydraulic head contours for case 3. (a) isotropic hydraulic conductivity, (b) $K_{yy} = K_{xx}/10$, (c) $K_{yy} = K_{xx}/100$, (d) $K_{yy} = K_{xx}/1000$.

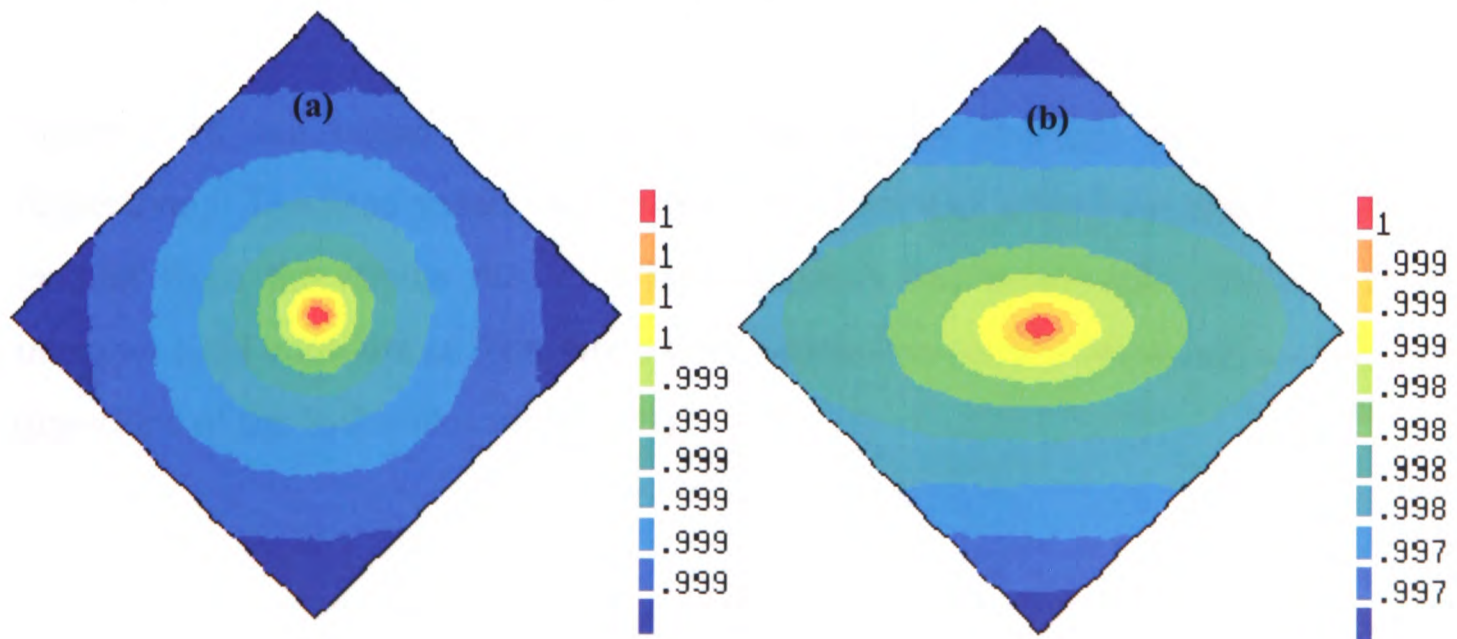


Figure 3-15. Head distribution for case 4 with (a) isotropic, (b) anisotropic hydraulic conductivity.

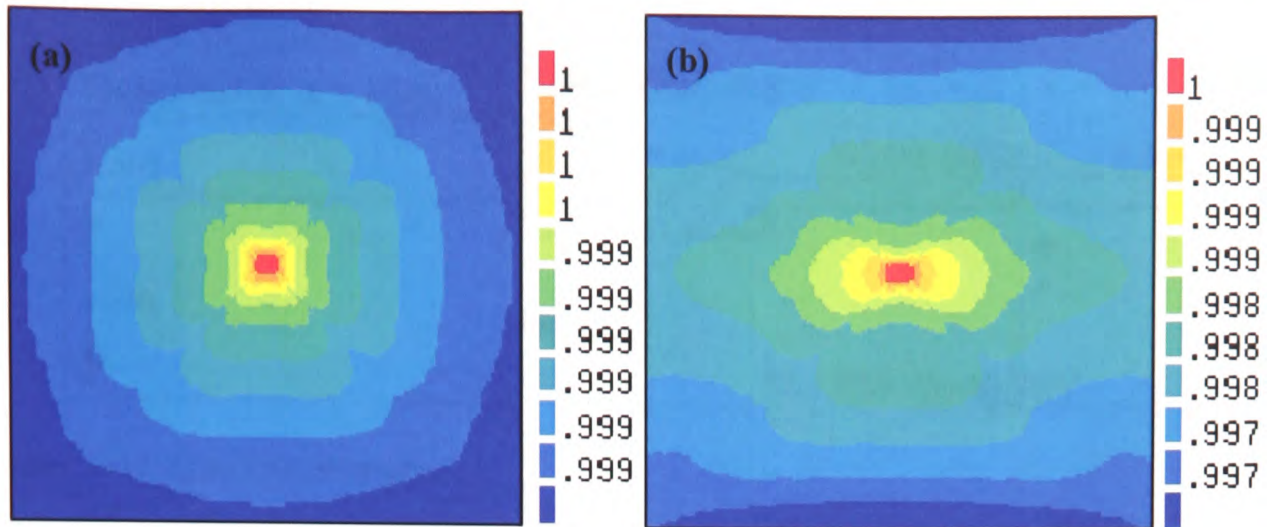


Figure 3-16. Head distribution for case 5 with (a) isotropic and (b) anisotropic hydraulic conductivity.

3.4.2.2 Comparison Case

The example below involves the computation of flow net and seepage under a weir and has been chosen as a mean of checking the model implementation and the accuracy of numerical code.

An impervious weir is partially embedded in a confined aquifer. The aquifer is assumed to be homogeneous with a hydraulic conductivity of 0.0005 m/s. The effective porosity, anisotropy ratio and thickness of the aquifer are given as 0.15, 0.2 and 9m respectively. A vertical cross-section of the aquifer with a uniform thickness of 1m as shown in Figure 3-17 is considered to compute the head distribution and the corresponding flowlines. The boundaries at the upstream and downstream of the weir are modelled as fixed-head boundaries with $h = 12\text{m}$ and $h = 10\text{m}$ above the reference level, respectively.

Figure 3-18 and Figure 3-19 show the flow net for isotropic and anisotropic cases respectively. The head values range from 10 to 12m with a head increment of 0.1m. It is evident from the results that in a homogeneous and anisotropic medium, flowlines intersect head contours at right angle only where flow is parallel to one of the principal directions of the hydraulic conductivity.

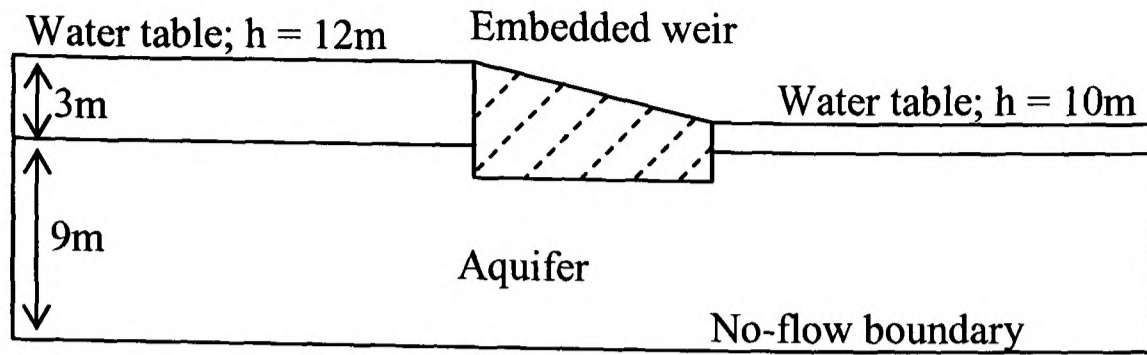


Figure 3-17. Problem description.

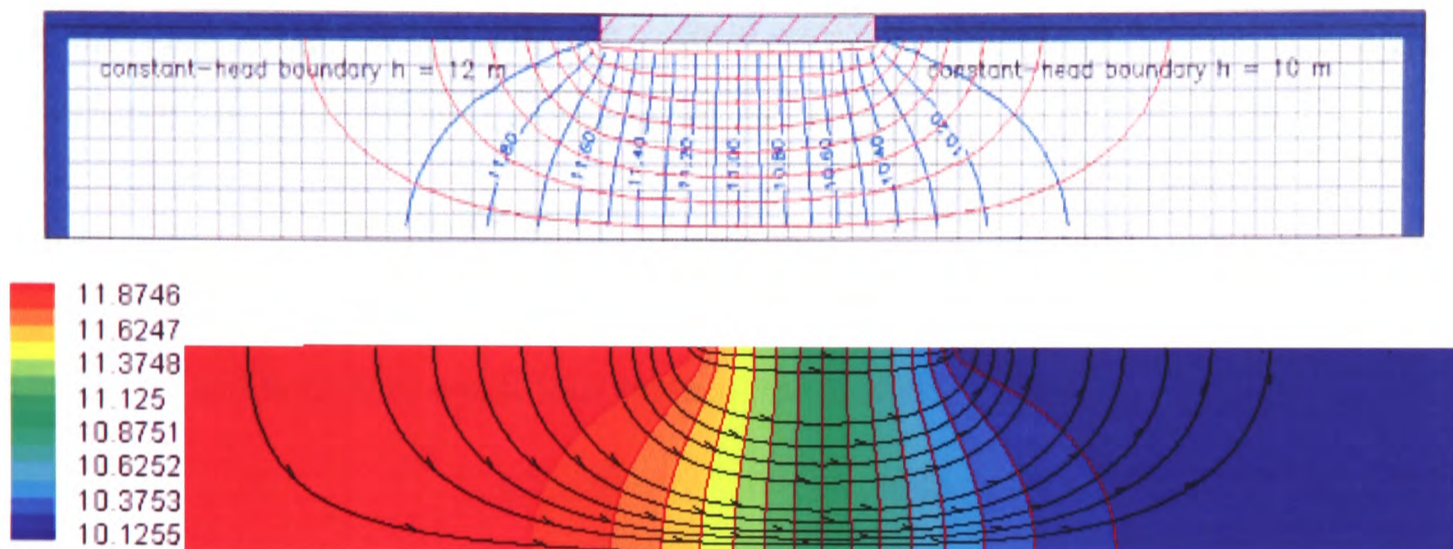


Figure 3-18. Comparison of flowlines and simulated hydraulic head contours for isotropic medium in Physica (bottom) and PMWIN (top) results.

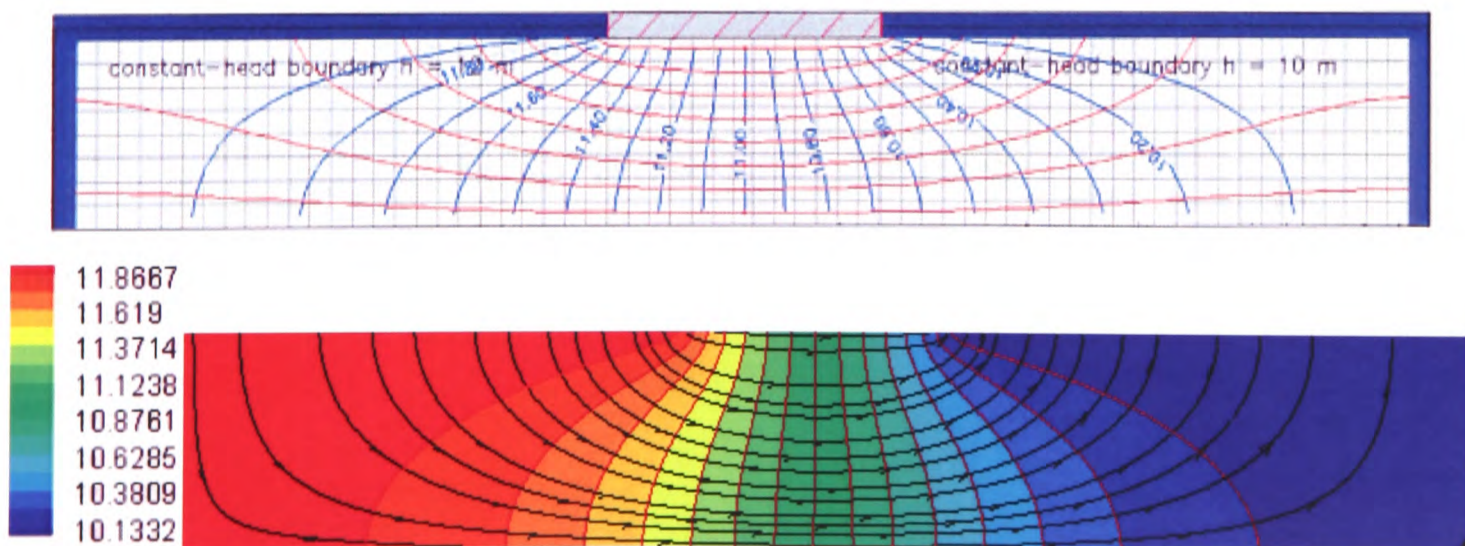


Figure 3-19. Comparison of flowlines and simulated hydraulic head contours for anisotropic medium in Physica (bottom) and PMWIN (top) results.

3.4.3 Conservative Solute Transport in Uniform Flow Fields

To examine contaminant transport in uniform flow fields two test cases are considered. The governing equation considering the advection, dispersion, linear adsorption and first order decay and can be presented as follows

$$R \frac{\partial C}{\partial t} = \nabla \cdot (\mathbf{D} \nabla C) - \nabla \cdot (\mathbf{v}C) - \lambda \eta C$$

where R is defined in equation (3.40)

3.4.3.1 Case 1

First test case simulates transport of a pollutant into a saturated homogeneous soil. As the transport of contaminant is conservative the physical parameters used are

$$v = 1 \text{ m/day}, \lambda = 0, R = 1, D_m = 0 \text{ and } \alpha_L = 1.0 \text{ m}$$

The initial and boundary conditions for this test case are

$$C(x, 0) = 0; \quad 0 < x < 300\text{m}$$

$$C(0, t) = 1$$

$$C(300, t) = 0$$

Simulated concentration profiles (Figure 3-20) in Physica for 200 days are compared with analytical solution (Kinzelbach [59]) given as

$$C(x, t) \frac{C_0}{2} \exp\left(\frac{x}{2\alpha_L}\right) \left[\exp\left(\frac{-x\gamma}{2\alpha_L}\right) \right] \operatorname{erfc}\left(\frac{x - vt\gamma / R}{2\sqrt{\alpha_L vt / R}}\right) + \exp\left(\frac{x\gamma}{2\alpha_L}\right) \operatorname{erfc}\left(\frac{x + vt\gamma / R}{2\sqrt{\alpha_L vt / R}}\right)$$

where

$$\gamma = \sqrt{1 + 4\lambda\alpha_L R / v}$$

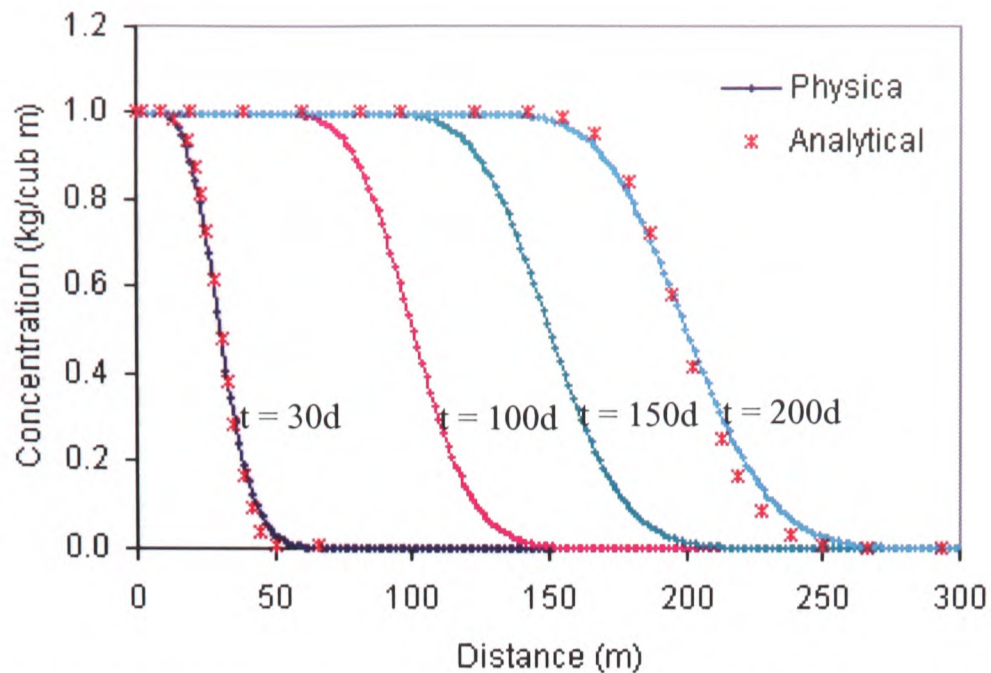


Figure 3-20. Concentration profiles at 4 different times for the case 1 with constant concentration at the entrance of the column.

3.4.3.2 Case 2

Second test case considers coupled groundwater flow and solute transport in a homogeneous saturated medium. The flow field parameters for a confined aquifer (equations (3.15), (3.16)) with anisotropic hydraulic properties (equation (3.22)) and the transport parameters of a conservative contaminant are given as follows

$$K_x = 45 \text{ m/day}, K_y = K_z = 15 \text{ m/day}, S = 0.00075,$$

$$\nu = 0.33 \text{ m/day}, \alpha_L = 10 \text{ m}, r = 0.3, C_0 = 5 \text{ kg/m}^3$$

where r = ratio of transverse to longitudinal dispersivity. Aquifer length, width and elevation are taken as 450m, 180m and 10m respectively (Figure 3-22). Initial concentration is assigned at a source 150m away from the west boundary. The contour maps of plume migration at different time steps are shown in Figure 3-22. A decrease in concentration and increase in spread of plume is observed due to dilution and dispersion processes as the plume migrates from west to east.

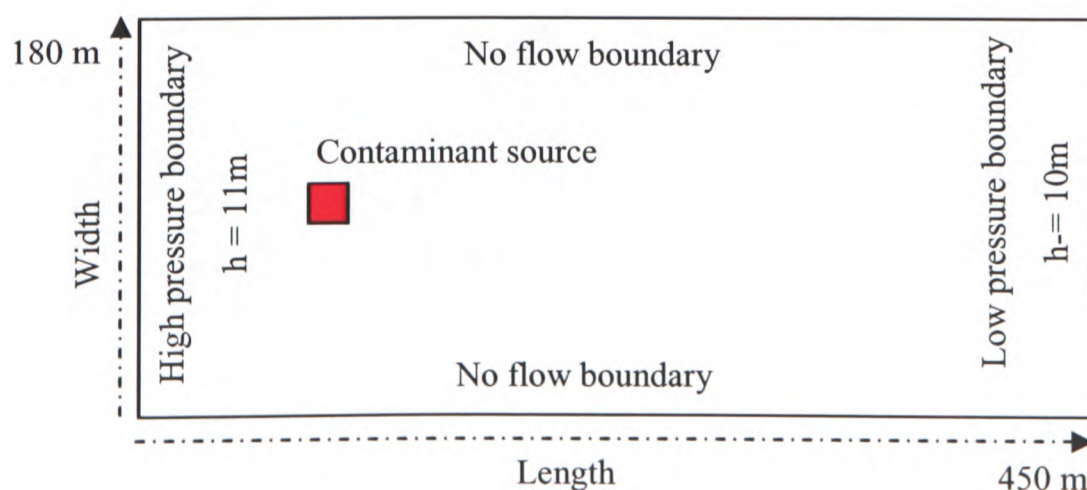


Figure 3-21 Problem description of case 2.

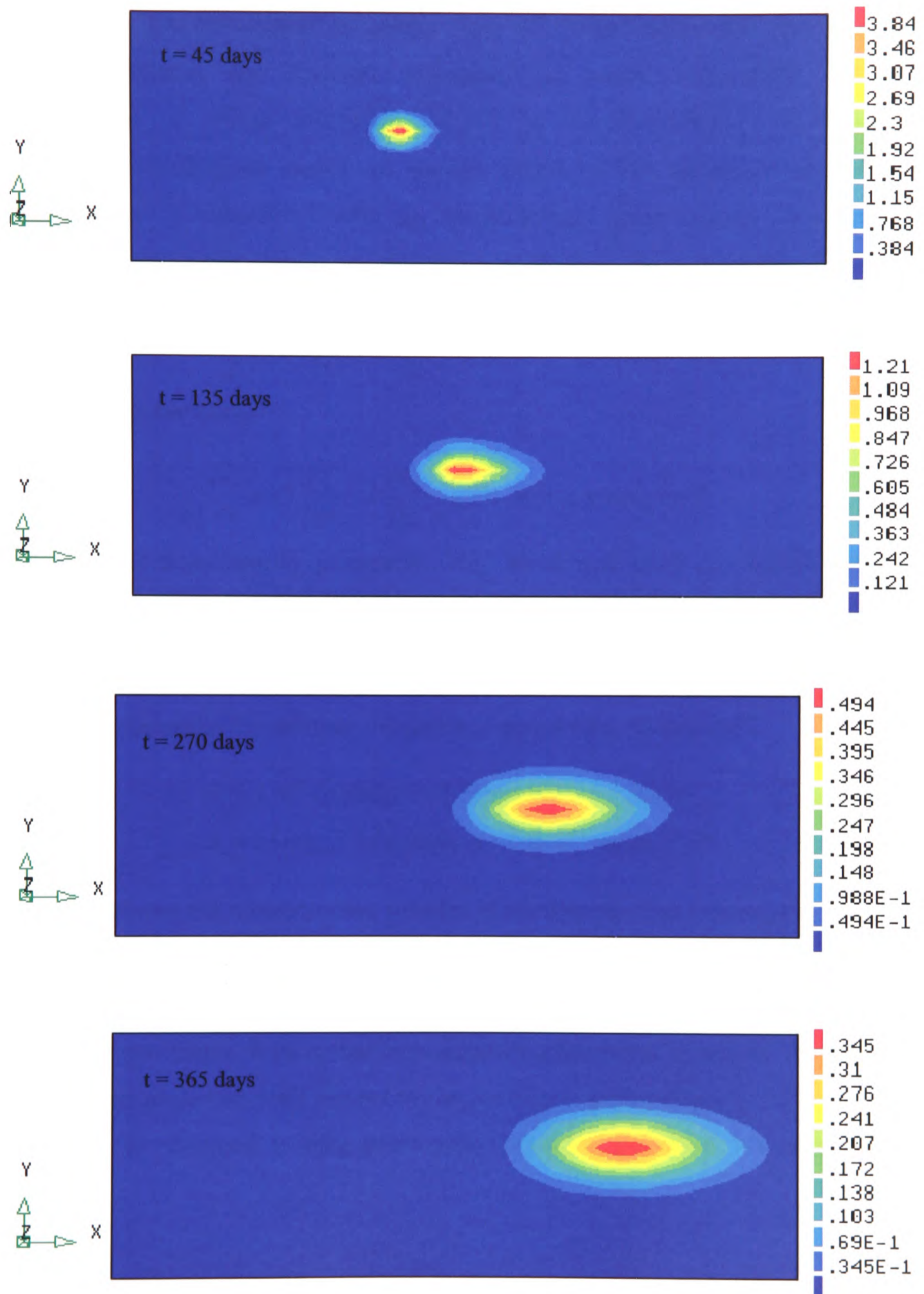


Figure 3-22. Simulated concentration distribution under anisotropic flow conditions at four different times subject to advection and dispersion.

3.4.4 Reactive Solute Transport under Non-Linear Sorption and Decay

One of the common approaches to model transport of reactive contaminants in porous media is to utilize adsorption isotherms. Fate of solute species has observed to be strongly influenced by sorption processes in many contaminant scenarios. Approximation of solute migration subject to linear/non-linear adsorption and radioactive (or biological) decay are subject matter of this section. Transport in an infinite aquifer is considered with an instantaneous point source. The governing advective-dispersive equation in one-dimension with linear decay is described as

$$\frac{\partial C}{\partial t} = D \frac{\partial^2 C}{\partial x^2} - v \frac{\partial C}{\partial x} - \lambda C, \quad -\infty < x < \infty, t > 0 \quad (3.53)$$

and with non-linear decay

$$\frac{\partial C}{\partial t} = D \frac{\partial^2 C}{\partial x^2} - v \frac{\partial C}{\partial x} - \lambda C^n, \quad -\infty < x < \infty, t > 0 \quad (3.54)$$

where n is the non-linearity parameter. The initial and boundary conditions are as follows

$$C(\pm\infty, t) = 0, \quad C(x, 0) = C_0 \delta(x)$$

To carry out numerical simulations the physical parameters chosen are

$$D = 1 \text{ m}^2 / \text{month}, \quad v = 1 \text{ m/month}, \quad t = 1 \text{ month}, \\ \lambda = 1 \text{ (mg/l)}^{1-n} / \text{month}, \quad n = 0.6, \quad C_0 = 100 \text{ mg/l}$$

Figure 3-23 shows the concentration profiles in the absence and presence of linear/non-linear decay one month after the spill. The amount of initial concentration is observed to have great impact on the degree of scaling the plume which is being controlled by the non-linearity parameter. With initial concentration greater than 1 and $n < 1$, most of the linear plume is scaled up with respect to the non-linear plume (Figure 3-23a). However, the opposite is observed to take place with initial concentration less than 1 (Figure 3-23b).

The effects of contaminant dispersion in long aquifer subject to linear and non-linear adsorption are examined by taking the equations (3.37), (3.39) and (3.41) into account along with the initial and the boundary conditions as described above. The physical parameters used for Langmuir model are:

$$K_1 = 0.001 \text{ l/mg}, K_2 = 1 \text{ g/kg}, \rho = 1000 \text{ kg/m}^3, C_0 = 10,000 \text{ mg/l},$$

$$\eta = 0.1, D = 1 \text{ m}^2 / \text{month}, v = 1 \text{ m/month}, t = 10 \text{ month}.$$

Figure 3-24 shows the comparison between simulated concentration profiles in Physica and the results presented by Serrano [60] in the absence of sorption and with linear/non-linear sorption after 10 months spill. As the Langmuir parameter are dimensions independent of magnitude of other parameters the quantitative effects on shape of plume are observed. Non-linearity causes an increase in the magnitude of concentration with respect to linear sorption. However, the plume concentration is observed to be most retarded under the effect of linear sorption.

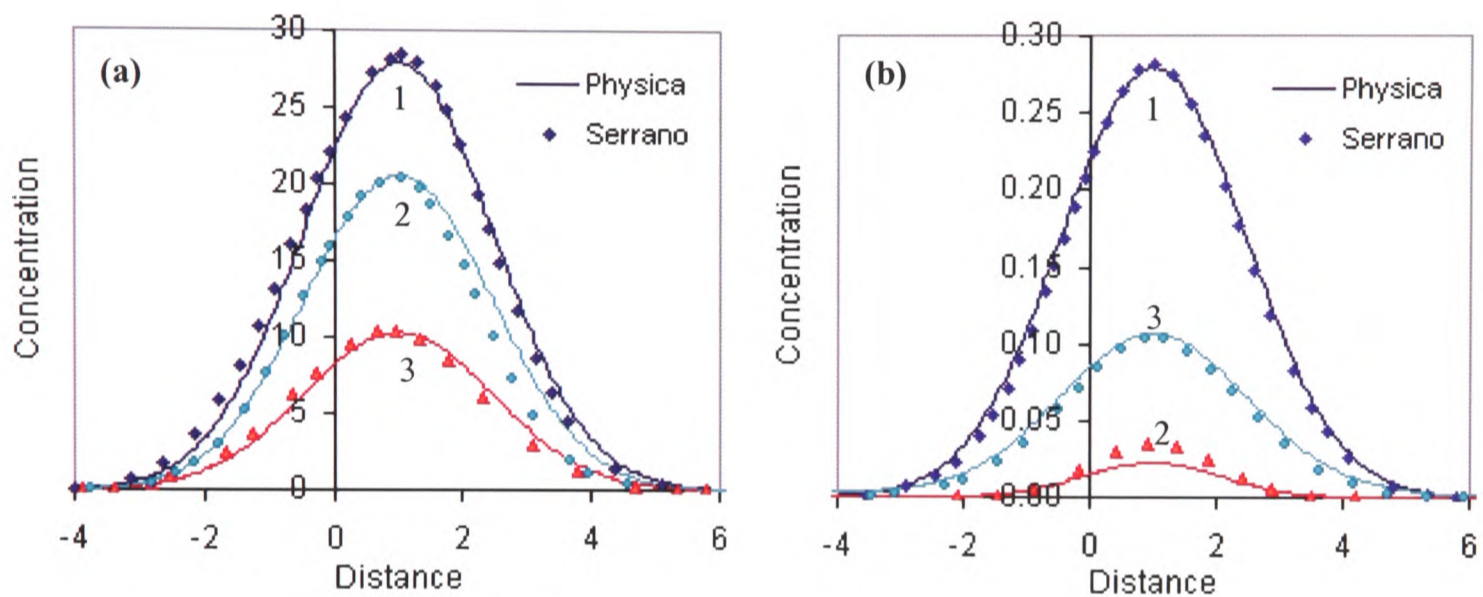


Figure 3-23. Comparison of concentration profiles subject to no-decay and linear/non-linear decay with (a) $C_0 > 1$, (b) $C_0 < 1$. Numbers 1, 2 and 3 represent cases with no decay, non-linear decay and linear decay respectively.

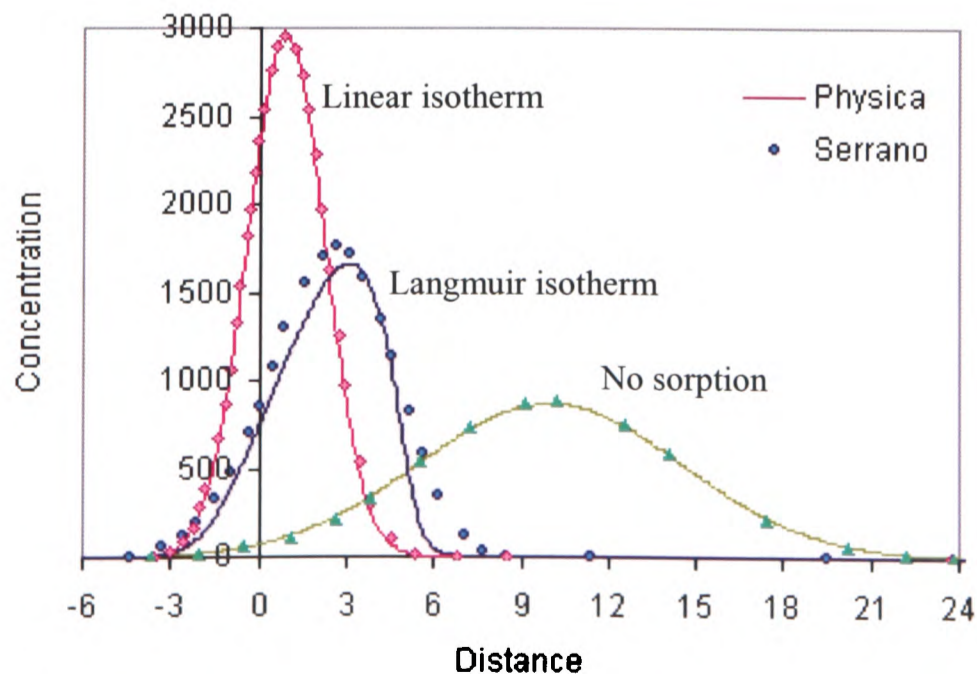


Figure 3-24. Comparison of concentration profiles subject to no sorption and linear/non-linear adsorption.

3.4.5 Colloid Transport in Geochemically Heterogeneous Porous Media

2-dimensional colloid transport in geochemically heterogeneous media is considered here. The transport model is validated with the physically homogeneous and geochemically heterogeneous test cases presented by Sun et al [55]. Physically homogeneous case involves a rectangular domain 3 m in length along x-axis and 1 m thick along z-axis. To predict the transport of colloid particles equation (3.47) is solved subject to favourable and unfavourable surface coverage rates for patchwise geochemical heterogeneity using equations (3.49) and (3.50). The basic model parameters, listed in Table 3-5, are close representative of colloid transport in sandy aquifer. The initial and boundary conditions for the colloid concentration are

$$\begin{aligned}
 N(x, z, t = 0) &= 0, \quad 0 \leq x \leq 3, \quad 0 \leq z \leq 1 \\
 \theta_f &= \theta_u = 0 \\
 \left. \begin{aligned}
 N(x = 0, z, t) &= 2.8 \times 10^{14} \\
 -D \frac{\partial N}{\partial x} \Big|_{x=3} &= 0
 \end{aligned} \right\}, \quad 0 < t \leq T_p
 \end{aligned}$$

where $T_p = 0.5$ days.

Shown in Figure 3-25 are the comparison results of Physica simulations with the numerical solution presented by Sun et al. As can be seen in Figure 3-25a, an increase in geochemical heterogeneity increases colloid deposition rate but decreases colloid concentration in the bulk solution. It is revealed from Figure 3-25b that at a constant hydraulic head gradient, increase in hydraulic conductivity increases colloid concentration spreading which is due to increase in colloid advection velocity.

Figure 3-26 shows the effect of varying the longitudinal dispersivity values over a small range. Large changes on colloid transport are resulted in response to minute changes in dispersivity.

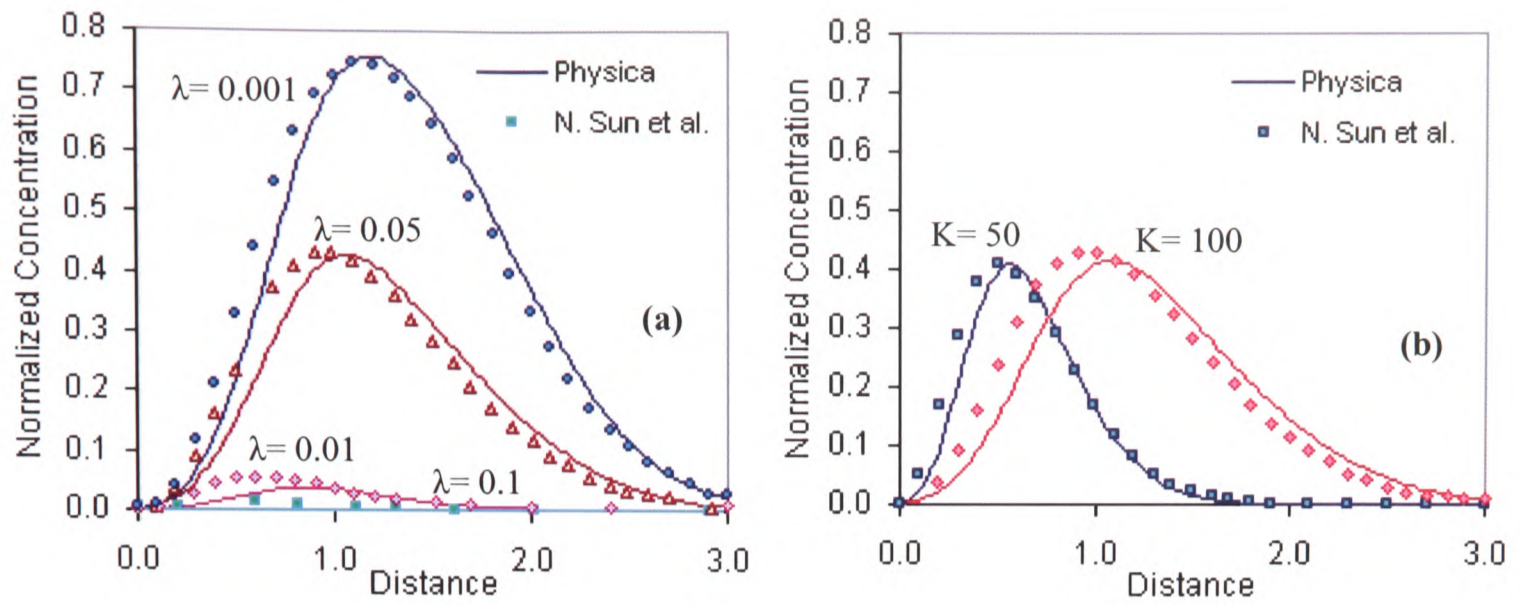


Figure 3-25. Effect of (a) geochemical heterogeneity, (b) hydraulic conductivity values variation on colloid transport for a period of 0.75 days.

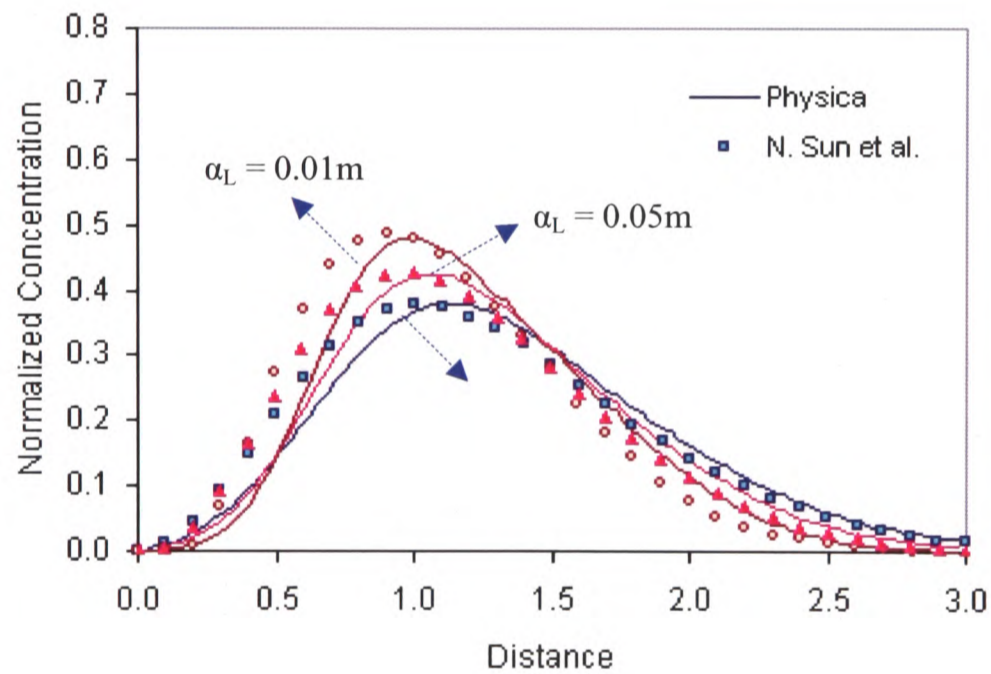


Figure 3-26. Effect of longitudinal dispersivity variation on colloid transport at 0.75 days.

Parameter	Basic value
Hydraulic gradient, ∇h	0.01
Hydraulic conductivity, K (m/day)	100
Longitudinal dispersivity, α_L (m)	0.05
Dispersivity ratio, $R = \alpha_L / \alpha_T$	5:1
Porosity, ε	0.4
Specific surface area, f (m^2/m^3)	3×10^4
Particle radius, a_p (μm)	0.15
Patchwise heterogeneity parameter, λ	0.001
Unfavorable particle deposition rate, $k_{dep,u}$ (m/day)	6.5×10^{-6}
Favorable particle deposition rate, $k_{dep,f}$ (m/day)	6.5×10^{-3}
Detachment rate from unfavorable surface, $k_{det,u}$ (h^{-1})	0.0
Detachment rate for favorable surface, $k_{det,f}$ (h^{-1})	0.0
Maximum attainable surface coverage, θ_{\max}	0.2

Table 3-5. Parameters and the basic values for colloid transport model. Source: Sun et al [55].

3.5 Concluding Remarks

In this chapter, the problems of modelling fluid flows and contaminant transport through homogeneous groundwater systems have been discussed. A detailed demonstration of using commercial CFD for such problems is given and some results for 1-, 2-, and 3-dimensional cases are shown. The key conclusions are high lighted as follows

- The numerical methods developed in this work for flow through spatially homogeneous flow field provide plausible results and show a good agreement where compared with the other commercial software and analytical solution. Numerical techniques are proposed to solve the fluid flow problems in an anisotropic confined aquifer. The non-orthogonality of flowlines and equipotential lines yields the construction of flownet in a transformed region. A bigger/smaller transformation of principal hydraulic conductivity in one coordinate direction results in an expansion/reduction of region of flow along that direction.

- Approximations of drawdown at short and long times of horizontal pumping well are obtained in real time domain. These are used for the pumping test interpretation of horizontal wells installed in confined and unconfined aquifers. The depth and extensiveness of the cones of depression depend on aquifer anisotropy, storage capacity, distance from the lower boundary and the location of the monitoring well. Hence, less drawdown is observed for a given interval of time and pumping rate in case of an unconfined aquifer.
- Anisotropy of the medium is also observed to have great influence on the migration of contaminant plume. The spread of plume along the axis of greater anisotropy is comparatively bigger than the others. The processes of sorption and decay also play a vital role in reducing the level of concentration for reactive solute species.
- The effects of medium properties have been determined on colloid transport through geochemically heterogeneous systems. The spread and shape of particle breakthrough curves are observed to be strongly influenced by alteration in conductivity and elementary volume surface fractions. Geochemical heterogeneity of the medium plays a key role in altering the physical and mechanical behaviour of colloids migration.

**FLOW AND TRANSPORT MODELS:
VADOSE ZONE**

This chapter provides a detailed description of flow and transport mechanisms through unsaturated zone. Several problems associated with fluid flow and solute migration subject to infiltration and reactive/non-reactive transport are discussed and the results of numerical simulations are provided for these problems.

4.1 Introduction

The study of water movement and storage in unsaturated zone also called vadose zone is important in many aspects. The processes on which fluid flow in vadose zone may have the major influence can be high lighted as

- Generation of runoff: water discharge to streams and rivers
- Infiltration to water table: generation of recharge to underlying groundwater, quantification of replenishment rates of water table in aquifers
- Cultivation of plants and vegetation
- Movement of pollutants entering into soil and underlying aquifer subject to thermodynamic interactions and chemical reaction in the unsaturated zone

A proper representation and understanding of these phenomena requires a detailed description of physical and chemical processes and the soil properties in the vadose zone. Soil water is thus dealt as an important subject in many branches of hydrology, soil mechanics, fluid dynamics and agricultural and environmental engineering.

Mathematical description of soil water system involves macroscopic view with continuum basis necessary for considerations of density, viscosity, temperature, compressibility, matric potential and other properties and the microscopic view for understanding the mechanisms governing discrete entities such as diffusion of solutes

and solute-water-solid interactions present in the molecular structures of the clay-mineral surfaces.

This chapter briefly describes water flow in vadose zone, including the modelling concepts of flow and transport mechanisms undergoing various physical and chemical processes. The current study also emphasis only on the flow of water in homogeneous and isotropic media under transient conditions.

4.2 Soil Water Storage

In natural conditions, some water is always present in soil even at the end of long dry periods. The presence and storage of water in soils depends on their physical properties and retention forces resulting from liquid-solid interactions in porous medium.

4.2.1 Physical Properties of Soil Water System

The flow process in vadose zone is a two-phase flow with liquid-phase below atmosphere and vapour-phase at atmospheric pressure. Whereas the zone itself, in nature, is a three-phase system of liquid, solid and vapour. According to Jury et al [61], the solid phase contains mineral grains and organic matter. The organic matter represents the remains of plants and animals that are undergoing decay. The liquid phase is water containing dissolved solutes of varying concentration from one pore to the next. The vapour phase includes water vapour and other gases that may not be present in the same proportions as the atmosphere.

Reflecting this complexity in its nature, the characterisation of infiltration, evapotranspiration and drainage depends on a number of factors including the shape, size and distribution of pores. This, in turn, influences the amount of water stored and rate of transfer of the fluid through the system. The physical properties of this three-phase system depend on the soil texture and structure and vary in space as well as in time. Soil texture which defines the size distribution of soil particles influences the attributes such as water holding capacity and infiltration capacity. Water drains more quickly through coarse soils such as sand than through fine soils such as clays which are slower to absorb and slower to drain of water. Soil structure which defines the aggregation of soil particles influences the movement and ease of flow of water through

a soil. Well aggregated soils contain large and interconnected pores that permit good water movement through them.

Soil texture is the proportion of three sizes of soil particles: sand (0.05-2 mm diameter), silt (0.002-0.05 mm diameter) and clay (<0.002 mm diameter). The sand and silt fractions mainly comprise quartz and minerals that have undergone little chemical alteration. Clays, on the other hand, result from chemical weathering and possess a variety of properties. The main features that distinguish clays from other soil types are their platy shape providing much higher specific surface and negatively charged surfaces. The negatively charged surfaces are generally balanced externally by cations and can result in the ion exchange processes between the soil surface and the soil solution (liquid-phase). Swelling on wetting and shrinking on drying are also properties possessed by many clay soils. These properties can influence the porosity and hydraulic conductivity of soils. Soils can be classified into four Hydrologic Soil Groups based on their runoff potential and transmission capacity as described in Table 4-1.

Soil group	Soil type	Properties
A	Sand, loamy sand, sandy loam	Low runoff potential, high infiltration rate, high rate of water transmission
B	Silt loam, loam	Moderate infiltration rate, moderate rate of water transmission
C	Sandy clay loam	Low infiltration rate, impede downward movement of water
D	Clay loam, silty clay loam, sandy clay, silty clay, clay	Highest runoff potential, very low infiltration rates, high swelling potential, nearly impervious to water transmission

Table 4-1 Hydrologic Soil Groups

4.2.2 Pressure Head and Water Content

Water in the unsaturated zone is generally held at a pressure less than atmospheric due to tension of the soil-surface-water contact. If h represents the total potential or hydraulic head in the unsaturated zone then mathematically

$$h = \psi + z \tag{4.1}$$

where z represents the elevation head and ψ is the pressure head [L] which being negative also referred as suction or tension head. The pressure head or matric pressure (matric suction/matric potential) in the theory of unsaturated hydrology is of major importance as it substantially influences the chief transport processes.

The amount of water present in the unsaturated zone is expressed in terms of moisture or water content [L^3/L^3] which is defined as

$$\theta = \frac{V_W}{V_T} \quad (4.2)$$

where V_T is the total volume of soil and V_W is the volume of water. The value of water content varies between zero and the total porosity of the soil. Hence

$$0 \leq \theta \leq \eta$$

A greater matric pressure generally describes higher water content whereas a zero matric pressure is associated with saturated or nearly saturated water content. A decrease in pressure causes a nonlinear decrease in the water content which is also hysteretic i.e. depends on the moisture history of the soil. It will be greater for a soil that is being dried than for one that is being re-wetted. The relationship between pressure and amount of water in soil is described by a function known as the soil water or soil moisture characteristic or retention curves (SWCC). The shape of the curve is a characteristic of porous medium and depends on the pore size distribution. In general, the SWCC in sandy soil is a much curved relationship due to large pore sizes than clayey soils which represent a SWCC of more uniform slope. The behaviour of SWCC at low water content generally predicts that soils never completely lose all of their water even under very dry conditions. This lower limit in water content is termed as residual water content.

4.2.3 Soil Water Constants

All available water in unsaturated zone is found mainly in three regions defined as

- a capillary fringe, which saturates the soil pores above the water table completely due to surface tension of the air-water interface and the molecular attraction of the liquid and solid phases
- a soil-water zone, extending from land surface to the depth of plant roots

- an intermediate zone, which occupies area between capillary fringe and the soil-water zone

Soil moisture at a location varies with change in the amount of precipitation and evaporation. Large amount of infiltration provides high soil moisture. A water withdrawal from the soil by evapotranspiration, on the other hand, drops the moisture content down. When the soil moisture content of a soil layer reaches the point at which the force of gravity which pulls the water downward equals the surface tension, gravity drainage ceases. Under this condition the soil is said to be at field capacity which specifies the water held in soil against gravity.

If evapotranspiration continues over a large time such as summer periods, soil moisture becomes lower than the field capacity. If soil moisture drops too low the remaining moisture is too tightly bound to the soil particles for the plant roots to extract it. The minimum water content at which the plants can extract water is termed as wilting point. The comparison between different soils is made on the basis of these two soil water constants. Fine-textured soils have higher values of field capacity and wilting point (Figure 4-1) owing to their greater surface area. The available water capacity of a soil is the difference between the field capacity and the wilting point.

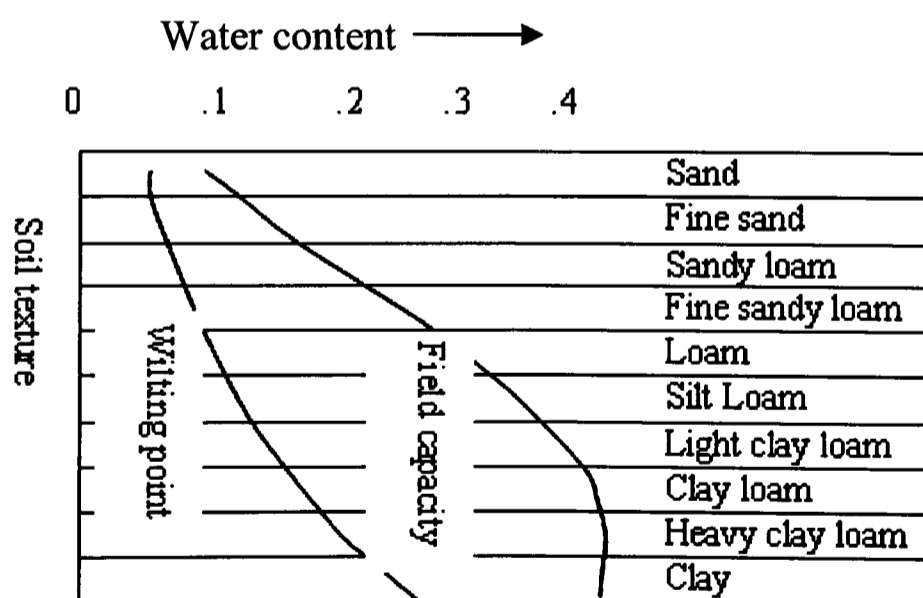


Figure 4-1. Soil water constants for different soil types. Source: Fetter [2].

4.3 Soil water Movement

The description of soil water movement depends upon the quantification of the force field as well as the specification of the solid matrix geometry. The dominant force field

factors can be described in terms of the components of total potential as: (1) gravity potential, which relates to the position in the gravitational field with respect to a reference elevation; (2) matric potential, which relates to capillary and adsorption forces between solid surfaces and water, including the effect of cohesive forces between water molecules; and (3) osmotic potential, which relates to forces of attraction between ions and water molecules (Marshall and Holmes [62]). These controlling forces exhibit a tendency to operate either from the ground surface or from the bottom layers of unsaturated zone. The resulted soil water potential gradients are in vertical direction yielding vertical movement of water either upwards or downwards.

Vertical movement of water subject to infiltration and the accompanying transport of solutes are the main focus of current chapter.

4.3.1 Water Movement during Infiltration

The non-uniformity of soil properties and water content and hysteresis of retention curves make the infiltration process a complex phenomenon. For a wetted column of soil there are a number of zones through which infiltration takes place. They can be summarized as

Saturated zone: a saturated layer about a centimetre in thickness at the ground surface.

Transition zone: a few centimetres in thickness shallow zone in which water content decreases drastically from top to bottom.

Transmission zone: a transmission of water from above two zones takes place in this zone with almost no change in water content.

Wetting zone: constitutes very steep moisture gradients with a significant change in water content with time.

Wetting front: characterized by very steep moisture gradients, this zone marks the limit between the wetted soil above and the dry soil below.

A changing pattern of infiltration alters the depth of wetted soil instead of continuously increasing the water content of surface layers. Figure 4-2 shows the schematic diagram of moisture zones during infiltration.

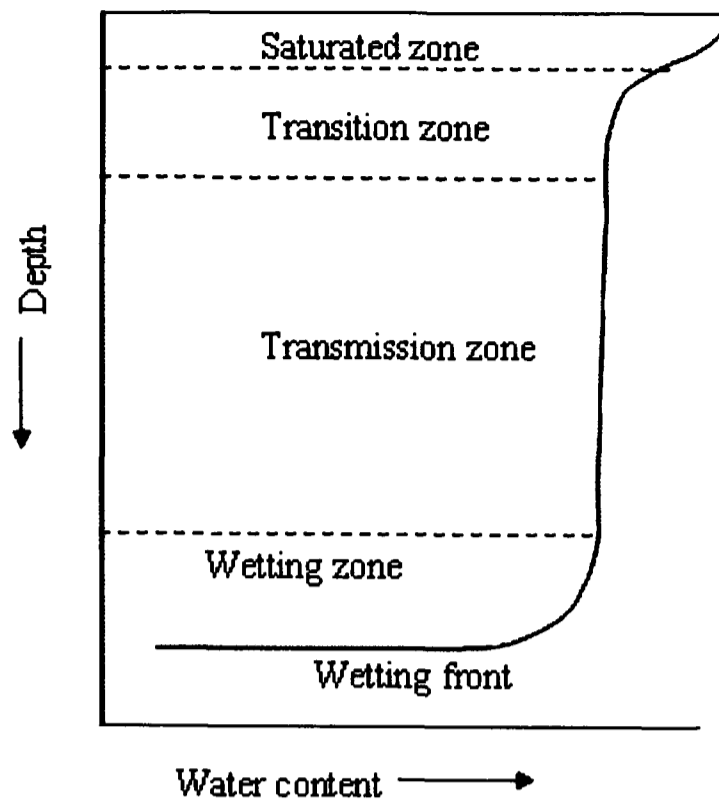


Figure 4-2. Moisture zones during ponded water infiltration. Source: Ward and Robinson [54].

4.3.2 Governing Flow Equations

Flow of water through anisotropic and non-homogeneous unsaturated zone can be described by combining extended form of Darcy's law with continuity equation. Darcy's law in mathematical form is

$$\begin{aligned}
 q_x &= -K_x(\theta) \frac{\partial h}{\partial x} = -K_x(\psi) \frac{\partial h}{\partial x} \\
 q_y &= -K_y(\theta) \frac{\partial h}{\partial y} = -K_y(\psi) \frac{\partial h}{\partial y} \\
 q_z &= -K_z(\theta) \frac{\partial h}{\partial z} = -K_z(\psi) \frac{\partial h}{\partial z}
 \end{aligned} \tag{4.3}$$

where q_x , q_y and q_z represent the flux in x, y and z-directions. K_x , K_y and K_z represent the unsaturated hydraulic conductivity [L/T] along the principal directions.

For an incompressible fluid and non-deformable media, the equation of continuity is given as

$$\frac{\partial \theta}{\partial t} = -\frac{\partial q_x}{\partial x} - \frac{\partial q_y}{\partial y} - \frac{\partial q_z}{\partial z} \tag{4.4}$$

Substitution of equation (4.3) into (4.4) implies

$$\frac{\partial \theta}{\partial t} = \frac{\partial}{\partial x} K_x(\psi) \frac{\partial h}{\partial x} + \frac{\partial}{\partial y} K_y(\psi) \frac{\partial h}{\partial y} + \frac{\partial}{\partial z} K_z(\psi) \frac{\partial h}{\partial z} \tag{4.5}$$

Using equation (4.1), equation (4.5) in terms of pressure head can be written as

$$\frac{\partial \theta}{\partial t} = \frac{\partial}{\partial x} K_x(\psi) \frac{\partial \psi}{\partial x} + \frac{\partial}{\partial y} K_y(\psi) \frac{\partial \psi}{\partial y} + \frac{\partial}{\partial z} K_z(\psi) \left(\frac{\partial \psi}{\partial z} + 1 \right) \quad (4.6)$$

For an isotropic medium equation (4.6) changes to

$$\frac{\partial \theta}{\partial t} = \text{div} \left(K(\psi) \text{grad}(\psi) \right) + \frac{\partial K(\psi)}{\partial z} \quad (4.7)$$

Equations (4.6) and (4.7) are called the mixed form of Richard's [63] equation as they contain two dependent variables θ and ψ . For one-dimensional vertical flow equation (4.7) reduces to

$$\frac{\partial \theta}{\partial t} = \frac{\partial}{\partial z} \left(K(\psi) \frac{\partial \psi}{\partial z} \right) + \frac{\partial K(\psi)}{\partial z} \quad (4.8)$$

If pressure head and water content are uniquely related then left hand side of equation (4.8) can be simplified to

$$\frac{\partial \theta}{\partial t} = \frac{\partial \theta}{\partial \psi} \frac{\partial \psi}{\partial t} = C(\psi) \frac{\partial \psi}{\partial t}$$

Then pressure-head based Richard's equation can be written as

$$C(\psi) \frac{\partial \psi}{\partial t} = \frac{\partial}{\partial z} \left(K(\psi) \frac{\partial \psi}{\partial z} \right) + \frac{\partial K(\psi)}{\partial z} \quad (4.9)$$

where $C(\psi)$ is the specific moisture capacity [1/L] and vertical distance z is assumed positive upward. The head-based formulation of the equation describing variably saturated flow in a compressible porous medium (Miller et al [21]) can be written as

$$\left[C(\psi) + S_a(\psi) S_s \right] \frac{\partial \psi}{\partial t} = \frac{\partial}{\partial z} \left(K(\psi) \frac{\partial \psi}{\partial z} \right) + \frac{\partial K(\psi)}{\partial z} \quad (4.10)$$

where S_s = specific storage [L^{-1}] and S_a = saturation of the aqueous phase [dimensionless].

A moisture-based Richard's equation can be derived from (4.8) by considering the following relationship

$$K(\psi) \frac{\partial \psi}{\partial z} = K(\psi) \frac{\partial \psi}{\partial \theta} \frac{\partial \theta}{\partial z} = \frac{K(\psi)}{C(\psi)} \frac{\partial \theta}{\partial z} = D(\theta) \frac{\partial \theta}{\partial z}$$

Equation (4.8) then implies

$$\frac{\partial \theta}{\partial t} = \frac{\partial}{\partial z} \left(D(\theta) \frac{\partial \theta}{\partial z} \right) + \frac{\partial K}{\partial z} \quad (4.11)$$

where $D(\theta)$ is the hydraulic diffusivity. All forms of Richard's equations described above are non-linear, parabolic and partial-differential equations and constitute complicated relationship among dependent variables θ , ψ and parameters K , C and D . Moisture-based form of the Richard's equation has major advantage to use that hydraulic diffusivity does not vary with moisture as much as unsaturated hydraulic conductivity varies with it. But there are various issues which have to be considered while dealing with this formulation which are described as follows

- Hydraulic diffusivity approaches to infinity as saturation is reached since $C(\psi)$ approaches to zero.
- Since $0 \leq \theta \leq \eta$, at saturation water content takes up the porosity values. Hence this equation is useful for describing flow in unsaturated zone only.
- For a non-homogeneous medium, this equation is not useful for describing soil parameters and their dependence on space coordinate.

4.3.3 Constitutive Relationships

The solution of equations describing flow in unsaturated zone requires the information concerning initial boundary conditions, geometry of the problem as well as the specification of physical properties, for instance, the hydraulic conductivity and the water content. Generally unsaturated hydraulic conductivity and pressure head are described as some non-linear functions of water content. Several models are available to express these relationships. The models proposed by van Genuchten [64] and Haverkamp et al [14] are presented here.

4.3.3.1 van Genuchten Model

$\theta - \psi$ Relationship

$$s_e = \begin{cases} \left[1 + |\alpha \psi|^n \right]^{-m} & ; \psi < 0 \\ 1 & ; \psi \geq 0 \end{cases} \quad (4.12)$$

where effective saturation S_e is given by

$$S_e = \frac{\theta - \theta_r}{\theta_s - \theta_r} \quad (4.13)$$

where α = thickness of capillary fringe [m^{-1}], n = pore size distribution [dimensionless], θ_r = residual water content [m^3/m^3] and θ_s = saturated water content [m^3/m^3].

$\theta - K$ Relationship

$$K(\psi) = \begin{cases} K_s S_e^{1/2} \left[1 - (1 - S_e^{1/m})^m \right] & ; \psi < 0 \\ K_s & ; \psi \geq 0 \end{cases} \quad (4.14)$$

where

$$m = 1 - \left(\frac{1}{n} \right)$$

4.3.3.2 Haverkamp Model

$\theta - \psi$ Relationship

$$\theta = \frac{\lambda(\theta_s - \theta_r)}{\lambda + |\psi|^\gamma} + \theta_r \quad (4.15)$$

$K - \psi$ Relationship

$$K = K_s \frac{A}{A + |\psi|^\beta} \quad (4.16)$$

where A , λ , β and γ are dimensionless parameters.

4.3.4 Initial and Boundary Conditions for Flow

4.3.4.1 Initial Conditions

In order to model transient soil water flow problems a specification of initial distribution of pressure head or water content at each point within the flow domain is required. This can be described as

$$\begin{aligned} \psi(z, 0) &= \psi_0, 0 \leq z < L \\ \theta(z, 0) &= \theta_0, 0 \leq z < L \end{aligned} \quad (4.17)$$

where L is the domain length and ψ_0 , θ_0 are some constant values of pressure head and water content at the time before the simulation take place. In case when these data are unavailable, water content at field capacity or those in equilibrium with the water table might be considered as the initial values.

4.3.4.2 Boundary Conditions

4.3.4.2.1 Lower Boundary

In unsaturated flow models the lower boundary is usually taken where the pressure head is at atmospheric pressure. The boundary conditions of type Dirichlet, Neumann or Cauchy can be defined there.

Dirichlet condition: A zero pressure head boundary

$$\psi(L, t) = 0 \quad (4.18)$$

or a prescribed pressure head

$$\psi(L, t) = \psi_1 \quad (4.19)$$

can be specified at the bottom boundary in order to present a constant water table level or a fixed position respectively.

Neumann condition: An impermeable layer or a free drainage at the lower boundary can be specified by a zero flux

$$\frac{\partial \psi}{\partial z} = 0 \quad (4.20)$$

or specified flux

$$K \frac{\partial \psi}{\partial z} = q \quad (4.21)$$

respectively. As the flux is always directed downward and vertical gradient $d\psi/dz = 1$ hence equation (4.21) transforms to

$$q = K \quad (4.22)$$

Thus the Darcian flux is equal to the hydraulic conductivity for a free drainage boundary.

Cauchy condition: The Cauchy type boundary condition can be used when unsaturated flow models are combined with regional groundwater or surface water flow models. A flux-fixed head relation at the lower boundary is obtained by writing the lower boundary flux as a function of the dependent variable. The coupling between the two systems is done by considering water table as an internal moving boundary.

4.3.4.2.2 Upper Boundary Condition

The upper boundary condition, i.e. the condition at the soil surface is specified as a prescribed pressure head to represent a water ponding condition or the region where flow enters (infiltration) or exits (evapotranspiration) the system or a flux boundary condition to specify a known flux rate to simulate infiltration.

4.3.5 Governing Transport Equations

To show the transport of contaminants subject to advection, dispersion, adsorption and radioactive decay through vadose zone the processes and equations described in sections 3.3.5 and 3.3.6 are used. The general form of conservative/reactive transport equation is given as

$$\frac{\partial(\theta RC)}{\partial t} + \theta \mathbf{v} \cdot \nabla C = \nabla \cdot (\theta D \cdot \nabla C) - \lambda \theta RC \quad (4.23)$$

where the form of retardation factor R depends on the choice of the adsorption isotherm used. The governing equations describing the volatilization in vadose zone are however discussed here in detail.

4.3.5.1 Volatilization

The process of volatilization involves partitioning of organic chemicals from solid or liquid into gas or vapour phase. It is recognised as one of the major transport processes that causes groundwater contamination as a result of leaching from hazardous waste landfills or the distribution of agricultural pesticides in soils. Several physical and chemical factors contribute in controlling the volatilization of chemicals from soils. The tendency of organic contaminants to volatilize depends on the weather conditions and the structure of the chemical. The former leads to great volatilization losses under warm and wet condition and very little in case of cool and dry weather in soils with high clay content or organic matter. The latter performs an important role in determining the vapour pressure, adsorptivity and solubility in soil water.

4.3.5.1.1 Volatilization Model

The governing equations for transport mechanism subject to volatilization are expressed as (Jury et al [65])

$$\frac{\partial C}{\partial t} = D \frac{\partial^2 C}{\partial z^2} - V \frac{\partial C}{\partial z} - \lambda C \quad (4.24)$$

$$C = R_L C_L = R_G C_G$$

where C_L = concentration in the liquid, C_G = concentration in the gas and C is the total concentration of chemical in liquid, gas and solid phases per unit volume of soil. The coefficients R_L and R_G are expressed as

$$R_L = \rho_b K_{SL} + \theta + (\eta - \theta) K_H + \rho_b K_H K_{SG} \quad (4.25)$$

and

$$R_G = \frac{R_L}{K_H} = \rho_b \frac{K_{SL}}{K_H} + \frac{\theta}{K_H} + (\eta - \theta) + \rho_b K_{SG} \quad (4.26)$$

respectively. The value of parameter K_{SL} , which represents the solid-liquid distribution coefficient, can be calculated from the relationship

$$K_{SL} = K_{oc} f_{oc} \quad (4.27)$$

where K_{oc} = partition coefficient [L^3/M^3] and f_{oc} = fraction of organic carbon [dimensionless]. The value of K_{SG} (solid-gas distribution coefficient), on the other hand, is estimated from laboratory tests. The overall pore velocity V given in equation (4.24) is defined as the sum of Darcy's velocities of the liquid and gas phases as follows

$$V = \frac{v_L}{R_L} + \frac{v_G}{R_G} \quad (4.28)$$

The dispersion coefficients in the liquid and gas phases are calculated from the dispersivities and molecular diffusion coefficients in the liquid and gas phases respectively as

$$D_L = \alpha_L v_L + D_{LM}$$

$$D_G = \alpha_G v_G + D_{GM}$$

where the subscripts L and G represent liquid and gas phases respectively and M stands for molecular.

Molecular diffusion coefficients can be estimated by a formula presented in Shoemaker et al. [66] as

$$D_{LM} = \frac{\theta^{10/3}}{\eta^2} D_w \quad (4.29)$$

and

$$D_{GM} = \frac{(\eta - \theta)^{10/3}}{\eta^2} D_a \quad (4.30)$$

The subscripts w and a stand for water and air respectively. The overall dispersion coefficient given in equation (4.24) is then defined as

$$D = \frac{D_L}{R_L} + \frac{D_G}{R_G} \quad (4.31)$$

4.3.5.1.2 Volatilization Subject to Gas-phase Advection

To study the effect of gas-phase advection, the Darcy velocity of the gas phase in the vadose zone is estimated by the formula

$$v_G = \frac{k(\rho_G - \rho_A)g}{\mu} \quad (4.32)$$

where k and μ are the permeability and viscosity of gas phase respectively. The density of air-VOC mixture can be calculated using Amagat model (Sonntag and van Wylen [67]) given as

$$\rho_G = \left(1 - \frac{C_G}{\rho_{VOC}}\right) \rho_A + C_G \quad (4.33)$$

where ρ_{VOC} is the density of the VOC vapour which is calculated from the expression

$$\rho_{VOC} = \frac{M_{VOC}}{M_A} \rho_A \quad (4.34)$$

where M_A = molecular weight of air and M_{VOC} = molecular weight of VOC. Substitution of equation (4.34) into (4.33) implies

$$\rho_G - \rho_A = \left(1 - \frac{M_A}{M_{VOC}}\right) C_G \quad (4.35)$$

Replacing C_G by C/R_G and substituting from equation (4.35) into (4.32) we obtain

$$v_G = \left(1 - \frac{M_A}{M_{VOC}}\right) \frac{kgC}{\mu R_G} \quad (4.36)$$

Equation (4.36) indicates that the gas advection velocity is proportional to the total concentration which is a variable quantity.

4.4 Numerical Simulations and Validations

The well established commercial code Physica and its CFD algorithm and solvers described in chapter 2 have been used to model continuum physical processes of flow and transport in vadose zone over unstructured domains. The results of numerical simulations performed are discussed separately as flow and transport models to describe fluid flow problems and the fate of contaminants with realistic features, as would be encountered in actual field situations.

4.4.1 Flow Modelling

Flow modelling involves description of flow in unsaturated porous media for homogeneous soils. One-dimensional unsteady equation of flow is solved by employing control volume methods taking diffusion and source (contribution from gravity) terms into account. In order to validate the correct implementation of Richard's equation for compressible and incompressible fluids and VG and Haverkamp models to examine the constitutive relationship between flow variables parameters, the following test cases are performed

Section (4.4.1.1) Flow field analysis subject to infiltration

Section (4.4.1.2) Sensitivity analysis of flow parameters

4.4.1.1 Flow Field Analysis Subject to Infiltration

One-dimensional flow models are developed for predicting vertical flow in unsaturated zone of the homogeneous soil. The constructed models are based on the pressure head form of Richard's equation which is capable of coupling the unsaturated flow with the saturated flow model. The numerical solutions presented here describe the development of the water content profile during constant infiltration and are capable of predicting the time dependence of both soil water content and soil matric potential. Figure 4-3 represents the geometrical representation of flow through vadose zone.

4.4.1.1.1 Case 1

This test case involves investigation of infiltration into initially dry soils governed by equation (4.9). VG model as described in section 4.3.3.1 is used to evaluate the constitutive relationships for a vertical column of soil with 1 metre thickness.

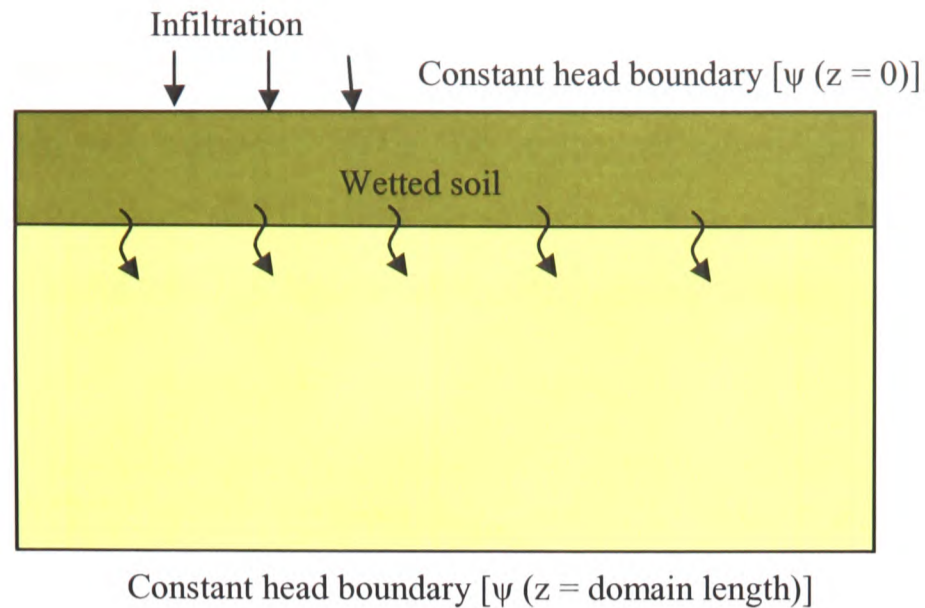


Figure 4-3. Graphical representation of flow processes under infiltration.

The initial and boundary conditions specified for the relevant grid node are given as follows

$$\psi(z, 0) = -10m, \quad 0 \leq z \leq 1.0m$$

$$\psi(0, t) = -10m$$

$$\psi(1.0, t) = -0.75m$$

The parametric values used are

$$\alpha = 3.35m^{-1}, \theta_s = 0.368, \theta_r = 0.102, n = 2, K_s = 9.22 \times 10^{-5}ms^{-1}$$

The results of one day simulations (Figure 4-4) are compared with Celia et al [15]. The dense grid solution with $\Delta t = 1$ second and $\Delta z \approx 0.0021mm$ gives a very close match. The effects of bigger time step and node spacing are also presented. The increase in Δt and Δz has been observed to under predict the infiltration depth.

4.4.1.1.2 Case 2

The second case computes infiltration into an unsaturated sand column with a depth $L = 120$ cm. The flow process is governed by equation (4.9) and the constitutive relationships are evaluated using Haverkamp model as described in section 4.3.3.2. The initial and boundary conditions are as follows

$$\psi(z, 0) = -61.5cm \quad (\theta = 0.10cm^3/cm^3)$$

$$\psi(0, t) = -20.73cm \quad (\theta = 0.267cm^3/cm^3)$$

$$\psi(L, t) = -61.5cm$$

The simulation results of water content profile (Figure 4-5) at three different times are compared with quasi-analytical solution by Philip and numerical methods solution presented by Gottardi and Venutelli [29]. The results of numerical simulations run by Physica are almost coincident and in good agreement with quasi-analytical solution. The good match obtained confirms the validity of the numerical methods used.

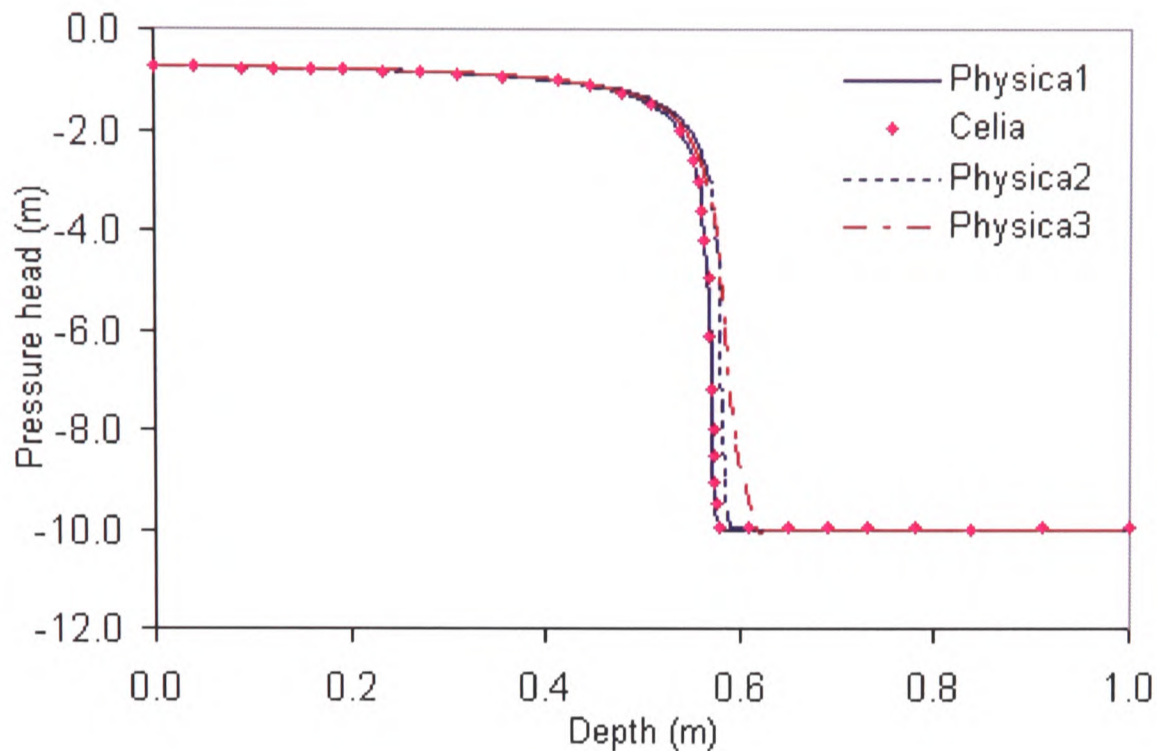


Figure 4-4. Comparison of results for case 1. Physica 1 ($\Delta t = 1$ sec, $\Delta z \approx 0.0021$ mm), Physica 2 ($\Delta t = 1$ min, $\Delta z \approx 0.0021$ mm), Physica 3 ($\Delta t = 1$ sec, $\Delta z \approx 1.11$ mm).

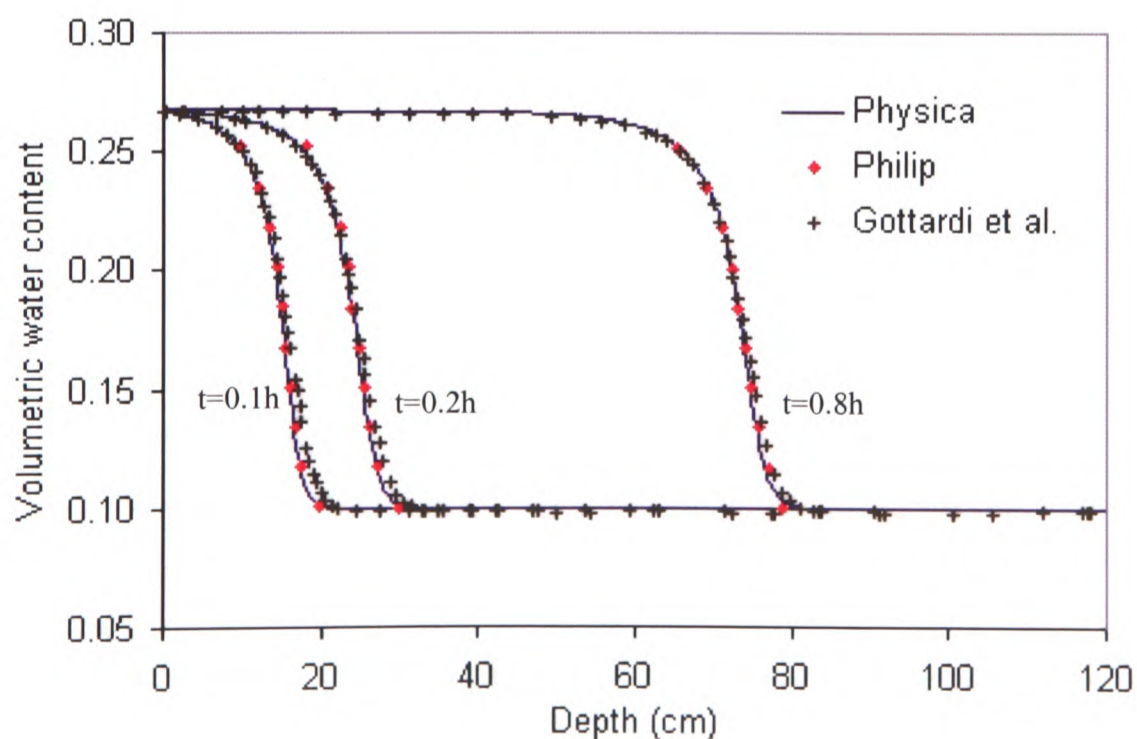


Figure 4-5. Water content profile for case 2 at times: 0.1, 0.2 and 0.8 hours.

4.4.1.1.3 Case 3

The last case considers infiltration into variably saturated media from ponded surface boundary condition (Miller et al [21]). The flow process in this case is governed by equation (4.10) and the constitutive relationships are evaluated using VG model as described in section 4.3.3.1. The chosen material parameters are those correspond to the average values for the loam and clay loam soil textural groups according to the USDA classification (van Genuchten and Leij [68]).

One-dimensional vertical columns of soil discretized into 400 nodes for loam material and 320 nodes for clay loam soil are used to perform a set of dense grid simulations. The material properties and spatial and temporal domain information for the two soil materials are listed in Table 4-2. The initial and boundary conditions are

$$\begin{aligned}\psi(z, t = 0) &= \psi_0(z) \\ \psi(z = 0, t > 0) &= \psi_1 \\ \psi(z = Z, t > 0) &= \psi_2\end{aligned}$$

where Z is the length of domain. ψ_0 , the initial pressure, is the function of space. ψ_1 and ψ_2 are constants.

The solutions of dense-grid simulations as shown in Figure 4-6 a & b illustrate a sharp infiltration front between unsaturated and saturated zones. A comparison of numerical results is made for pressure profiles with Miller et al. [21]. Water content and conductivity profiles are also presented in Figure 4-7a & b for the two materials.

Material type	θ_r	θ_s	α m ⁻¹	n	K_s ms ⁻¹	z m	t days	ψ_0 m	ψ_1 m	ψ_2 m	S_s m ⁻¹	Δz m
Loam	0.078	0.43	3.6	1.56	0.250	5.0	2.25	-z	0	0.1	1.0×10^{-6}	0.013
Clay loam	0.095	0.41	1.9	1.31	0.062	2.0	1.0	-z	0	0.1	1.0×10^{-6}	0.006

Table 4-2. Case 3 parameters.

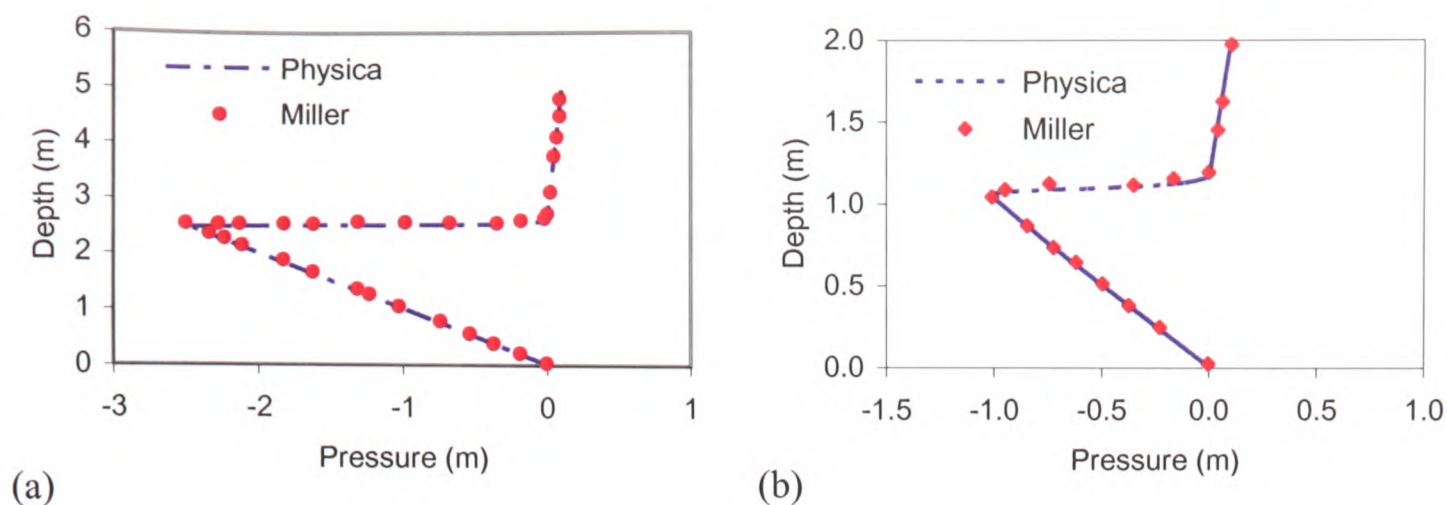


Figure 4-6. Pressure head profile for case 3 for (a) loam, (b) clay loam soil texture.

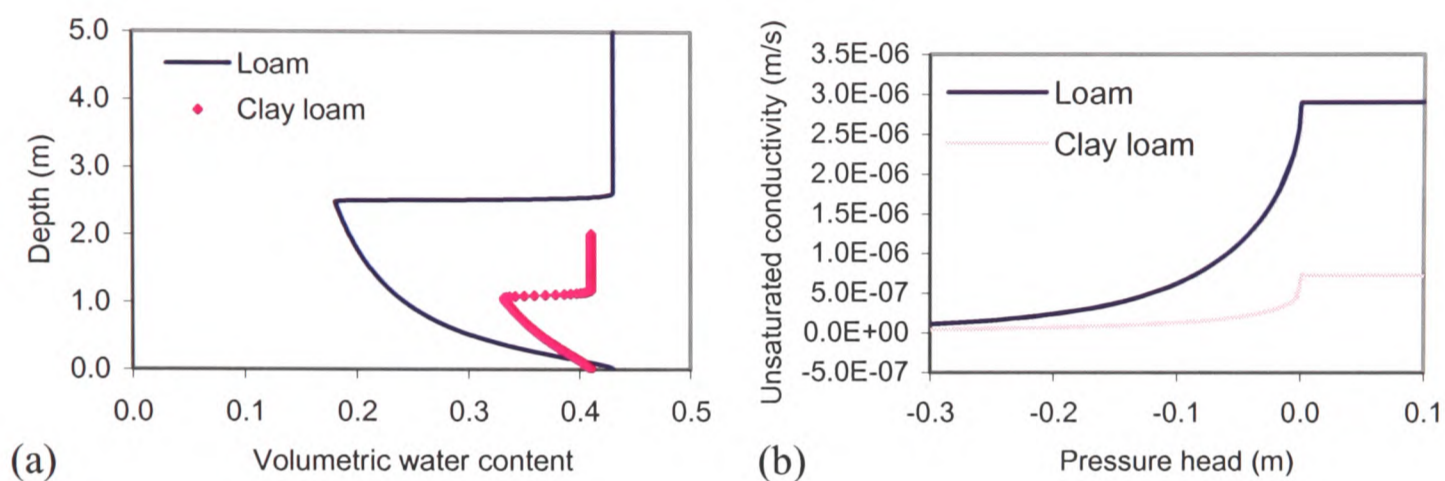


Figure 4-7. Water content (a) and unsaturated conductivity (b) profiles for loam and clay loam materials.

4.4.1.2 Sensitivity Analysis of Flow Parameters

To investigate the sensitivity of flow parameters used in VG model to the moisture movement through vadose zone, a sensitivity analysis is performed by undertaking the problem presented in case 1 section 4.4.1.1. The soil parameters considered in this study are capillary fringe thickness α and pore size distribution n whose values are varied over a range which covers most field soils. In order to judge the effects of these parameters the flow problem is examined for:

- Consistency of moisture gradients
- Depth of wetting front
- Variations in hydraulic conductivity

Effect of parameter α

The effect of parameter α is examined by varying its value from 2.0 to 3.35 m^{-1} while the other soil parameters of saturated hydraulic conductivity, saturated and residual water

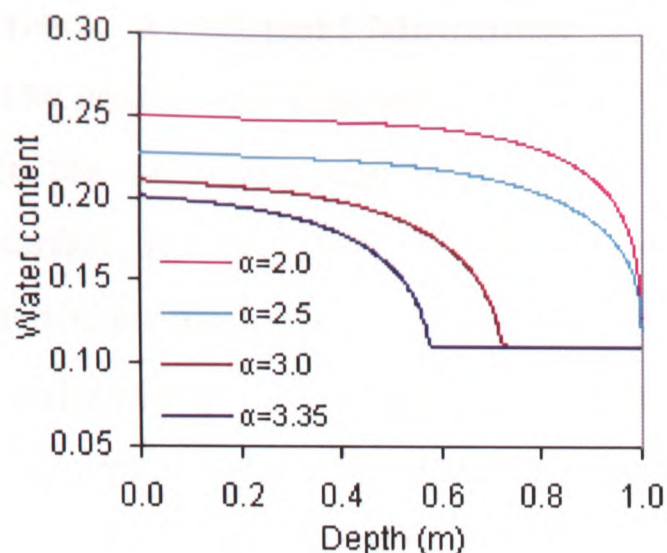
content and pore size distribution are kept constant. Figure 4-8a shows the moisture profile after one day infiltration at different values of α . A low value of α corresponds to a soil that has large capillary fringe thickness. Such soils are capable of storing and retaining less amount of water due to insufficient capillary forces. This fact is evident from Figure 4-8a which shows greater values of moisture content for lower values of α . A decrease in α tends to vary moisture gradients from uniform to steeper over the major portion of the soil column.

Figure 4-8c shows pressure head profile for different values of α . It can be seen that a decrease in α moves the wetting front to a greater depth which is due to the fact that the soils with larger capillary fringe thickness drain quickly as compared to the soils with small capillary fringe thickness. Movement of wetting front during infiltration is highly dependent on the hydraulic conductivity. Since hydraulic conductivity decreases with an increase in α (Figure 4-8e) the wetting front moves at slower rates as the value of α increases.

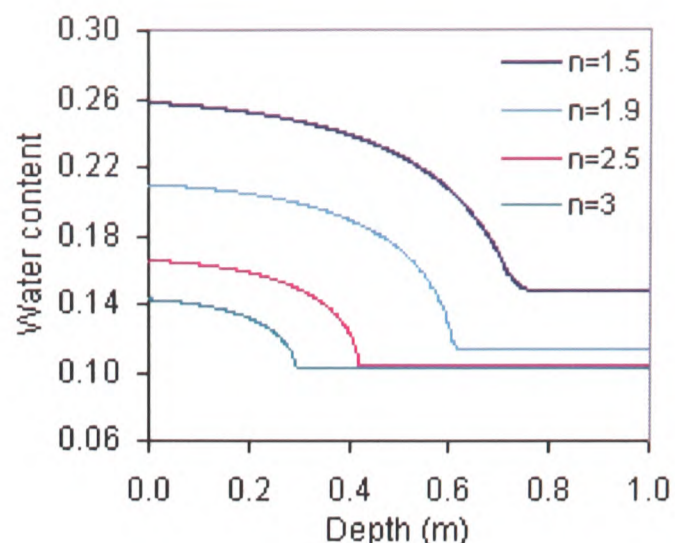
Effect of parameter n

The effect of parameter n is examined by varying it from 1.5 to 3.0 while keeping all other soil parameters to be constant. Figure 4-8b presents the water content profile for different values of n . As the width of pore size distribution increases the ability of soil to retain water decreases. Soils with low values of n contain small pores which are difficult to drain due to large viscous effects. It is observed that the moisture gradients are non-uniform and steeper with small values of n near the soil surface.

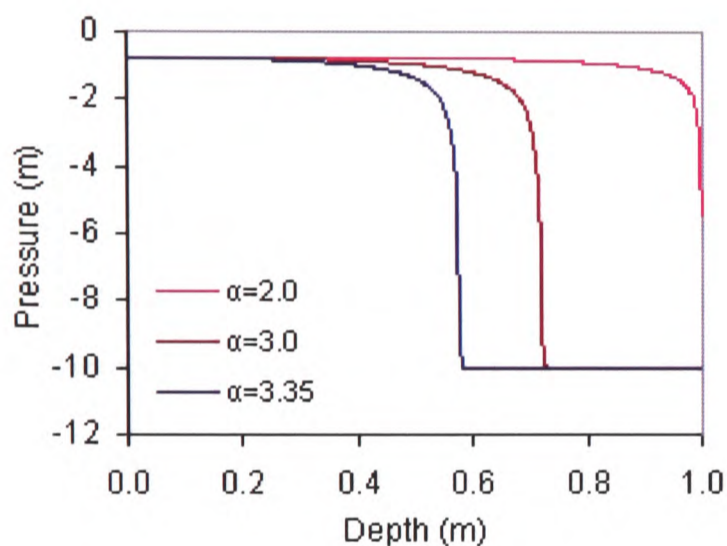
Figure 4-8d shows movement of wetting front for different values of n after one day simulations. An increase in the value of n causes a decrease in movement of wetting front. It is also evident that the soils with higher values of n possess sharp pressure gradients occurring near the soil surface. As the soil gets wetted, depending on initial pressure head applied a decrease in hydraulic conductivity (Figure 4-8f) is also observed with increase in the pore size distribution.



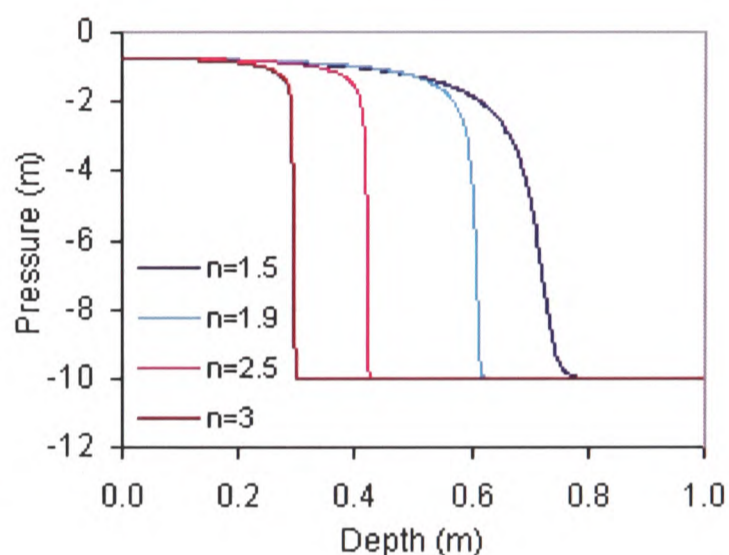
(a). Water content profile at different capillary fringe thickness values.



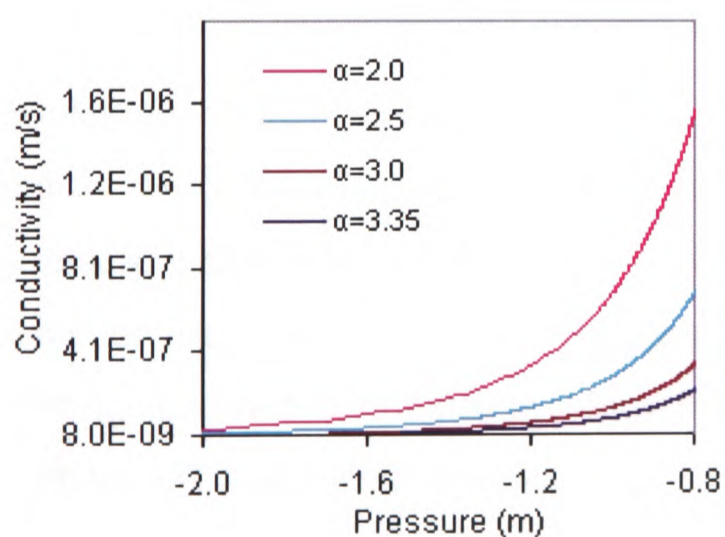
(b). Water content profile at different pore size distribution values.



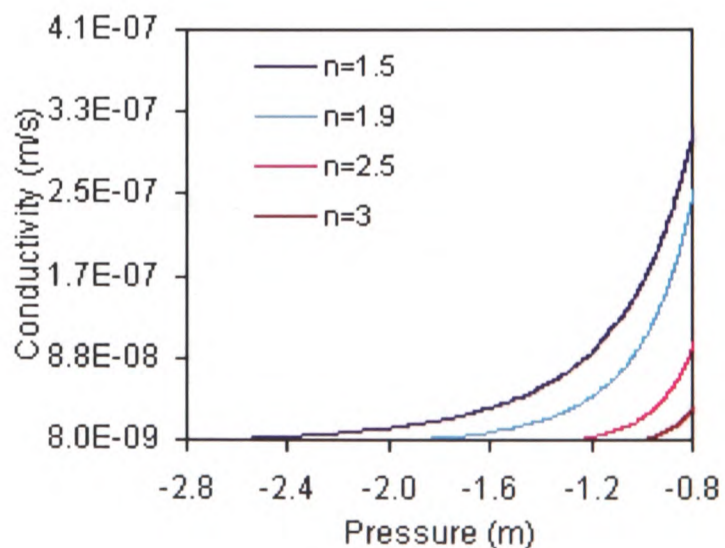
(c). Pressure profile at different capillary fringe thickness values.



(d). Pressure profile at different pore size distribution values.



(e). Conductivity profile at different capillary fringe thickness values.



(f). Conductivity profile at different pore size distribution values.

Figure 4-8. Flow profiles for sensitivity analysis.

4.4.2 Transport Modelling

The unsaturated zone plays a crucial role in the fate and transport of pollutants entering in the underlying aquatic systems. The pollutants present in water reaching ground surface, leaching from landfill sites, spills of chemicals at industrial sites, application of fertilizers and pesticides at agricultural sites and leakage of septic tanks and drains serve as the examples of sources of contaminants travelling through the unsaturated zone into the groundwater. The appropriate prediction of the movement and accumulation of contaminants in vadose zone is therefore essential in order to evaluate risk of groundwater pollution. Numerically based simulators can play a key part in improving understanding of fate of contaminants and prediction of future states under various loading scenarios. The effectiveness of the proposed numerical methodologies to correctly model the transport phenomena through vadose zone is described by means of various case scenarios in this section. Numerical simulations of conservative and reactive transport of solutes are calibrated for one and two-dimensional problems to examine the migration of leachate entering in the unsaturated zone from point or dispersed contaminant sources by considering the following

Section (4.4.2.1) Transport of conservative contaminants

Section (4.4.2.2) Transport of reactive contaminants

4.4.2.1 Transport of Conservative Contaminants

4.4.2.1.1 Pure Advection at Constant Velocity

Modelling of pure advection is one of the most complicated phenomena of solute transport problem. The principal difficulty in the solution comes from the introduction of artefacts which destroy the shape of concentration profiles when simple advection schemes are used (McGrail [69]). Searching for a suitable differencing scheme for solving advection-dominated problems has been the subject of intense study for several decades (McGrail [69], Zalesak [32], Gupta et al. [33]). Studies has shown that the problems of numerical diffusion and artefacts can be overcome by employing higher order schemes such as total variation diminishing (TVD) and flux-corrected transport (FCT) for approximating the advective term.

This section presents a specific example to analyse various advection schemes to assess their applicability to transport processes in porous media. Simulations are carried out for two linear schemes; Upwind and Quick and two TVD schemes; SMART and Van Leer. The problem considered involves transport of a solute through a soil column of 2 metres deep at constant velocity of 0.5 m/day. The initial concentration is set at 1 Kg/m³ at a source 15 cm in thickness at land surface. The transport mechanism is governed by equation (3.35) considering $D = 0$. In mathematical form the initial and boundary conditions are expressed as

$$\left. \begin{aligned} C(z, 0) &= 1, & 0 < z \leq 0.15 \\ C(z, 0) &= 0, & 0.15 < z \leq L \\ C(0, t) &= 0 \\ -D_m \frac{\partial C}{\partial z} \Big|_{z=L} &= 0 \end{aligned} \right\}, \quad 0 < t \leq t_{\max}$$

The simulated concentrations in Physica (Figure 4-9) for four differencing schemes are compared with the analytical solution and results from literature (McGrail [69]). The Upwind differencing scheme is bounded and stable but for the current 1-d problem it produces numerical dispersion which is generated due to the truncation error in terms of Fourier series expansion. This results in spreading of the original square wave shape of solute as it translates. 3rd order accuracy of quick differencing scheme helps minimizing the errors of false diffusion but suffers from the boundedness problem and produces undershoots and overshoots at leading and trailing edges. The generated negative concentrations are non-physical. TVD schemes have been formulated by using a flux limiter which enforces a boundedness criteria based on the local solution behaviour. Two of the TVD schemes used proved to be the best suitable for current advection-dominated problem to achieve the oscillation free solution.

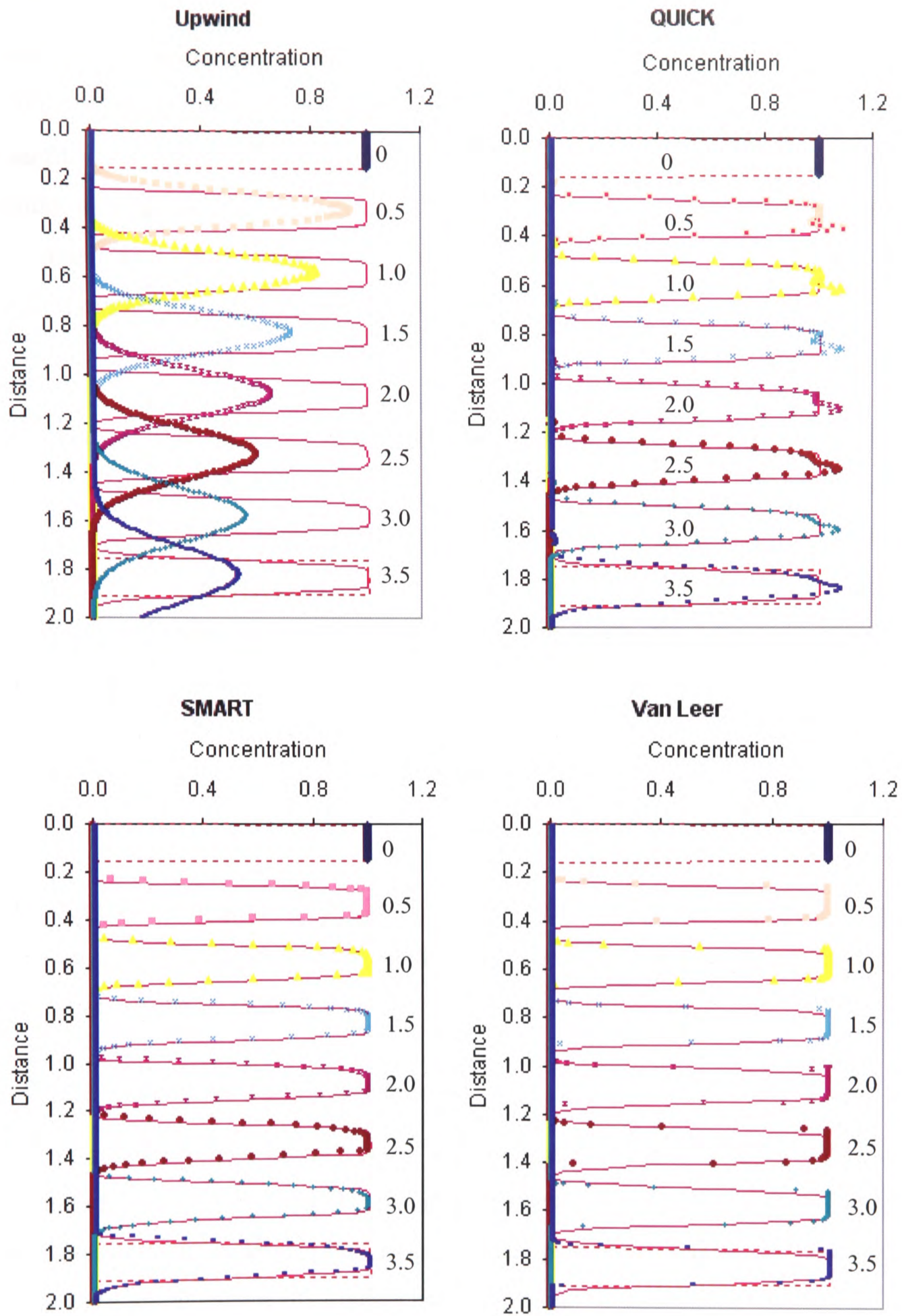


Figure 4-9. Concentration Profiles at 0, 0.5, 1, 1.5, 2, 2.5, 3 and 3.5 days. Symbols, solid lines and broken lines represent Physica, McGrail and analytical solutions respectively.

4.4.2.1.2 Pure Advection at Darcy Velocity

Transport of solute species through vadose zone takes place at the velocity of soil water which being a function of water content and unsaturated conductivity is a variable quantity. Coupling between fluid flow and solute transport equation in vadose zone results in non-linearities which arise firstly due to non-linear relationship between flow variables and soil parameters and secondly through the velocity dependent hydrodynamic dispersion and advection terms.

To illustrate the transport of contaminants at the Darcy velocity the flow problem discussed in case 1 of section 4.4.1.1 is adopted by considering a steady state solute plume that originates from a continuous solute source of constant concentration. The transport mechanism is governed by equation (3.35) considering $D = 0$. The initial and the boundary conditions are the same as described for the last case. The results of 10 days simulation for concentration profiles at constant and Darcy velocity and pressure profile at which Darcy velocity largely depends are presented at different times in Figure 4-10.

The concentration profile at Darcy velocity displays slow transport of contaminants depending on the moisture movement of the porous medium under infiltration due to dry initial conditions.

4.4.2.1.3 Advection and Dispersion

The combined effect of advection and dispersion phenomena at Darcy velocity is presented in Figure 4-11 for the previous problem. To account for the effects of changes in dispersion and molecular diffusion rates the parametric values are varied over a small range for a given source of constant concentration.

Simulation results show that at small dispersion and molecular diffusion rate the dilution and spread in the concentration is smaller over time as compared to the higher dispersion and molecular dispersion rate.

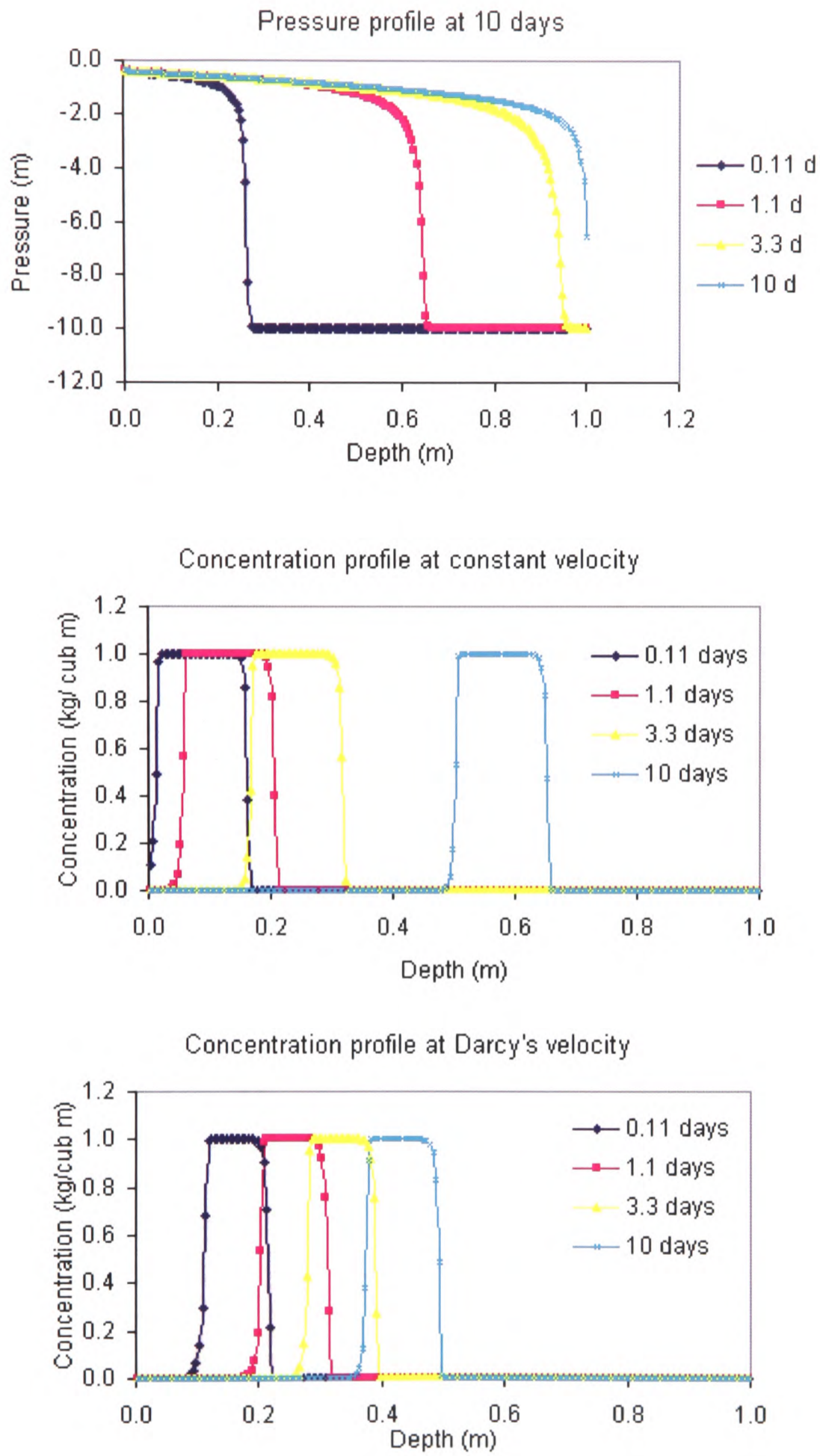


Figure 4-10. Pure advection of solutes at constant and Darcy velocity.

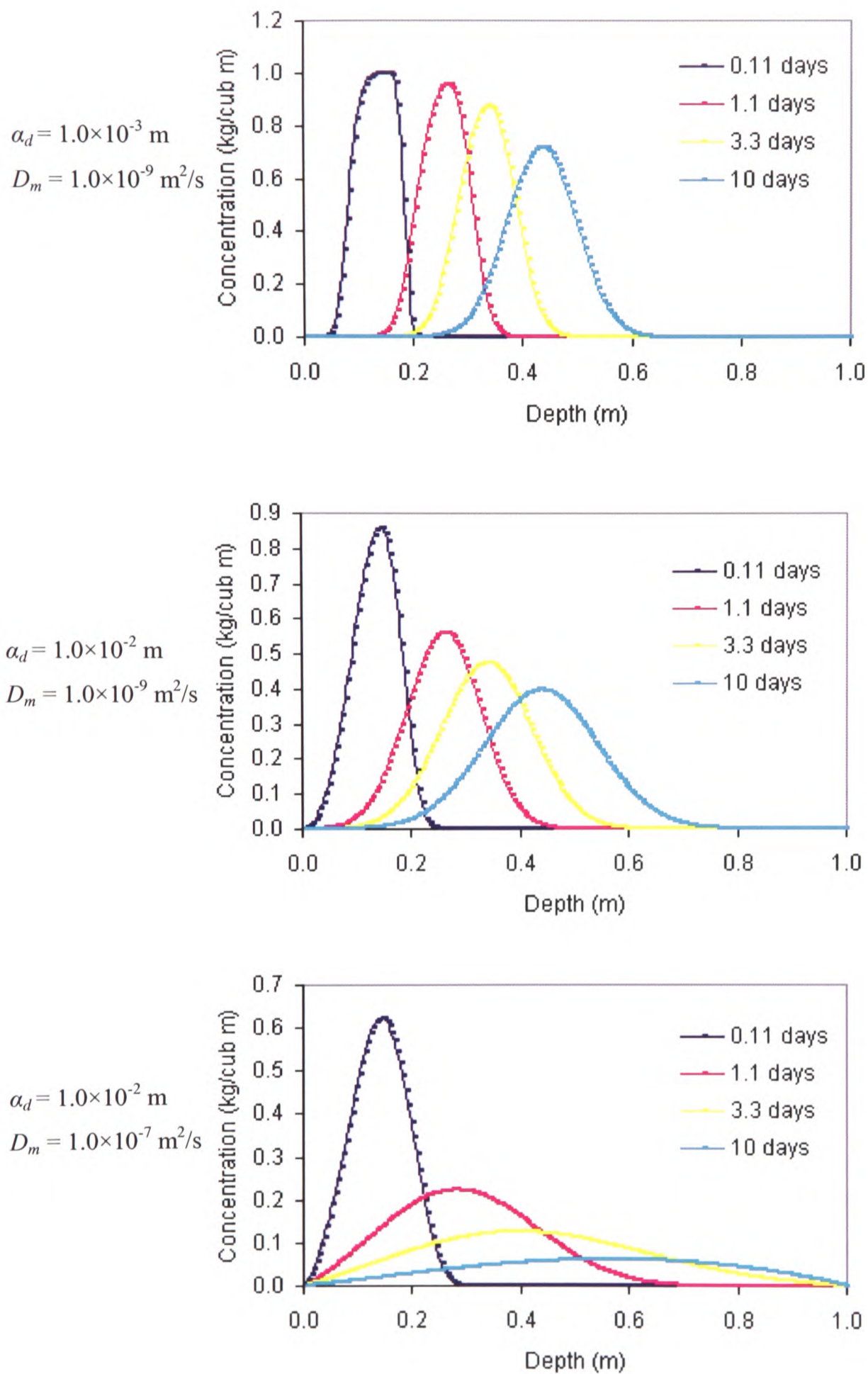


Figure 4-11. Advection and dispersion of solutes at Darcy's velocity.

4.4.2.2 Transport of Reactive Contaminants

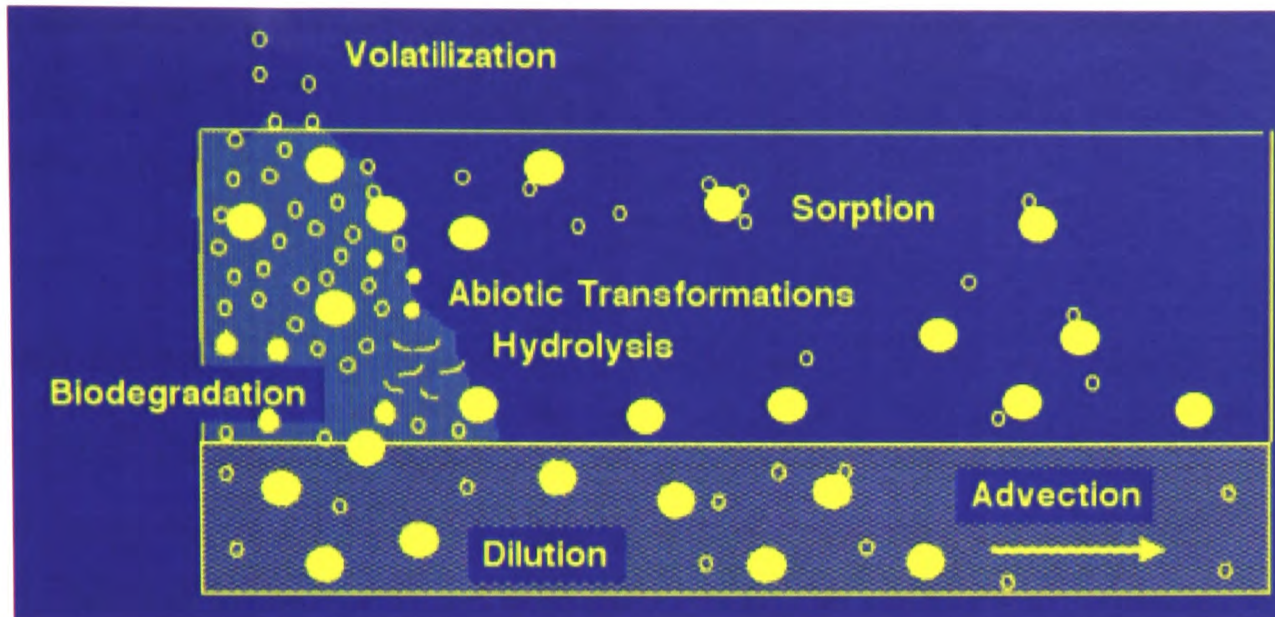


Figure 4-12. Fate of organic contaminants in subsurface.

4.4.2.2.1 Adsorption

Adsorption isotherms described in chapter 3 have been implemented and validated with analytical solutions and numerical results available in literature for the transport of reactive solutes in vadose zone. A comprehensive set of test cases has been performed with Physica for the purpose of verifying that the numerical methods correctly approximate the governing equation describing equilibrium and non-equilibrium adsorption.

Linear isotherm

Solute concentration profiles for one-dimensional linear adsorption model presented by equations (4.23) and (3.40) are obtained for this test case. The material properties considered for advection-dispersion problem are

$$D = 1.16 \times 10^{-6}, v = 5.787 \times 10^{-6}, \eta = 1.0, \rho_b = 1.0, L = 1.0$$

The results are compared with the analytical solution (Bear [70])

$$C(x,t) = \frac{C_0}{2} \operatorname{erfc} \frac{x-vt/R}{\sqrt{4Dt/R}} + e^{vx/D} \operatorname{erfc} \frac{x+vt/R}{\sqrt{4Dt/R}}$$

with initial and boundary conditions given as

$$\begin{aligned}
 &C(x, 0) = 0, 0 \leq x \leq L \\
 &\left. \begin{aligned}
 &C(0, t) = 1 \\
 &-D \frac{\partial C}{\partial x} \Big|_{x=L} = 0
 \end{aligned} \right\}, 0 < t \leq t_{\max}
 \end{aligned}$$

The results presented in Figure 4-13 show the concentration profile with six different K_d values. The contaminant concentration for $K_d = 0$ is compared with the corresponding analytical solution.

Langmuir isotherm

A set of cases have been considered in this example by accounting for Langmuir isotherm using equations (4.23) and (3.42). The material properties for these cases are shown in Table 4-3. The initial and boundary conditions are given as follows

Case I & II

$$\begin{aligned}
 &C(x, 0) = 0, 0 \leq x \leq 10 \\
 &\left. \begin{aligned}
 &C(0, t) = 1 \\
 &-D \frac{\partial C}{\partial x} \Big|_{x=10} = 0
 \end{aligned} \right\}, 0 < t \leq t_{\max}
 \end{aligned}$$

Case III

$$\begin{aligned}
 &C(x, 0) = 0, 0 \leq x \leq 10 \\
 &\left. \begin{aligned}
 &C(0, t) = 1 \\
 &C(x = 10, t) = 0
 \end{aligned} \right\}, 0 < t \leq t_{\max}
 \end{aligned}$$

For case I the simulated concentration in Physica for three differencing schemes is compared with the analytical solution presented by Sheng and Smith [71] (Figure 4-14). The effects of numerical dissipation and spurious oscillations are observed to be suppressed by the use of TVD scheme (Van Leer). A retardation in solute migration under the influence of equilibrium adsorption isotherm being considered is observed as shown in Figure 4-14b.

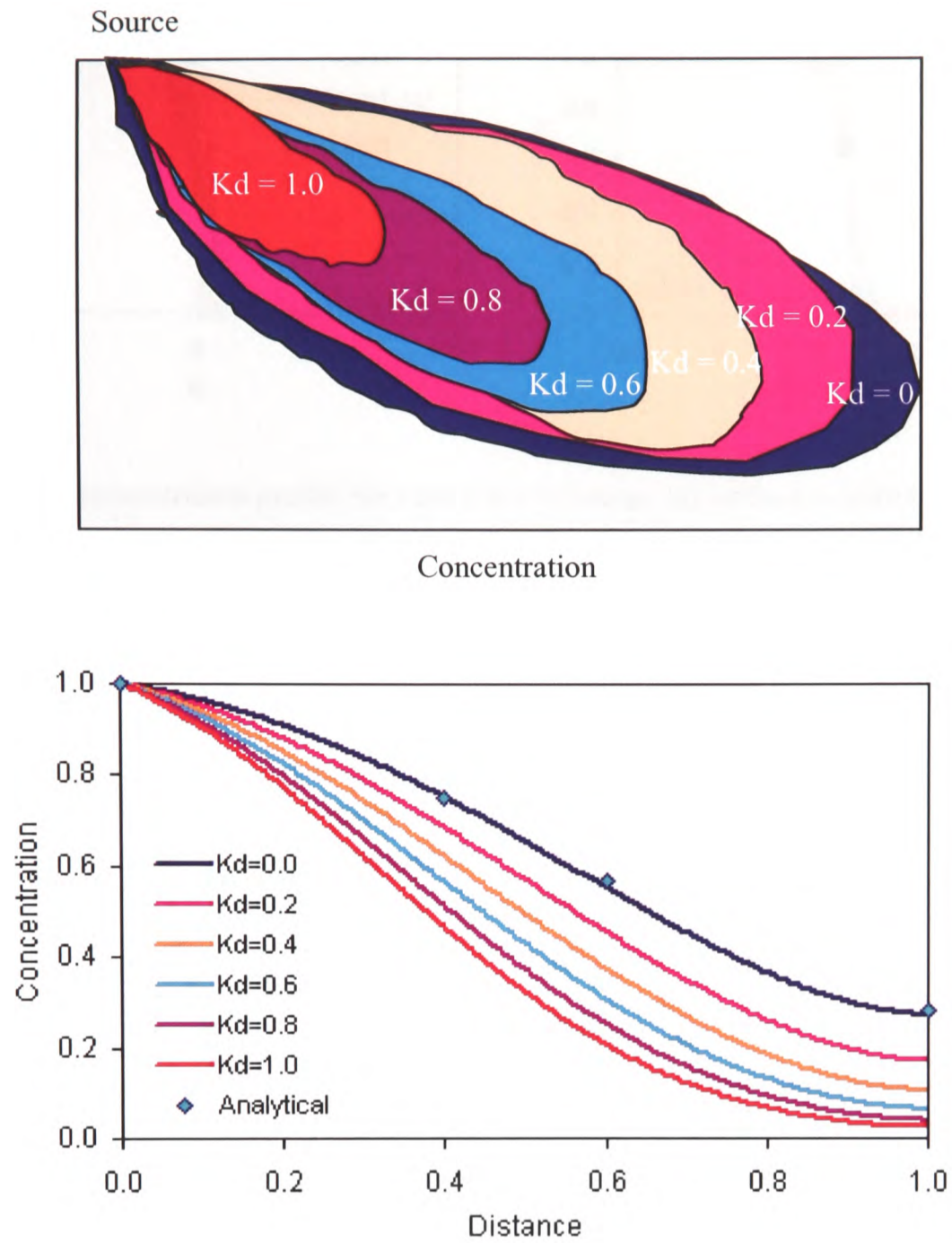


Figure 4-13 Concentration profile at 1 day for different K_d values.

Case	η	ρ_b	ν	D	Transport type
I	0.5	1.5	1.157×10^{-5}	0.0	Pure advection
II	0.5	1.5	1.157×10^{-5}	1.157×10^{-6}	Advection-diffusion
III	0.5	1.5	0.0	1.157×10^{-6}	Pure diffusion

Table 4-3. Material properties for Langmuir isotherm.

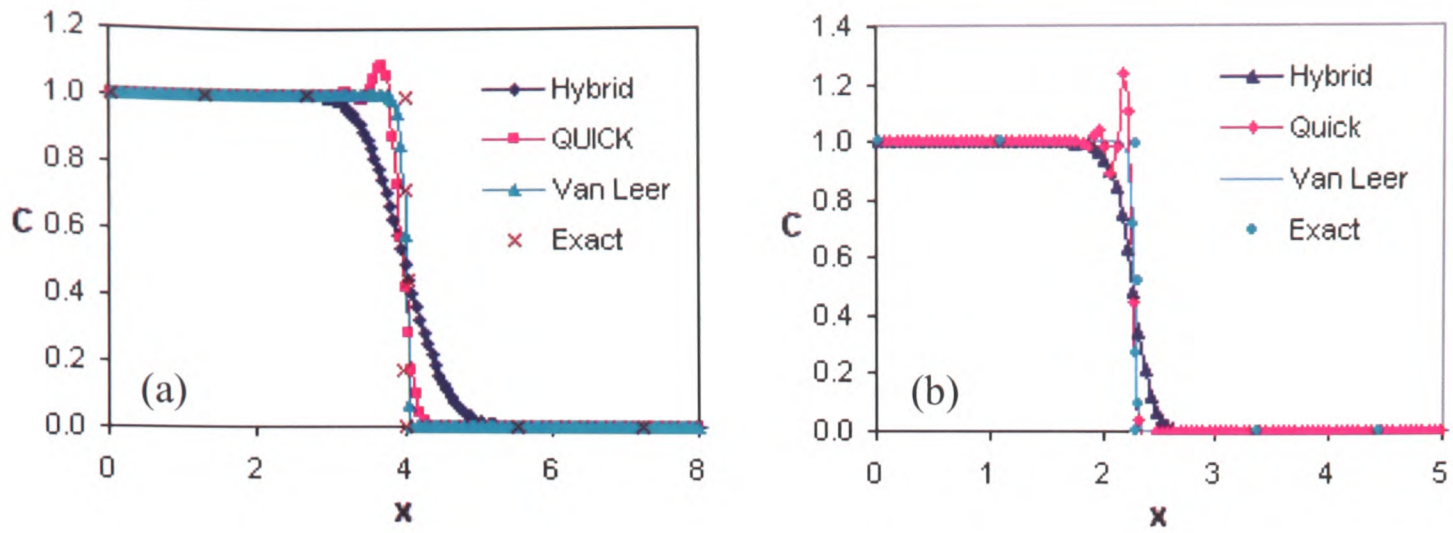


Figure 4-14. Concentration profile for case I at $t = 2$ days. (a) without adsorption, (b) with adsorption.

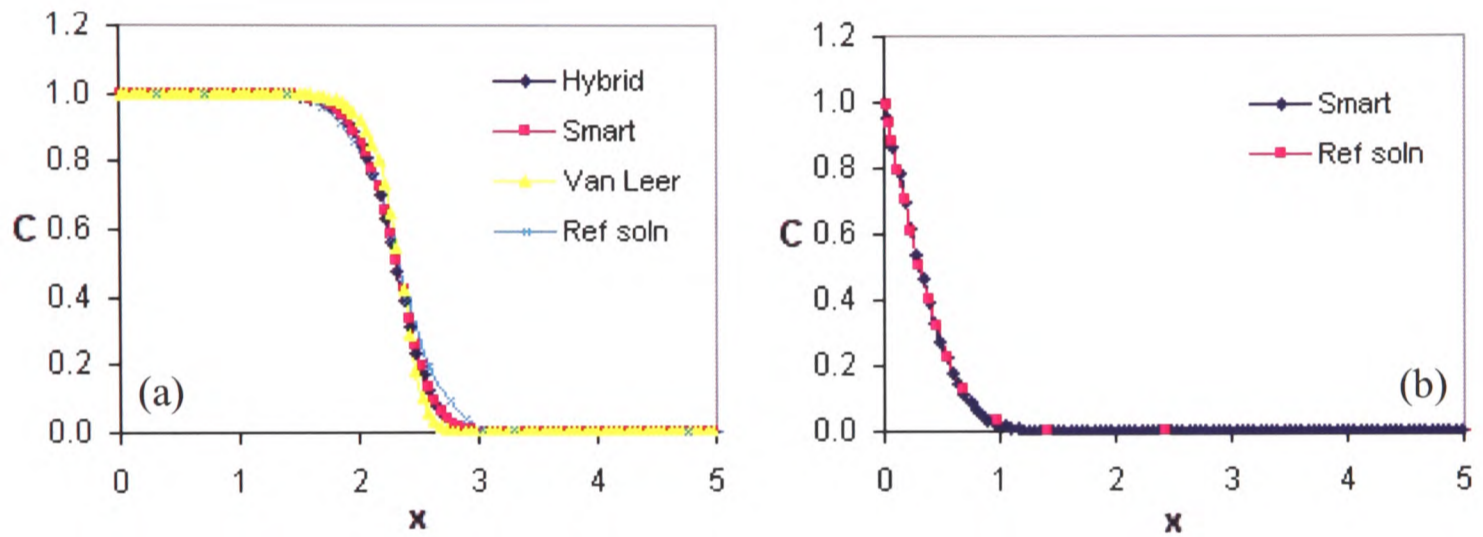


Figure 4-15. (a) Concentration profile for case II, (b) concentration profile for case III at $t = 2$ days.

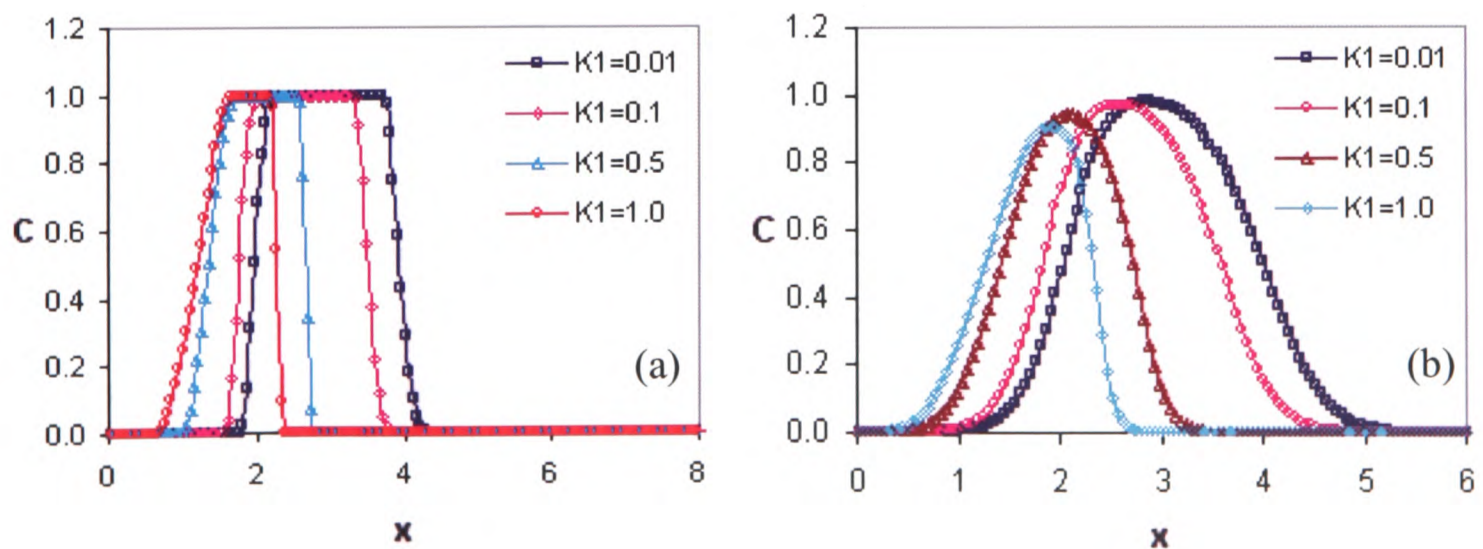


Figure 4-16. Contaminant distribution for different values of the Langmuir parameter K_1 .

The concentration profiles for advection-dispersion and pure dispersion cases are compared with reference solution presented by Sheng and Smith [71] in Figure 4-15a & b respectively. The sensitivity of Langmuir parameter K_1 which is related to the adsorbate bond strength is examined by varying its value over a range 0.01-1.0. The shape of the plume appears to be quite sensitive to the size of non-linearity for both case I and II. As the value of K_1 decreases in magnitude, there is less sorption at higher concentrations as can be seen in Figure 4-16a & b.

Freundlich isotherm

Nonlinear adsorptive transport through a homogeneous medium using Freundlich isotherm is presented in this example. The governing equations for transport in this case are (4.23) and (3.44). The problem considers a soil column 100 cm in depth subjected to a steady infiltration of 0.2 cm/day. The material properties are given as:

$$\rho_b = 1.5 \text{ g / cm}^3, \eta = 0.45, n = 1.5, K_f = 1 (\text{cm}^3 / \text{g}) (\text{L / mg})^{0.5}, \alpha = 0.01 \text{ cm}, D_d = 0.0 \text{ m}^2 / \text{s}$$

The initial and boundary conditions are:

$$\begin{aligned} C(z, 0) &= 0, 0 < z \leq 100 \\ C(z = 0, t) &= \begin{cases} 1, t \leq T_p \\ 0, t > T_p \end{cases} \\ C(z = 100, t) &= 0 \end{aligned}$$

where $T_p = 10$ days is the time period during which a constant concentration source is applied at the surface boundary.

Shown in Figure 4-17 is the comparison between Physica's simulation results and analytical and numerical solution presented by Wu et al. at $t = 10, 50$ and 100 days. A sensitivity analysis (Figure 4-18) is carried out to analyse the effect of hydrodynamic dispersion on concentration profile by considering higher dispersivity values. A downstream shift in concentration peak is observed with increasing dispersivity value (Wu et al [72]).

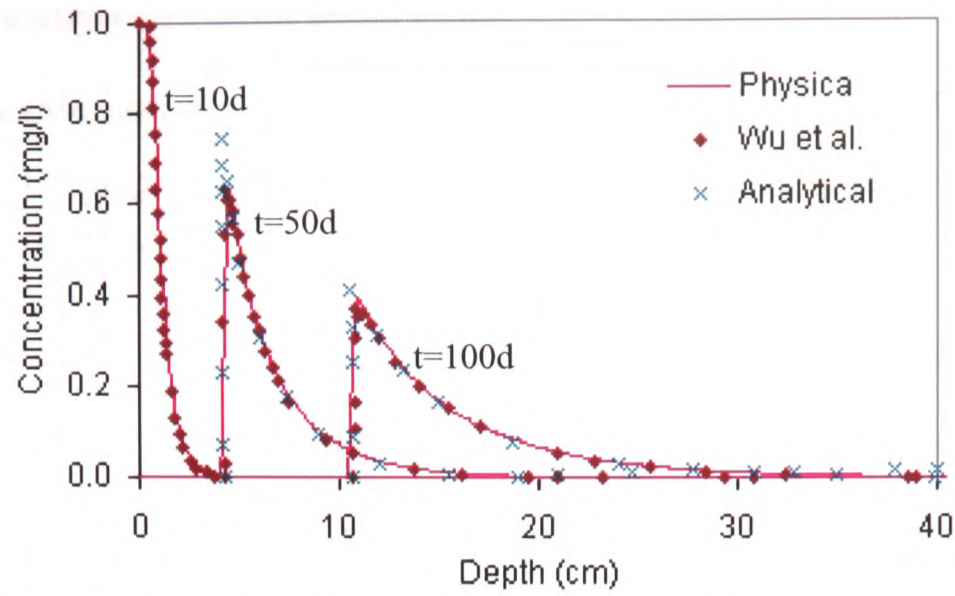


Figure 4-17. Concentration profile for case I at three different times.

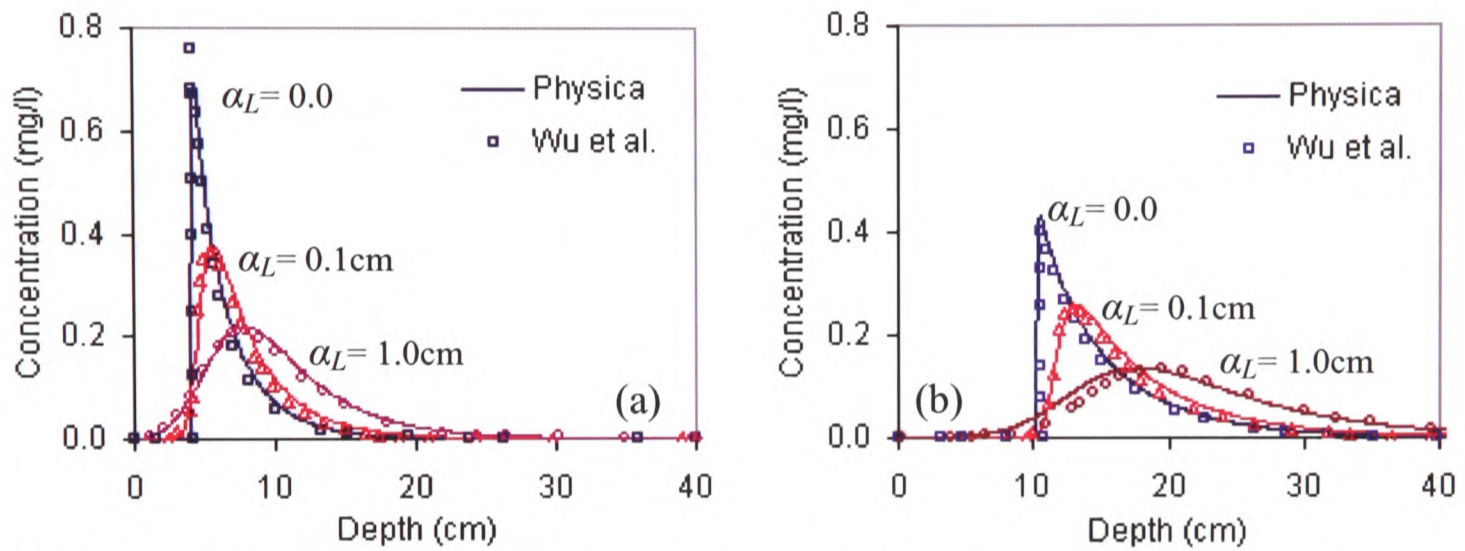


Figure 4-18. Comparison results for case I (sensitivity analysis) showing concentration profiles at (a) $t = 50d$ and (b) $t = 100d$.

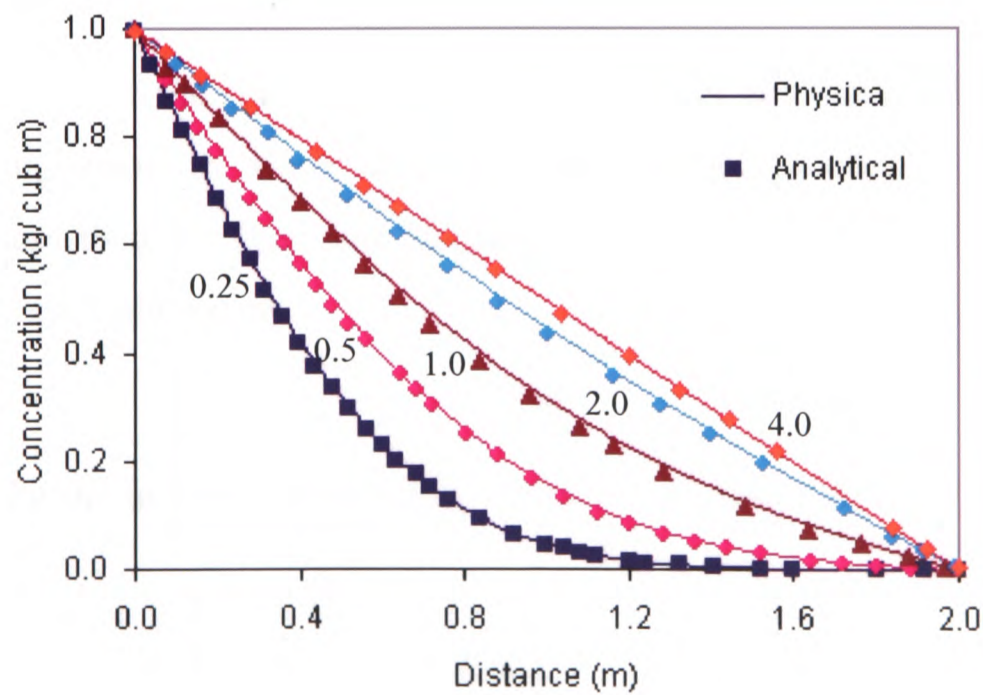


Figure 4-19. Concentration profiles comparison at 0.25, 0.5, 1, 2 and 4 days.

First order kinetically-controlled adsorption

This case computes the solution of one-dimensional pure diffusion problem i.e. equation (3.35) with $v = 0$ coupled with equation (3.45). Simulations are carried out by considering following material properties:

$$D = 0.5m^2/d, v = 0.0, \eta = 1.0, \rho_b = 1.0kg/m^3, k_1 = 0.1m/d, k_2 = 0.5d^{-1}$$

The initial and boundary conditions chosen are:

$$\begin{aligned} C(x, 0) &= 0, 0 \leq x \leq 2m \\ \left. \begin{aligned} C(0, t) &= 1.0 \\ C(x = 2, t) &= 0 \end{aligned} \right\}, 0 < t \leq t_{\max} \\ S(x, 0) &= 0 \\ S(0, t) &= 0 \end{aligned}$$

Shown in Figure 4-19 are comparison results from Physica's simulation with analytical solution presented by McGrail [69]. The two results for kinetically controlled linear adsorption are in good agreement.

4.4.2.2.2 Volatilization

The models described in sections (4.3.5.1.1) and (4.3.5.1.2) are used to investigate the transport of volatile organic chemicals (VOC) through the vadose zone. The effects of water table and gas-phase advection are analysed by means of different test cases.

Effect of water table

The first case considers the transport processes of steady advection of water and gas, diffusion and dispersion in water and gas, as well as adsorption and first-order degradation as described by Shan and Stephens [73]. In order to solve equation (4.24) the initial conditions assumed are

$$C(z, 0) = C_i$$

where C_i stands for the initial concentration, which is considered as

$$\begin{aligned} C_i &= 0 \quad (0 \leq z \leq d_1 \text{ and } d_2 \leq z \leq d_3) \\ C_i &= C_0 \quad (d_1 \leq z \leq d_2) \end{aligned}$$

where C_0 is a non-zero constant; and d_1 , d_2 and d_3 ($0 < d_1 < d_2 < d_3 < \infty$) represent the depth to the top and the bottom of the contaminant source, and to the groundwater table, respectively. The boundary conditions assumed are

$$C(0,t) = 0$$
$$\left(\frac{\partial C}{\partial z}\right)_{z=d_3} = 0$$

The numerical simulations are carried out by considering the transport of trichloroethylene (TCE) in vadose zone of a finite depth (10 m) with water table as the lower boundary. The parameters used in the calculations are listed in Table 4-4. As the transport of TCE displays small variation to hydrodynamic dispersion and biodegradation, their effects have been neglected in all calculations. The effect of water table at a depth of 10 m is examined by taking four different cases into account. In all four cases Jury's [65] solution was calculated using a boundary layer of thickness 0.475 cm. Case A assumes a source located within the depth interval 300-310 cm and a recharge rate of $v_L = 10$ cm/day.

The simulated concentration profiles are compared with Jury's solution at three different times in Figure 4-20a. A good agreement is found in this case for early times. In case B, the recharge rate is lowered to accommodate more realistic dry conditions at given porosity and water content. The value thus adopted is 0.01 cm/day. The simulated concentration profiles are compared with Jury et al. and Shan et al. solution in Figure 4-20b. A good agreement is found among all solutions at early times ($t = 100$ days). However, as the front is significantly blocked by the water table at longer times ($t = 500, 1000$ days), a higher concentration above the water table is observed contrasting to Jury's solution. A shift in source to a depth of 700-710 cm is presented in Figure 4-20c. Large differences in concentration profiles are observed in this case at late times as compared to Jury's [65] solution.

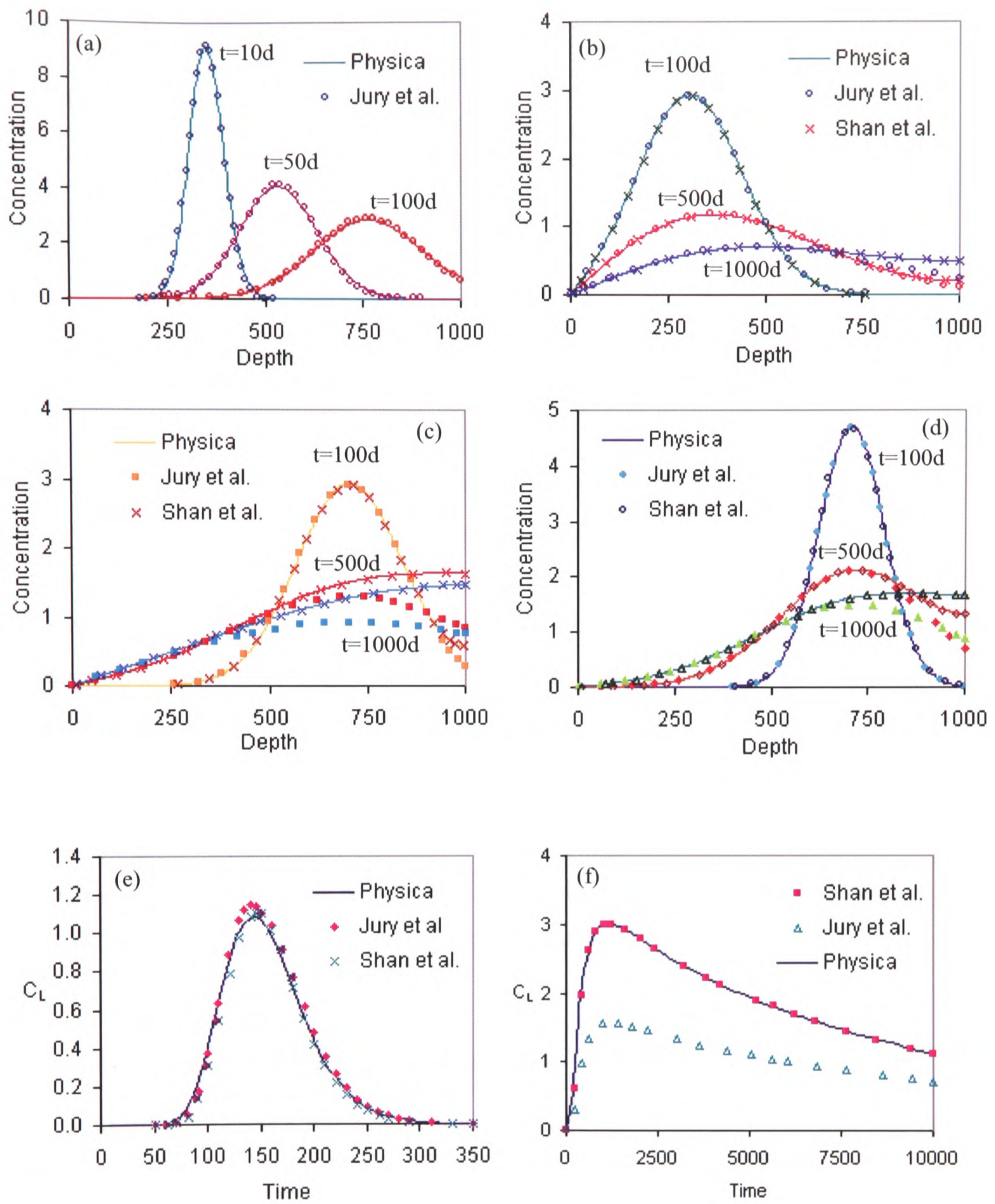


Figure 4-20. Comparison of total concentrations: (a)-(d) and aqueous phase concentrations: (e) & (f).

C_0	$100 \mu\text{g cm}^{-3}$	η	0.5	K_H^*	0.397
d_1	300 cm	θ	0.2	D_w^*	$0.8304 \text{ cm}^2 \text{ day}^{-1}$
d_2	310 cm	α_L	0.0	D_a^*	$7030 \text{ cm}^2 \text{ day}^{-1}$
d_3	1000 cm	α_G	0.0	K_{oc}^*	$61.1 \text{ cm}^3 \text{ g}^{-1}$
v_L	0.01 cm day^{-1}	λ	0.0	f_{oc}	0.0125
v_G	0.0	ρ_b	1.35 g cm^{-3}	K_{SG}	$2 K_{SL}$

Table 4-4. Basic parameters used for concentration calculations. * properties of TCE

Finally, the reduction in available pore space for gas diffusion and adsorption rate are calculated by increasing the values of water content to 0.35 and decreasing the value of fraction of organic carbon to 0.001 (with source depth 700-710). The simulated profiles again present differences in concentration (Figure 4-20d) above the water table at late times from Jury's solution. However, an excellent match is obtained in all cases with the solution presented by Shan et al.

Shown in Figure 4-20e & f are the time-dependent concentration profiles in the aqueous phase at water table for cases A and D. It can be observed that the lower water table has the effect of raising the concentration peak at initial times.

Comparison with commercial numerical model

The validity of Physica's functionality to correctly model transport of VOC in vadose zone is checked against the numerical code VLEACH which is a one-dimensional finite difference vadose zone leaching model initially developed for U.S. Environmental Protection Agency to evaluate groundwater impacts and volatilization of volatile organic contaminants. The main processes simulated by the code are aqueous-phase advection, gas-phase diffusion, solid-phase sorption and three-phase equilibrium.

Simulated results by Shan et al. using VLEACH for case B are compared with physica's solution considering $K_{SG} = 0$ (VLEACH is unable to simulate vapour-phase sorption). An

excellent match (Figure 4-21a) in the results of two codes is found. However, in order to achieve the results for gas concentration presented in Figure 4-21a, a modification in VLEACH was performed by Shan et al. to calculate gas diffusion coefficient. The adopted Millington [74] model in the diffusion equation was expressed as

$$D_{GE} = \frac{(\eta - \theta)^{7/3}}{\eta^2} D_a \quad (4.37)$$

Shown in Figure 4-21b are the Physica results for gas concentration with the modified gas diffusion coefficient according to equation (4.37). Clearly, a modification in gas diffusion estimates the concentration roughly a factor of two less than the expected solution. Apparently, the code with a modification will underestimate the gas diffusion in the vadose zone and correspondingly overestimate the potential risk posed on groundwater resources.

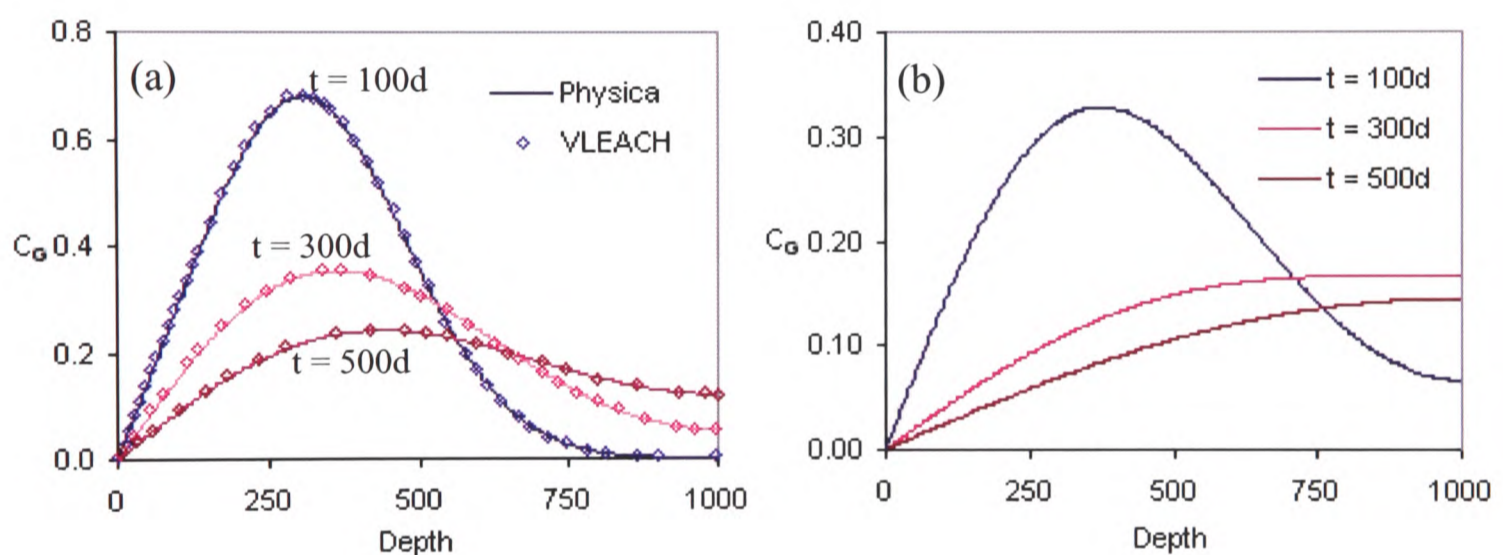


Figure 4-21. Gas concentration profiles (a) without and with (b) modification in gas diffusion coefficient according to equation (4.32).

Effect of gas-phase advection

To calculate the concentration profile for TCE a mean velocity for gas-phase advection is computed by replacing C with $C_0/2$ in equation (4.36). The other parameters to compute v_G for trichloroethylene are given in Table 4-5. Two different values of initial concentration are considered

$$\text{Case1: } C_0 = 100 \mu\text{g cm}^{-3} \Rightarrow v_G = 0.336 \text{ cm day}^{-1}$$

$$\text{Case2: } C_0 = 1000 \mu\text{g cm}^{-3} \Rightarrow v_G = 3.36 \text{ cm day}^{-1}$$

The concentration profiles are calculated for case B for the two cases and are compared with the concentration profiles with no gas advection assumptions (Figure 4-22). A small concentration source produces an insignificant effect on gas-phase advection (Figure 4-22a & b). A fast transport by density-driven gas phase advection is observed on the other hand, when the source concentration is relatively high (Figure 4-22c and d).

μ (Nsm ⁻¹)	k (m ²)	R_G	M_A	M_{TCE}
1.8×10^{-5}	10^{-11}	5.463	29	131.4

Table 4-5. Parametric values for TCE.

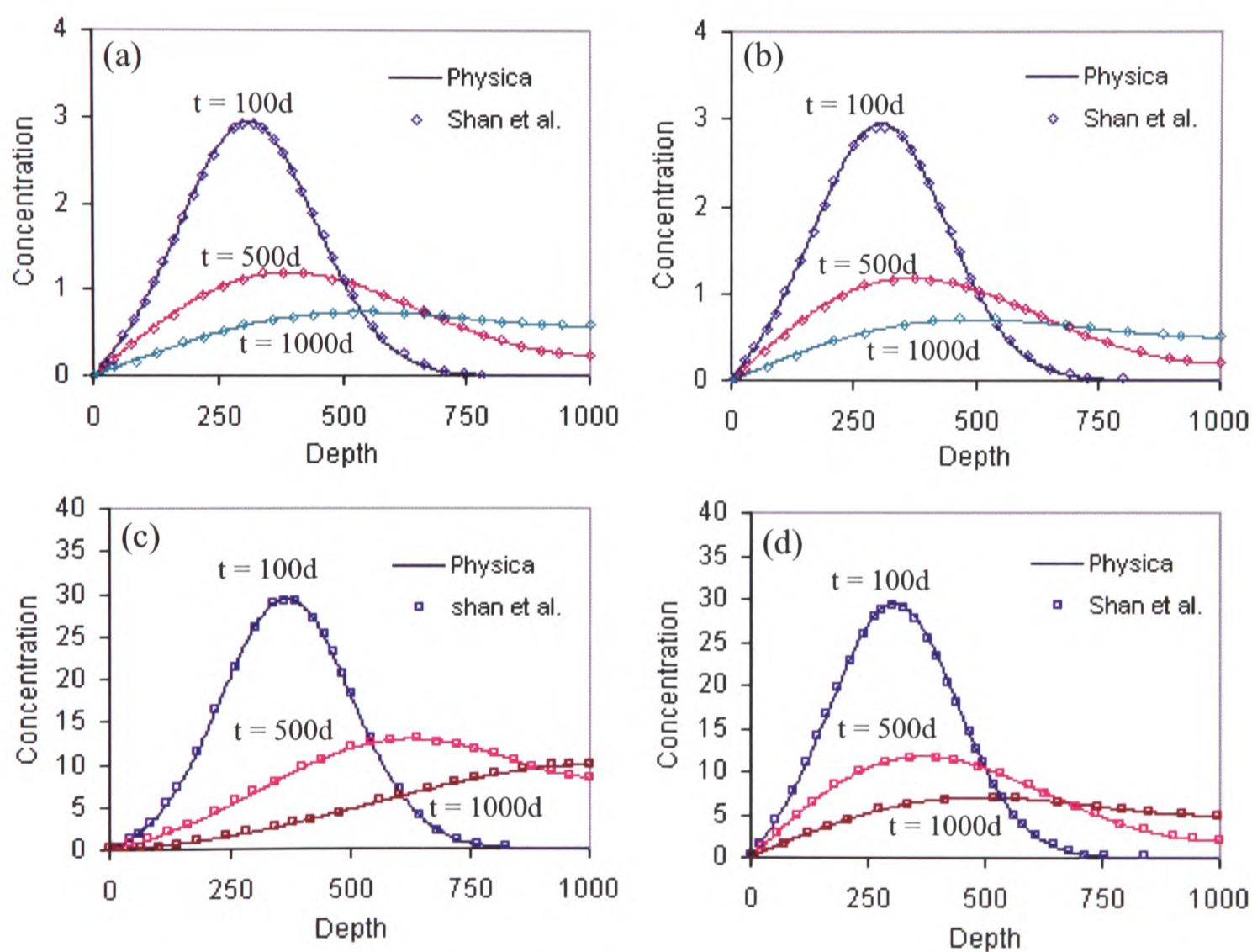


Figure 4-22. Effect of gas-phase advection for case B: (a) $V_G = 0.333$ cm/d, $C_0 = 100$ $\mu\text{g}/\text{cm}^3$, (b) $V_G = 0.0$ cm/d, $C_0 = 100$ $\mu\text{g}/\text{cm}^3$, (c) $V_G = 3.36$ cm/d, $C_0 = 1000$ $\mu\text{g}/\text{cm}^3$ and (d) $V_G = 0.0$ cm/d, $C_0 = 1000$ $\mu\text{g}/\text{cm}^3$.

4.5 Concluding Remarks

The key conclusions for the current study of flow and transport through unsaturated zone are summarised as below

- The unsaturated conductivity and moisture content are greatly influenced by the pressure variation subject to infiltration in the vadose zone. A more advancing wetting front is observed for problems where the pressure gradient presents rapid changes or higher initial values over a specified interval of time.
- At constant velocity the solute migration is constant over time whereas, in case of Darcy velocity the flow field depends on the unsaturated conductivity, pressure gradient and moisture content which are variable quantities in time. Hence the migrating solute presents diversity in two cases in terms of plume spread and transportation.
- For convection-dominated problems, by employing higher order differencing schemes, the breakthrough curves of concentration distribution can be obtained with minimum oscillations and false-diffusion.
- Sensitivity analysis of transport parameters such as dispersivity, molecular diffusion and dispersion shows that different solute species migrate in different ways and under different hydrogeological conditions.
- Breakthrough curves of solute transport subject to non-linear adsorption (advection-dominant problems) exhibit concentration shocks and sharp fronts with a retarded plume velocity as opposed to the linear adsorption. Owing to different transport processes, the extent to which the migration of dissolved solute species entering the subsurface flow systems is retarded can be investigated using appropriate adsorption isotherm.

FLOW AND TRANSPORT MODELS: HETEROGENEOUS (LAYERED) SYSTEMS

In this chapter the flow and transport analysis is studied for hydrogeological systems involving spatial heterogeneity in their physical properties. The flow and transport mechanisms described in chapter 3 and 4 are analysed for heterogeneous systems here.

5.1 Introduction

Being mixture of organic, inorganic materials and decomposed rocks geologic deposits display spatial variation in soil properties at various length scales. The spatial variability of physical properties such as hydraulic conductivity is quite common.

Heterogeneous configurations can be classified into four broad types as follows

Layered: The stratigraphic layering within the medium where individual geologic units possess different hydraulic properties. Within each layer the medium is homogeneous with known material properties (Figure 5-1).

Discontinuous: Comprises the presence of faults or large scale stratigraphic features.

Trending: Shows the variation in sedimentation patterns.

Random: It is the small scale variation of soil properties from one point to another within the formation due to different deposition conditions.

5.2 Layered Heterogeneity

To model the flow and transport mechanisms through the layered heterogeneous systems following approach is adapted

- Implementation of spatially varying hydraulic properties.
- Bedding of varying thickness is possible.

- Implementation of conductivity contrasts between the layers to monitor downward (vertical) flow under variably saturated conditions.
- Implementation of spatial distribution of solute species across the layers.
- Execution of convection velocity across the layers and its effects on the hydrodynamic dispersion coefficient.

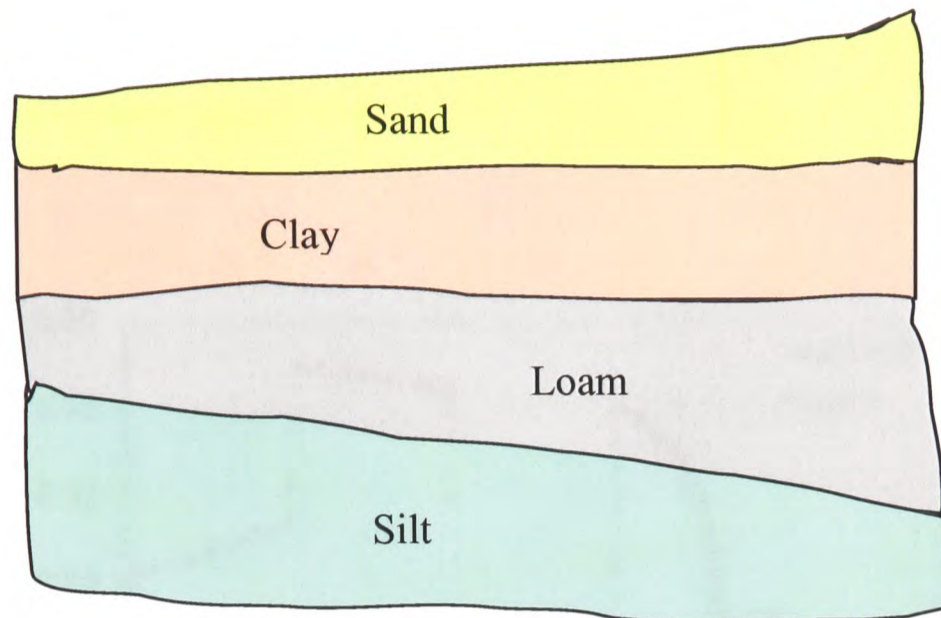


Figure 5-1. Layering configuration of a heterogeneous medium. Soil materials sand, clay, loam and silt possess different hydraulic properties.

5.2.1 Test Cases

Geological systems comprised of stratigraphic layering of contrasting physical properties have a great influence on over all vertical flow of the fluid. The spatial variability of geologic medium can also have a great impact on the distribution and accumulation of pollutants in the subsurface system. Flow and transport problems presented in the subsequent sections analyse these impacts in brief details.

5.2.1.1 Flow Problems

To demonstrate the potential application of flow through such a non-homogeneous system and the correct implication of proposed finite volume techniques a test problem involving infiltration into field scale layered lysimeter is presented here. The layered soil structure follows Hills et al [28]. The flow process is governed by equation (4.9) and the simulations are carried out by considering alternating layers of Berino loamy fine sand and Glendale clay loam (each 20 cm thick) with a total soil depth of 1 metre. Both soil types are described by VG hydraulic function as described in section 4.3.3.1 with parameters (Table 5-1) as reported by Hills et al [28]. The initial and the boundary conditions incorporated are

$$\psi(z, 0) = -10000\text{cm}, 0 \leq z \leq 1\text{m}$$

$$\psi(0, t) = -50\text{cm}$$

$$\psi(1\text{m}, t) = -10,000\text{cm}$$

The results of two days simulations (Figure 5-2) with $\Delta z = 0.4$ cm and $\Delta t = 1$ second are compared with fine grid solution presented by Gasto et al [75]. A change in the movement of wetting front is observed (Figure 5-3) by increasing the initial pressure to -1000 cm. These results illustrate that using wetter initial conditions will cause the wetting front to move faster than it should.

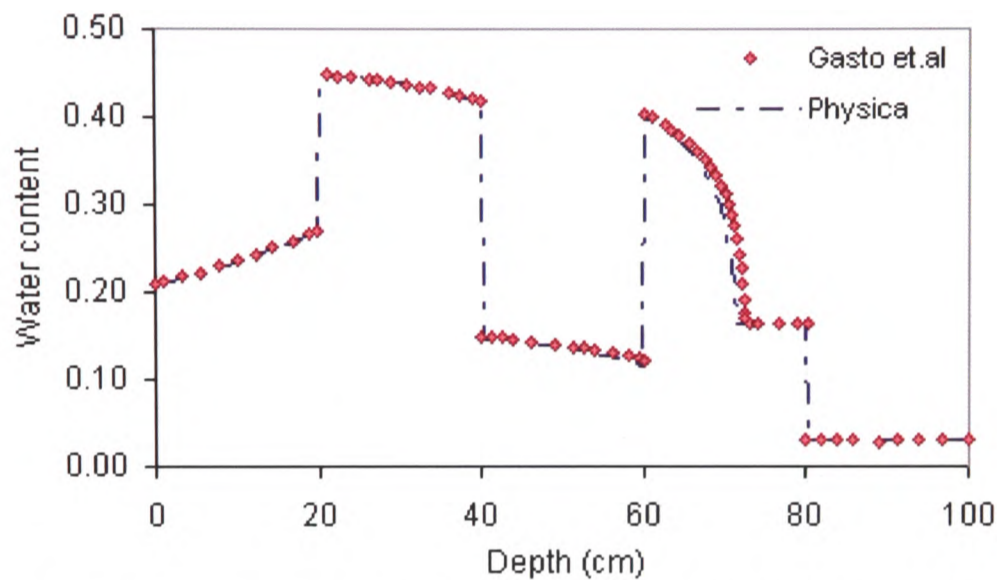


Figure 5-2. Water content profile with initial pressure head of -10,000 cm at 48 hours.

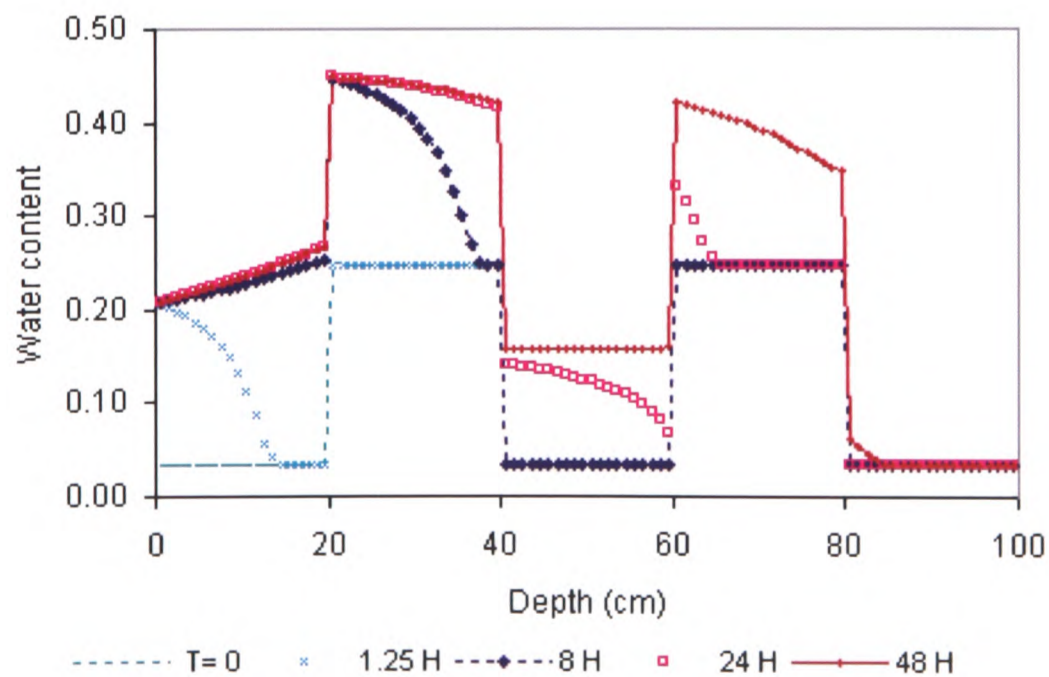


Figure 5-3. Water content profile with initial pressure head of -1000 cm at 4 different times.

Material type	K_s (cms^{-1})	θ_r	θ_s	α (cm^{-1})	n
Berino loamy fine sand	6.2616	0.0286	0.3658	0.0280	2.2390
Glendale clay loam	1.561×10^{-4}	0.1060	0.4686	0.104	1.3954

Table 5-1. Soil parameters.

5.2.1.2 Transport Problems

To demonstrate the potential application of transport through a layered heterogeneous system two test problems involving reactive transport are presented here.

5.2.1.2.1 Non-linear Adsorption Isotherm

Nonlinear adsorptive transport governed by equation (3.37) through a layered heterogeneous medium is presented in this case using Freundlich isotherm equation (3.43). The problem involves one-dimensional solute transport through a two layered heterogeneous medium. Layer 1 is taken to be 100 cm deep and the second layer is considered as semi-infinite. The medium is subjected to a steady infiltration of 0.4 cm/day with material properties for the two layers given as

Layer 1:

$$\rho_b = 1.5 \text{ g/cm}^3, \eta = 0.4, n = 1.5, K_f = 0.64 (\text{cm}^3/\text{g})(\text{l/mg})^{0.5}$$

Layer 2:

$$\rho_b = 1.6 \text{ g/cm}^3, \eta = 0.25, n = 5, K_f = 0.25 (\text{cm}^3/\text{g})(\text{l/mg})^4$$

The initial and boundary conditions for this problem are:

$$C(z, 0) = 0$$

$$C(z = 0, t) = \begin{cases} 10, & t \leq T_p \\ q, & t > T_p \end{cases}$$

$$C(z = \text{outflow boundary}, t) = 0$$

Comparison results for simulated concentration profile in Physica and those presented by Wu et al. [69] are shown in Figure 5-4. An abrupt change in the slope of concentration is observed at the interface of two layers which is due to contrasting material properties and the velocity variation across the interface.

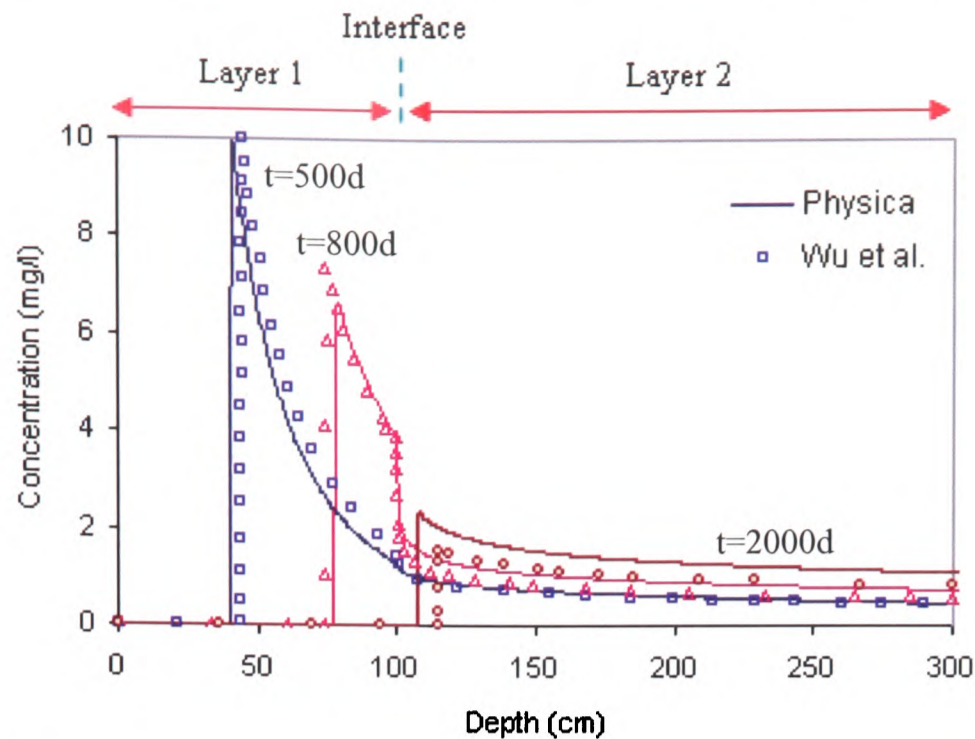


Figure 5-4. Concentration profile for Freundlich isotherm at three different times.

5.2.1.2.2 Colloid Transport

2-dimensional colloid transport in physically and geochemically heterogeneous medium is considered in this case. The transport mechanism, governing equations and initial conditions are same as those described in section 3.4.5. The problem considers physical heterogeneity which involves a rectangular domain 3 m in length along x-axis and 1 m thick along z-axis with the distribution of model domain into three horizontal layers along x-axis. Layer I (0-0.3 m) and III (0.7-1.0 m) are assigned the same material properties and parametric values. A different set of parameter values is assigned to layer II (0.3-0.7 m) in order to incorporate the heterogeneity. The boundary conditions are assumed as

$$N(x=0, z, t) = 2.8 \times 10^{14}$$

$$-D \frac{\partial N}{\partial x} \Big|_{x=3} = 0$$

Figure 5-5 illustrates the effect of layered physical heterogeneity on colloid transport under different conditions as described in Table 5-2. In case (a) higher conductivity value causes faster flow through the central layer and faster accompanying colloid transport. The results in case (b) show that the increased deposition rate of colloid particles onto the favourable surface fractions of layer I and III (more heterogeneous) can result in preferential flow of colloid particles through central layer (Sun et al [55]).

Case	Constant property	Constrasting property		
		Layer I	Layer II	Layer III
a	$\lambda = 0.001$	$K = 50\text{m/d}$	$K = 100\text{m/d}$	$K = 50\text{m/d}$
b	$K = 100\text{m/d}$	$\lambda = 0.025$	$\lambda = 0.001$	$\lambda = 0.025$
c	$\lambda = 0.001$	$R = 5$	$R = 1$	$R = 5$
d	$\lambda = 0.001$	$R = 5$	$R = 10$	$R = 5$
e	-	$\lambda = 0.001$ $K = 50\text{m/d}$	$\lambda = 0.025$ $K = 100\text{m/d}$	$\lambda = 0.001$ $K = 50\text{m/d}$
f	-	$\lambda = 0.025$ $K = 50\text{m/d}$	$\lambda = 0.001$ $K = 100\text{m/d}$	$\lambda = 0.025$ $K = 50\text{m/d}$

Table 5-2. Parametric values for simulated cases for colloid transport.

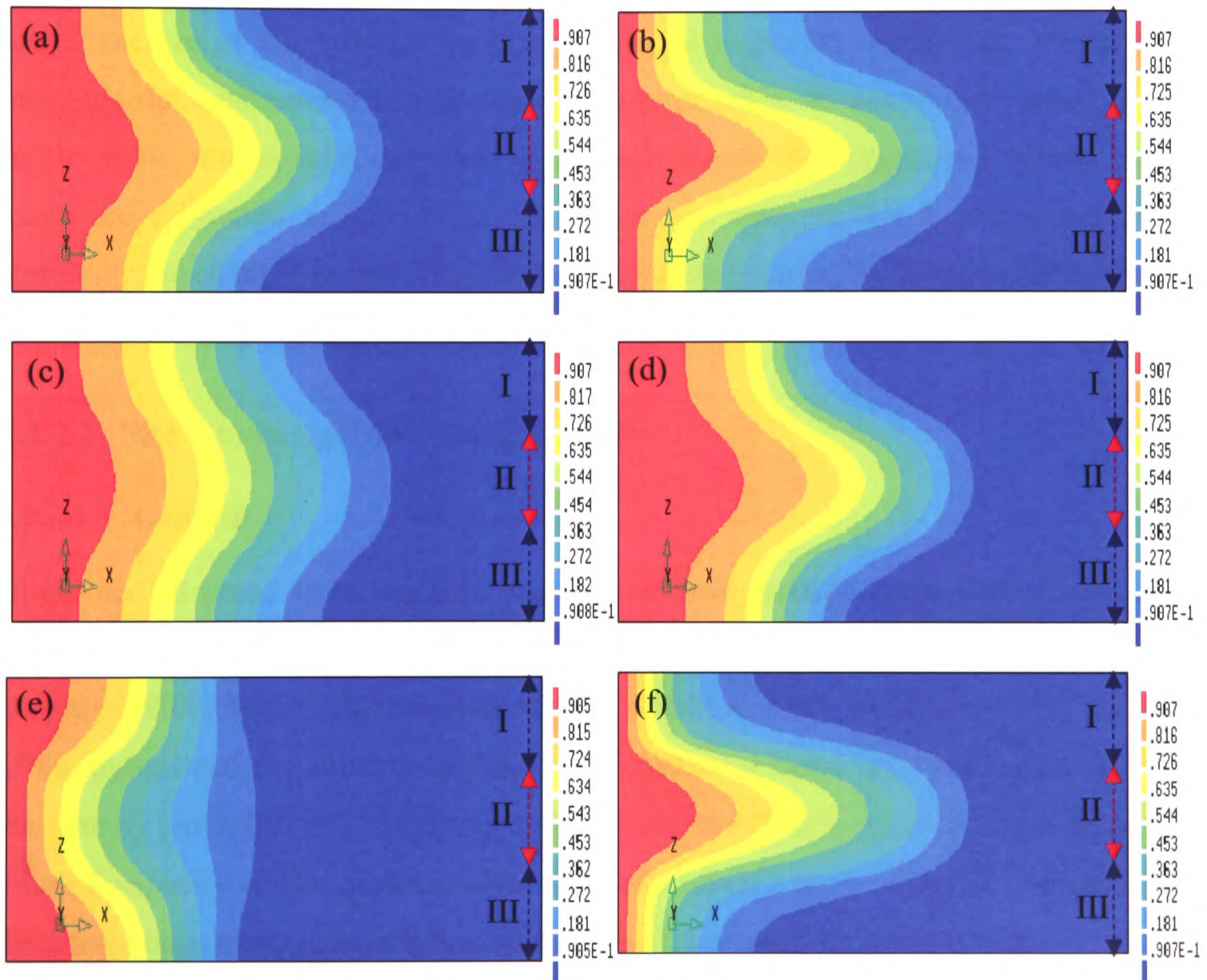


Figure 5-5. Concentration contours showing the effect of (a) physical layered heterogeneity, (b) geochemical layered heterogeneity, (c) dispersivity ratio $R = 1$ and (d) dispersivity ratio $R = 10$ on colloid transport at an observation time of 0.75 day. (e) & (f) show combined effect of physical and geochemical heterogeneity. The basic parameters used are given in table (3.5).

It can be seen from (c) and (d) that a large transverse dispersivity value ($R = 1$) leads to a reduced preferential flow in the central layer whereas a small transverse dispersivity value ($R = 10$) results in enhanced preferential colloid transport through the central layer. The results in (e) that the effects of geochemical heterogeneity are dominated on physical heterogeneity showing no preferential flow path for colloid transport. In (f) however, the preferential flow path is enhanced with higher conductivity and lower geochemical heterogeneity values.

5.2.2 Case Study: Burnstump

The CFD analysis conducted in this case study involves field-scale flow/transport investigation in vadose zone with layering heterogeneity. The numerical simulations are performed on the data (see Appendix A) collected from Burnstump landfill site in collaboration with Imperial College London. In order to simulate the effects of heterogeneities in the hydrogeology on downward migration of leachate several one-, two-, and three-dimensional simulations are performed by accounting for transient flow and transport mechanisms described in earlier sections. Heterogeneities within landfill waste are calibrated using a time varying source term for the contaminants which represents the changes in the composition of leachate entering the unsaturated zone from the ‘dilute and disperse’ types of landfills.

5.2.2.1 Site Characterisation and Details

5.2.2.1.1 Landfill

Dilute and disperse style landfills were a common practice until 1980’s before the reassessment of the ‘dilute and disperse’ principle introduced by European Groundwater Directive (80/68/EEC). The previous method of filling involved little or no engineering of the unconfined site prior to landfilling. The practice relied on the attenuation of the leachate by biological and physico-chemical processes within the geology along with the diluting capacity of the groundwater. Although suitable under normal circumstances, there have been many cases when it resulted in the pollution of groundwater.

5.2.2.1.2 Geography

The old style dilute and disperse landfill site considered here is situated 8km north of Nottingham (UK). The site is located on major (Sherwood Sandstone) aquifer with a substantial unsaturated zone and was infilled during 1970’s. It covers an area of roughly

0.5 km². There are no major surface water features within the vicinity of Burnstump. It is therefore concluded that the site does not have any effect on the surface waters.

5.2.2.1.3 Geology

The Triassic Sherwood Sandstones are red sands that are medium to coarse grained in texture with an average grain size of 0.3 mm. The aquifer at the site has a massive cross-bedded structure that is interspersed with lenses of mudstones and siltstones, as well as bands of pebbles and clays. It also overlies Permian mudstones that comprise the lower aquitard. The aquifer at Burnstump is unconfined in general. The small amount of calcium carbonate cement present in the sandstone means that it has a low buffering capacity.

5.2.2.1.4 Hydrogeology

The unconfined aquifer at the site is approximately 100 m thick in depth. The regional groundwater levels below the site are in the range 50-55m with an unsaturated zone of 45-55m through which the leachate must travel prior to reaching groundwater. The Triassic sandstone has a mean intergranular porosity of approximately 24% and has an average saturated hydraulic conductivity of 3 m/day. A minute fluctuation in water levels is found which characterises an aquifer with no indication of faulting or fissuring. The groundwater discharges into River Trent and is extracted from water supply boreholes.

5.2.2.1.5 Site Investigations

Site investigation and monitoring was commenced in 1978 and a series of boreholes was drilled between 1978 and 2000. Over the years many different sets of analysis have been conducted at the site focusing on the migration of ammonia, TOC, chloride, sulphates and nitrates (Lewin et al [76]). An interpretation of the data has demonstrated significant attenuation of organic carbon and ammoniacal-nitrogen occurring within the vadose zone.

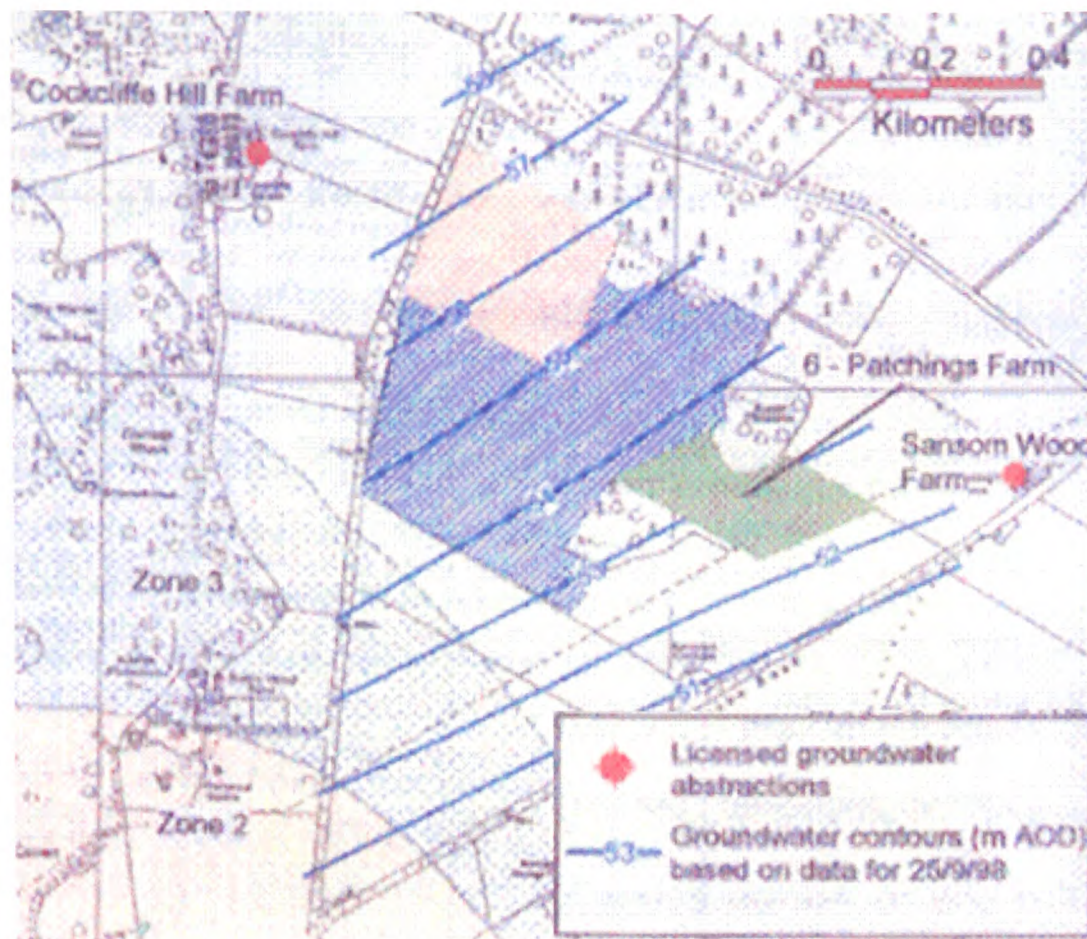


Figure 5-6. Hydrogeological map of the area.

Soil type	K_s (cmh ⁻¹)	θ_s	θ_r	α	n	L
Clay	4	0.4	0.15	0.03	1.5	-1.3
Sand1	8	0.3	0.08	0.09	1.8	-1.2
Sand2	35	0.24	0.08	0.09	2.0	-1.6
Gravel	30	0.20	0.03	0.20	2.5	-1.5

Table 5-3. Soil parameters values for the calibrated simulations.

5.2.2.2 Simulation Results and Discussions

To investigate the spatial distribution of solute species entering the vadose zone from the landfill site (Figure 5-6), numerical simulations are performed on hydrological and geochemical data collected from the landfill site (Thornton et al [77]). The key contaminants, which this investigation concentrates on, are chloride (Cl) and ammoniacal-nitrogen (NH₃-N). Chloride being highly soluble with infinite half-life is used as a tracer to illustrate the movement of the leading edge of the contaminant plume. Ammoniacal-nitrogen, on the other hand, is used as a nutrient indicator to represent the inorganic phase contaminants.

Contaminant	K_d ($m^3 kg^{-1}$)	α (m)	D_m ($m^2 s^{-1}$)	$T_{1/2}$ (yrs)	λ (s^{-1})
Cl	0.0	0.01	1.0×10^{-9}	12	1.83×10^{-9}
NH_3-N	1.2×10^{-4}	0.01	1.0×10^{-9}	2.2	1.0×10^{-8}

Table 5-4. Contaminant parameters and associated values.

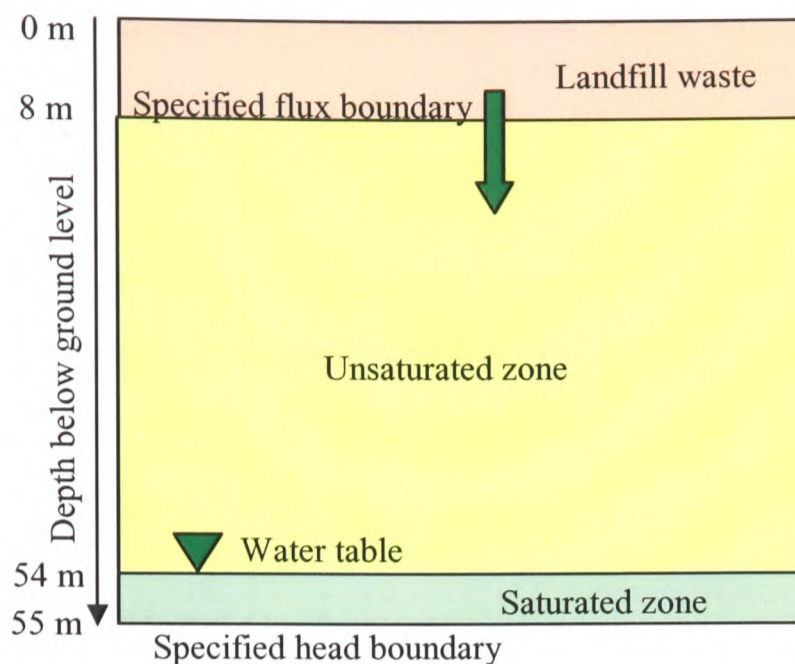


Figure 5-7. Conceptual model of the subsurface underneath Burnstump.

The hydrological quantities of volumetric water content and pore water velocity are calibrated by solving flow equations subject to constitutive relationships presented in equations (4.10), (4.12) and (4.14). For contaminant transport equation (4.23) is used with $R = 1$. The sandstone below the landfill is modelled with three different hydrological settings: (1) homogeneous, (2) three soil types and (3) four clay lenses in order to compare with observed migration of the plume between 1978 and 2000. The hydrological/contaminant parameters used are listed in Table 5-3 and Table 5-4. The active physical, biological and chemical processes taking place in the waste are ignored and a time dependent source term at the upper boundary of the model (base of the landfill) is used to represent the heterogeneity within the waste. The lower boundary, 1 meter below the groundwater table, is at a pressure of 100 cm. The upper boundary is set as a specified flux boundary with an effective rainfall rate of 0.03 cm/day (Figure 5-7).

5.2.2.2.1 Homogeneous Model Calibration

The hydrological model (Figure 5-8) shows the variation in water content against the pressure profile. The initial pressure for hydrological model is set to -225 cm. The transport model is calibrated as soon as the results of flow model become available. Results of one-dimensional transport of chloride tracer using the homogeneous model

with bulk hydrological parameters of sand1 type are presented in Figure 5-9. In comparison to the observed data the simulation results show no decrease in mass over time and a very little dispersion of the mass. This reveals that chloride plume does not exhibit a non-conservative behaviour as one should expect. In order to calibrate the non-conservative behaviour displayed by chloride plume a half-life of 12 years is used as shown in Figure 5-10.

Although the results of this simulation present good match in terms of plume peak and arrival position in most cases, the shape of plume is unable to predict the sharp leachate front for Cl. In case of NH₃-N the simulated migration of plume is non-representative of observed field situation (Figure 5-11).

5.2.2.2 Heterogeneous Model Calibration

In order to understand how heterogeneity within the profile affects the migration rate of the leachate plume, small scale layers or lenses with different hydrological parameters are introduced within the model. Two different hydrological profiles are simulated here in this contest namely; three soil types and four clay lenses.

Three soil types

To determine the influence of different lithologies on contaminant transport, this simulation is run with three sets of parameters in order to represent clay, sandstone (sand 2) and gravel layers. The model consists of sand, within which there are two layers, one of clay between 13 and 18m depth and one of gravel between 23 and 28m depth below ground level.

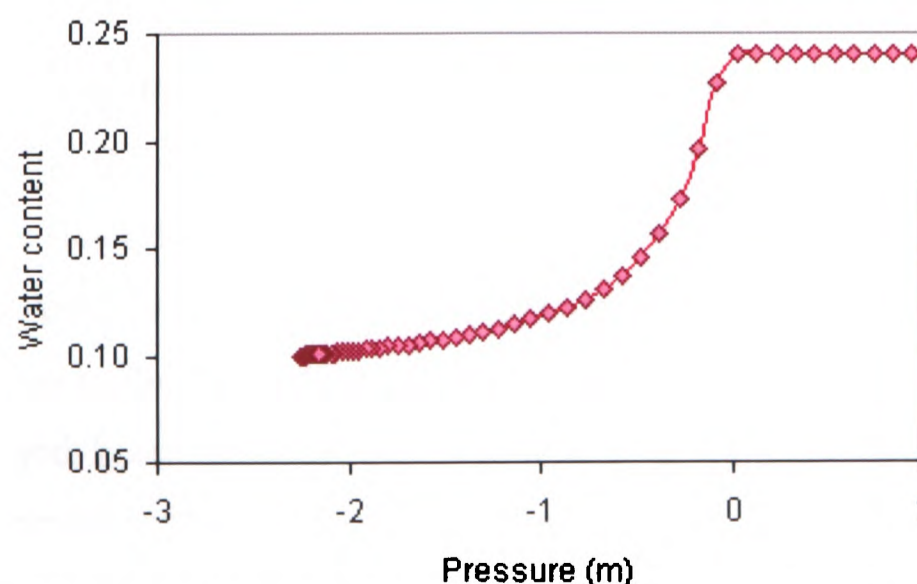


Figure 5-8. Calibrated soil water characteristic curve for homogeneous geologic settings.

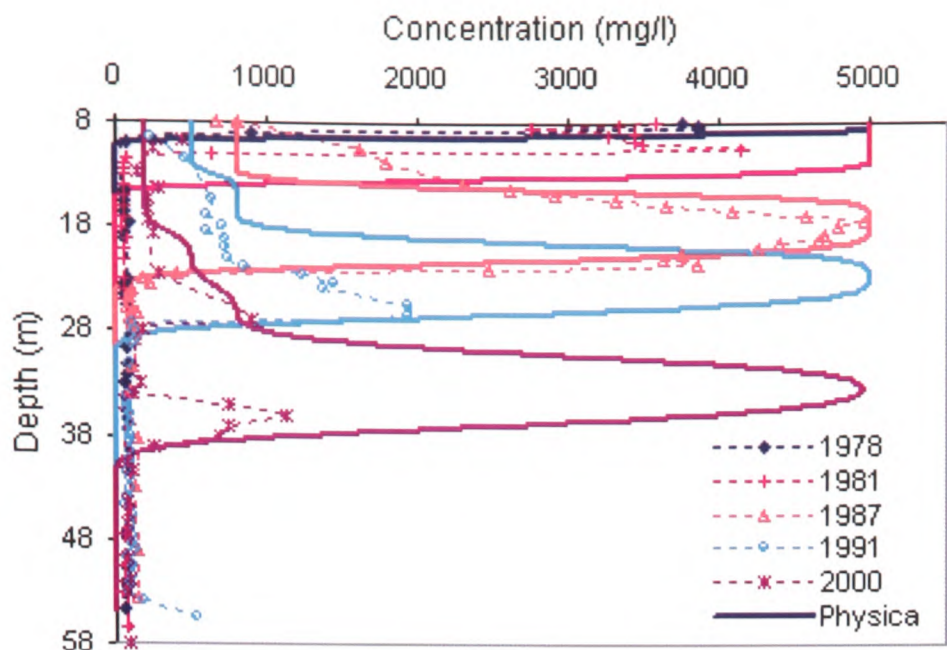


Figure 5-9. Observed (broken lines with symbols) and simulated (solid lines) chloride concentration profiles. The predicted profiles consider the conserved behaviour of chloride.

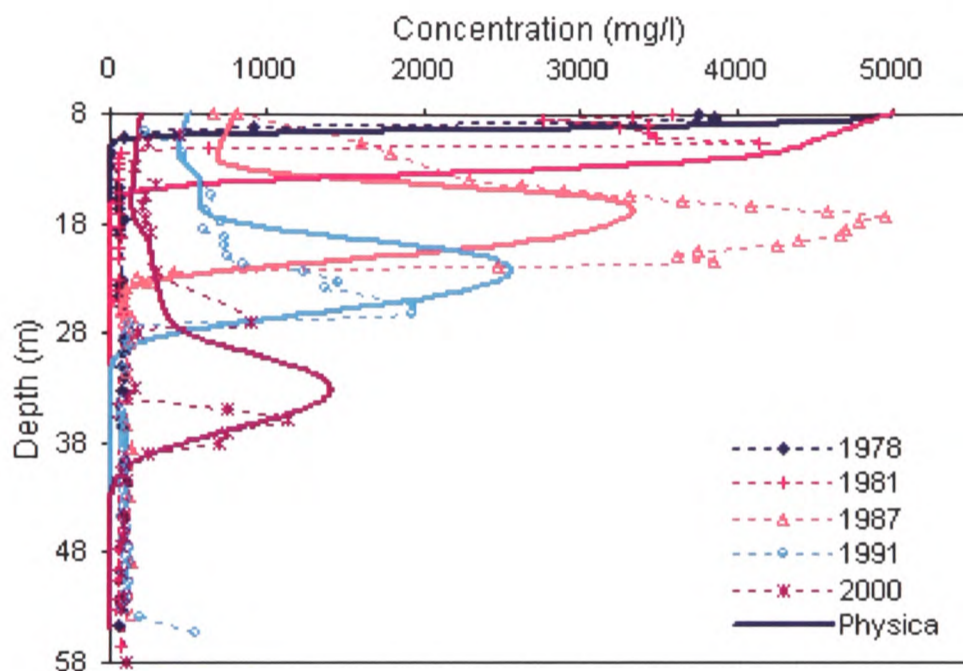


Figure 5-10. Comparison of observed and simulated chloride concentration profiles with an associated half-life of 12 years.

The results of chloride migration over 23 years are presented in Figure 5-13. The distance travelled by the leading edge of the plume and the area of the plume are observed to vary as functions of soil type; greatest in the gravel and smallest in the clay. This is due to the pore water velocity variation across the layers and the contrasting moisture content due to the interaction of the conditions between each soil type (Figure 4-12). The employed heterogeneous model is unable to correctly match the observed contaminant distribution at the different time intervals.

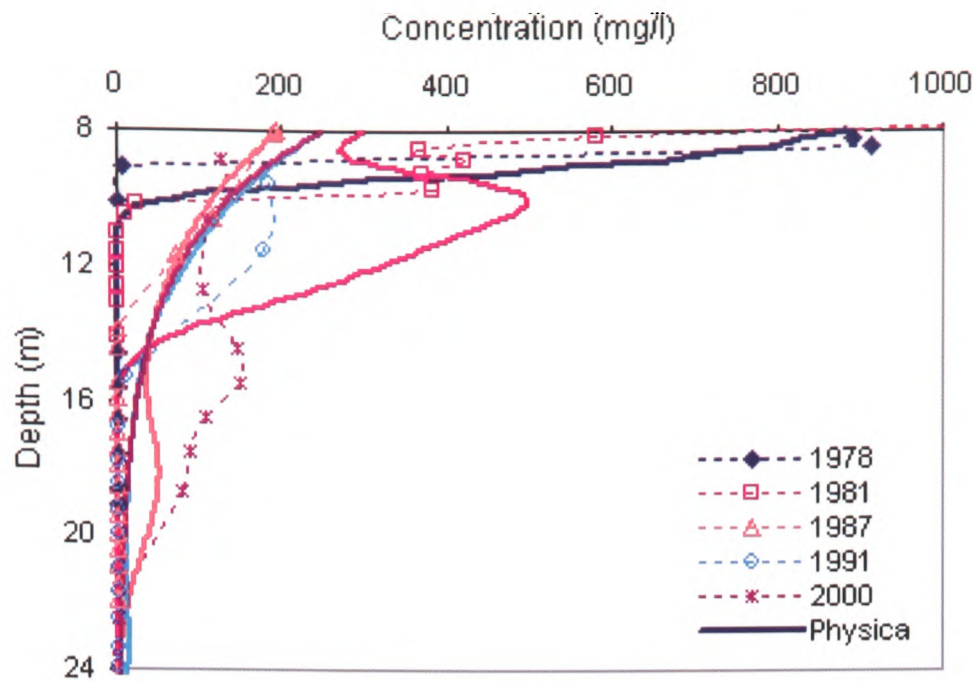


Figure 5-11. Comparison of observed and simulated $\text{NH}_3\text{-N}$ concentration profiles under homogeneous geologic setting.

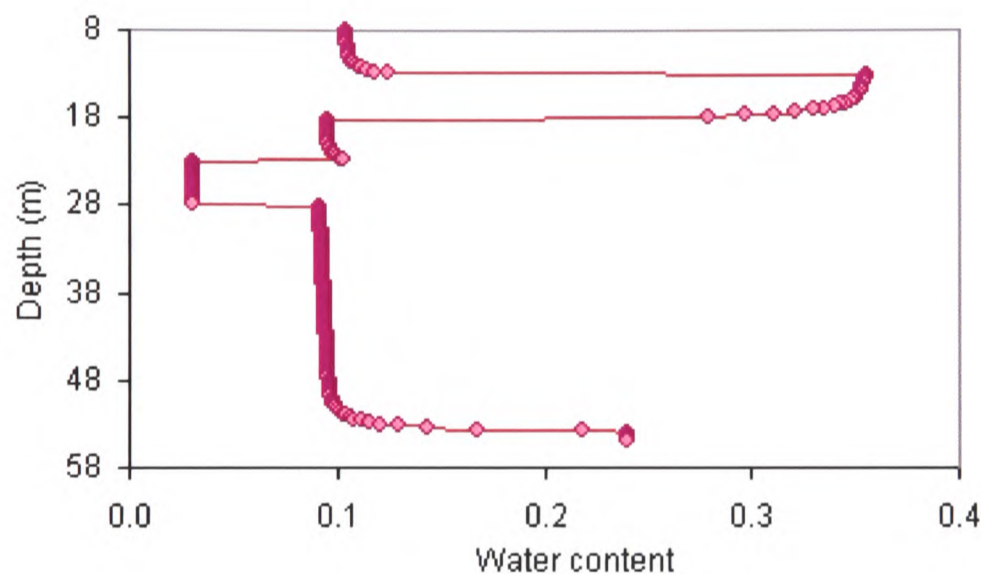


Figure 5-12. Simulated water content profile at one year for three soil types case.

Four clay lenses

To improve the performance of the model more heterogeneity is added to this simulation by means of a number of thin clay lenses. A lower conductivity zone at the top of the profile is created by introducing lower conductivity sand (sand1) and a clay lens to simulate the slow progress of the pore water in this region. The geologic setting and the position of clay lenses are shown in Figure 5-14. The results of chloride and ammonical-nitrogen transport over 23 years are presented in Figure 5-15 and Figure 5-16 respectively. This simulation gives a better comparison to the observed data in terms of the plume's position and pronounced leachate front.

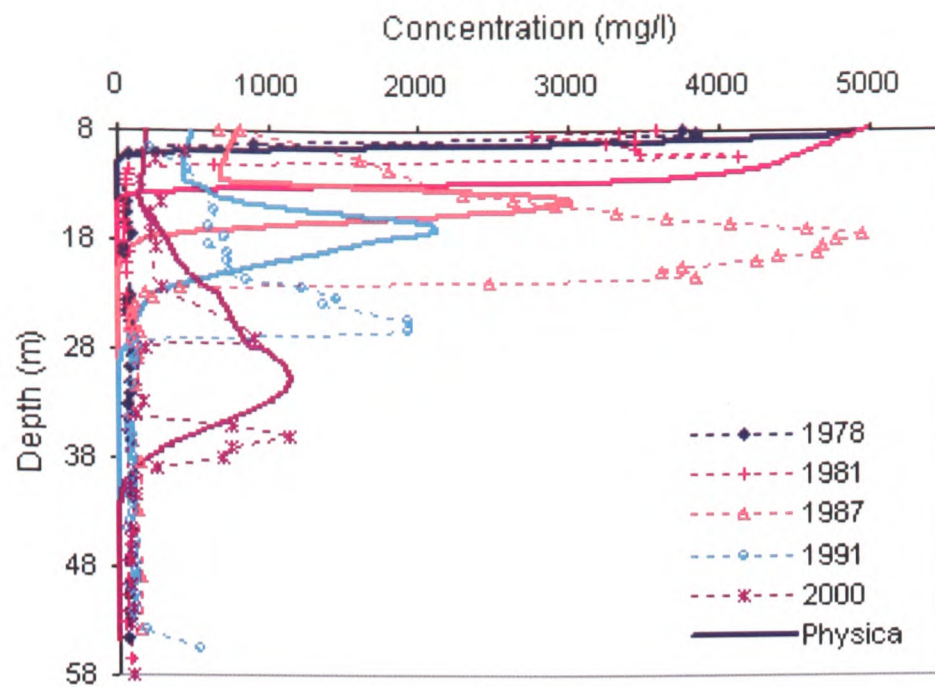


Figure 5-13. Comparison of observed and simulated chloride concentration profiles for three soil type case.

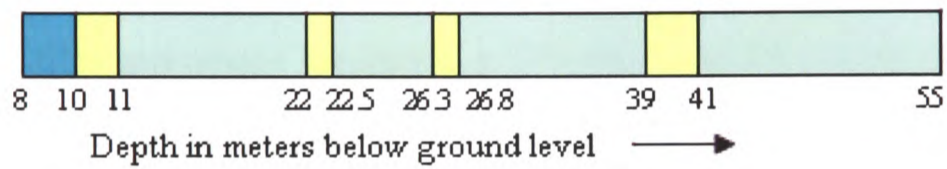


Figure 5-14. Geologic profile setting for four clay lenses case. Turquoise, light turquoise and yellow colours represent materials of type sand1, sand2 and clay respectively.

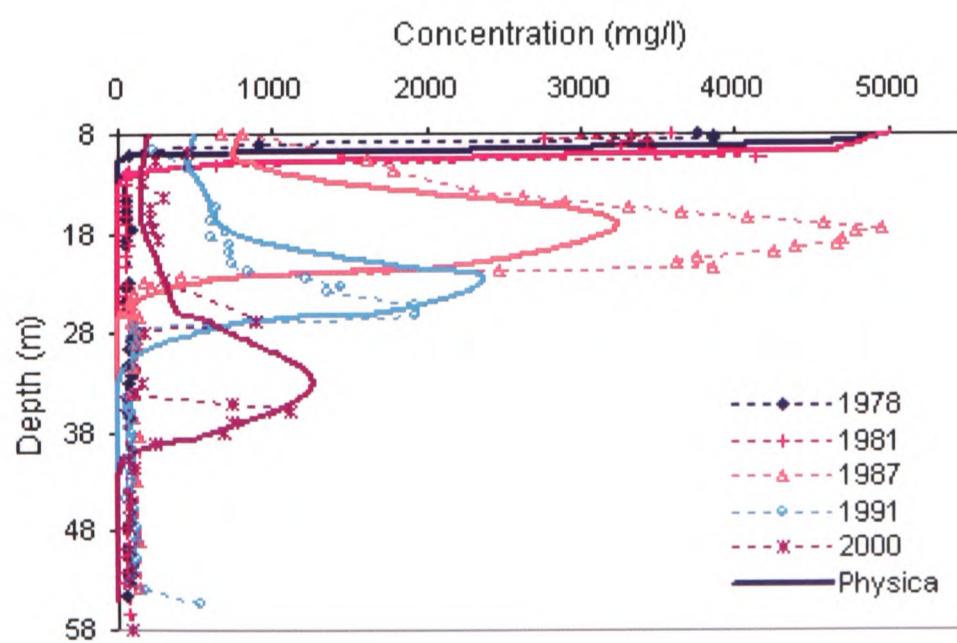


Figure 5-15. Comparison of observed and simulated chloride concentration profiles for four clay lenses case.

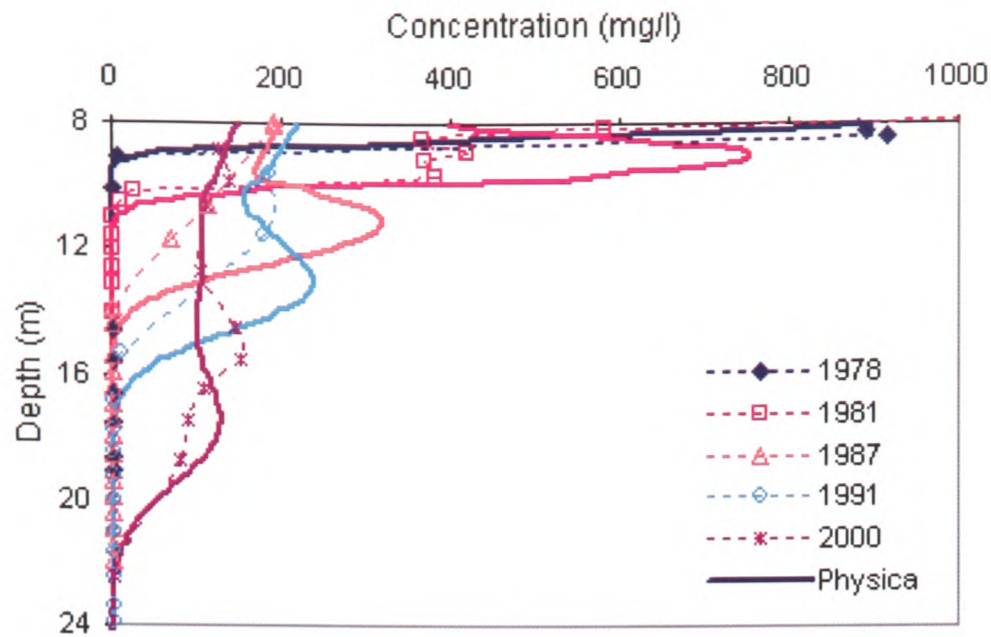


Figure 5-16. Comparison of observed and simulated $\text{NH}_3\text{-N}$ concentration profiles for four clay lenses case.

5.2.2.2.3 2-D Simulations

To gain an insight into how the heterogeneity of subsurface leads to a range of concentration profiles at various locations, a 2-D model is simulated using chloride as a tracer. The calibrated model serves as a general purpose transport model rather than specific to the landfill site under discussion. The model area involves a rectangular domain 20m thick along z-axis and 14m in length along x-axis. The upper boundary receives rainfall flux at a rate of 0.03cm/day and at lower boundary a fixed pressure is set as 100 cm. Numerical simulations are performed considering two different cases: one clay lens, two offset clay lenses (Figure 5-17). The geologic profile of one clay lens case consists of a single clay lens positioned at -6 to -6.7m along z- and 4 to 10m along x-axes in a homogeneous sand material. The two offset clay lenses profile consists of two clay lenses both 100 cm thick by 600 cm wide. They are positioned at 500 to 600 cm depth, extending between 800 and 1400 cm and 1000 to 1100 cm depth, extending laterally between 400 to 1000 cm. Shown in Figure 4-18 and Figure 5-20 are the simulated concentration profiles every two years from Julian date 2,001 until Julian date 20,001 for the two cases respectively.

The presence of low conductivity clay lens results a in more pronounced front of chloride plume reaching the peak values in a much smaller vertical distance than that of seen in the sand.

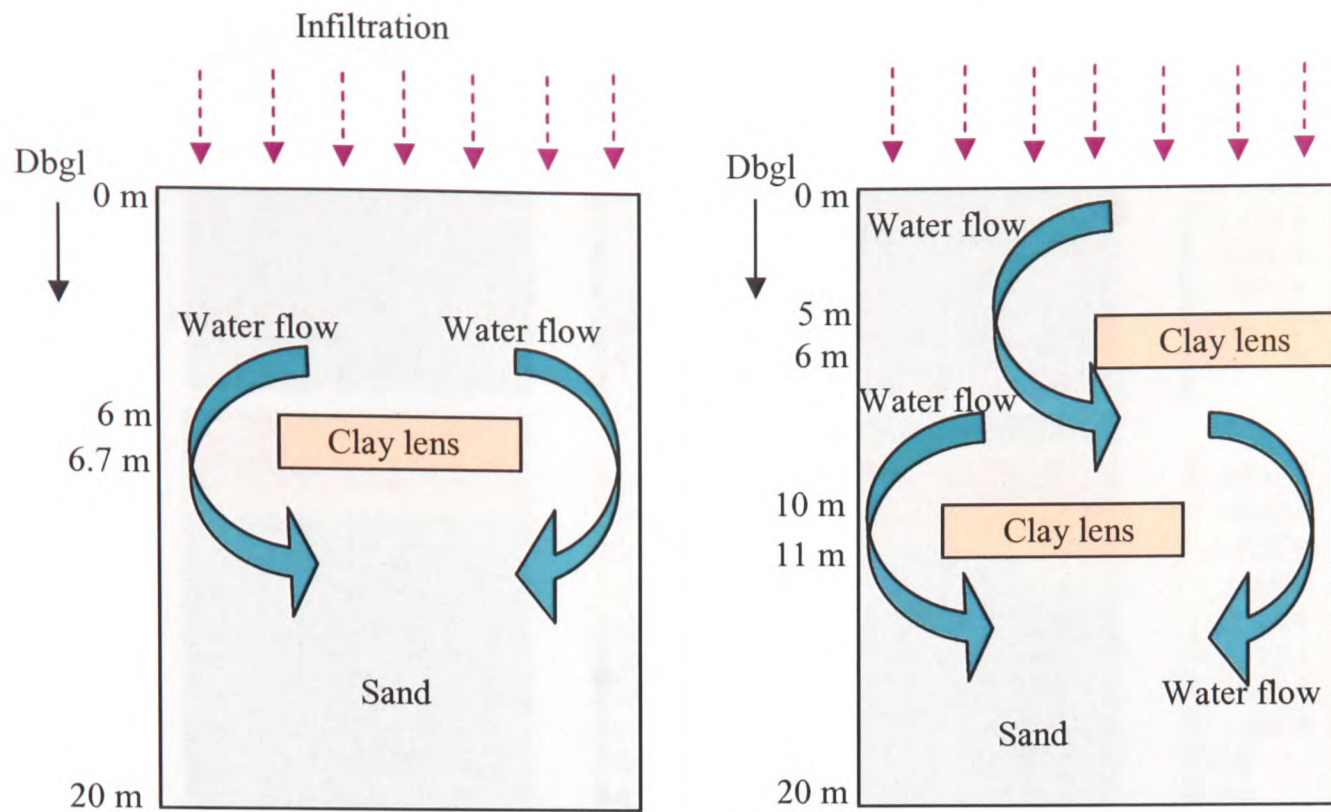


Figure 5-17. Geologic profile of 2-d model. Left: one clay lens, right: two offset clay lenses cases. Dbgl = depth below ground level.

5.2.2.2.4 3-D Simulations

A 3-d implementation of the 2-d model with two offset clay lenses is presented (Figure 5-18). The simulated concentration profiles every three years from Julian date 2,001 until Julian date 17, 001 are shown in Figure 5-21.

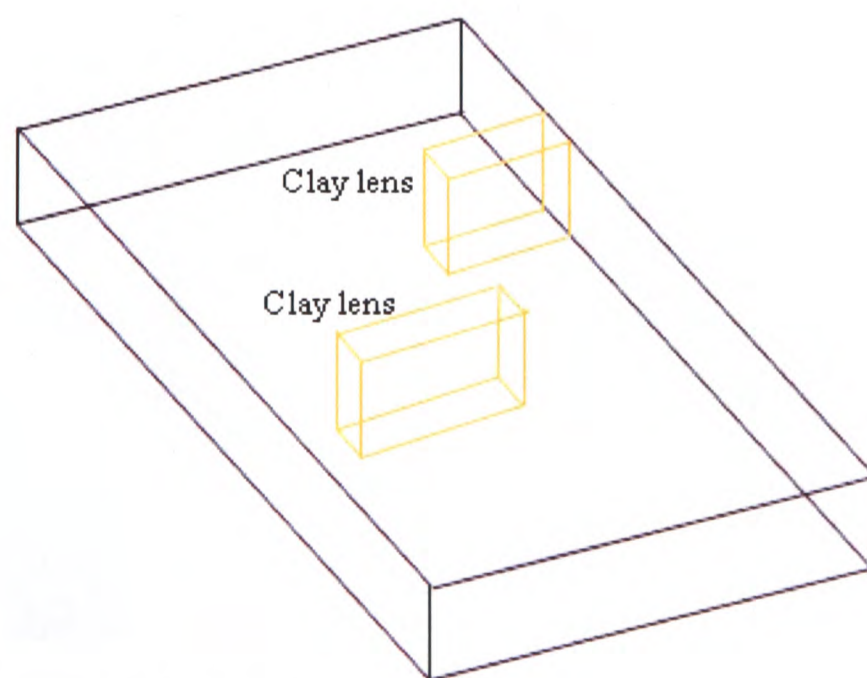


Figure 5-18. Geometry of 3-d case.

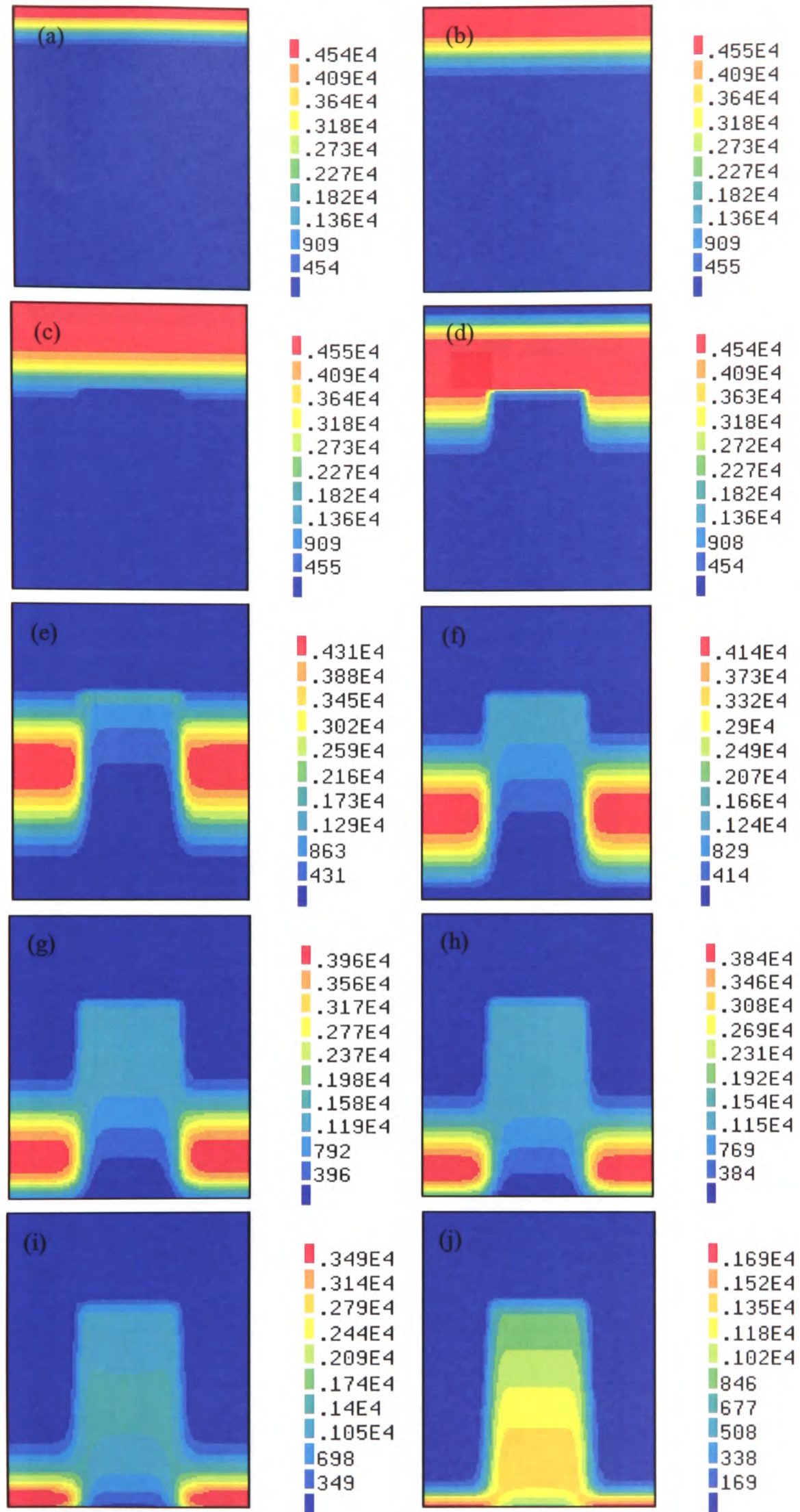


Figure 5-19. Contours of chloride concentration for two-d simulation (one clay lens case). Plots a-j show transport at Julian date 2001-20001 with a time interval of two years.

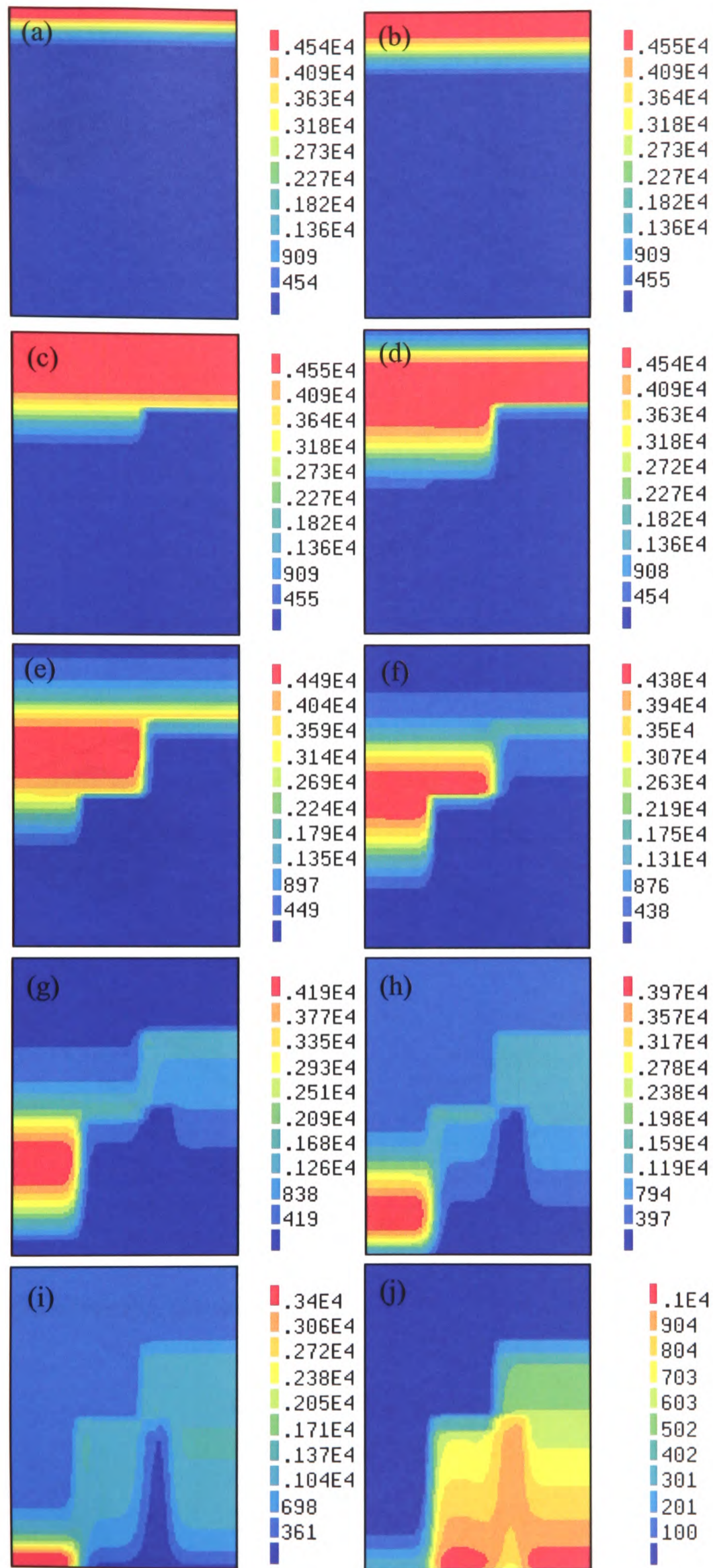
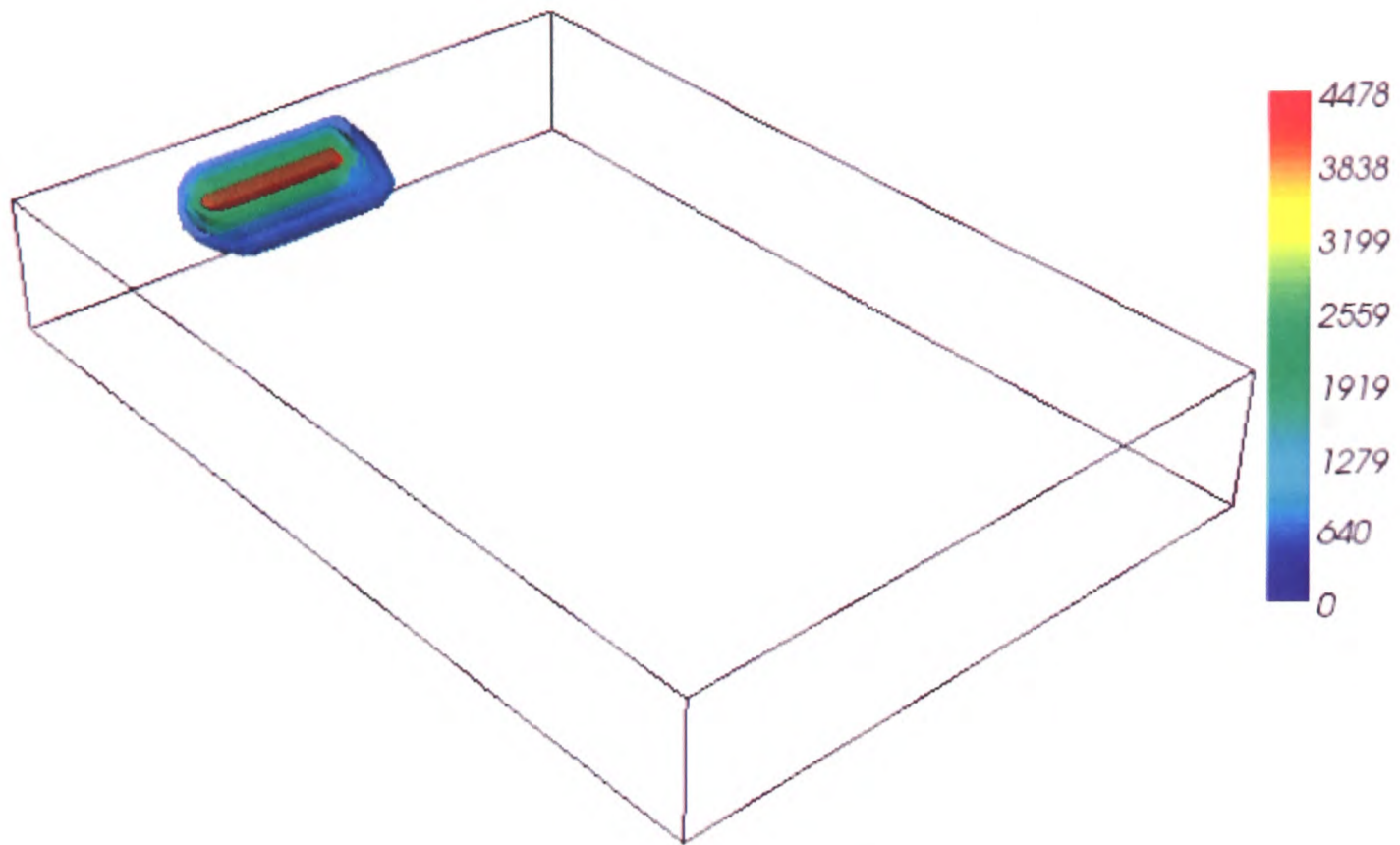
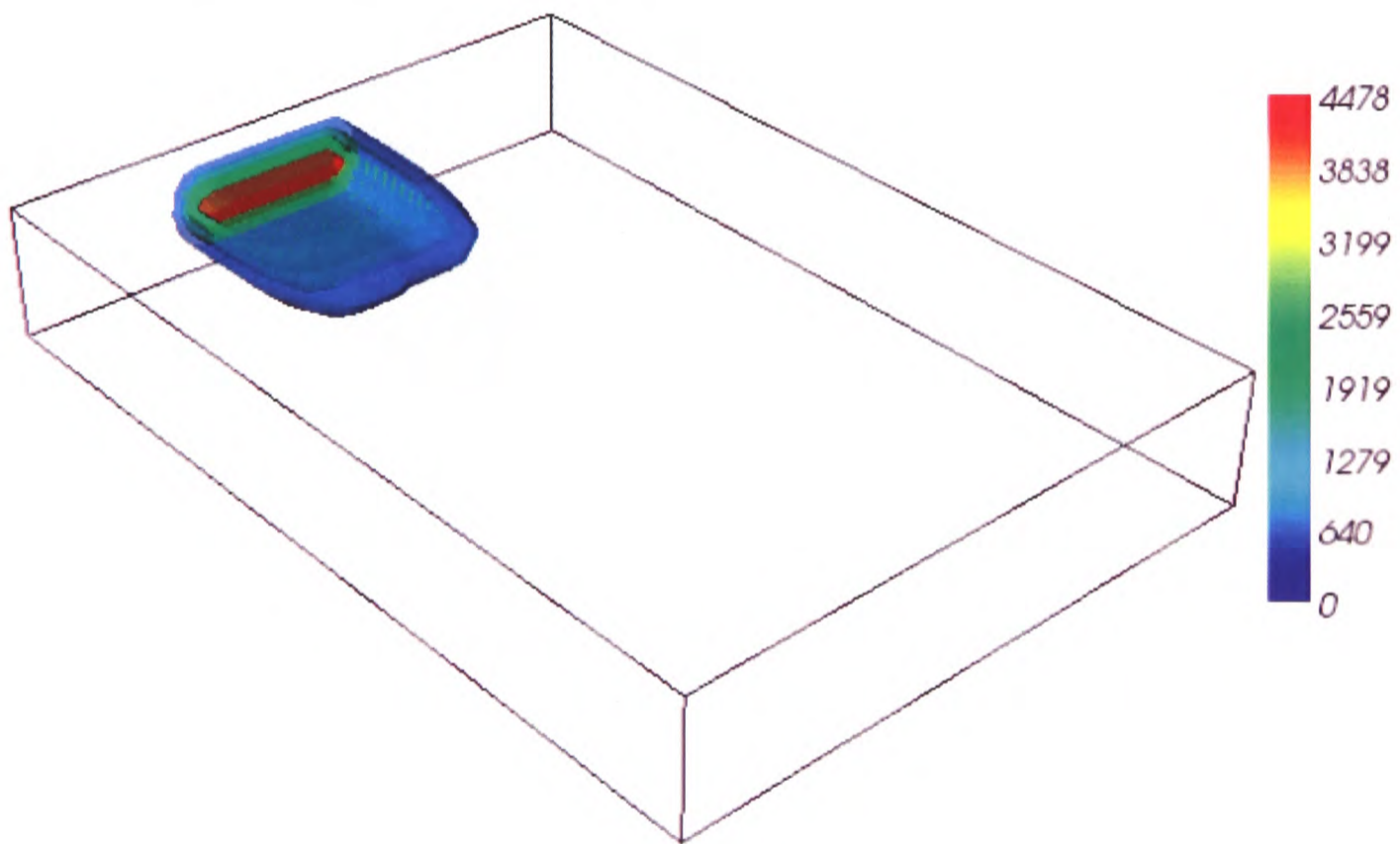


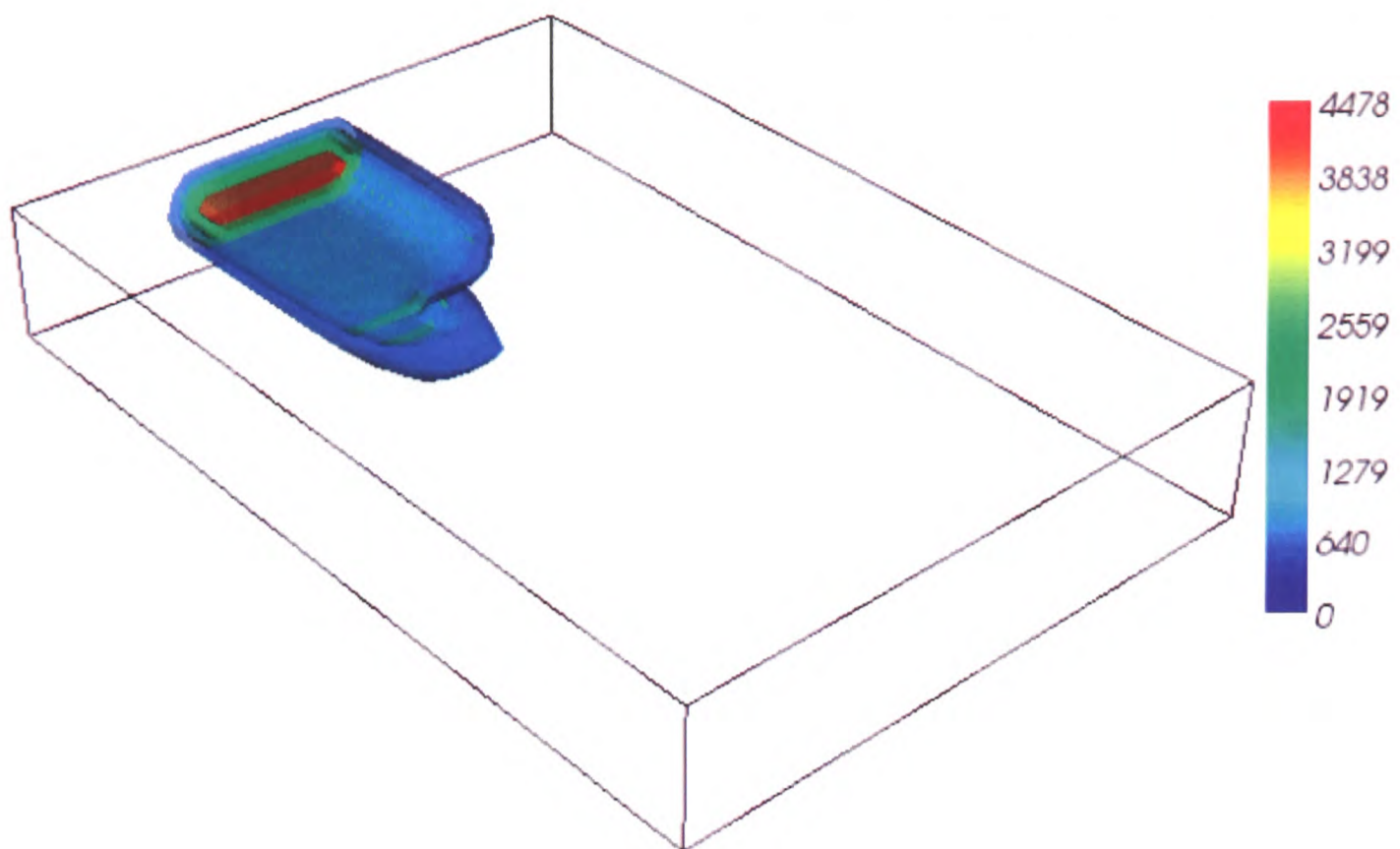
Figure 5-20. Contours of chloride concentration for two-d simulation (two offset clay lenses case). Plots a-j show transport at Julian date 2001-20001 with a time interval of two years.



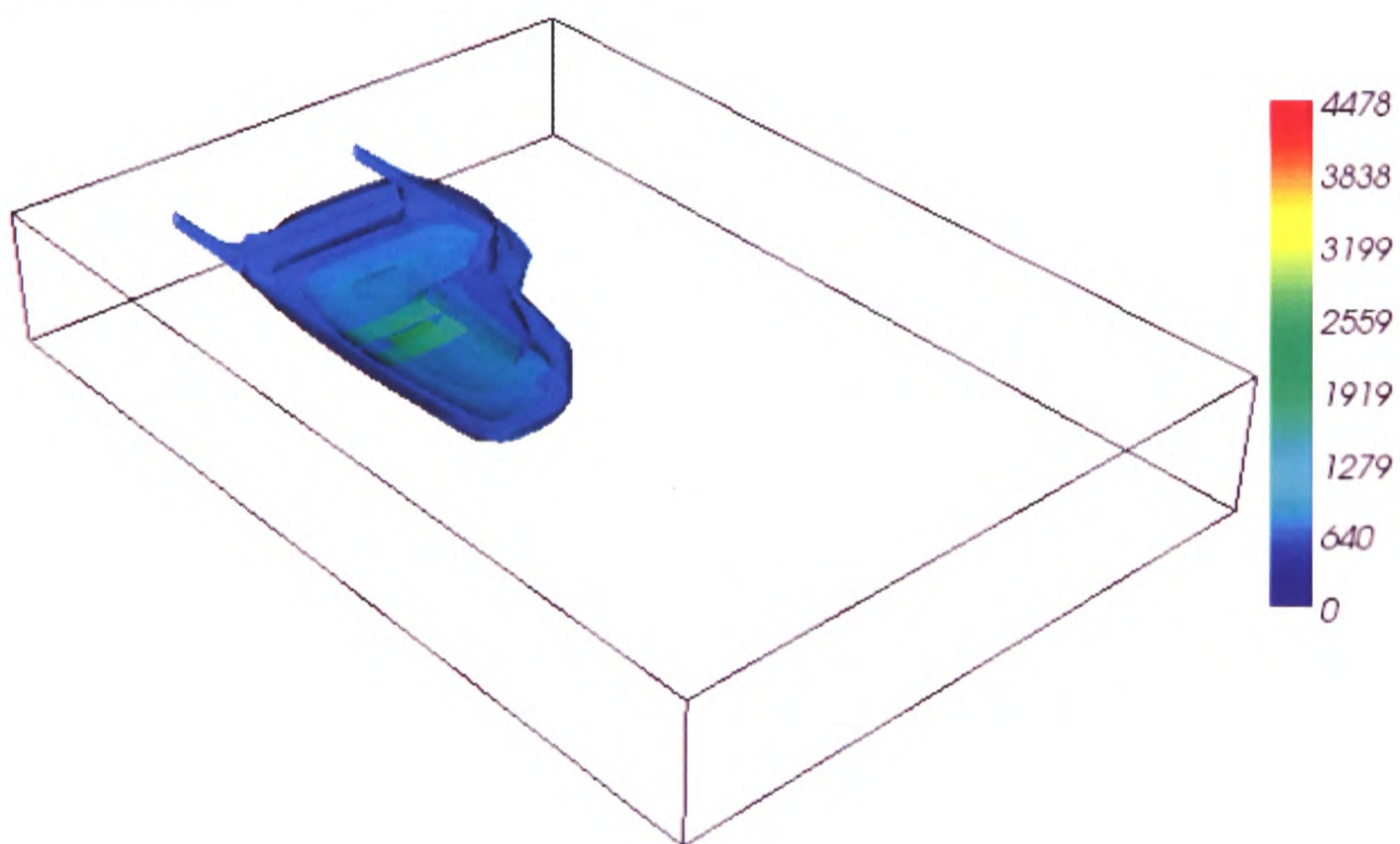
(a). Chloride concentration at Julian date 2001.



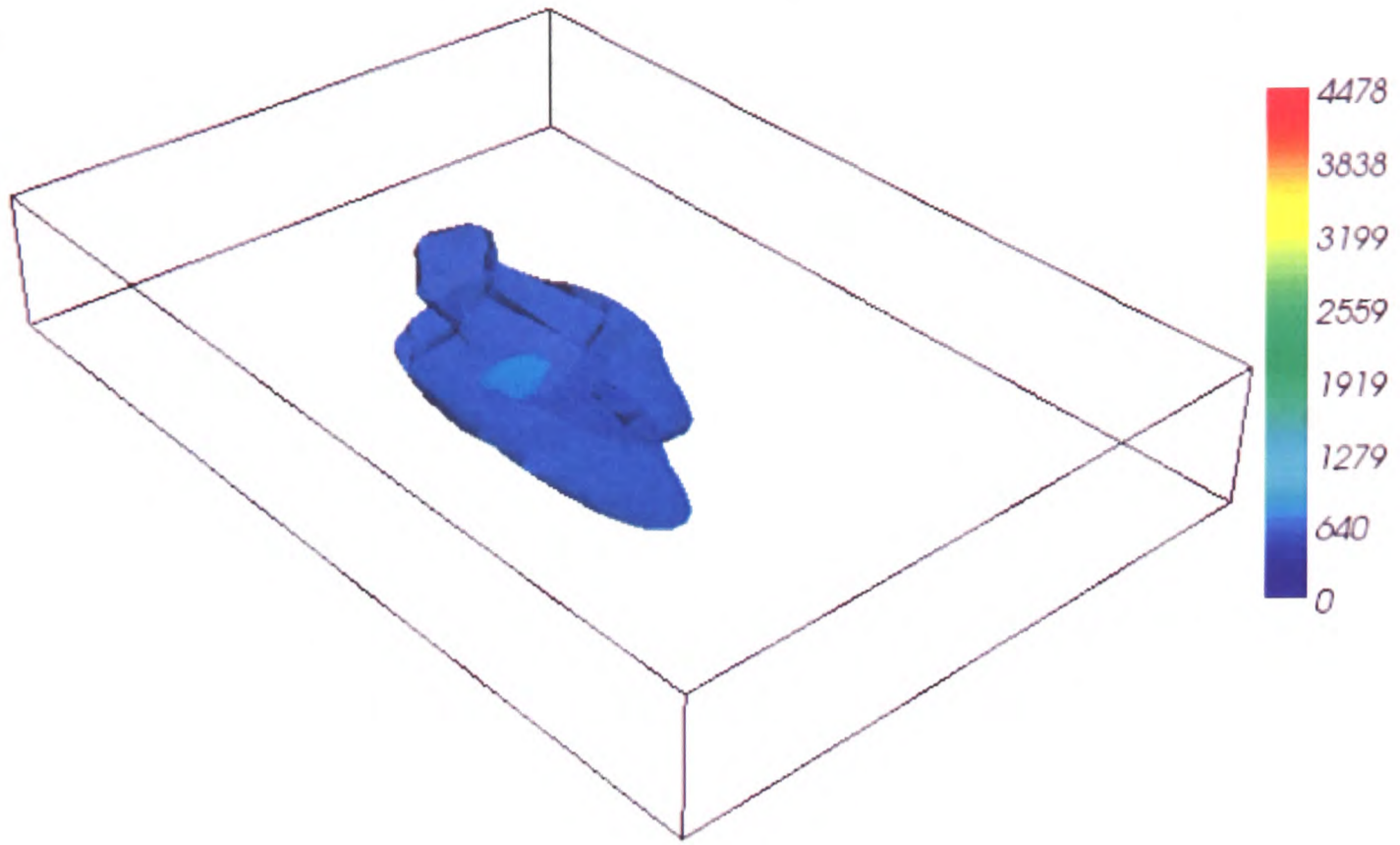
(b). Chloride concentration at Julian date 5001.



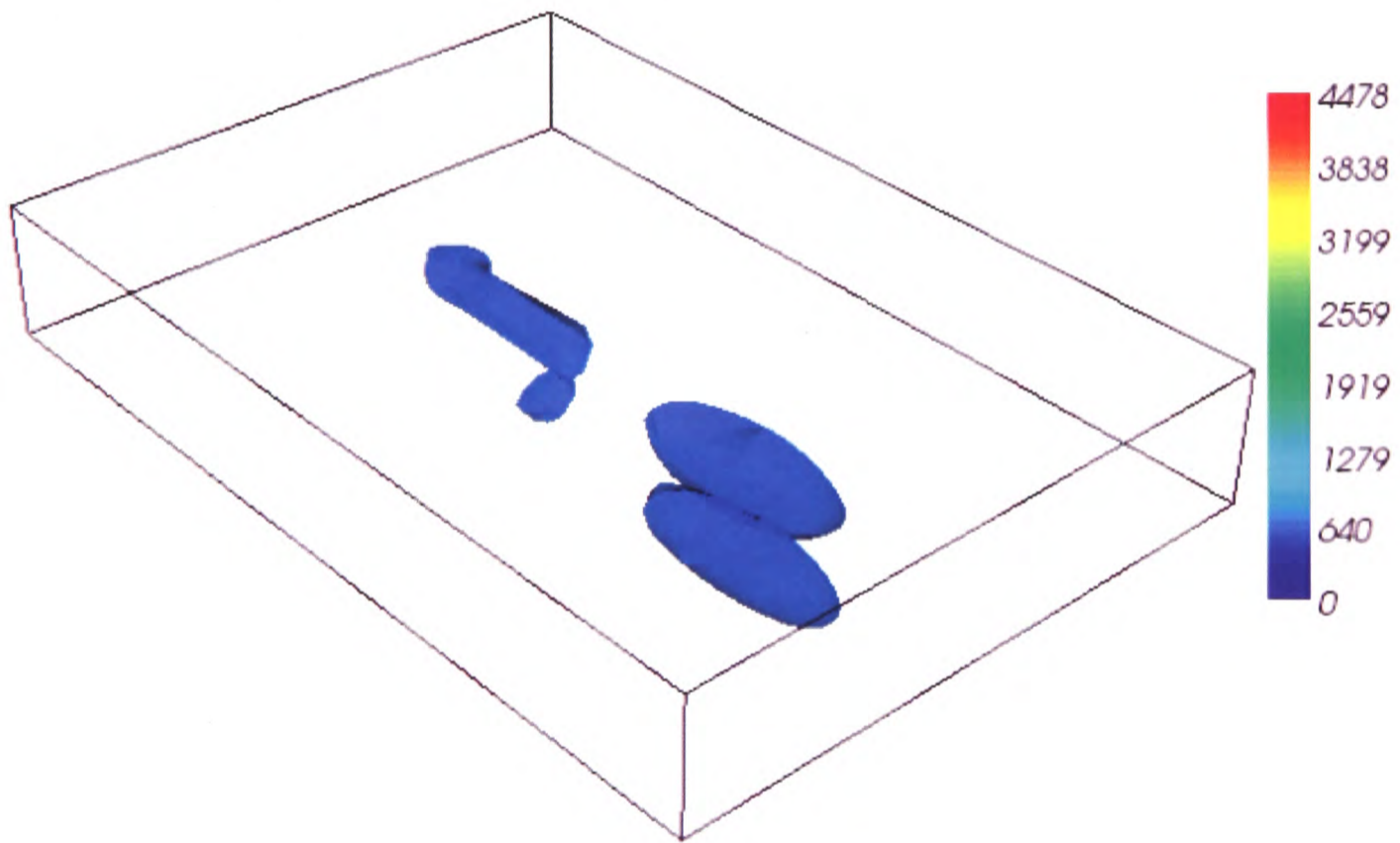
(c). Chloride concentration at Julian date 8001.



(d). Chloride concentration at Julian date 11001.



(e). Chloride concentration at Julian date 14001.



(f). Chloride concentration at Julian date 17001.

Figure 5-21. 3D results of simulated chloride concentration at different time intervals.

5.3 Concluding Remarks

Computational techniques have been implemented within a multi-physics environment to predict the behaviour of heterogeneities within the porous media on fluid flow prediction and plume migration. Investigated test cases of predominant layering heterogeneity are observed to give a range of different flow and concentration profiles within the subsurface. This reveals the fact that these profiles are affected by the nature of medium as a function of its position. In case of colloid migration phenomenon through such systems, the system heterogeneities can result in preferential colloid particle transport.

It is also concluded that the predicted results for Burnstump case study are comparable to observed data in instances where enough information is available to describe the geology. In instances where sufficient data is not available about the geology, the tool can be used to undertake “what-if” type simulations to understand the likely impact such as risk assessment of the underlying groundwater resources.

STRESS ANALYSIS

This chapter provides a theoretical background and numerical solution algorithm for the coupled transient fluid flow and deformation analysis of unsaturated soils. The effects of volume change due to dissipation of excess pore water pressure or suction as a result of applied loads are revealed in expansive clay materials.

6.1 Introduction

The theory of elasticity which forms the central core of solid mechanics abounds applications in a wide range of engineering and scientific disciplines. During recent years considerable progress has been made in finding the solution of problems arising in structural mechanics, material science, geophysics and medicine using the methods of theory of elasticity.

In geotechnical problems the process of soil consolidation, deformation and failure are governed by the stresses acting on the soil skeleton. The design, operation and maintenance of geotechnical and geo-environmental structures such as retaining walls, pavements, earth dams and soil liners and covers can well understood by employing the theories related to the determination of mechanical behaviour of soils.

In accordance with the stress level involved, the deformation problems that are dealt in soil mechanics can be divided into two main categories (Fredlund and Rahardjo [51]) (Figure 6-1). Elasticity theories are usually employed for the problems involving low deviator stress levels. Such systems undergo deformation that is recoverable. Plasticity theories, on the other hand, are more suitable for the problems that come across relatively high stress levels. Such systems may undergo deformations that are irreversible. Current study deals with the problems based on the assumption that the soil behaves perfectly plastic and the plasticity analysis is conducted using the stress state variable approach.

6.2 Assessment of Mechanical Behaviour of Soils

The application of stress causes deformation in soil matrix in general. In fully saturated soil where the soil particles are considered incompressible the applied load results in a change of volume of voids leading to a corresponding change in pore pressure. The state of stress in a soil consists of certain combination of stress variables generally referred to as stress state variables which are independent of physical properties of the soil. The number of stress state variables required for the description of stress state of a soil depends primarily upon the number of phases involved.

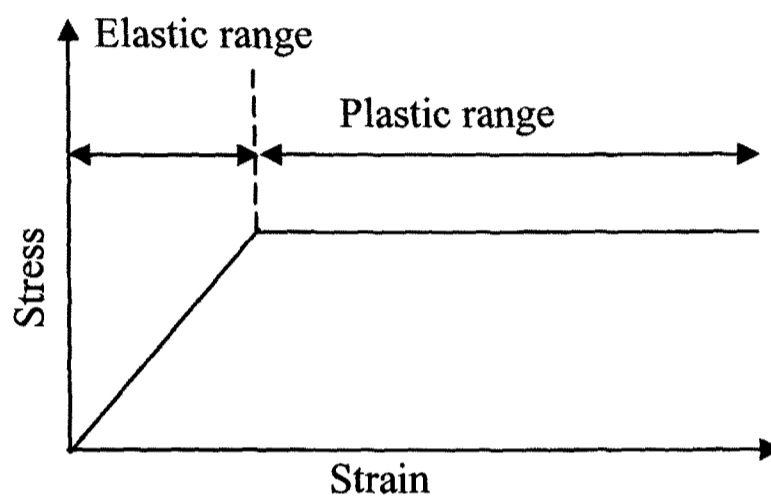


Figure 6-1. Idealized elastic-plastic behaviour giving rise to two categories of deformation analysis. Source: Fredlund and Rahardjo [51].

It is assumed that any deformation in the saturated soil mass takes place due to changes in the stress variable, effective stress, which uniquely describes a mechanical state on which the behaviour of soil skeleton depends. In mathematical form the effective stress variable is represented by Terzaghi [78] principal as follows

$$\sigma' = \sigma - u_w \quad (6.1)$$

where σ' = effective normal stress, σ = total normal stress and u_w = pore water pressure.

All mechanical aspects of a saturated soil (i.e. volume change and shear strength behaviour) are governed by the effective stress.

The unsaturated soils being a two-phase system of water and air form a more compressible medium and allow more deformation in response to the applied stresses. A given change in the volume of the soil mass would result in a volume change of water of less magnitude, with the difference being the volume change of the air phase.

The saturated soil theory in an extended form can be used to present the stress analysis for an unsaturated soil. Due to more complex nature of the unsaturated porous systems the single-valued effective stress approach, however, has studied to be faced with many difficulties. A two independent stress state variable approach is adopted instead for unsaturated soils.

6.2.1 Stress State Variables for Unsaturated Soils

The study of mechanical behaviour of unsaturated soil was initiated in late 1950's. The widely cited effective stress equation proposed by Bishop [79] is represented as

$$\sigma' = (\sigma - u_a) + \chi(u_a - u_w) \quad (6.2)$$

where u_a = pore air pressure and χ = parameter related to the degree of saturation of the soil varying from zero for dry soil to unity for fully saturated state. $(\sigma - u_a)$, the net normal stress, is the stress component which is conducted through the soil skeleton and $(u_a - u_w)$ is the matric suction.

Jennings and Burland [80] suggested that the Bishop equation for unsaturated soil is unable to provide a suitable relationship between volume change and effective stress for soils below a critical degree of saturation. The parameter χ was found to be unable to fit into the soil mechanics framework described by Terzaghi. The concept of two independent stress state variables was introduced by Bishop and Blight [81]. They suggested that the effective stress σ' and net normal stress $(\sigma - u_a)$ correspond to dissimilar changes with a variation in matric suction $(u_a - u_w)$. Another form of effective stress equation was presented by Richards [82] with the addition of a solute suction component. In mathematical terms it can be written as

$$\sigma' = (\sigma - u_a) + \chi_m(h_m + u_a) + \chi_s(h_s + u_a) \quad (6.3)$$

where χ_m = effective stress parameter for matric suction, h_m = matric suction, χ_s = effective stress parameter for solute suction and h_s = solute suction.

Not much reference is found to the equation (6.3) in the literature. The stress state variables that form the basis of most current studies were presented theoretically by

Fredlund and Morgenstern [83]. They described three possible combinations which can be used as stress state variables for an unsaturated as follows

- i. $(\sigma - u_a)$ and $(u_a - u_w)$
- ii. $(\sigma - u_w)$ and $(u_a - u_w)$
- iii. $(\sigma - u_a)$ and $(\sigma - u_w)$

The stress state variables can be used to construct the constitutive equations which describe the shear strength behaviour and the volume change behaviour of unsaturated soils.

As the soils are most commonly subjected to compressive normal stresses the set of three independent normal stresses can be expressed in terms of $(\sigma - u_a)$, $(u_a - u_w)$ and (u_a) (Fredlund and Rahardjo [51]). For the cases where the soil and the water particles are considered incompressible the stress component (u_a) can be ignored. The complete form of stress state for unsaturated soil in terms of shear and normal stresses can be represented as two independent stress tensors as

$$\begin{bmatrix} (\sigma_x - u_a) & \tau_{yx} & \tau_{zx} \\ \tau_{xy} & (\sigma_y - u_a) & \tau_{zy} \\ \tau_{xz} & \tau_{yz} & (\sigma_z - u_a) \end{bmatrix} \quad (6.4)$$

and

$$\begin{bmatrix} (u_a - u_w) & 0 & 0 \\ 0 & (u_a - u_w) & 0 \\ 0 & 0 & (u_a - u_w) \end{bmatrix} \quad (6.5)$$

Since the stress variables have different soil properties therefore the above tensors cannot be combined into one matrix. For compressible soil or fluid particles the third stress tensor (u_a) can be described as

$$\begin{bmatrix} u_a & 0 & 0 \\ 0 & u_a & 0 \\ 0 & 0 & u_a \end{bmatrix} \quad (6.6)$$

where the pore-air and the pore-water pressures are usually expressed in terms of gauge pressure.

6.2.2 Volume Change Analysis

Earth retaining structures constructed on clayey expansive soils have tendency to undergo considerable changes in volume as a consequence of changing environmental conditions. The volume change conditions can be associated with water uptake by vegetation, water infiltration into soil due to watering at soil surface etc. the prediction of volume change behaviour of unsaturated soils can be analysed by computing the state variables along with the soil suction measurements empirically or the other experimental tests such as odometers.

The volume change associated with an unsaturated soil involves the description of two sets of deformation state variables, for instance, those related to soil structure deformation such as void ratio changes or porosity changes and those related to water phase deformation such as changes in water content. The deformation state variables in conjunction with the stress state variables form the constitutive equations for volume change analysis of unsaturated soils. The constitutive relations can be expressed in terms of elasticity, compressibility or soil mechanics forms, each of which leads to a particular class of geotechnical problems.

Under an applied stress gradient the deformations in the unsaturated soil are associated with the total volume change of the soil element. This total change in volume, according to continuity requirement, must be equal to the sum of volume changes associated with air and the water phases. For incompressible soil particles it can be expressed as

$$\frac{\Delta V_v}{V_0} = \frac{\Delta V_w}{V_0} + \frac{\Delta V_a}{V_0} \quad (6.7)$$

where V_0 = initial overall volume of an unsaturated soil element, V_v = volume of soil voids, V_w = volume of water and V_a = volume of air.

Considering a Cartesian coordinate system the changes corresponding to the deformation and distortion in response to an applied stress can be expressed in terms of normal and shear strain in tensor form as

$$\begin{bmatrix} \varepsilon_x & \frac{1}{2}\gamma_{xy} & \frac{1}{2}\gamma_{xz} \\ \frac{1}{2}\gamma_{yx} & \varepsilon_y & \frac{1}{2}\gamma_{yz} \\ \frac{1}{2}\gamma_{zx} & \frac{1}{2}\gamma_{zy} & \varepsilon_z \end{bmatrix} \quad (6.8)$$

where ε_x , ε_y , ε_z = normal strain in x-, y- and z-direction and γ_{xy} , γ_{yz} , γ_{zx} = shear strain on the z-, x- and y-plane.

The sum of normal strain components is called volumetric strain ε_v and is defined as

$$\varepsilon_v = \frac{\Delta V_v}{V_0} = \varepsilon_x + \varepsilon_y + \varepsilon_z$$

or in incremental form

$$d\varepsilon_v = \frac{dV_v}{V_0} = d\varepsilon_x + d\varepsilon_y + d\varepsilon_z \quad (6.9)$$

The volumetric strain, which defines the soil structure volume change resulting from deformation, can be used as a deformation state variable for the soil structure.

6.2.2.1 Constitutive Relationships

Under the assumption that the deformation state variables satisfy the continuity requirements the constitutive relations for unsaturated soils can be formulated by linking the deformation state variables to the stress state variables of net normal stress and matric suction. The volume change in soil due to externally applied loads and the environmental changes can be predicted by making use of constitutive relations. The constitutive relations are discussed in the following section in elasticity, compressibility and volume mass forms.

6.2.2.1.1 Elasticity Form

Soil structure constitutive relations: The theoretical basis for constitutive relations was provided by Biot [84]. His work is based on the assumption that the soil material is isotropic and Darcy's law is applicable. His work was further developed by Fredlund and Rahardjo [51]. The basic stress strain relations for saturated soils assuming linear elastic behaviour in the x-, y-, and z-direction have the following form (Fredlund and Rahardjo [51])

$$\begin{aligned}
 \varepsilon_x &= \frac{(\sigma_x - u_w)}{E} - \frac{\mu}{E}(\sigma_y + \sigma_z - 2u_w) \\
 \varepsilon_y &= \frac{(\sigma_y - u_w)}{E} - \frac{\mu}{E}(\sigma_x + \sigma_z - 2u_w) \\
 \varepsilon_z &= \frac{(\sigma_z - u_w)}{E} - \frac{\mu}{E}(\sigma_x + \sigma_y - 2u_w)
 \end{aligned} \tag{6.10}$$

where E = modulus of elasticity for the soil structure with respect to a change in net normal stress and μ = Poisson's ratio.

Using the appropriate stress state variables the constitutive relations for unsaturated soil can be formulated as an extension of the equation (6.10). The soil structure constitutive relations associated with normal strains in the x-, y-, and z-direction then can be written as

$$\begin{aligned}
 \varepsilon_x &= \frac{(\sigma_x - u_a)}{E} - \frac{\mu}{E}(\sigma_y + \sigma_z - 2u_a) + \frac{(u_a - u_w)}{H} \\
 \varepsilon_y &= \frac{(\sigma_y - u_a)}{E} - \frac{\mu}{E}(\sigma_x + \sigma_z - 2u_a) + \frac{(u_a - u_w)}{H} \\
 \varepsilon_z &= \frac{(\sigma_z - u_a)}{E} - \frac{\mu}{E}(\sigma_x + \sigma_y - 2u_a) + \frac{(u_a - u_w)}{H}
 \end{aligned} \tag{6.11}$$

Adding and subtracting $\frac{\mu}{E}(\sigma - u_a)$ to each component of equation (6.11) it can be written in the following form

$$\begin{aligned}
 \varepsilon_x &= \frac{(1+\mu)}{E}(\sigma_x - u_a) - \frac{\mu}{E}(\sigma_x + \sigma_y + \sigma_z - 3u_a) + \frac{(u_a - u_w)}{H} \\
 \varepsilon_y &= \frac{(1+\mu)}{E}(\sigma_y - u_a) - \frac{\mu}{E}(\sigma_x + \sigma_y + \sigma_z - 3u_a) + \frac{(u_a - u_w)}{H} \\
 \varepsilon_z &= \frac{(1+\mu)}{E}(\sigma_z - u_a) - \frac{\mu}{E}(\sigma_x + \sigma_y + \sigma_z - 3u_a) + \frac{(u_a - u_w)}{H}
 \end{aligned} \tag{6.12}$$

where H is the modulus of elasticity for the soil structure with respect to a change in matric suction. A change in the volumetric strain of the soil for each increment, $d\varepsilon_v$, can be obtained by adding the changes in normal strains in x-, y-, and z-directions and making use of equation (6.9) as

$$d\varepsilon_v = 3\left(\frac{1-2\mu}{E}\right)d\left(\frac{\sigma_x + \sigma_y + \sigma_z}{3} - u_a\right) + \frac{3}{H}d(u_a - u_w)$$

or in simplified form

$$d\varepsilon_v = 3\left(\frac{1-2\mu}{E}\right)d(\sigma_{mean} - u_a) + \frac{3}{H}d(u_a - u_w) \quad (6.13)$$

The constitutive equations associated with the shear deformations are

$$\begin{bmatrix} \varepsilon_x \\ \varepsilon_y \\ \varepsilon_z \\ \gamma_{xy} \\ \gamma_{yz} \\ \gamma_{zx} \end{bmatrix} = \frac{1}{E} \begin{bmatrix} 1 & -\mu & -\mu & 0 & 0 & 0 \\ -\mu & 1 & -\mu & 0 & 0 & 0 \\ -\mu & -\mu & 1 & 0 & 0 & 0 \\ 0 & 0 & 0 & 2(1+\mu) & 0 & 0 \\ 0 & 0 & 0 & 0 & 2(1+\mu) & 0 \\ 0 & 0 & 0 & 0 & 0 & 2(1+\mu) \end{bmatrix} \begin{bmatrix} (\sigma_x - u_a) \\ (\sigma_y - u_a) \\ (\sigma_z - u_a) \\ \tau_{xy} \\ \tau_{yz} \\ \tau_{zx} \end{bmatrix} \\ + \frac{1}{H} \begin{bmatrix} 1 & 0 & 0 & 0 & 0 & 0 \\ 0 & 1 & 0 & 0 & 0 & 0 \\ 0 & 0 & 1 & 0 & 0 & 0 \\ 0 & 0 & 0 & 0 & 0 & 0 \\ 0 & 0 & 0 & 0 & 0 & 0 \\ 0 & 0 & 0 & 0 & 0 & 0 \end{bmatrix} \begin{bmatrix} u_a - u_w \\ u_a - u_w \\ u_a - u_w \\ u_a - u_w \\ u_a - u_w \\ u_a - u_w \end{bmatrix}$$

$$\gamma_{xy} = \frac{\tau_{xy}}{G}, \quad \gamma_{yz} = \frac{\tau_{yz}}{G}, \quad \gamma_{zx} = \frac{\tau_{zx}}{G} \quad (6.14)$$

Combining equations (6.12) and (6.14) gives

$$(6.15)$$

Rearranging equation (6.15) provides

$$\begin{bmatrix} \sigma_x - u_a \\ \sigma_y - u_a \\ \sigma_z - u_a \\ \tau_{xy} \\ \tau_{yz} \\ \tau_{zx} \end{bmatrix} = \frac{E}{(1+\mu)(1-2\mu)} \begin{bmatrix} 1-\mu & \mu & \mu & 0 & 0 & 0 \\ \mu & 1-\mu & \mu & 0 & 0 & 0 \\ \mu & \mu & 1-\mu & 0 & 0 & 0 \\ 0 & 0 & 0 & \frac{1-2\mu}{2} & 0 & 0 \\ 0 & 0 & 0 & 0 & \frac{1-2\mu}{2} & 0 \\ 0 & 0 & 0 & 0 & 0 & \frac{1-2\mu}{2} \end{bmatrix} \times \\ \begin{bmatrix} \varepsilon_x - \frac{u_a - u_w}{H} \\ \varepsilon_y - \frac{u_a - u_w}{H} \\ \varepsilon_z - \frac{u_a - u_w}{H} \\ \gamma_{xy} \\ \gamma_{yz} \\ \gamma_{zx} \end{bmatrix} \quad (6.16)$$

This can be reduced to

$$\{\sigma\} - \{u_a\} = [D] \left(\varepsilon - \frac{u_a - u_w}{H} \right) \quad (6.17)$$

or

$$\{\sigma\} = [D] \varepsilon - [D] \left(\frac{u_a - u_w}{H} \right) + \{u_a\} \quad (6.18)$$

where D is given as

$$D = c \begin{bmatrix} 1-\mu & \mu & \mu & 0 & 0 & 0 \\ \mu & 1-\mu & \mu & 0 & 0 & 0 \\ \mu & \mu & 1-\mu & 0 & 0 & 0 \\ 0 & 0 & 0 & \frac{1-2\mu}{2} & 0 & 0 \\ 0 & 0 & 0 & 0 & \frac{1-2\mu}{2} & 0 \\ 0 & 0 & 0 & 0 & 0 & \frac{1-2\mu}{2} \end{bmatrix}$$

where c is given as

$$c = \frac{E}{(1+\mu)(1-2\mu)}$$

Water phase constitutive relations: For unsaturated soils the soil structure constitutive relationship is not sufficient to describe the volume change behaviour. A second constitutive relationship is required either in form of water or the air phase. Assuming water is incompressible, the water phase constitutive relations can be formulated as follows

$$\frac{dV_w}{V_0} = \frac{1}{E_w} d(\sigma - 3u_a) + \frac{1}{H_w} d(u_a - u_w) \quad (6.19)$$

where E_w = water volumetric modulus associated with a change net normal stress and H_w = water volumetric modulus associated with a change in matric suction.

The elasticity forms can be used to solve non-linear elastic volume change problems associated with unsaturated soils in two- or three-dimensions.

6.2.2.1.2 Compressibility Form

For a saturated soil the compressibility form of the constitutive equation (Fredlund and Rahardjo [51]) is represented as

$$d\varepsilon_v = m_v d(\sigma - u_w)$$

where m_v = coefficient of volume change. Using the stress state variables the compressibility form of soil structure constitutive equation for an unsaturated soil can be written as

$$d\varepsilon_v = m_1^s d(\sigma_{mean} - u_a) + m_2^s d(u_a - u_w) \quad (6.20)$$

The compressibility form of the water phase constitutive equation for an unsaturated soil can be presented as

$$\frac{dV_w}{V_0} = m_1^w d(\sigma_{mean} - u_a) + m_2^w d(u_a - u_w) \quad (6.21)$$

where σ_{mean} = mean net normal stress $[(\sigma_x + \sigma_y + \sigma_z)/3]$,

m_1^s = coefficient of volume change with respect to net normal stress $[= 3(1 - 2\mu)/E]$,

m_2^s = coefficient of volume change with respect to matric suction $[3/H]$,

m_1^w = coefficient of water volume change with respect to net normal stress $[= 3/E_w]$,

m_2^w = coefficient of water volume change with respect to matric suction $[= 1/H_w]$.

6.2.2.1.3 Volume-Mass Form

The constitutive relation for volume-mass form for saturated soil can be constructed by incorporating the void ratio of the medium. It can be represented by mean of the following equation

$$de = a_w d(\sigma - u_w)$$

where a_w = coefficient of compressibility. For unsaturated soil the deformation state variables of void ratio and gravimetric water content can be used to construct the constitutive relations for soil structure and the water phase as follows

$$de = a_t d(\sigma_{mean} - u_a) + a_m d(u_a - u_w)$$

$$dw = b_t d(\sigma_{mean} - u_a) + b_m d(u_a - u_w)$$

where e = void ratio,

a_t = coefficient of compressibility with respect to a change in net normal stress,

a_m = coefficient of compressibility with respect to a change in matric suction,

b_t = coefficient of water content change with respect to a change in net normal stress,

b_m = coefficient of water content change with respect to a change in matric suction.

6.2.3 Use of SWCC in Volume Change Prediction

Soil properties associated with an unsaturated soil e.g. coefficient of permeability and coefficient of water storage are functions of stress state variables of net normal stress and matric suction. The soil water characteristic curve SWCC is defined as the relationship between water content and suction for a soil. The slope of the SWCC is used to express the water storage of a soil as a result of a change in the pore water pressure. Several equations, mainly empirical in nature, have been proposed in the research literature to simulate the soil water characteristic curve e. g. van Genuchten [64], Gardner [85], Haverkamp et al [14] and Brooks and Corey [86] etc. Each equation appears to apply for a particular group of soils. A general equation describing the soil water characteristic curve over the entire suction range (i.e. 0 to 1000,000 kPa) is given by Fredlund and Xing [87] as

$$\theta = \theta_s C(\psi) \left[\frac{1}{\ln(e + (\psi/a)^n)} \right]^m \quad (6.22)$$

where $c(\psi)$ = a correction factor for high soil suctions, defined as

$$C(\psi) = \left[1 - \frac{\ln(1 + \psi/\psi_r)}{\ln(1 + 1000,000/\psi_r)} \right] \quad (6.23)$$

where e = natural log base [= 2.71828], ψ_r = total suction corresponding to the residual water content, a = soil parameter related to the air entry value of the soil, n = soil parameter which controls the slope at the inflection point in the soil water characteristic curve and m = soil parameter which is related to the residual water content of the soil. There are several permeability functions that have been proposed in the literature to describe the permeability function of an unsaturated soil. The equation described by Leong and Rahardjo [88] is used in the current study. Using equation (6.22) with $C(\psi) = 1$, the permeability function takes the following form

$$k = k_s \left[\frac{1}{\ln(e + (\psi/a)^n)} \right]^{mp} \quad (6.24)$$

The parameter p can be determined by using a curve fitting of the coefficient of permeability data. The slope of soil water characteristic curve (i.e. coefficient of water storage = m_2^w) is obtained by differentiating the SWCC equation (6.22) (see appendix C). For correction factor $C(\psi) = 1$, the water storage function is given as

$$m_2^w = -mn \frac{\theta_s}{\left[\ln(e + (\psi/a)^n) \right]^{m+1}} \frac{\psi^{n-1}}{ea^n + \psi^n} \quad (6.25)$$

The coefficient of permeability, k , and the water storage function, m_2^w , are the soil properties required for transient water flow analysis of unsaturated soils. For water flow analysis if the pore-air pressure is assumed to be atmospheric, the distribution of pore-water pressure is equivalent to the matric suction distribution. Assuming that the total stress remains constant during a transient process and the pore-air pressure is atmospheric, the differential equation for water flow through a heterogeneous, isotropic saturated/unsaturated soil can be presented for the three-dimensional case as

$$\frac{\partial}{\partial x} \left(k \frac{\partial h}{\partial x} \right) + \frac{\partial}{\partial y} \left(k \frac{\partial h}{\partial y} \right) + \frac{\partial}{\partial z} \left(k \frac{\partial h}{\partial z} \right) = m_2^w \gamma_w \frac{\partial h}{\partial t} \quad (6.26)$$

where γ_w = unit weight of water.

6.2.4 Stress-Deformation Analysis

The equations of equilibrium for the soil structure of an unsaturated soil are

$$\begin{aligned} \frac{\partial \sigma_x}{\partial x} + \frac{\partial \tau_{xy}}{\partial y} + \frac{\partial \tau_{xz}}{\partial z} &= b_x \\ \frac{\partial \tau_{xy}}{\partial x} + \frac{\partial \sigma_y}{\partial y} + \frac{\partial \tau_{yz}}{\partial z} &= b_y \\ \frac{\partial \tau_{xz}}{\partial x} + \frac{\partial \tau_{yz}}{\partial y} + \frac{\partial \sigma_z}{\partial z} &= b_z \end{aligned} \quad (6.27)$$

where b_i ($i = x, y, z$) = components of the body forces acting in the direction represented by i . The total strains are related to the displacement via the equation given by

$$\varepsilon^T = Ld \quad (6.28)$$

The partial differential equations for plane strain loading for the soil structure can be derived from equations (6.16), (6.27) and (6.28) as follows

$$\frac{\partial}{\partial x} \left\{ C \left[(1-\mu) \frac{\partial u}{\partial x} + \mu \frac{\partial v}{\partial y} + \mu \frac{\partial w}{\partial z} - \frac{(1+\mu)}{H} (u_a - u_w) \right] \right\} + \frac{\partial}{\partial y} \left\{ G \left(\frac{\partial v}{\partial x} + \frac{\partial u}{\partial y} \right) \right\} + \frac{\partial}{\partial z} \left\{ G \left(\frac{\partial u}{\partial z} + \frac{\partial w}{\partial x} \right) \right\} = 0 \quad (6.29)$$

$$\frac{\partial}{\partial x} \left\{ G \left(\frac{\partial v}{\partial x} + \frac{\partial u}{\partial y} \right) \right\} + \frac{\partial}{\partial y} \left\{ C \left[\mu \frac{\partial u}{\partial x} + (1-\mu) \frac{\partial v}{\partial y} + \mu \frac{\partial w}{\partial z} - \frac{(1+\mu)}{H} (u_a - u_w) \right] \right\} + \frac{\partial}{\partial z} \left\{ G \left(\frac{\partial v}{\partial z} + \frac{\partial w}{\partial y} \right) \right\} = -\rho g \quad (6.30)$$

$$\frac{\partial}{\partial x} \left\{ G \left(\frac{\partial u}{\partial z} + \frac{\partial w}{\partial x} \right) \right\} + \frac{\partial}{\partial y} \left\{ G \left(\frac{\partial v}{\partial z} + \frac{\partial w}{\partial y} \right) \right\} + \frac{\partial}{\partial z} \left\{ C \left[\mu \frac{\partial u}{\partial x} + \mu \frac{\partial v}{\partial y} + (1-\mu) \frac{\partial w}{\partial z} - \frac{(1+\mu)}{H} (u_a - u_w) \right] \right\} = 0 \quad (6.31)$$

where g = acceleration due to gravity. Soil property functions required for stress-deformation analysis are the elastic parameter function, E , with respect to change in net normal stress, elastic parameter function, H , with respect to change in matric suction, and Poisson's ratio. The elastic moduli, E and H , can be calculated from the volume change indices, initial void ratio and Poisson's ratio as follows (Hung and Fredlund [89])

$$E = n_t (\sigma_{avg} - u_a)_{avg}; n_t = \frac{4.605(1+\mu)(1-2\mu)(1+e_0)}{C_s} \quad (6.32)$$

$$H = n_m (u_a - u_w)_{avg}; n_m = \frac{4.605(1+\mu)(1+e_0)}{C_m} \quad (6.33)$$

where n_t = coefficient that relates net normal stress with elastic modulus E , n_m = coefficient that relates matric suction with elastic modulus H , $(\sigma_{avg} - u_a)_{avg}$ = average of the initial and final net normal stress for an increment, $(u_a - u_w)_{avg}$ = average of the initial and final matric suction for an increment, C_s = volume change index from net normal stress plane, and C_m = volume change index from matric suction plane. The volume change index C_s (or C_m) is a slope of the void ratio versus logarithm of net normal stress (or matric suction) as shown in Figure 6-2. The semi-logarithmic plots of void ratio constitutive surface for an unsaturated soil is linear on the extreme planes (i.e. $\log(\sigma - u_a) = 0$ plane and $\log(u_a - u_w) = 0$ plane) (Fredlund and Rahardjo [51]).

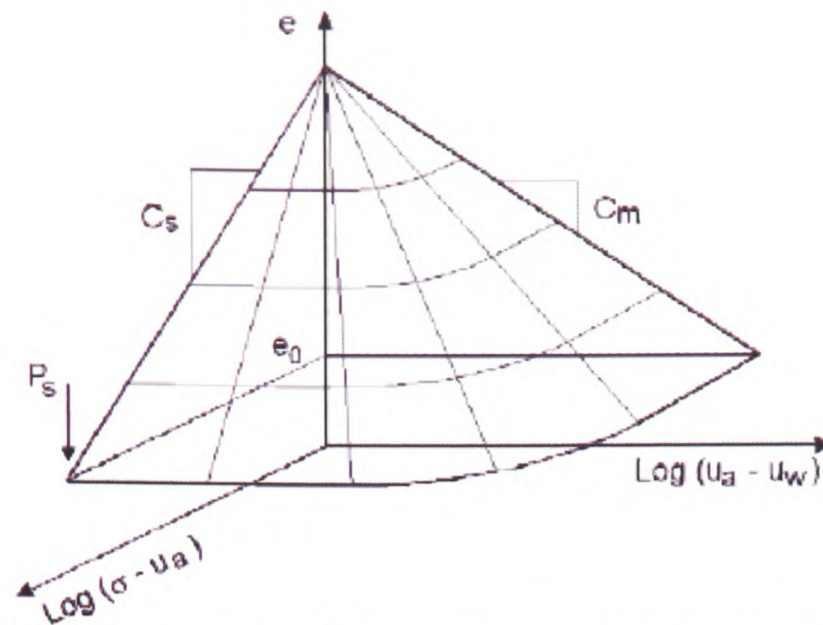


Figure 6-2. Semi-logarithmic plot of void ratio versus net normal stress and matric suction.
Source: Fredlund and Rahardjo [51].

Equations (6.29)-(6.31) can be used to compute the displacements under an applied load or due to changes in matric suction.

6.3 Implementation

Current methods for deformation analysis of unsaturated soil problems use either an uncoupled hydrological approach or a fully coupled hydro-mechanical approach (Sheng et al [90]). The uncoupled hydrological approach seeks the solution of continuity equations first considering a non-deformable body. The information thus obtained is used to solve mechanical equilibrium equations for the displacements. This approach suffers the inconsistency between the continuity equations for a non-deformable body and the mechanical equilibrium equations for a deformable body. Although simple, this approach is restricted to soil that do not experience significant volume change over time.

The coupled hydro-mechanical approach, also adopted in this study, is based on the continuity equations for deformable media. The coupling between the continuity equations and mechanical equilibrium relations is performed through volumetric strain rate and the relationships between the stress state variables which are solved simultaneously. The stress-deformation analysis in this study is carried out using the elastic-visco-plastic (EVP) algorithm to formulate the stress-strain relations and elasticity problems. The objectives of the study are

- To adapt a two-dimensional finite element model which is capable of predicting the volume change behaviour of an unsaturated soil in response to externally applied loads.
- To evaluate the magnitude of deformation in the soil profile due to applied load and matric suction changes.
- To investigate the influence of different input stress parameters, soil property data, initial-boundary conditions and the processes such as leakage of water underneath flexible covers.
- To display the spatial distribution of matric suction and cumulative displacement profiles due to wetting and loading at various elapsed times.

6.3.1 Comparisons and Validation

The example presented here shows a comprehensive volume change problem in an unsaturated medium. The problem to be analysed is illustrated in Figure 6-3 and Figure 6-4 for flow prediction and the deformation analysis respectively. For flow predictions the problem considers a 5 metre deep deposit of unsaturated swelling clay that rests underneath a flexible cover (Hung and Fredlund [89]). Swelling due to leakage of water under the cover is predicted for various predetermined elapsed times. The initial matric suction in the soil mass is assumed to be constant and with a value equal to 400 kPa. The assumed soil properties for flow analysis are listed in Table 6-1.

For deformation analysis a load of 10 kPa is applied in the form of a concrete slab on the soil surface as shown in the Figure 6-4. The boundary conditions are specified for stress-deformation analysis as follows. At the left and right sides of the domain, the soil is free to move in the vertical direction while it is fixed in the horizontal direction. The lower boundary is fixed in both directions. The deformations are predicted for various predetermined elapsed times as well. The assumed soil properties for deformation analysis are listed in Table 6-2.

The analysis is considered to be purely elastic where the plastic part in Model's EVP module is switched off by considering a very high value (1.0×10^{20}) of the yield stress.

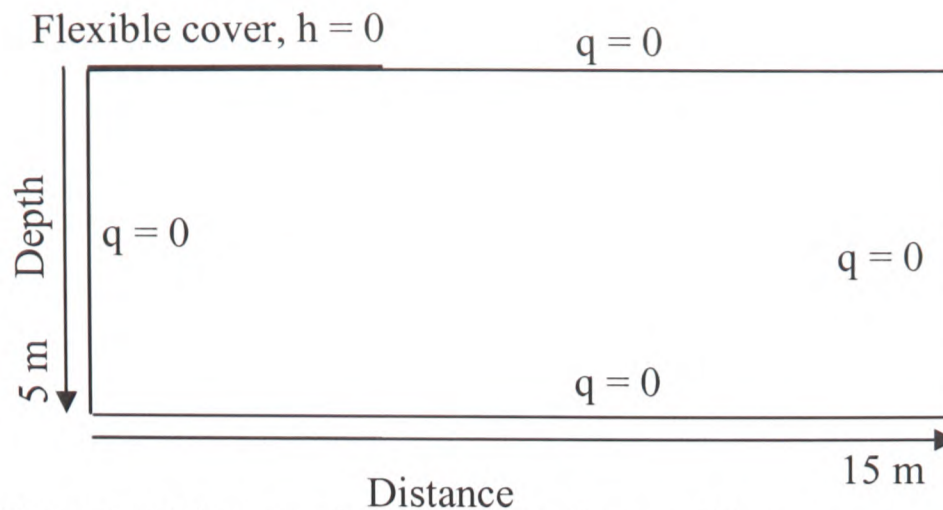


Figure 6-3. Geometry of the example problem with flow conditions.

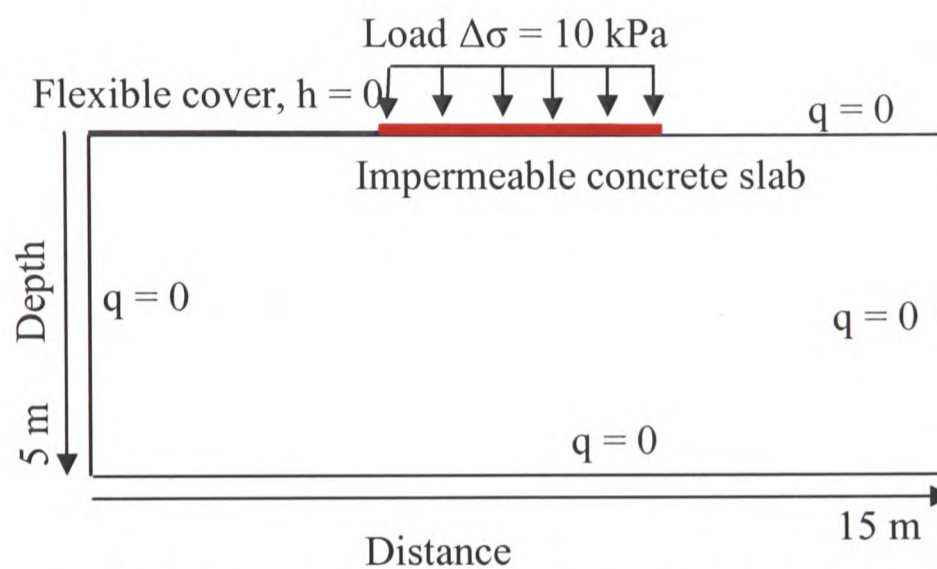


Figure 6-4. Geometry of the problem with flow conditions and applied load.

Soil properties	k_s (m/s)	θ_s	$(u_a - u_w)_{ini}$ (kPa)	a (kPa)	n	m	p
Values	1.157×10^{-8}	0.45	400	100	1.5	1	1

Table 6-1. Assumed soil properties for flow analysis.

Properties	e_0	μ	E	H
Values	1.0	0.4	$12.89 (\sigma_{avg} - u_a)_{avg}$	$184.20 (u_a - u_w)$

Table 6-2. Assumed soil properties for stress-deformation analysis.

The transient seepage analysis is conducted to predict matric suction changes with time as the wetting front advances into the soil mass. The stress-deformation is then performed to predict the displacements due to changes in matric suction and under the

influence of applied load. The comparison between contour plots of matric suction at day 100 presented by Hung and Fredlund [89] and Physica simulations is shown in Figure 6-5. The simulated contour plots of matric suction at day 200 are also shown in Figure 6-6. Development of matric suction below the cover versus time is presented in Figure 6-7. After 200 days of wetting, matric suction below the cover reduces to about 80 kPa.

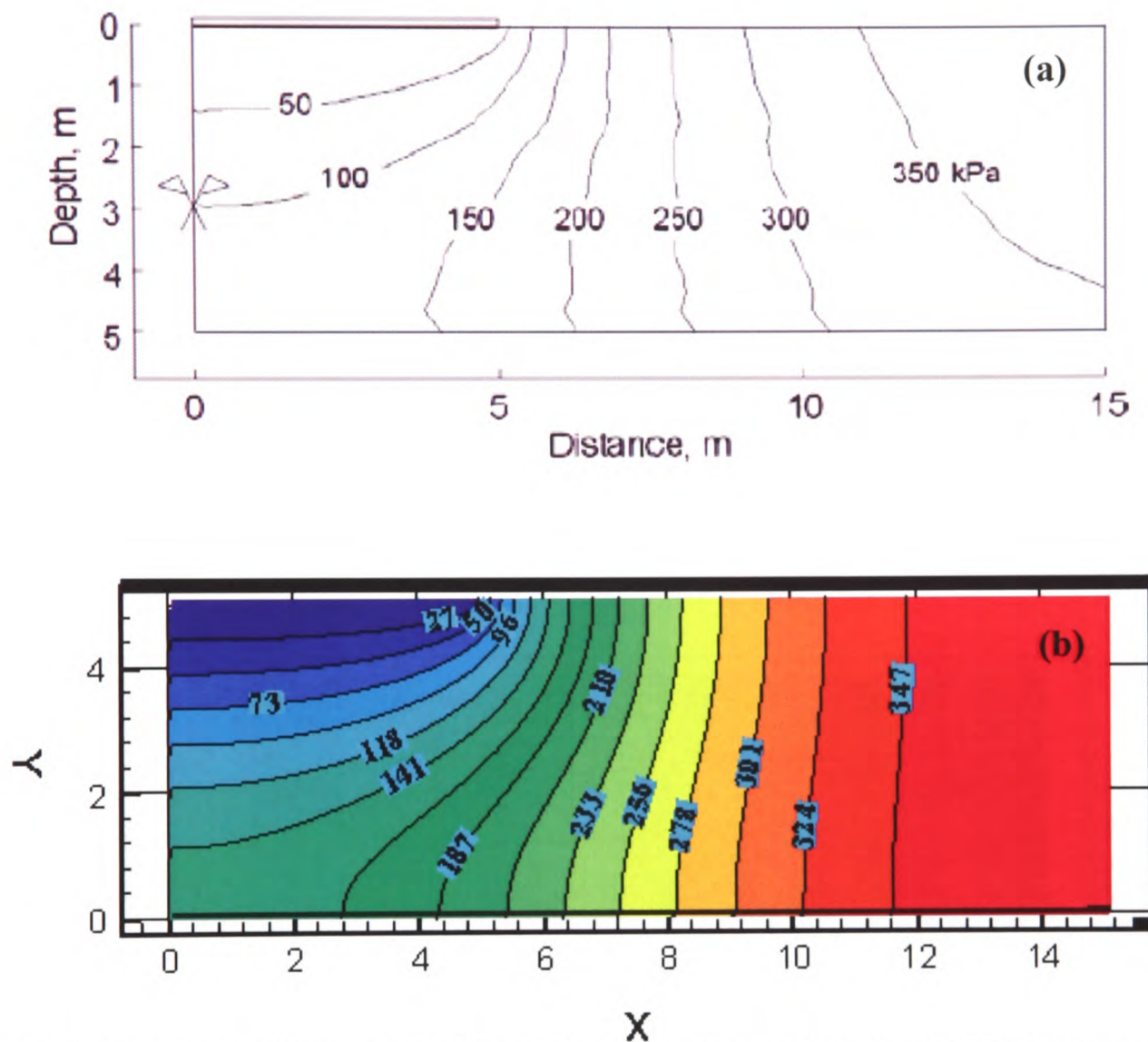


Figure 6-5. Matric suction distribution at day 100. (a) Hung and Fredlund [89]. (b) Physica results.

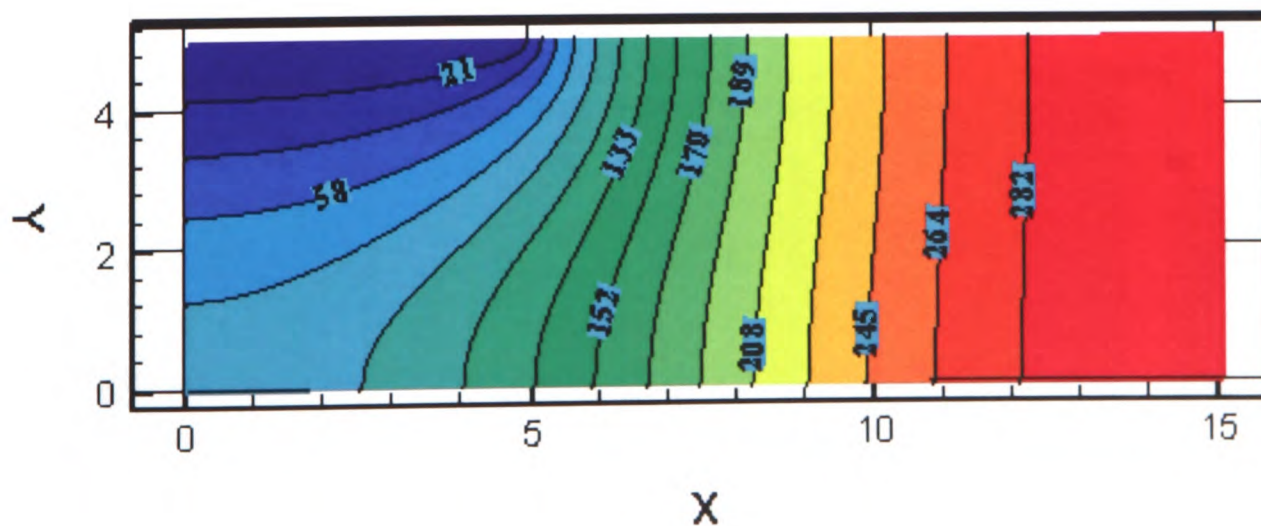


Figure 6-6. Matric suction distribution at day 200.

Because the parameter $p = 1$, the shapes of the soil-water characteristic curve and the permeability are similar. The contour plots of SWCC and the permeability function are shown in Figure 6-8a & b respectively.

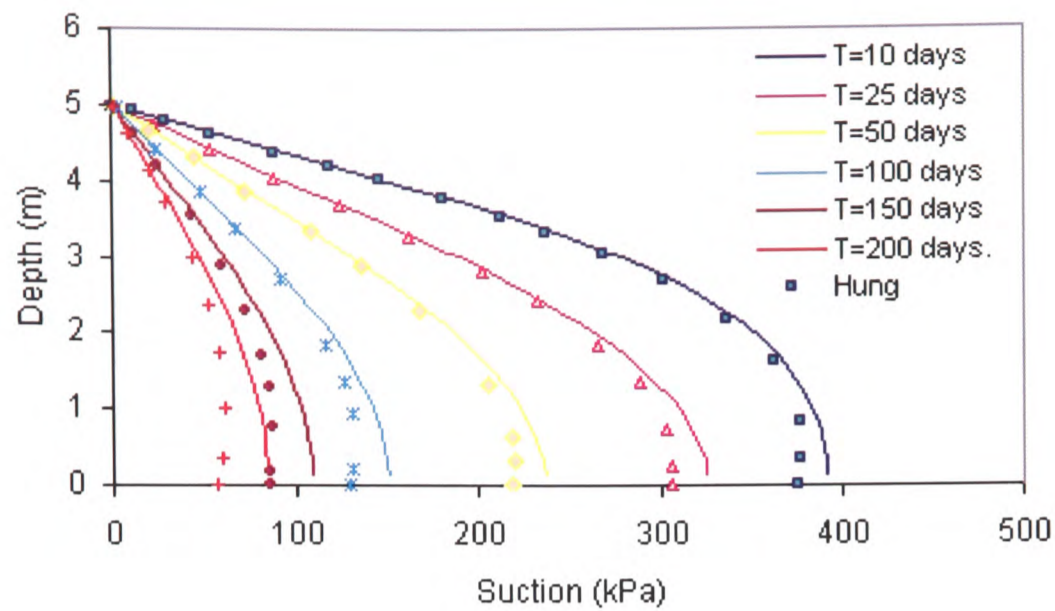


Figure 6-7. Comparison of matric suction development below the cover versus depth with time. Solid lines = Physica results, symbols = Hung and Fredlund.

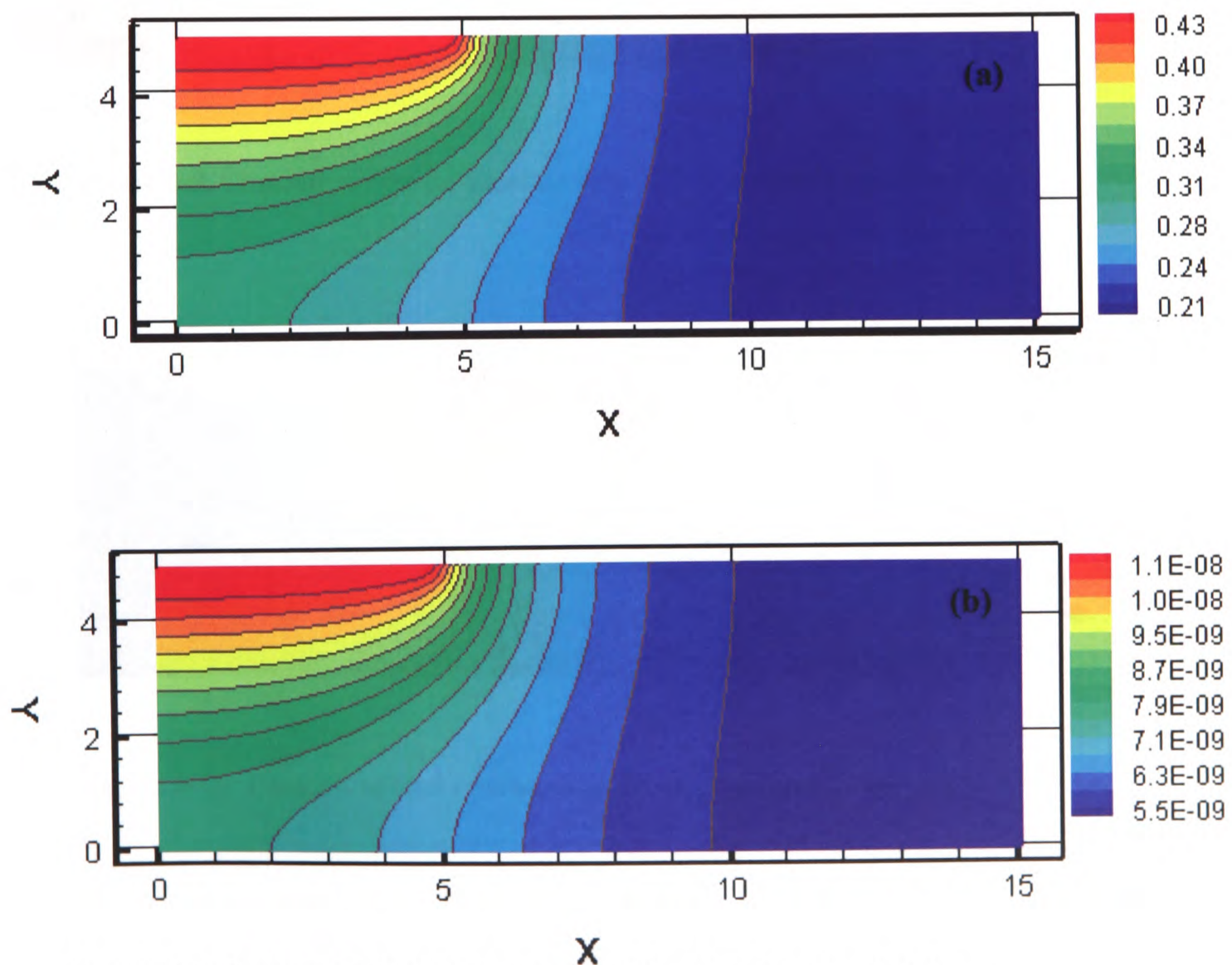


Figure 6-8. Contours of SWCC (a) and permeability function (b) at 100 day.

The stress-strain analysis is performed in two stages. One stage is for changes in net normal stress and the other is for changes in suction. Deformation due to changes in matric suction is a time dependent process, whereas the deformation in a soil mass due to loading are assumed to response immediately. At an initial matric suction of 400 kPa the contours of vertical displacement caused by loading are presented in Figure 6-9. The maximum displacement of 120 mm is predicted for the concrete slab. Figure 6-10 shows the displacement contours due to wetting and loading after 100 days. The maximum heave of about 60 mm is predicted under the concrete slab for this example. The distribution of deformation vectors and total cumulative displacements at the surface due to wetting and loading after 100 days are also shown in Figure 6-11 and Figure 6-12 respectively.

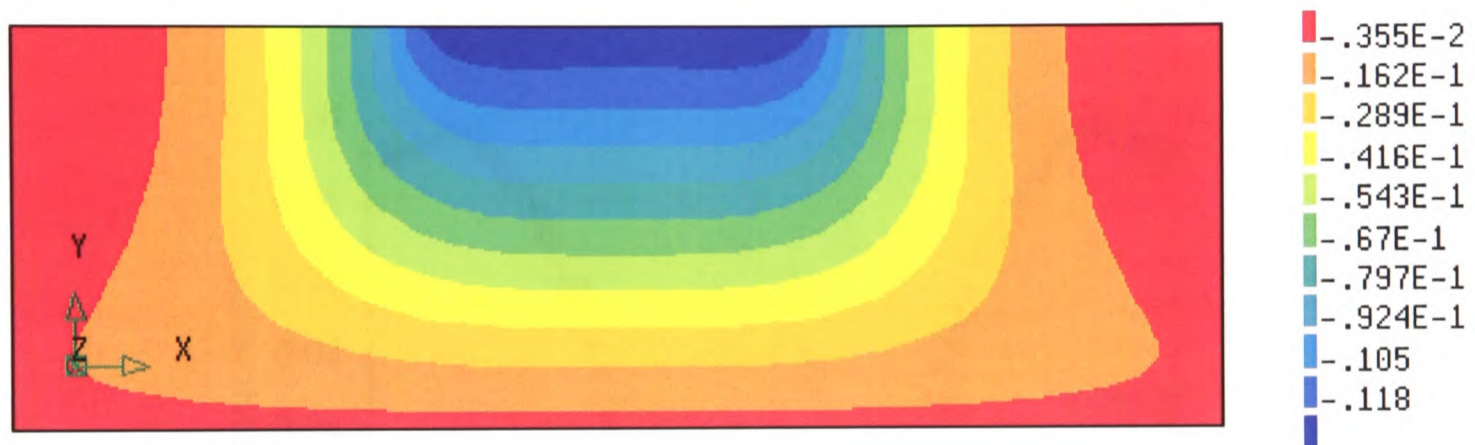


Figure 6-9. Contours of vertical displacement (m) due to loading at 100 days.

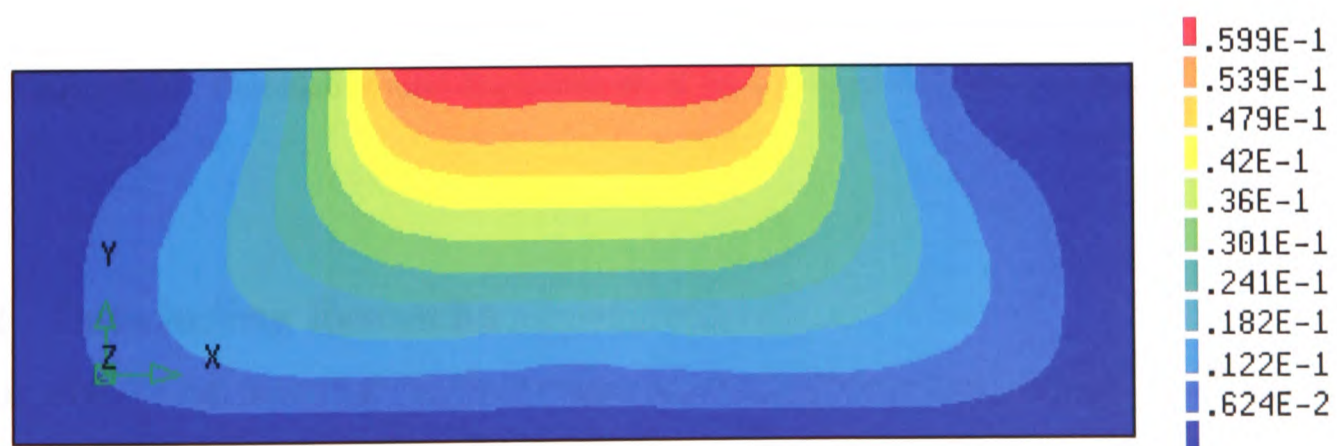


Figure 6-10. Contours of total displacement due to wetting and loading at 100 days.

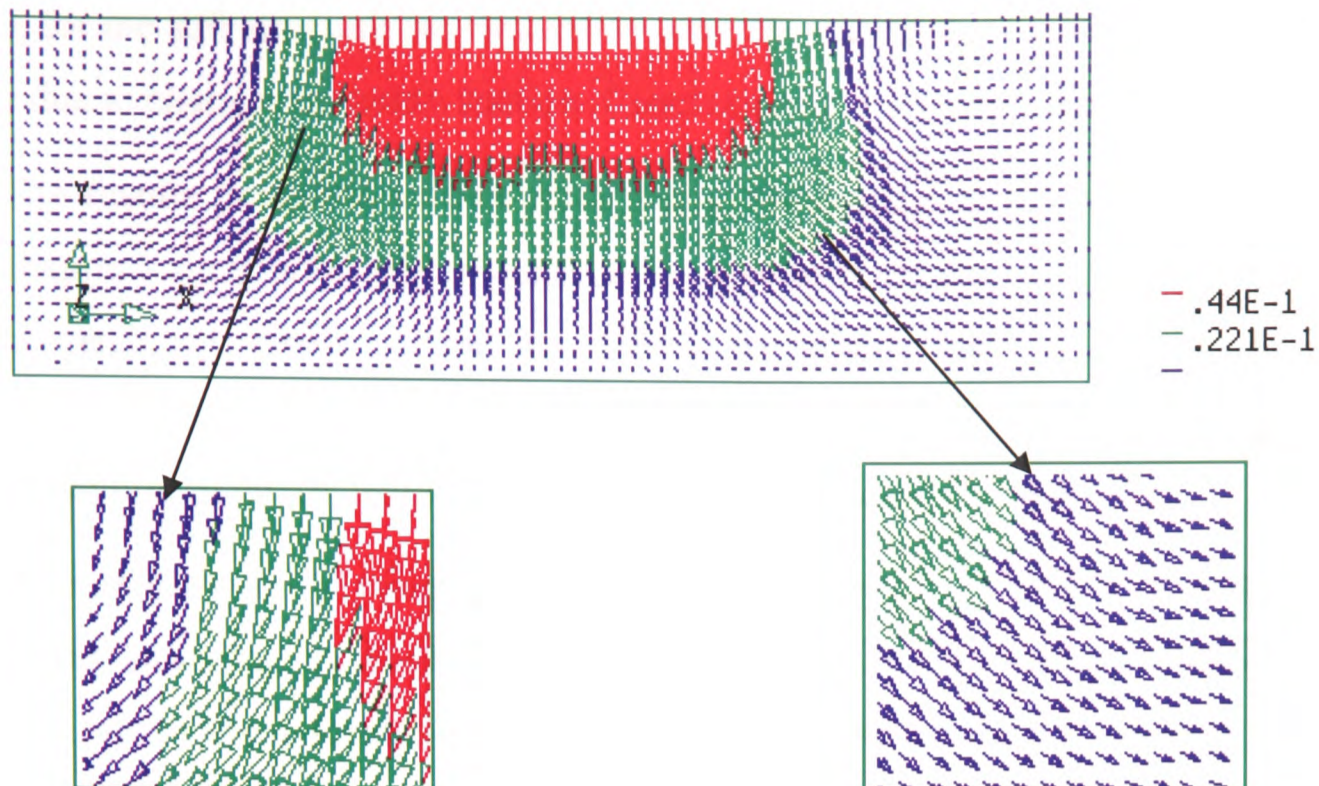


Figure 6-11. Distribution of deformation vectors due to loading and wetting after 100 days.

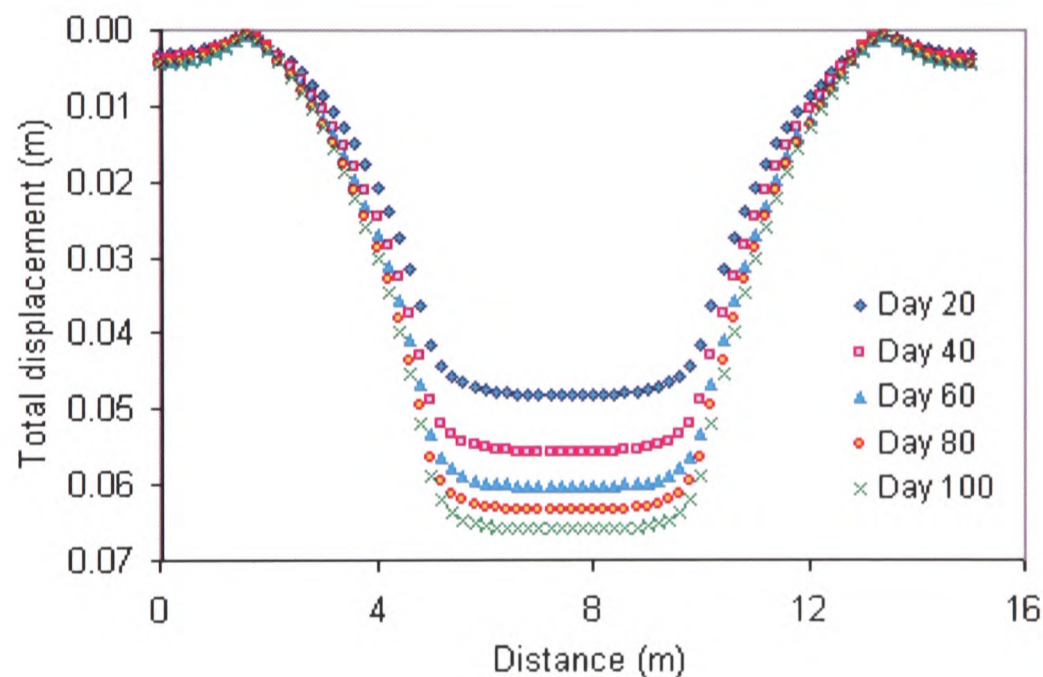


Figure 6-12. Cumulative total displacements at the surface at five different times.

6.3.2 Concluding Remarks

In this chapter the essential features required in the stress-strain modelling for expansive unsaturated soils are discussed taking into account the role of stress state variables in the mechanical behaviour of soils. The stress state variables of net normal stress and matric suction along with deformation state variables are used to construct the constitutive relations for unsaturated soils in soil structure and water phase forms. General empirical equations are proposed to describe the SWCC for evaluating the relationship between flow parameters and the stress state variables. Finally the equations for plane strain

loading for the soil structure are derived to compute the displacements under an applied load or due to changes in matric suction. Conclusions are summarised as follows

1. The results predicted in this study using the numerical procedures proposed in chapter 2 show good agreement with the published data on measured coefficient of permeability, matric suction and SWCC for unsaturated soils. The equation for SWCC proposed by Fredlund and Xing [87] was found to be effective in the prediction of coefficients of permeability and the water storage.
2. An interpretation of volume change behaviour of unsaturated soil using stress state theory proposed by Fredlund and Rahardjo [51] is presented and applied to the analysis of the deformations in a swelling clay profile under a concrete floor slab due to applied load. The results appear to be satisfactory. Further studies are however required to examine the proposed framework on different soils and environmental problems.
3. The total vertical displacement due to loading and resultant displacement due to combined effects of loading and wetting are investigated. The maximum displacement of 60 mm and a minimum displacement of 6 mm is predicted at the surface and at about 4.5 m depth below the concrete slab.

CHAPTER 7

CONCLUSIONS

A comprehensive mathematical analysis based on Finite Volume discretisation approach has been carried out for determining the flow and transport processes in natural hydrogeological systems. The conclusions drawn from the research methods described can be summarised as follows

7.1 Finite Volume Methodology

FV methodology adapted for CFD modelling of deterministic flow/transport mechanisms and CSM modelling of stress state analysis in porous media has proven to perform well within PHYSICA framework. The employed cell-centred FV method for CFD and cell-vertex based FV method for CSM problems provide the conservation of underlying physical properties together with the ease of presenting the complex domains on unstructured meshes. Although the current procedure for evaluating the flow field across the grid cells produced reasonable results, the accuracy and efficiency in case of non-uniform medium can be enhanced by incorporating further modifications to the interpolation methods or by mesh refinement.

7.2 Integrated Modelling Framework

The research undertaken presents an integrated system for modelling water flow and contaminant transport with the aim of bringing various aspects of concern in a complete simulation environment. The model provides added option and features for supporting isotropic/anisotropic, homogeneous/heterogeneous, saturated/unsaturated fluid flow and transport of reactive/conservative contaminants through subsurface systems. The model also enables a coupled simulation environment between transient fluid flow and deformations prediction under applied loads accurately.

7.3 Validation of Results

The performance of the model as a reliable tool is accomplished by means of a number of standard verification test case comparisons. The following remarks can be made in this contest

- Cell-centred FV convention performs well for estimating the infiltration depth through uniform and non-uniform soil textures.
- The proposed numerical algorithms display very accurate results in terms of computational time with mass-balance errors of less than one percent in most cases.
- Numerical predictions of fate of contaminants are of vital interest in terms of peak concentration, change in concentration over time and change in vertical extent of plume through hydrologic environments in order to evaluate the risk of subsurface pollution.

7.4 Fluid Flow Analysis

The methodology proposed for the simulation of groundwater flow is a useful tool to perform preliminary analysis using variable medium properties alongside the constant values. Heterogeneous and anisotropic material properties can be approximated and layering heterogeneities can be treated in flow analysis.

Modelling the flow through the unsaturated zone is complicated by the difficulty to quantify unsaturated hydraulic properties and the spatial variability of those properties. The applied approach is very stable and robust for solving accurately and efficiently complex non-linear problem of unsaturated flow through vadose zone and the estimation of subsurface hydraulic properties during transient one-dimensional infiltration redistribution. Study of flow field estimation in response to varying hydraulic properties has provided valuable information for locating optimally the moisture measurement depth for different textured soils. The stability of the solution is further investigated by performing sensitivity analysis of hydraulic parameters and by incorporating different plausible levels of moisture measurement errors. The employed adjustments are observed to have little influence on the prediction of the implemented strategy as designed is well-posed to enable unique and reliable estimation of the soil hydraulic parameters.

7.5 Solute Transport Analysis

Fate and transport of solute through 1-, 2-, and 3-dimensional saturated/unsaturated porous media is examined for a variety of different solute species. The implemented numerical techniques for contaminant transport can account for advection,

hydrodynamic dispersion, equilibrium/non-equilibrium sorption, first order degradation and volatilisation processes. The processes of dispersion, adsorption and decay are observed to have great impact in reducing the level of solute concentration over time. The attenuation of solute migration can assist to predict the future extent and concentration of a dissolved contaminant plume at a site as well to assess the potential for downgradient receptors to be exposed to the contamination that exceeds regulatory levels.

7.6 Effectiveness of the Model

The effectiveness of the model can be analysed in terms of the following

- **Subsurface Water Resources Investigation**
 - The numerical solutions are developed to simulate water table variation in response to withdrawal of groundwater from wells installed in confined and unconfined aquifers. The model can be used to test the effectiveness of the pump and treat systems and can simulate the effects of various pumping strategies with equivalent and lesser pumping rates and duration once the system reaches the new equilibrium. It can also be used for testing the results of numerical models under developing stages and for sensitivity analysis of the effects of variable controlling parameters such as location and dimension of abstraction wells and recharge basins.
 - The proposed flow model describes adequately the hydrodynamic behaviour of soils and therefore is promising for estimating effective subsurface hydraulic properties. Moreover, as it allows the prediction of large number of flow parameters, it facilitates the assessment of complex phenomena in the direct flow modelling.
- **Subsurface Contaminant Investigation**
 - The proposed model can predict the rate of plume migration and extent subject to different geologic settings. It can be effectively used to determine the natural attenuation of organic compounds as well as to assist in the design of monitoring programs and remedial schemes.

Owing to the fact that PHYSICA [91] provides an open framework for multi-physics computational mechanics modelling, a number of geophysical and geochemical phenomena can be analysed in the context of future research to the current work (Figure 8-1) as under

8.1 Heat Transfer

The simultaneous flow of heat and subsurface water is a coupled process controlled by hydraulic as well as the thermal gradients. Heat is transported through a porous medium by conduction, convection and radiation. A further research can be undertaken by including a conductive transport controlled by the thermal conductivity of geological medium in static groundwater and a convective transport where heat is carried along the flowing groundwater. For the analysis of forced convection where the fluid motion is under the influence of buoyancy effects, the Boussinesq approximation can be used. However, the effects of forced convection and radiation can be modelled by solving the general transport equation with temperature as solved variable.

8.2 Random Heterogeneity

Water flow and solute transport in natural soils are significantly influenced by the occurrence of macropore and the spatial variability of the hydraulic properties of the medium. The dynamic states of such systems i.e. pressure, water content and fluxes are associated with an uncertainty in their predictions. A further research is required to conduct the stochastic analysis by treating the hydraulic parameters as random fields. One way to accomplish the randomisation is the use of Fast Fourier Transform. The method performs the computation of first two statistical moments of mean and (co)variance to provide an estimate of the system state and the uncertainty associated with the estimate.

8.3 Analysis of Flow through Fractures

A great deal of further research is possible with regard to CFD modelling of preferential flow and transport in the vadose zone. The phenomenon of preferential flow occurs if the soil matrix is composed of fractures and interconnected discontinuities in its texture. The consequence of such a flow is the irregular wetting of the soil profile as a result of fluid moving faster in certain parts of the soil than in others. A potentially rapid migration of contaminants through the unsaturated zone to underlying groundwater is a direct impact of preferential flow problems. Various approximations for modelling fluid flow and solute transport in fractured porous media have evolved in the past few decades. Two of the most commonly used approaches are dual-porosity and dual-permeability models. The porous medium is considered to be comprised of two interacting regions, one associated with macropores or the fractures, and one consisting micropores inside the soil matrix. The dual porosity model proposed by van Genuchten and Wierenga [92] assumes the partitioning of fluid phase into mobile, θ_f , and immobile, θ_m , regions as

$$\theta = \theta_f + \theta_m$$

8.4 Complex Chemical Reactions

A further analysis of physical/chemical reactions can be conducted by taking into account dissolution, precipitation, complexation and oxidation-reduction reactions.

8.5 Shear Strength Analysis

The research can be further extended to the analysis of problems that are related to the shear strength of soils. The simple examples are the prediction of the stability of slopes and embankments, the bearing capacity of foundations and earth retaining structures.

The prediction of shearing strength of unsaturated soils can be carried out by employing the two stress state variables theory of Fredlund et al [93] given as

$$\tau = c' + (\sigma_n - u_a) \tan \phi' + (u_a - u_w) \tan \phi^b$$

where c' , ϕ' and ϕ^b are the effective cohesion, effective angle of internal friction and the angle indicating the rate of increase in shear strength τ relative to a change in the matric suction.

8.6 Multi-Phase Flow

An extension of single-phase flow to three-phase flow (oil, gas, water) can be included in the current PHYSICA framework. Traditional mathematical models of multi-phase flow in porous media incorporate an extension of Darcy's equation. A great deal of processes of practical interest e.g. oil production with movable water, water floods, steam and immiscible CO₂ floods and contaminant intrusions into vadose zone require the predictions of flow of three-phase fluid systems.

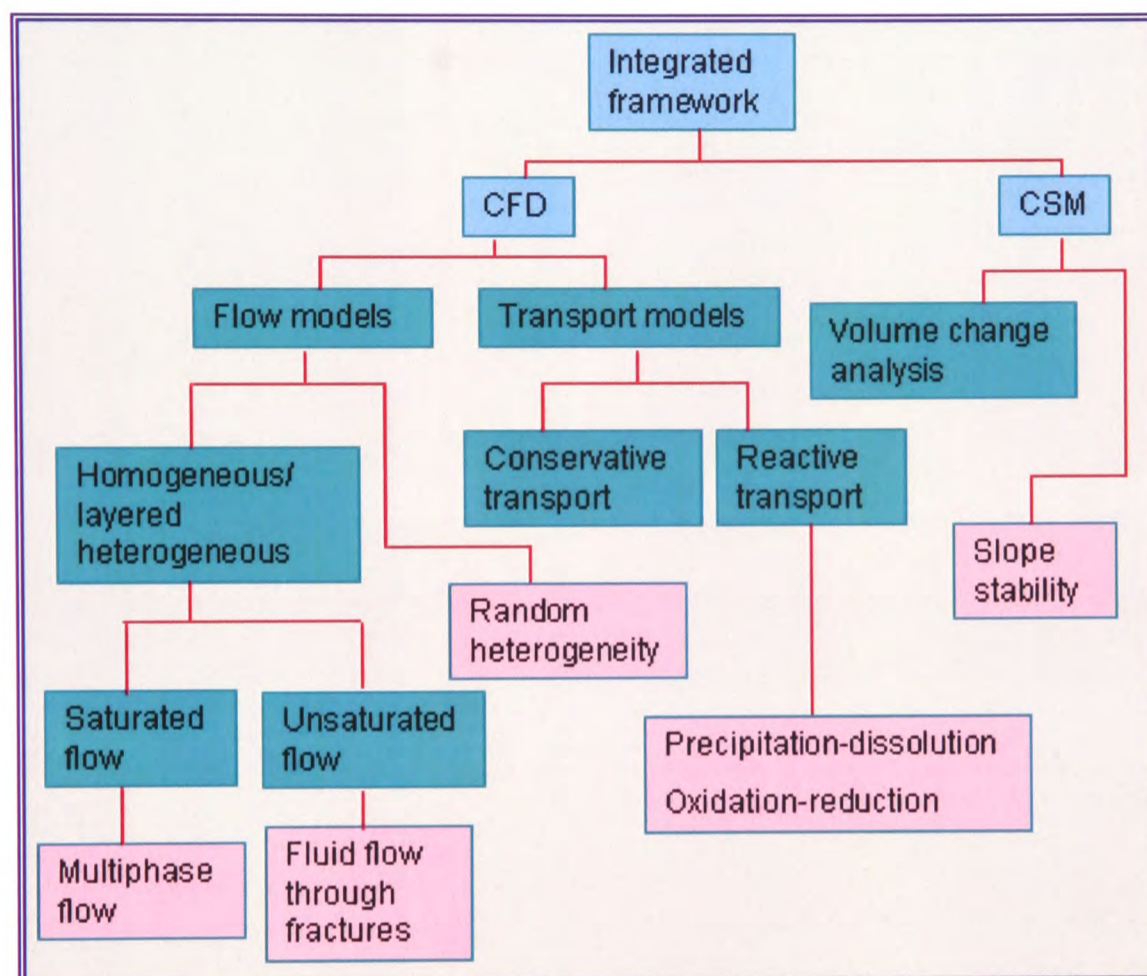


Figure 8-1. Route map for future work. Blue boxes = modelling environment, Turquoise boxes = tasks accomplished, pink boxes = future work.

APPENDICES

A	BOREHOLE DATA FOR BURNSTUMP CASE STUDY.....	194
A1	BOREHOLE SURVEY FOR CHLORIDE CONCENTRATION	194
A2	BOREHOLE SURVEY FOR AMMONOCAL-NITROGEN	196
B	PRINCIPAL DIRECTIONS AND ANISOTROPY	198
C	CALCULATION OF COEFFICIENT OF WATER STORAGE	199

A Borehole data for Burnstump case study

A1 Borehole survey for chloride concentration

Following are the results of the borehole surveys for chloride concentrations below the landfill site at the particular year of observation.

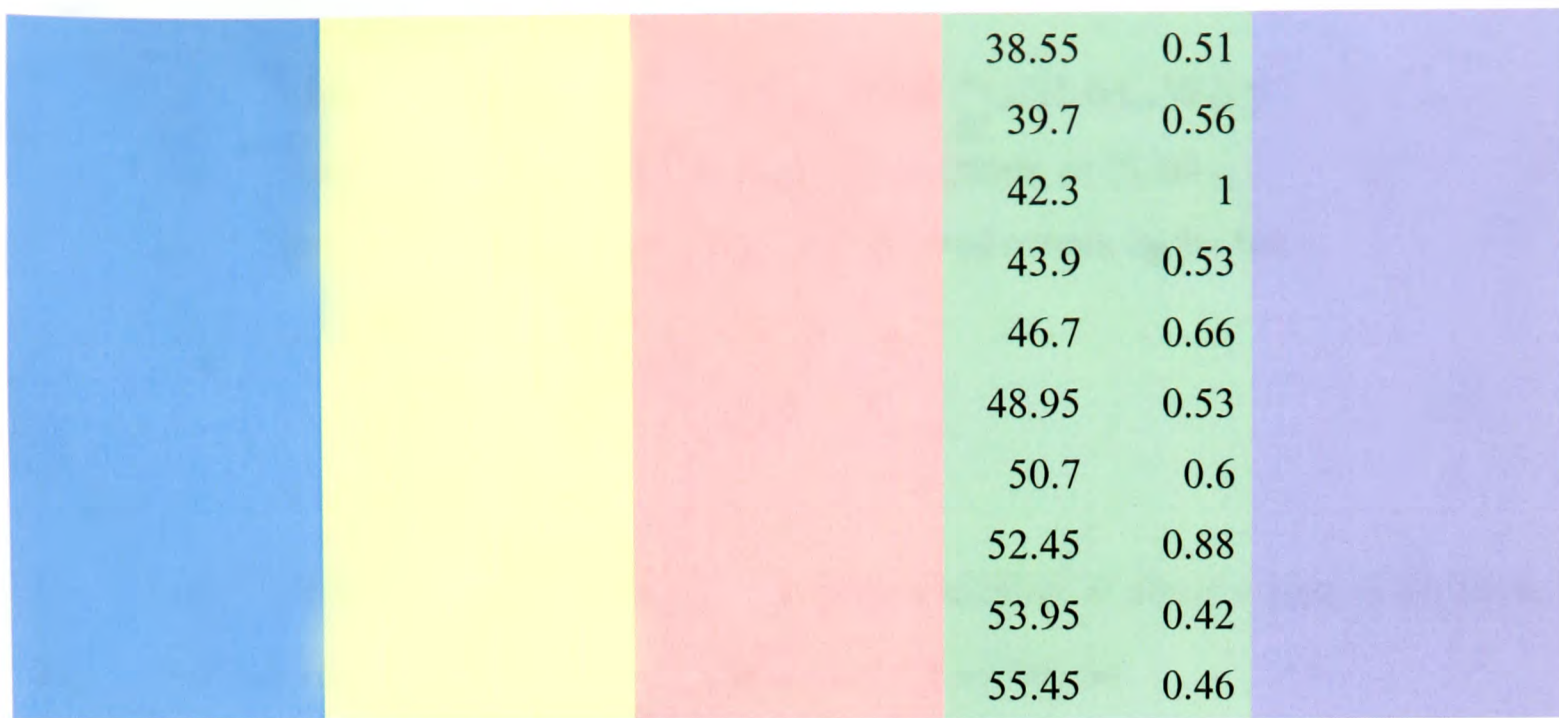
1978		1981		1987		1991		2000	
Depth (m)	Conc. (mg/l)	Depth (m)	Conc. (mg/l)	Depth (m)	Conc. (mg/l)	Depth (m)	Conc. (mg/l)	Depth (m)	Conc. (mg/l)
7.95	3750	7.925	3580	8	664	9.6	220	9.9	442
8.25	3850	8.175	3325	8.1	813	11.55	450	10.65	241
8.45	3850	8.525	2750	10.6	1604	15.35	635	12.75	148
9.125	900	8.9	3430	11.7	1790	16.85	600	14.5	287
10.125	77	9.225	3250	13.95	2290	17.85	700	15.5	211
14.625	45	9.725	3430	14.45	2618	18.5	595	16.5	208
15.625	53	10.1	3480	14.95	2900	19.25	715	17.5	217
16.625	57	10.525	4130	15.45	3310	20	715	18.75	253
17.6	85	11.075	630	15.95	3650	21	735	22.5	288
18.625	44	11.625	65	16.45	4080	21.75	845	27	893
19.125	44	12.075	58	16.95	4580	22.5	1220	28	171
23.025	68	12.625	54	17.45	4950	23.4	1440	33	150
23.525	48	13.15	50	17.95	4780	23.9	1360	34	97.8
24.625	50	14.125	47	18.6	4690	25.3	1920	35	733
25.625	64	15.125	44	19.1	4660	26.3	1920	36	1122
28.625	85	16.225	44	19.45	4390	27.3	111	37	739
29.625	77	17.125	48	19.95	4250	28.05	120	38	689
31.125	65	18.225	43	20.45	3750	28.55	92	39	238
32.125	78	19.225	64	20.95	3620	29.05	114	40.75	74.5
33.125	61	20.275	50	21.45	3850	29.55	100	41.5	99.2
34.4	57	21.275	57	21.95	2470	31.3	83	44.5	76.8
35.625	55	23.05	54	22.45	406	34.3	62	45.5	76.5
36.525	73	24.125	56	22.95	171	35.05	69	46.5	76.8
39.525	85	25.125	50	23.45	229	35.55	65	47.5	72.6
41.625	96	26.25	66	23.95	101	36.05	92	49.75	74.2
44.875	81	34.4	57	24.45	92	36.55	67	52	83.6
47.6	52	35.63	55	24.95	83	37.05	82	53.25	67.8

49.625	56	56.53	73	25.45	92	37.55	77	58	93.6
50.625	45	39.53	85	25.95	74	38.05	82		
52.125	46	41.63	96	26.45	133	38.55	88		
53.125	61	44.88	81	26.95	88	39.7	80		
54.575	48	47.6	52	27.45	101	40.45	82		
		49.63	56	27.95	141	40.95	81		
		50.63	45	28.45	116	41.55	76		
		52.13	46	28.95	116	42.3	80		
		53.13	32.29	31.45	97	43.15	93		
				33.95	93	43.9	77		
				36.45	96	44.7	59		
				38.45	140	45.7	98		
				42.95	119	46.7	91		
				48.95	134	47.7	113		
				53.75	140	48.45	102		
						48.95	114		
						49.45	98		
						49.95	78		
						50.7	112		
						51.7	102		
						52.45	96		
						52.95	74		
						53.95	177		
						55.45	534		

A2 Borehole survey for ammonocal-nitrogen

Following are the results of the borehole surveys for ammonocal-nitrogen concentrations below the landfill site at the particular year of observation.

1978		1981		1987		1991		2000	
Depth (m)	Conc. (mg/l)	Depth (m)	Conc. (mg/l)	Depth (m)	Conc. (mg/l)	Depth (m)	Conc. (mg/l)	Depth (m)	Conc. (mg/l)
7.95	880	7.952	1020	8	191	9.6	183	8.85	124
8.25	890	8.175	580	8.1	190	11.55	177	9.9	136
8.45	915	8.525	365	10.6	114	15.35	9.6	10.65	109
9.125	5	8.9	420	11.7	69	16.85	0.4	12.75	103
10.125	0.5	9.225	368	13.95	0.7	17.85	1.3	14.5	143
14.625	0.2	9.725	380	14.45	0.5	18.5	0.5	15.5	149
15.625	0.2	10.2	24	15.45	0.9	19.25	1.2	16.5	105
16.625	0.3	10.525	10	15.95	0.9	20	1	17.5	88
17.6	0.4	11.075	0.4	16.45	0.5	21	0.7	18.75	77
18.625	0.2	11.625	0.4	16.95	0.7	21.75	0.7	22.5	1.11
19.125	0.3	12.075	0.1	17.45	1.2	22.5	0.6	27	0.556
		12.625	0.3	17.95	1	23.4	0.7	28	1.1
		13.15	0.1	18.6	1.2	23.9	1.2	33	0.15
		14.125	0.1	19.1	1.5	25.3	0.6	34	0.51
				19.45	1.1	26.3	0.8	36	0.75
				19.95	1	27.3	0.7	37	0.27
				20.45	0.7	28.05	0.7	38	0.5
				20.95	0.9	28.55	0.7	39	0.57
				21.45	1	29.05	0.6	41.5	0.05
				21.95	0.6	29.55	0.1	44.5	0.25
						31.3	0.5	46.5	0.29
						34.3	0.7	49.75	0.07
						35.05	0.4	52	0.16
						35.55	0.5	53.25	0.11
						36.05	0.5		
						36.55	0.3		
						37.05	0.4		
						37.55	0.4		
						38.05	0.47		



			38.55	0.51	
			39.7	0.56	
			42.3	1	
			43.9	0.53	
			46.7	0.66	
			48.95	0.53	
			50.7	0.6	
			52.45	0.88	
			53.95	0.42	
			55.45	0.46	

B Principal directions and anisotropy

Assuming the conductivity along the principal directions coinciding initially with the Cartesian coordinate axes x, y is represented as diagonal matrix in the form

$$K_{ij}^P = \begin{bmatrix} K_{\xi\xi} & 0 \\ 0 & K_{\eta\eta} \end{bmatrix}$$

If the coordinate system is rotated to ξ and η by a rotation θ about z axis as shown in Figure 3-3 the rotation matrix in 2-dimension can be written as

$$(a_{ij}) = \begin{bmatrix} a_{11} & a_{12} \\ a_{21} & a_{22} \end{bmatrix} = \begin{bmatrix} \cos \theta & -\sin \theta \\ \sin \theta & \cos \theta \end{bmatrix}$$

This rotation will transform an anisotropic, diagonal tensor in the x, y coordinate system to a tensor with off diagonal terms in the ξ, η coordinate system.

The components of conductivity tensor K_{ij} ($i, j = 1, 2$) in the global coordinate system x, y can be determined by making use of directional cosines (a_{ij}) through the following relation

$$K_{ij} = a_{mi} K_{mn}^P a_{nj}$$

which implies that

$$K_{ij} = \begin{bmatrix} K_{xx} & K_{xy} \\ K_{yx} & K_{yy} \end{bmatrix} = \begin{bmatrix} \cos \theta & -\sin \theta \\ \sin \theta & \cos \theta \end{bmatrix} \begin{bmatrix} K_{\xi\xi} & 0 \\ 0 & K_{\eta\eta} \end{bmatrix} \begin{bmatrix} \cos \theta & \sin \theta \\ -\sin \theta & \cos \theta \end{bmatrix}$$

Hence the components of the two-dimensional anisotropic conductivity lead to

$$\begin{aligned} K_{xx} &= K_{\xi\xi} \cos^2 \theta + K_{\eta\eta} \sin^2 \theta \\ K_{yy} &= K_{\xi\xi} \sin^2 \theta + K_{\eta\eta} \cos^2 \theta \\ K_{xy} &= K_{yx} = (K_{\xi\xi} - K_{\eta\eta}) \sin \theta \cos \theta \end{aligned}$$

C Calculation of coefficient of water storage

The soil water characteristic curve for an unsaturated soil is given as

$$\theta = \theta_s C(\psi) \left[\frac{1}{\ln(e + (\psi/a)^n)} \right]^m$$

The coefficient of water storage (i.e. slope of soil water characteristic curve) can be obtained by differentiating SWCC with respect to suction ψ .

Taking $C(\psi) = 1$ and rearranging the above equation it can be written as

$$\theta = \theta_s \left[\ln(e + (\psi/a)^n) \right]^{-m}$$

Differentiating with respect to ψ

$$\frac{d\theta}{d\psi} = m_2^w = -m\theta_s \left[\ln(e + (\psi/a)^n) \right]^{-m-1} \frac{1}{e + (\psi/a)^n} \times n(\psi/a)^{n-1} \frac{1}{a}$$

or

$$m_2^w = -mn \frac{\theta_s}{\left[\ln(e + (\psi/a)^n) \right]^{m+1}} \frac{1}{\left[e + (\psi/a)^n \right]} \frac{\psi^{n-1}}{a^n}$$

or

$$m_2^w = -mn \frac{\theta_s}{\left[\ln(e + (\psi/a)^n) \right]^{m+1}} \frac{\psi^{n-1}}{ea^n + \psi^n}$$

REFERENCES

- [1] Viessman, W.Jr. and Lewis, G.L. 1996. Introduction to Hydrology, *Harper Collins College Publishers*, New York.
- [2] Fetter, C.W. 2001. Applied hydrogeology, *Prentice-Hall*, New Jersey.
- [3] Rudland, D.J., Lancefield, R.M. and Mayell, P.N. 2001. Contaminated land risk assessment: A guide to good practice, *CIRIA Publication C552*, London.
- [4] Marsland, P.A. and Carey, M.A. 1999. Methodology for the derivation of remedial targets for soil and groundwater to protect water resources, *Environment Agency R & D Publication 20*, Bristol.
- [5] Manglik, A. and Rai, S.N. 2000. Modeling of water table fluctuations in response to time-varying recharge and withdrawal, *Water Resources Management*, **14**:339-347.
- [6] Zhan, H., Wang, L.V. and Park, E. 2001. On the horizontal-well pumping tests in anisotropic confined aquifers, *Journal of Hydrology*, **252**:37-50.
- [7] Moore, J.E. 1979. Contribution of ground-water modeling to planning, *Journal of Hydrology*, **43**:121-128.
- [8] Prickett, T.A. 1979. Ground-water computer models_ state of art, *Groundwater*, **17**:121-128.
- [9] Freeze, R.A. and Cherry, J.A. 1979. Groundwater, *Englewood Cliffs, NJ:Prentice-Hall*.
- [10] van Dam, J.C. and Feddes, R.A. 2000. Numerical simulation of infiltration, evaporation and shallow groundwater levels with the Richards equation, *Journal of Hydrology*, **233**:72-85.
- [11] Ataie-Ashtiani, B., Volker, R.E. and Lockington, D.A. 1999. Numerical and experimental study of seepage in unconfined aquifers with a periodic boundary condition, *Journal of Hydrology*, **222**:165-184.
- [12] Bakker, M. 1999. Simulating groundwater flow in multi-aquifer systems with analytical and numerical Dupuit-model, *Journal of Hydrology*, **222**:55-64.
- [13] Freeze, R.A. 1969. The mechanism of natural groundwater recharge and discharge: 1. One-dimensional vertical, unsteady, unsaturated flow above a recharging or discharging groundwater flow system, *Water Resources Research*, **5**: 153-171.

-
- [14] Haverkamp, R., Vauclin, M., Touma, J., Wierenga, P. and Vuchaud, G. 1997. A comparison of numerical simulation models for one-dimensional infiltration, *Soil Science Society of America Journal*, **41**: 285-294.
- [15] Celia, M.A, Bouloutas, E.T. and Zarba, R.L. 1990. A general mass-conservative numerical solution for the unsaturated flow equation, *Water Resources Research*, **26**: 1483-1496.
- [16] Parsad, H.K.S., Kumar, M.M.S. and Sekhar, M. 2001. Modelling flow through unsaturated zones: Sensitivity to unsaturated soil properties, *Sadhana*, **26**: 517-528.
- [17] Cooley, R.L. 1983. Some new procedures for numerical solution of variably saturated flow problems, *Water Resources Research*, **19**: 1271-1285.
- [18] van Genuchten, M.Th. 1982. A comparison of numerical solutions of the one-dimensional unsaturated-saturated flow and mass transport equations, *Advances in Water Resources*, **5**: 47-55.
- [19] Paniconi, C., Aldama, A.A. and Eric, F.W. 1991. Numerical evaluation of iterative and noniterative methods for the solution of the nonlinear Richards equation, *Water Resources Research*, **27**: 1147-1163.
- [20] Simpson, M.J and Clement, T.P. 2003. Comparison of finite difference and finite element solutions to the variably saturated flow equation, *Journal of Hydrology*, **270**: 49-64.
- [21] Miller, C.T., Glenn, A.W., Kelley, C.T. and Michael, D.T. 1998. Robust solution of Richards' equation for nonuniform porous media, *Water Resources Research*, **34**: 2599-2610.
- [22] Kim, J.M. and Parizek, R.R. 1997. Numerical simulation of the Noordbergum effect resulting from groundwater pumping in a layered aquifer system, *Journal of Hydrology*, **202**:231-243.
- [23] Pruess, K. 2004. A composite medium approximation for unsaturated flow in layered sediments, *Journal of Contaminant Hydrology*, **70**:225-247.
- [24] Ng, C-O. 1999. Macroscopic equations for vapour transport in a multi-layered unsaturated zone, *Advances in Water Resources*, **22**:611-622.

-
- [25] Butts, M.B. and Jensen, K.H. 1996. Effective parameters for multiphase flow in layered soils, *Journal of Hydrology*, **183**:101-116.
- [26] Mattson, E.D., Bowman, R.S. and Lindgren, E. R. 2002. Electrokinetic ion transport through unsaturated soil: 2. Application to a heterogeneous filed site, *Journal of Contaminant Hydrology*, **54**:121-140.
- [27] Prechtel, A., Knabner, P., Schneid, E. and Totsche, K.U. 2002. Simulation of carrier-facilitated transport of phenanthrene in a layered soil profile, *Journal of Contaminant Hydrology*, **56**:209-225.
- [28] Hills, R.G., Porro, I., Hudson, D.B. and Wierenga, J. 1989. Modelling one-dimensional infiltration into very dry soils: 1. Model development and evaluation, *Water Resources Research*, **25**: 1259-1269.
- [29] Gottardi, G. and Venutelli, M. 1993. Richards: computer program for the numerical simulation of one-dimensional infiltration into unsaturated soil, *Computers & Geosciences*, **19**: 1239-1266.
- [30] Gerke, H.H., Molson, J.W. and Frind, E.O. 1998. Modelling the effect of chemical heterogeneity on acidification and solute leaching in over burden mine spoils, *Journal of Hydrology*, **209**:166-185.
- [31] Wu, J., Hu, B.X., Zhang, D. and Shirley, C. 2003. A three-dimensional numerical method of moments for groundwater flow and solute transport in a nonstationary conductivity filed, *Advances in Water Resources*, **26**:1149-1169.
- [32] Zalesak, S.T. 1979. Fully multidimensional flux corrected transport algorithms for fluids, *Journal of Computational Physics*, **31**:335-362.
- [33] Gupta, A.D., Lake, L.W., Pope, G.A., Sepehrnoori, K. and King, M.J. 1991. High-resolution monotonic schemes for reservoir fluid flow simulation, *In Situ*, **15**:289-317.
- [34] Rubin, B. 1993. Extension of the TVD midpoint scheme to higher accuracy in time. In: 12th SPE symposium on reservoir simulation, *Society of Petroleum Engineers*, New Orleans, Louisiana, pp:375-385.
- [35] Morton, K.W. 1996. Numerical solution of convection-diffusion problems, *Chapman & Hall*, London.

- [36] Schnoor, J.L. 1996. Environmental modeling: Fate and transport of pollutants in water, air and soil, *John Wiley & Sons Inc.*, New York.
- [37] Lichtner, P.C., Steefel, C.J. and Oelkers, E.H. 1996. Reactive transport in porous media, *The Mineralogical Society of America*, Washington.
- [38] Indelman, P., T-Yasur, I., Yaron, B. and Dagan, G. 1998. Stochastic analysis of water flow and pesticides transport in a field experiment, *Journal of Contaminant Hydrology*, **32**:77-97.
- [39] Thomasson, M.J. and Wierenga, P.J. 2003. Spatial variability of the effective retardation factor in an unsaturated field soil, *Journal of Hydrology*, **272**:213-225.
- [40] Morshed, J. and Kaluarachchi, J.J. 1998. Application of artificial neural network and genetic algorithm in flow and transport simulation, *Advances in Water Resources*, **22**:145-158.
- [41] Piggott, J.H. and Cawlfild, J.D. 1996. Probabilistic sensitivity analysis for one-dimensional contaminant transport in the vadose zone, *Journal of Contaminant Hydrology*, **24**:97-115.
- [42] Kim, J.Y., Edil, T.B. and Park, J.K. 1997. Effective porosity and seepage velocity in column tests on compacted clay, *Journal of Geotechnical and Geoenvironmental Engineering*, **123**:1135-1142.
- [43] Mazzieri, F., Vanlmpe, P.O., van Impe, W.F. and Constales, D. 2002. A simulation model for consolidation and contaminant coupled flows in clay layers, *Environmental Geotechnics (4th ICEG)'02*, Swets & Zeitlinger, Rio de Janeiro, Brazil, pp:183-188.
- [44] Hardisty, J. 1993. Computerised environmental modelling: A practical introduction using Excel, *John Wiley & Sons*, Chichester.
- [45] Versteeg, H.K and Malalasekera, W. 1995. An introduction to computational fluid dynamics: The finite volume method, *Prentice Hall*, Harlow.
- [46] Courant, R., Isaacson, E. and Rees, M. 1952. On the solution of nonlinear hyperbolic differential equations by Finite Difference, *Communications in Pure and Applied Mathematics*, **5**:243-255.

-
- [47] Spalding, D.B. 1972. A novel Finite Difference formulation for differential expressions involving both first and second derivatives, *International Journal for Numerical Methods in Engineering*, 4:551-559.
- [48] Patankar, S.V. 1980. Numerical heat transfer and fluid flow, *McGraw-Hill*, New York.
- [49] Leonard, B. P. 1979. A stable and accurate convective modelling procedure based on quadratic upstream interpolation, *Computational Methods in Applied Mechanical Engineering*, 23:293-312.
- [50] Hayase, T., Humphrey, J.A.C. and Grief, R. 1992. A consistently Formulated QUICK scheme for fast and stable convergence using Finite-Volume iterative calculation procedures, *Journal of Computational Physics*, 98:108-118.
- [51] Fredlund, D.G. and Rahardjo, H. 1993. Soil mechanics for unsaturated soils, *John Wiley & Sons*, New York.
- [52] Domenico, P.A. and Schwartz, F.W. 1998. Physical and chemical Hydrology, *John Wiley & Sons, Inc.*, New York.
- [53] Company, R.M. 1990. Handbook of ground water development, *John Wiley & Sons*, New York.
- [54] Ward, R.C. and Robinson, M. 1990. Principles of Hydrology, *McGraw-Hill*, Cambridge.
- [55] Sun, N., Elimelech, M., Sun, Ne-Z. and Ryan, J.N. 2001. A novel two-dimensional model for colloid transport in physically and geochemically heterogeneous porous media, *Journal of Contaminant Hydrology*, 49:173-199.
- [56] Johnson, P.R., Sun, N. and Elimelech, M. 1996. Colloid Transport in geochemically heterogeneous porous media: Modeling and measurements, *Environmental Science & Technology*, 30:3284-3293.
- [57] Johnson, P.R. and Elimelech, M. 1995. Dynamics of colloid deposition in porous media: Blocking based on random sequential adsorption. *Langmuir*, 11:801-812.
- [58] Alley, W.M., Reilly, T.E. and Franke, O-L. 1999. Sustainability of ground-water resources, *U.S. Geological Survey Circular 1186*, Denver.

-
- [59] Kinzelbach, W. 1986. groundwater modeling- An introduction with simple programs in BASIC, *Elsevier*, 270-294.
- [60] Serrano, S.E. 2001. Solute transport under non-linear sorption and decay, *Water Resources*, **35**:1525-1533.
- [61] Jury, W., Gardner, W.R and Gardner, W.H. 1991. Soil physics, *John Wiley & Sons*, New York.
- [62] Marshall, T.J. and Holmes, J.W. 1979. Soil physics, *Cambridge University Press*, Cambridge.
- [63] Richards, L.A. 1931. Capillary conduction of liquids in porous media, *Physics*, **1**:318-333.
- [64] Van Genuchten, M.Th. 1980. A closed-form equation for predicting the hydraulic conductivity of unsaturated soils, *Soil Science Society of America Journal*, **44**:892-898.
- [65] Jury, W.A., Russo, D., Streile, G. and Abd, H.E. 1990. Evaluation of volatilization by organic chemicals residing below the soil surface, *Water Resources Research*, **26**:13-20.
- [66] Shoemaker, C.A., Culver, T.B., Lion, L.W. and Peterson, M.G. 1990. Analytical models of the impact of two-phase sorption on subsurface transport of volatile chemicals, *Water Resources Research*, **26**:745-758.
- [67] Sonntag, R.E. and Van Wylen, G.J. 1982. Introduction to thermodynamics: Classical and statistical, *John Wiley*, New York.
- [68] Van Genuchten, M.Th. and Leij, F.J. 1992. On estimating the hydraulic properties of unsaturated soils: Direct methods for estimating the hydraulic properties of unsaturated soils, *Proceedings of the International Workshop on Indirect Methods for Estimating the Hydraulic Properties of Unsaturated Soils*, Riverside, California.
- [69] McGrail, B.P. 2001. Inverse reactive transport simulator (INVERTS): An inverse model for contaminant transport with nonlinear adsorption and source terms. *Environmental Model Software*, **16**: 711-723.
- [70] Bear, J. 1972. Dynamics of fluids in porous media, *American Elsevier*, New York.

-
- [71] Sheng, D. and Smith, D.W. 2000. Numerical modelling of competitive components transport with non-linear adsorption, *International Journal of Numerical and Analytical Methods in Geomechanics*, **24**:47-71.
- [72] Wu, Y.S., Kool, J.B., Huyakorn, P.S. and Saleem, Z.A. 1997. An analytical model for nonlinear adsorptive transport through layered soils, *Water Resources Research*, **33**:21-29.
- [73] Shan, C. and Stephens, D.B. 1995. An analytical solution for vertical transport of volatile chemicals in the vadose zone, *Journal of Contaminant Hydrology*, **18**:259-277.
- [74] Millington, R.J. 1959. Gas diffusion in porous media, *Science*, **130**:100-102
- [75] Gasto, J.M, Grifoll, J. and Cohen, Y. 2002. Estimation of internodal permeabilities for numerical simulation of unsaturated flows, *Water Resources Research*, **38**:1326.
- [76] Lewin, K., Young, C.P., Bradshaw, K., Fleet, M. and Blakey, N.C. Landfill monitoring investigations at Burnstump landfill, Sherwood Sandstone, Nottingham, *DoE Report No: CWM 035/94*, WRc., 1978-1993.
- [77] Thornton, S.F., Tellam J.H. and Lerner D.N. 2000. Attenuation of Leachate by UK Triassic Sandstone Aquifer materials: 1. fate of inorganic pollutants in laboratory columns, *Journal of Contaminant Hydrology*, **43**:327-354.
- [78] Terzaghi, K. 1936. The shear resistance of saturated soils, *Proc. First International Conference on Soil Mechanics & Foundation Engineering*, Cambridge, MA, **1**:54-56.
- [79] Bishop, A.W. 1959. The principle of effective stress, *Teknisk Ukeblad*, **39**:859-863.
- [80] Jennings, J.B. and Burland, J.B. 1962. Limitations to the use of effective stresses in partially saturated soils, *Geotechnique*, **12**:125-144.
- [81] Bishop, A.W. and Blight, G.E. 1963. Some aspects of effective stress in saturated and partly saturated soils, *Geotechnique*, **13**:177:197.

-
- [82] Richards, B.G. 1966. The significance of moisture flow and equilibria in unsaturated soils in relation to the design of engineering structures built on shallow foundations in Australia, *Symposium on permeability and capillary*, American Society of Testing Materials, Atlantic City, NJ.
- [83] Fredlund, D.G. and Morgenstern, N.R. 1977. Stress state variable for unsaturated soils, *Journal of Geotechnical Engineering Division, Proceedings, American Society of Civil Engineering (GT5)*, 103:447-466.
- [84] Biot, M.A. 1941. General theory of three dimensional consolidation, *Journal of Applied Physics*, 12:155-164.
- [85] Gardner, W.R. 1958. Some steady state solutions of the unsaturated moisture flow equation with application of evaporation from a water table, *Soil Science*, 85:228-232.
- [86] Brooks, R.H. and Corey, A.T. 1964. Hydraulic properties of porous media, *Hydrology Paper No. 3*, Civil Engineering Dept., Colorado State Univ., Fort Collins, Colorado.
- [87] Fredlund, D.G. and Xing, A. 1994. Equation for the soil-water characteristic curve, *Canadian Geotechnical Journal*, 31:521-532.
- [88] Leong, E.C. and Rahardjo, H. 1997. Permeability functions for unsaturated soils, *Journal of Geotechnical and Geoenvironmental Engineering*, ASCE, pp:1118-1126.
- [89] Hung, V.Q. and Fredlund, D.G. 2000. Volume change predictions in expansive soils using a two-dimensional Finite Element Method, *Proceeding of Asian Conference on Unsaturated soils*, Singapore, pp:231-236.
- [90] Sheng, D., Sloan, S.W., Gens, A. and Smith, D.W. 2003. Finite Element formulation and algorithms for unsaturated soils, Part I: Theory, *International Journal for Numerical and Analytical Methods in Geomechanics*, 27:745-765.
- [91] PHYSICA+, <http://www.multi-physics.com>.
- [92] van Genuchten, M.Th. and Wierenga, P.J. 1976. Mass transfer studies in sorbing porous media. I. Analytical solutions, *Soil Science Society of America Journal*, 40:473-481.

- [93] Fredlund, D.G., Morgenstern, N.R. and Widger, R.A. 1978. The shear strength of unsaturated soils, *Canadian Geotechnical Journal*, **15**:313-321.